2-9-2010

Mineralogy and bulk chemistry of chondrules and matrix in petrologic type 3 chondrites : implications for early solar system processes

Jana Berlin

Jana Berlin
Candidate

Earth and Planetary Sciences
Department

This dissertation is approved, and it is acceptable in quality and form for publication:

Approved by the Dissertation Committee:

Alan Brawley, Chairperson

Brian Jones

Jana Schwertner

Jeffrey N. Grossman

MINERALOGY AND BULK CHEMISTRY OF CHONDRULES AND MATRIX IN PETROLOGIC TYPE 3 CHONDRITES: IMPLICATIONS FOR EARLY SOLAR SYSTEM PROCESSES

BY

JANA BERLIN

Diplom, Mineralogy, Free University Berlin, 2003

DISSERTATION

Submitted in Partial Fulfillment of the
Requirements for the Degree of

Doctor of Philosophy
Earth and Planetary Sciences

The University of New Mexico
Albuquerque, New Mexico

December, 2009

DEDICATION

To Emil Johansson Bergholtz,
who brought me back to life.

ACKNOWLEDGEMENTS

Funding for this study was provided by NASA Cosmochemistry grants NNG06GG37G to Dr. Adrian J. Brearley and NNG06GF73G to Dr. Rhian H. Jones.

I am indebted to my advisors Adrian Brearley and Rhian Jones for their guidance and support during this journey. Special thanks also to my committee: Zachary Sharp, Jane Selverstone and Jeffrey Grossman (USGS, Reston).

A big THANK YOU goes to Mike Spilde (Institute of Meteoritics), without whom I would never have learned so much about EPMA. Thank you also to Jeff Davis (National Institute of Standards and Technology), who introduced me to the Lispix software, which made producing the phase images of chondrules a lot faster. This dissertation and many of my conference talks also benefited from discussions with fellow grad students: Neyda Abreu, Rena Ford, Hollis Kovach, Mark Tyra and Paul Burger.

I thank Cindy Jaramillo for all her logistical help and the Department of Earth and Planetary Sciences for the scholarships I received.

I am indebted to my parents, Margrit and Heinz Berlin, for their continuing support during all these years, and to my friends Rachel Dwarzski, Johny Chaklader, Caitlin N. Callahan, Shannon Clark and Jeannette Gericke, who helped keeping me sane during this endeavor.

Finally, I would like to thank all the courageous people in Eastern Germany, who helped tearing down the Wall 20 years ago – without you, I certainly would not be where I am at right now.

MINERALOGY AND BULK CHEMISTRY OF CHONDRULES AND MATRIX IN PETROLOGIC TYPE 3 CHONDRITES: IMPLICATIONS FOR EARLY SOLAR SYSTEM PROCESSES

BY

JANA BERLIN

ABSTRACT OF DISSERTATION

Submitted in Partial Fulfillment of the
Requirements for the Degree of

Doctor of Philosophy
Earth and Planetary Sciences

The University of New Mexico
Albuquerque, New Mexico

December, 2009

MINERALOGY AND BULK CHEMISTRY OF CHONDRULES AND MATRIX IN PETROLOGIC TYPE 3 CHONDRITES: IMPLICATIONS FOR EARLY SOLAR SYSTEM PROCESSES

by

Jana Berlin

Diplom, Mineralogy, Free University Berlin, 2003
Ph.D., Earth and Planetary Sciences, University of New Mexico, 2009

ABSTRACT

A detailed electron microprobe (EMP) study was performed on chondrules of various textural types in four petrologic type 3 chondrites: MET 00526 (L3.05), MET 00426 (CR3.0), Kainsaz (CO3.2) and Kakangari (K3). Bulk compositions of twenty chondrules in each meteorite were determined with modal recombination analysis. This study provides a self-consistent dataset that combines chondrule textures with mineralogy and bulk chemical compositions. It allows us to make comparisons between different chondrite groups. In order to interpret the compositional relationship between chondrules and matrix, bulk matrix compositions were obtained as well, using EMP defocused beam analyses.

In Chapter 1, we compare the mineralogy and bulk chemistry of chondrules and matrix in MET 00526 (L), MET 00426 (CR) and Kainsaz (CO). These three chondrites represent some of the most pristine material that formed in the solar nebula. Chondrule characteristics and the complementary relationship between the compositions of chondrules and matrix suggest open system behavior during chondrule formation, in the form of evaporation and recondensation of volatile and siderophile elements.

While chondrules of the same textural types (e.g., FeO-poor (type I) and FeO-rich (type II) porphyritic chondrules) are present in all three chondrites and show similar characteristic features, there are also significant differences between the chondrite groups. This indicates that they probably formed in different regions of the solar nebula. One significant difference can be found in the Fe-Mn systematics of FeO-rich porphyritic

olivine (type IIA) chondrules (Chapter 2). We also recognized that Fe-Mn systematics can be used to identify relict grains in type IIA chondrules.

Chapter 3 deals with the chondrite Kakangari, which has been thought of as a very pristine chondrite in previous studies. Our study reveals that it records a complex series of events including reduction, thermal metamorphism, sulfidization and low-temperature aqueous alteration. Kakangari chondrules, as they are preserved in the meteorite, are quite different from chondrules in unequilibrated ordinary and carbonaceous chondrites. Kakangari appears to have undergone processing similar to that experienced by the enstatite chondrites.

TABLE OF CONTENTS

LIST OF FIGURES

CHAPTER 1:

CHAPTER 2:

CHAPTER 3:

APPENDIX A:

LIST OF TABLES

CHAPTER 1:

CHAPTER 2:

CHAPTER 3:

APPENDIX A:

APPENDIX B:

PREFACE

This dissertation consists of three independent chapters, two appendices and a supplementary CD. Each chapter is written as a separate manuscript. Therefore, some repetition in the introduction and analytical method sections was unavoidable. All of the literature references cited in the chapters and appendices have been combined into one list, which appears at the end of the dissertation. Each chapter represents a collaborative effort, but the majority of the analytical work, data interpretation and writing was done by myself and I will be the lead author on each manuscript.

Chapter 1 presents a detailed electron microprobe (EMP) study of chondrules and matrix in three chondritic meteorites from different groups: MET 00526 (L3.05), MET 00426 (CR3.0) and Kainsaz (CO3.2). Neyda M. Abreu and Adrian J. Brearley provided additional EMP data for matrix in MET 00426 (CR3.0) and ALHA 77307 (CO3.0), respectively. Adrian J. Brearley and Rhian H. Jones contributed significantly to the ideas and interpretations presented in this work. Preliminary results of this chapter were presented at the Annual Meeting of the Meteoritical Society in Zurich, Switzerland in 2006 (Berlin et al. 2006a). This chapter will be submitted to *Geochimica et Cosmochimica Acta* for publication.

The focus of Chapter 2 is the characteristic Fe-Mn trends of type IIA chondrules in unequilibrated ordinary, CR and CO chondrites. Rhian H. Jones provided previously obtained EMP data for Semarkona type IIA chondrules (Jones 1990) as well as for experimental run products (Jones and Lofgren 1993), both of which played a significant role in understanding the Fe-Mn trends. Paul V. Burger provided EMP data for several CR type IIA chondrules. Rhian H. Jones and Adrian J. Brearley contributed significantly to the ideas and interpretations presented in this chapter. This study also benefited from insightful discussions with James J. Papike and Jeffrey N. Grossman (USGS, Reston). Preliminary results of this chapter were presented at the Lunar and Planetary Science Conference in Houston in 2008 and 2009 (Berlin et al. 2008a, 2009). This chapter will be submitted to *Meteoritics and Planetary Science* for publication.

Chapter 3 deals with the meteorite Kakangari. This meteorite has been thought of as a very pristine chondrite, but our study reveals that it records a very complex history.

Harry Y. McSween Jr. (University of Tennessee, Knoxville) provided his previously obtained EMP data for Kakangari bulk chondrule compositions (McSween 1977a) for comparison with our data. Adrian J. Brearley and Rhian H. Jones contributed significantly to the ideas and interpretations presented in this work. Preliminary results of this chapter were presented at the Lunar and Planetary Science Conference in Houston, the Annual Meeting of the Meteoritical Society in Tucson and the Goldschmidt Conference in Cologne, Germany in 2007 (Berlin et al. 2007a,b,c). This chapter will be submitted to *Geochimica et Cosmochimica Acta* for publication.

In Appendix A, we discuss why we chose modal recombination analysis (MRA) over defocused beam analyses (DBA) as a technique to obtain the bulk compositions of chondrules. Discussions with Michael N. Spilde provided very helpful insights. A poster on this topic was presented at the Lunar and Planetary Science Conference in Houston in 2006 (Berlin et al. 2006b) and an invited talk was given at the Microscopy and Microanalysis conference in Albuquerque in 2008 (Berlin et al. 2008b).

In Appendix B, we describe and compare the two protocols that were used to obtain the phase images of chondrules and to determine the modal abundances of the phases present. Until Jeffrey M. Davis from the National Institute of Standards and Technology (NIST) made us aware of the program Lispix at the Microscopy and Microanalysis meeting in August 2008, we used a more time-consuming technique that involved producing the phase images in Adobe Photoshop® and determining the modal abundances of the phases with Scion Image software.

The supplementary CD contains Microsoft® Office Excel files with the collected data for each chondrule, including EMP analyses of individual phases, backscattered electron (BSE) images, corresponding phase images and results of the modal recombination analysis.

The meteorite samples for this study were provided by the Astromaterials Curation Facility at the Johnson Space Center in Houston (one thin section of MET 00526, two thin sections of MET 00426, one thin section of QUE 97008), the Smithsonian National Museum of Natural History in Washington D.C. (one thin section of Kainsaz), and the IOM meteorite collection at the University of New Mexico in Albuquerque (one thin section of Kainsaz and two thin sections of Kakangari).

CHAPTER 1 – MINERALOGY AND BULK CHEMISTRY OF CHONDRULES AND MATRIX: A COMPARISON OF PRISTINE CHONDRITES FROM DIFFERENT GROUPS

ABSTRACT

A detailed electron microprobe (EMP) study was performed on chondrules of various textural types in three fairly pristine chondrites: MET 00526 (L3.05), MET 00426 (CR3.0) and Kainsaz (CO3.2). Bulk compositions of twenty chondrules in each meteorite were determined using modal recombination analysis. This study provides a self-consistent dataset for chondrules from pristine members of three different chondrite groups integrating mineralogical and bulk chemical data with chondrule textural types. In order to address the compositional relationship between chondrules and matrix, bulk matrix compositions were obtained as well.

While chondrules of the same textural types are present in all three chondrites and show similar characteristic features, there are also significant differences between the chondrite groups. For example, type I (FeO-poor) chondrules in Kainsaz (CO) and MET 00526 (L) contain sulfides, while those in MET 00426 (CR) do not. A significant difference between type II (FeO-rich) chondrules in the three chondrites studied was found in the Fe-Mn systematics of their olivines and in the FeO content of their bulk chondrule compositions. Such differences imply that chondrules of the same textural type found in the different chondrite groups cannot all have formed within one single reservoir in the solar nebula, but that each chondrite accreted chondrules that formed in a parcel of the solar nebula under conditions and from precursor materials that are specific to that chondrite group.

We also observed a strong complementary relationship between chondrule and matrix compositions in MET 00426 (CR3.0), which indicates that they formed within the same nebular reservoir and supports a local chondrule forming mechanism such as shock waves. Our compositional data for chondrules and matrix in MET 00526 (L3.05) and Kainsaz (CO3.2) record a more complex history.

INTRODUCTION

Chondritic meteorites are fragments of undifferentiated asteroids and represent the oldest and most primitive solar system materials. They consist of a mixture of components that formed under a wide range of conditions during the earliest stages of solar system formation. The four major components are chondrules (igneous spherules), matrix (fine-grained material), refractory inclusions and Fe,Ni metal/sulfides. In the most pristine chondrites, i.e., those that did not experience significant parent-body processing such as thermal metamorphism and/or aqueous alteration, these components are far from chemical, isotopic and textural equilibrium. As a consequence, they provide valuable information about processes that occurred within the first 10 million years of formation of the solar system.

The (sub)-millimeter-sized ferromagnesian chondrules, which can comprise up to 80 vol% of chondrites, are widely considered to have formed by a brief heating event (or events) that reached peak temperatures between ~1200 and 1900ºC (e.g., Zanda 2004). They exhibit various igneous textures (e.g., porphyritic, granular, barred, radial, or cryptocrystalline) that are thought to be the result of several factors, such as different cooling rates, variable bulk compositions of the precursor material and different numbers of viable nuclei surviving at the peak temperature reached in relation to the liquidus (e.g., Lofgren 1989; Hewins et al. 2005). Scott and Taylor (1983) noted many similarities between chondrules in carbonaceous, ordinary, and enstatite chondrites, indicating that chondrules in different chondrite groups share a common formation mechanism. The mineralogy, petrography, bulk chemistry and isotopic compositions of chondrules provide valuable information about the nature and variability of precursor materials, nebular heterogeneities, conditions during chondrule formation such as varying oxygen fugacity, and reheating/recycling of material (e.g., Jones et al. 2005; Grossman et al. 1988). These constraints can then be used by astronomers and astrophysicists for models of young stellar disks, including understanding the mechanism that was responsible for the formation of chondrules. This has been one of the main challenges in meteoritics over the past decades and is still under active debate (e.g., Boss 1996; Ciesla 2005). Currently favored models for chondrule formation are the shock wave model (e.g., Desch et al. 2005) and the X-wind model (Shu et al. 1997, 2001).

In contrast to chondrules, matrices are texturally and mineralogically very variable among the different chondrite groups (e.g., Scott et al. 1988; Brearley 1996), but recently a very similar picture has emerged for the matrix in the most pristine chondrites found to date (Scott and Krot 2005; Nuth et al. 2005), which include the CO3.0 chondrite ALHA 77307 (Brearley 1993), the unique carbonaceous chondrite Acfer 094 (Greshake 1997) and the two CR3.0 chondrites, MET 00426 and QUE 99177 (Abreu 2007; Abreu and Brearley, Forthcoming). The fine-grained (<5 μm) matrix materials in these pristine chondrites preserve an extreme disequilibrium and contain high abundances of amorphous silicate material, nanosulfides (<300 nm) and interstellar grains.

In ordinary chondrites, matrix is much less abundant than in carbonaceous chondrites and a higher percentage of clastic matrix is observed, which is consistent with an origin by fragmentation of chondrules (e.g., Alexander et al. 1989b; Brearley 1996). Fine-grained rims around chondrules (and refractory inclusions) are found in both ordinary and carbonaceous chondrites. They are clearly petrographically distinct from, though probably related to, the interchondrule matrix (e.g., Alexander et al. 1989b; Metzler et al. 1992; Brearley 1993; Zolensky et al. 1993; Brearley et al. 1995).

Compositional relationships between chondrules and fine-grained materials provide important constraints on how the chondrule-forming mechanism may have operated in the solar nebula (e.g., Ciesla 2005). Examining and comparing the bulk chemical compositions of chondrules and matrix can help address questions that are important for chondrule formation models, such as: (1) Did chondrules and matrix form in the same or in different regions of the solar nebula? and (2) Could matrix be a sink for the volatile elements that were possibly lost from chondrules during the chondrule formation event(s)? Several authors (Wood 1985; Klerner and Palme 1999a,b, 2000; Palme and Klerner 2000; Bland et al. 2005; Hezel and Palme 2008) have argued that chondrules and matrix must have formed in the same region of the solar nebula, because their compositions appear to be complementary, meaning that their separate compositions are significantly different, but when put together they are closer to the solar composition (or CI chondrites). Such a relationship supports local chondrule formation models, for example the shock wave model (e.g., Desch et al. 2005) or nebular lightning (e.g., Horányi et al. 1995). However, it specifically contradicts the X-wind model (Shu et al.

1997; Shu et al. 2001), which suggests that chondrules were formed close to the sun and were subsequently transported into the asteroidal region, where they combined with matrix. Brearley (1996) and Huss et al. (2005) stimulated the discussion about the relationship between chondrules and matrix by drawing attention to the fact that not only secondary processing, but also the origin of matrix needs to be taken into account when discussing the relationship between chondrules and matrix.

There are currently very few data for bulk chondrule compositions of pristine chondrites available in the literature (see reviews in Jones et al. 2005; Grossman and Wasson 1983a; Grossman et al. 1988). These include data for LL3.0 chondrite Semarkona determined by INAA (Grossman and Wasson 1983b) and by electron microprobe (EMP) defocused beam analyses (Jones and Scott 1989; Jones 1990, 1994, 1996a), as well as INAA data for the ungrouped type 3.0 carbonaceous chondrite LEW 85332 (Wasson et al. 2000). Data for other chondrite groups are compromised to varying extents by secondary processes (see review in Jones 2005 and references therein). Even for the existing data, there are significant discrepancies when different techniques were used. For example, EMP data by McSween (1977a,b) for chondrules from CO chondrites (Kainsaz, CO3.2 and Ornans, CO3.4) show two populations on a Fe-Mg-Si ternary plot, while INAA data for Ornans chondrules from Rubin and Wasson (1988) do not (Jones et al. 2005). The best EMP method for obtaining bulk compositions is modal recombination analysis (MRA). There are currently only a few studies available that use this approach correctly, i.e. including phase densities (e.g., Dodd 1978a; Simon and Haggerty 1980). Because there are very few internally consistent datasets available for the most pristine chondrites, we currently only have a limited understanding as to how bulk compositions of chondrules with the same texture compare between different chondrite groups (e.g., Scott and Taylor 1983; Grossman and Wasson 1983a).

Many authors have obtained bulk matrix compositions in a variety of chondrite groups (e.g., McSween and Richardson 1977; Huss et al. 1981; Scott et al. 1984; Alexander et al. 1989b; Brearley et al. 1989; Brearley 1993; Zolensky et al. 1993; Brearley et al. 1995; Alexander 1995; Klerner 2001; Bland et al. 2005; Grossman and Brearley 2005; Abreu and Brearley, Forthcoming). Most of these data are also compromised by secondary overprints to varying extents, just like most data for bulk

chondrule compositions as discussed above. While there are several studies containing bulk matrix data for some of the most pristine chondrites, such as ALHA 77307, Acfer 094, MET 00426 and QUE 99177 (Brearley 1993; Brearley et al. 1995; Bland et al. 2005; Abreu and Brearley, Forthcoming), bulk chondrule data were not obtained at the same time.

The motivation for this study was to obtain a self-consistent dataset of bulk chondrule and matrix compositions for some of the least altered chondrites in order to (1) relate the bulk composition of chondrules to their texture and mineralogy, (2) examine the compositional relationship between different chondrule types within a chondrite group, (3) compare mineralogy and bulk composition of chondrules with the same texture in different chondrites and (4) examine the compositional relationship between chondrules and matrix. Only with such a detailed study can we begin to address questions about the heterogeneity of dust in the nebular disk. In order to be able to address the points above in a comprehensive way, we adopted what we consider the best two-dimensional analytical approach, while recognizing and discussing 3D issues. Using an electron microprobe, we obtained bulk compositions for 20 chondrules via modal recombination in each of three primitive chondritic meteorites: L3.05 chondrite MET 00526, CR3.0 chondrite MET 00426 and CO3.2 chondrite Kainsaz. We also present matrix data for all three chondrites, obtained by defocused beam analysis. The main goals of this study are to provide further information about the conditions during chondrule formation and to contribute to the discussion of compositional complementarity between chondrules and matrix with respect to current chondrule formation models.

SAMPLES AND ANALYTICAL CONDITIONS

In order to be able to explore the pristine nebular record contained in chondrules and matrix, we tried to select chondrites for this study that experienced minimal parent-body processing and/or terrestrial weathering. However, as Huss et al. (2005) pointed out, there is virtually no chondrite that did not experience any kind of secondary processing. Therefore, we account for secondary overprints in the discussion of our data.

The samples examined in this study include one thin section of the L3.05 chondrite MET 00526 (JSC–,25), two thin sections of the CR3.0 chondrite MET 00426 (JSC–,16-1 and JSC–,16-2) and two thin sections of the CO3.2 chondrite Kainsaz (UNM 1050 and USNM 2486-5). Even though Kainsaz has been classified as petrologic type 3.2 (e.g., Chizmadia et al. 2002; Grossman and Brearley 2005) or even higher (Bonal et al. 2007), we included it in this study because it is an observed fall and it made sense to produce a bulk chondrule data set via MRA to be able to compare it directly to McSween (1977a)'s DBA data for Kainsaz chondrules. Abreu (2007) and Abreu and Brearley (Forthcoming) recognized MET 00426 as one of the most pristine CR chondrites (type 3.0) known to date. Floss and Stadermann (2009) have further shown that MET 00426 has high interstellar grain abundances comparable to ALHA 77307 and Acfer 094, supporting the classification of MET 00426 as a very pristine chondrite. Its weathering grade is B (Russell et al. 2002). MET 00526 was originally classified as H3.2 chondrite (Connolly et al. 2007b), however, Grossman and Brearley (2005) suggested a petrologic type 3.05 and found that chondrule sizes may indicate an L or LL group classification. The L3.0 classification of this meteorite has been confirmed by Righter (2007). The weathering grade of MET 00526 is B/C (Connolly et al. 2007b).

All thin sections were studied in detail by optical and electron microscopy. Electron imaging (BSE), semi-quantitative EDS, X-ray mapping, and quantitative analyses were obtained on a JEOL 8200 Superprobe in the Department of Earth and Planetary Sciences, University of New Mexico. This electron microprobe is equipped with a tungsten filament, a Thermo Noran EDS system and five wavelength dispersive spectrometers, including two high intensity H-type spectrometers with smaller Rowland circles for precise minor element analysis.

Twenty chondrules were selected in each of the three chondrites (MET 00526, MET 00426 and Kainsaz) for petrographic characterization and determination of bulk compositions. In Appendix A, we demonstrate in more detail why we chose modal recombination analysis (MRA) over defocused beam analyses (DBA) for the determination of bulk chondrule compositions.

In order to avoid Na loss (e.g., Grossman and Brearley 2005), analyses of mesostasis glass (when possible, areas free of crystallites) were obtained first, using an accelerating

voltage of 15 keV, a beam current of 10 nA and a 5 μm beam diameter. When crystallites were large enough to analyze (width >2 μm), it was preferred to analyze them separately with a focused beam. If only small patches of glass were present, the beam diameter was decreased to 3 μm. A rhyolitic glass standard (3.75 wt% Na_2O) and a basaltic glass standard (2.66 wt% Na_2O) were analyzed along with the meteorite samples in order to maintain a reasonable accuracy for our Na values (±10%).

Subsequently, WDS element maps were obtained for each chondrule using a beam current of 30 nA and a pixel-size between 0.5 and 1.5 μm (depending on chondrule size) for a suite of 5 elements (Al, Ca, Mg, Fe, S). The collected element maps were then used to select spots for point analyses. The number of analyses obtained on a certain mineral phase was between 1 and 15, roughly based on its modal abundance. Silicate and oxide (e.g., chromite in type II chondrules) minerals were analyzed with an accelerating voltage of 15 keV and a beam current of 20 nA. Metals and sulfides were analyzed at 20 keV and a beam current of 40 nA. ZAF corrections were applied to the data, and standards used included Taylor olivine (Si, Fe, Mg), diopside (Ca, Mg, Si), spessartine (Mn), albite (Na), orthoclase (K, Al), corundum (Al), rutile (Ti), chromite (Cr), apatite (P), pyrite (S), Ni metal (Ni), and Co metal (Co), as well as JEOL Fe-metal (Fe) and Si-metal (Si). To account for the interference of the Fe Kβ peak with the Co Kα peak, a background subtraction correction was applied.

Phase images of chondrules were assembled based on the collected X-ray maps, either with the 'Phase Tool' in Lispix (public domain image analysis program for Windows, written and maintained by David Bright, National Institute of Standards and Technology) or with Adobe Photoshop®. Modal abundances (vol. %) of the different phases present were provided in Lispix or determined with Scion Image analysis software when the phase images had been assembled in Adobe Photoshop®. Detailed instructions and a comparison of both methods are provided in Appendix B.

Bulk chemical compositions of chondrules were calculated by combining mineral compositions with their weighted modal proportions according to the following equation (for each element):

$$Element\ Z = conc^{Element\ Z}_{phase\ 1} \cdot \left[\frac{vol\%_{phase\ 1} \cdot \rho_{phase\ 1}}{\sum_{1}^{n} (vol\%_{phase} \cdot \rho_{phase})} \right] + conc^{Element\ Z}_{phase\ 2} \cdot \left[\frac{vol\%_{phase\ 2} \cdot \rho_{phase\ 2}}{\sum_{1}^{n} (vol\%_{phase} \cdot \rho_{phase})} \right] + \ ... \ + \ conc^{Element\ Z}_{phase\ n} \cdot \left[\frac{vol\%_{phase\ n} \cdot \rho_{phase\ n}}{\sum_{1}^{n} (vol\%_{phase} \cdot \rho_{phase})} \right]$$

where ρ is the density of the phase analyzed and the concentration (*conc*) is given in element wt%. Mineral densities from Deer et al. (1992) and at http://www.webmineral.com were used. Densities for mesostasis glass were determined using a model calculation by Fluegel (2007).

In each chondrite, several matrix regions were analyzed with a defocused beam (10 μm diameter), a beam current of 20 nA and an accelerating voltage of 15 keV. Analyses were placed randomly and small metal/sulfide grains (<5 μm) within the matrix were not avoided. Elements were measured as oxides and most resulting totals were between 85 and 95 wt%. Analyses with totals lower than 80 wt%, which are probably due to a higher porosity of some matrix regions, were discarded. High totals, which are due to mixed metal/sulfide/silicate analyses and the fact that Fe, Ni and S were measured as FeO, NiO and SO_3, were not discarded. For the presentation of our matrix data, oxide wt% were converted to element wt%.

RESULTS

Based on a combination of optical examination and SEM imaging, twenty chondrules covering a range of textural types were selected in each of the three chondrites (MET 00526 (L), MET 00426 (CR), and Kainsaz (CO)) for petrographic characterization and determination of bulk compositions. The supplementary CD contains Microsoft® Office Excel files with data for each chondrule, including EMP analyses of individual phases, backscattered electron (BSE) images, corresponding phase images and results of the modal recombination analysis. As an example, BSE images of FeO-poor porphyritic olivine-pyroxene (type IAB) chondrules from each of the three chondrites and their corresponding phase images are shown in **Figure 1.1**.

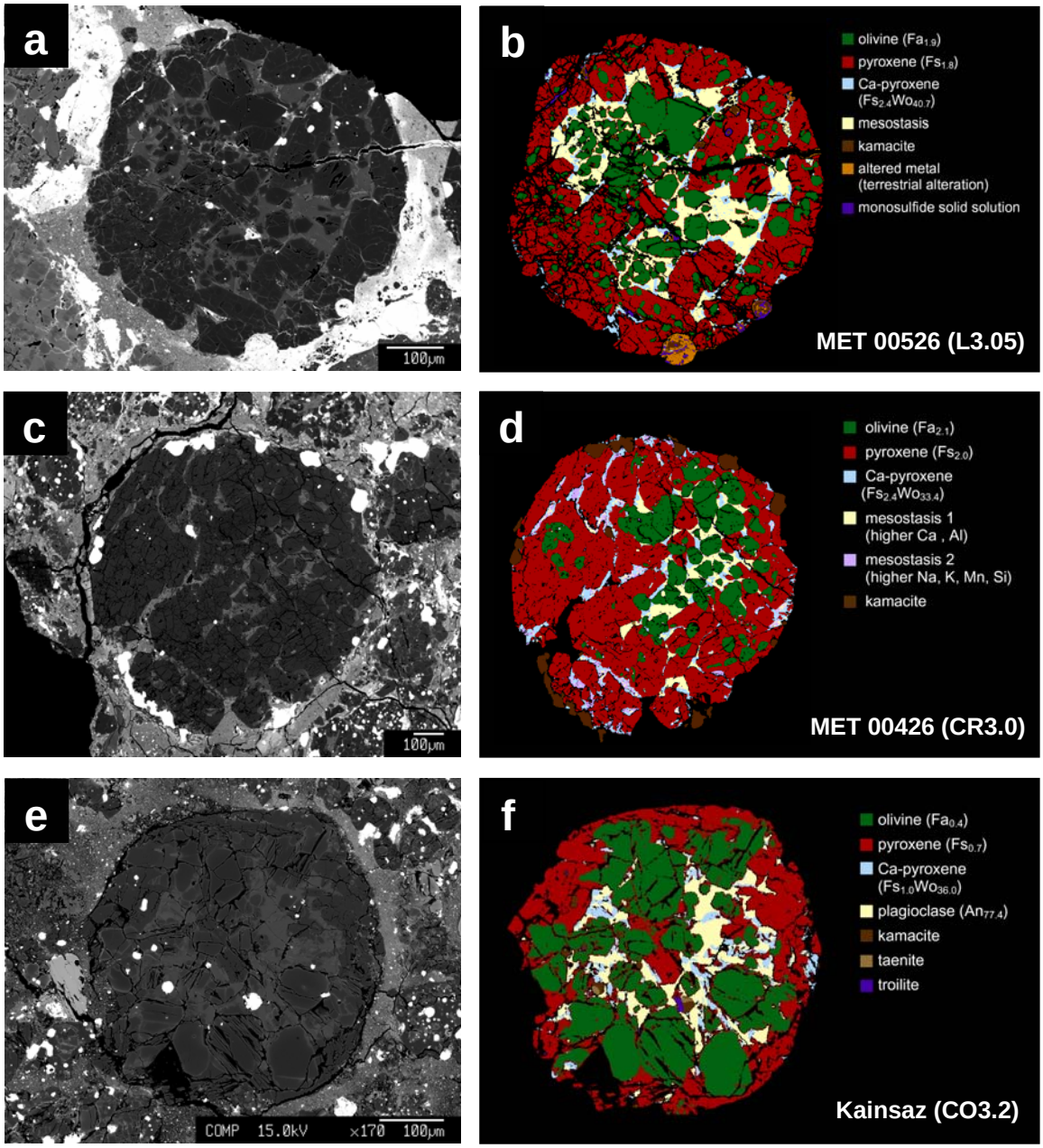

Fig. 1.1. Backscattered electron (BSE) images of typical FeO-poor POP (type IAB) chondrules and their corresponding phase images used for modal analysis. a) and b) MET 00526 (L3.05) chondrule L-Ch12. c) and d) MET 00426 (CR3.0) chondrule CR-Ch1. e) and f) Kainsaz (CO3.2) chondrule K2-Ch8.

Chondrule textures

We did not evaluate the relative proportions of the different textural types of chondrules in each chondrite in a quantitative way, but **Table 1.1** shows a comparison between available literature data and the relative proportions of textural types of the chondrules selected for this study. Granular and cryptocrystalline chondrules were not included in this study, as they were either absent or very rare in the thin sections we examined. For MET 00426 (CR) and Kainsaz (CO), we have included a higher percentage of FeO-rich porphyritic chondrules than what is typically observed in CR and CO chondrites (**Table 1.1**; Weisberg et al. 1993a; Grossman et al. 1988). For MET 00426 (CR), we included every FeO-rich porphyritic chondrule that we found in the two thin sections we studied (four chondrules).

Table 1.1. Relative proportions of textural types of the chondrules selected for this study (20 chondrules per chondrite) compared to literature data.

	MET 00526 (L3.05)	**OC[a]**	**MET 00426 (CR3.0)**	**CR[b]**	**Kainsaz (CO3.2)**	**CO[c]**
porphyritic	85%	81%	90%		95%	95-96%
low-FeO (type I)	41%	50-90%	78%	most abundant	68%	97%
high-FeO (type II)	47%	10-50%	22%	<1%[d]	32%	3%
reduced	12%	-	-		-	-
PO	41%	28%	17%		26%	8%
POP	47%	60%	78%		53%	73%
PP	12%	12%	5%		21%	19%
non-porphyritic	5%	15%	5%		5%	2-3%
RP/C	100%	80%	100%		100%	100%
G	-	20%	-	rare	-	-
barred	10%	4%	5%		-	2

[a]Grossman et al. (1988)
[b]Weisberg et al. (1993a)
[c]Grossman et al. (1988) and Rubin (2000)
[d]fragmental

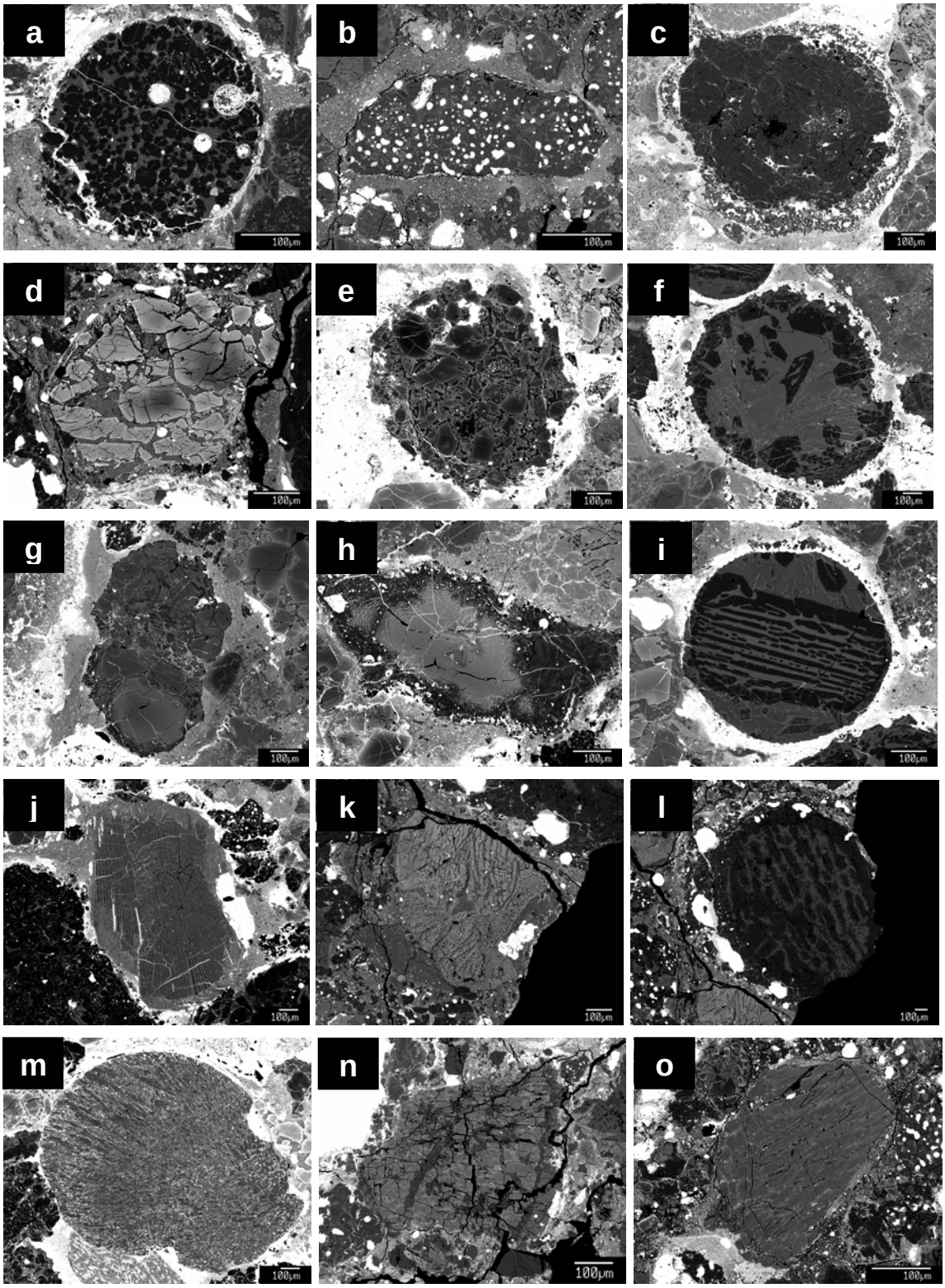

Fig. 1.2. BSE images of chondrules selected for this study showing different textural types. a) type IA chondrule (L-Ch13) in MET 00526, b) metal-rich type IB chondrule (K1-Ch17) in Kainsaz, c) type IB chondrule (L-Ch16) with an igneous rim in MET 00526, d) type IIA chondrule (CR-Ch13) in MET 00426, e) type IIAB chondrule (L-Ch10) in MET 00526, f) glass-rich type IA chondrule (L-Ch17) in MET 00526, g) and h) FeO-rich POP chondrules (L-Ch20 and L-Ch14) in MET 00526 with large relict grains, showing

evidence for solid-state reduction in form of micron-size metal blebs, i) FeO-poor compound BO/POP chondrule (L-Ch1) in MET 00526, j) FeO-rich BO chondrule (L-Ch19) in MET 00526, k) FeO-rich type IIA chondrule (CR-Ch16) in MET 00426 showing a textural continuum between porphyritic and barred, l) FeO-poor BO chondrule (CR-Ch11) with an igneous rim in MET 00426, m) FeO-rich RP chondrule (L-Ch5) in MET 00526, n) FeO-rich silica-bearing RP chondrule fragment (CR-Ch17) in MET 00426, and o) FeO-rich RP chondrule (K1-Ch19) in Kainsaz – the texture of this chondrule might be better described as barred pyroxene (BP).

To demonstrate the variety of porphyritic textures studied, BSE images of several chondrules are shown in **Figure 1.2a-h**. All BO and RP chondrules included in this study are shown in **Figure 1.2i-o**. As is typical for ordinary and most carbonaceous chondrites, two distinct populations of porphyritic chondrules (e.g., McSween 1977a; Scott and Taylor 1983) are present in all three chondrites examined in this study: FeO-poor (type I) and FeO-rich (type II) chondrules. FeO-poor porphyritic olivine (PO), porphyritic olivine-pyroxene (POP) and porphyritic pyroxene (PP) chondrules are described as type IA (**Fig. 1.2a**), IAB (**Fig. 1.1**) and IB (**Fig. 1.2b,c**), respectively, while FeO-rich porphyritic chondrules are described as type IIA (**Fig. 1.2d**), IIAB (**Fig. 1.2e**) and IIB in the same manner (e.g., Scott et al. 1994). Type I and type II chondrules show some textural differences (e.g., Scott and Taylor 1983), such as higher amounts of Fe,Ni metal in type I chondrules (e.g., **Fig. 1.2b**) and larger olivine phenocrysts in type II chondrules (e.g., **Fig. 1.2d,e**), but the main differences are in their olivine and low-Ca pyroxene compositions (see below).

Of the three chondrites studied, the ordinary chondrite MET 00526 (L) shows the highest variety of chondrule textures (**Table 1.2**, **Fig. 1.2**). In addition to the textural types typically found in ordinary chondrites (e.g., Gooding and Keil 1981; Grossman et al. 1988), we included a glass-rich type IA chondrule (**Fig. 1.2f**), a compound BO/POP chondrule (**Fig. 1.2i**), and two chondrules with large relict grains that show textural evidence for solid-state reduction in form of micron-size metal blebs (**Fig. 1.2g,h**). An FeO-rich BO chondrule and a RP chondrule from MET 00526 (L) are shown in **Figures 1.2j** and **1.2m**.

Table 1.2. Characteristics of the MET 00526 (L3.05) chondrules selected for this study.

	texture	ol/px[a]	Fa[b]	Fs[c]	Wo[c]	notes
FeO-poor chondrules:						
L-Ch13	PO		0.9	-	-	metal heavily weathered
L-Ch8	PO		0.8	-	-	metal heavily weathered
L-Ch17	PO	7.6/1	0.4	1.3	5.0	glass-rich, pyroxene at periphery
L-Ch12	POP	1/1.9	1.9	1.8	0.4	
L-Ch6	POP	1/3.2	1.9	2.1	0.4	
L-Ch16	PP	1/36.5	1.9	2.0	0.2	igneous rim
L-Ch15	PP	1/82.0	3.3	3.0	0.3	
L-Ch1	BO/POP	8.2/1	0.7	1.0	5.9	compound chondrule
FeO-rich chondrules:						
L-Ch4	PO		10.3 – 26.8	-	-	
L-Ch7	PO		15.5 – 30.3	-	-	
L-Ch9	PO		8.8 – 25.0	-	-	
L-Ch2	PO	4.7/1	8.9 – 36.4	22.2	3.4	pyroxene = quenched crystals
L-Ch11	POP	5.6/1	14.6 – 50.7	25.1	5.5	
L-Ch10	POP	1.5/1	6.1 – 18.2	9.6	1.1	relict grains
L-Ch18	POP	1/1.5	15.6 – 36.1	19.3 – 30.2	0.5 – 6.7	
L-Ch3	POP	1/3.3	10.8 – 16.7	12.1 – 19.8	0.8 – 1.6	poikilitic olivine
L-Ch14	POP*	1.3/1	23.1 – 11.8	17.0 / 5.7	2.5 / 1.9	*reduced, FeO-rich relict olivine
L-Ch20	POP*	1/1.4	18.9 – 3.6	14.1 / 2.1	1.3 / 1.6	*reduced, FeO-rich relict olivine
L-Ch19	BO	6.1/1	20.0	18.7	7.4	
L-Ch5	RP		-	10.5 / 17.5	0.4 / 5.8	

[a]Olivine/pyroxene ratio (modal abundance).
[b]Mean Fa content is given for type I olivine and range of Fa contents for zoned type II olivine.
[c]Mean Fs and Wo content are given for low-Ca pyroxene or pigeonite in type I, ranges for zoned type II chondrules.

Most chondrules in MET 00426 (CR) are FeO-poor and have porphyritic textures (**Table 1.3**), as is very typical for CR chondrites (e.g., Weisberg et al. 1993a). Many of them are surrounded by a continuous or discontinuous layer of metal grains (e.g., **Fig. 1.1c,d**). As mentioned above, type II chondrules are not very common in CR chondrites – according to Weisberg et al. (1993a), they make up less than 1% of the chondrule population and many are fragmental. In the two thin sections of MET 00426, we found two larger type IIA chondrule fragments (e.g., **Fig. 1.2d**), an FeO-rich chondrule showing a textural continuum between porphyritic and barred (**Fig. 1.2k**), as well as a type IIAB chondrule (**Table 1.3**). An FeO-poor BO chondrule and a silica-bearing RP chondrule from MET 00426 (CR) are shown in **Figures 1.2l** and **1.2n**.

Table 1.3. Characteristics of the MET 00426 (CR3) chondrules selected for this study.

	texture	ol/px[a]	Fa[b]	Fs[c]	Wo[c]	notes
FeO-poor chondrules:						
CR-Ch12	POP	3.1/1	2.0	3.6	0.9	
CR-Ch14	POP	2.1/1	0.7	1.0	0.7	
CR-Ch2	POP	1.5/1	5.1	5.1	0.7	
CR-Ch3	POP	1.4 /1	1.5	1.6	0.8	
CR-Ch5	POP	1.3/1	1.2	1.6	0.8	
CR-Ch10	POP	1.2/1	1.4	1.3	0.9	partial silica rim
CR-Ch8	POP	1/1.7	1.7	1.9	0.9	
CR-Ch15	POP	1/1.75	1.5	1.2	1.0	
CR-Ch19	POP	1/1.8	3.3	3.0	0.7	discontinuous silica rim
CR-Ch18	POP	1/2.7	2.8	3.5	1.0	silica present within chondrule
CR-Ch1	POP	1/3.3	2.1	2.0	0.6	
CR-Ch7	POP	1/5.5	0.9	1.4	1.5	
CR-Ch20	POP	1/7.6	1.0	0.9	1.0	
CR-Ch9	PP	1/29.4	2.4	2.2	0.8	
CR-Ch11	BO	1.6/1	2.3	2.6	0.7	metal-rich igneous rim
FeO-rich chondrules:						
CR-Ch6	PO		17.0 – 31.7	-	-	chondrule fragment
CR-Ch13	PO		13.5 – 57.2	-	-	chondrule fragment
CR-Ch16	PO (BO)		29.7 – 39.1	-	-	chondrule fragment
CR-Ch4	POP	1/1.6	31.6	26.6	5.5	chondrule fragment
CR-Ch17	RP		-	10.1 / 17.8	0.4 / 5.3	silica-bearing chondrule fragment

[a]Olivine/pyroxene ratio (modal abundance).
[b]Mean Fa content is given for type I olivine and range of Fa contents for zoned type II olivine.
[c]Mean Fs and Wo content of low-Ca pyroxene.

Even though CO chondrites have the smallest chondrules of any chondrite group (apart from CH chondrites) (e.g., Rubin 1989), they show the same textural types as chondrules in ordinary and other carbonaceous chondrites (e.g., Scott and Taylor 1983; see also **Fig. 1.1**, **Table 1.4**). However, a significant textural characteristic of type I chondrules in CO chondrites is that they frequently have non-spherical shapes and contain abundant metal grains in their interiors (**Fig. 1.2b**; Rubin and Wasson 2005). Type I chondrules are more abundant than type II (**Table 1.1**; Grossman et al. 1988). Most of the type II chondrules are type IIA, while type IIAB chondrules are less common. **Figure 1.2o** shows a Kainsaz chondrule that we placed into the RP category, although the texture might be better described as coarse-barred pyroxene (e.g., Jones 1996a).

Table 1.4. Characteristics of the Kainsaz (CO3.2) chondrules selected for this study.

	texture	ol/px[a]	Fa[b]	Fs[d]	Wo[d]	notes
FeO-poor chondrules:						
K2-Ch9	POP	2.0/1	0.4	0.3	0.9	
K1-Ch9	POP	1.4/1	3.1[c]	1.0	1.2	
K1-Ch21	POP	1.1/1	2.3[c]	0.6	0.8	
K2-Ch8	POP	1.1/1	0.4	0.7	1.1	
K1-Ch12	POP	1/1.3	3.0[c]	1.1	1.0	
K1-Ch1	POP	1/1.5	1.0	0.7	3.2	
K1-Ch10	POP	1/2.0	4.6[c]	1.1	1.2	
K1-Ch13	POP	1/2.8	5.7[c]	1.5	1.0	
K1-Ch14	POP	1/5.9	5.0[c]	1.1	1.0	metasomatized rim[e]
K1-Ch11	PP	1/14.1	5.5[c]	1.4	0.9	
K2-Ch14	PP	1/15.2	13.2[c]	1.5	0.9	
K1-Ch17	PP	1/27.7	6.0[c]	1.3	0.8	
K1-Ch20	PP			4.1	0.3	
FeO-rich chondrules:						
K1-Ch7	PO		11.3 – 48.4	-	-	
K1-Ch8	PO		9.0 – 44.3	-	-	relict grains
K1-Ch16	PO		31.6 – 59.3	-	-	
K2-Ch4	PO		6.4 – 42.5	-	-	
K2-Ch7	PO		13.5 – 41.5	-	-	
K1-Ch15	POP	1/1.7	55.3	43.0	1.5	
K1-Ch19	RP		-	12.6	0.8	texture of this chondrule might be better described as barred pyroxene (BP)

[a]Olivine/pyroxene ratio (modal abundance).
[b]Lowest measured Fa content of olivine is given for type I and range of Fa contents for zoned type II olivine.
[c]Fa contents of type I chondrule olivines are high due to Fe-Mg exchange with the matrix (Scott and Jones 1990).
[d]Lowest measured Fs content of low-Ca pyroxene. Wo content is from the same analysis.
[e]Metasomatized rim (e.g., Kring 1991) was not included in bulk chondrule composition.

Chondrule mineralogy

Olivine and pyroxene

Individual olivine and pyroxene analyses and average compositions for each chondrule are given in the Microsoft® Office Excel files on the supplementary CD. In **Tables 1.2, 1.3** and **1.4**, Fa contents of olivine and/or Fs and Wo contents of low-Ca pyroxene (in some cases pigeonite) are listed for all chondrules that were selected for detailed study. When zoning is present in the silicate minerals, the range of compositions is given. Otherwise, the values are means, except for Kainsaz type I chondrules (**Table 1.4**), for which the lowest measured Fa and Fs contents are shown. Type I chondrules in the two most pristine chondrites, MET 00526 (L) and MET 00426 (CR), typically have mean olivine and low-Ca pyroxene compositions with an Fe/(Fe+Mg) atomic ratio <5%

(**Table 1.2** and **1.3**). The lowest measured Fa contents in Kainsaz type I chondrules range from 0.4 up to 13.2 mol%, while Fs contents are below 5 mol% (**Table 1.4**). These data will be further addressed in the Discussion section on secondary alteration.

Figure 1.3 shows mean Fs contents of low-Ca pyroxene (or in some cases pigeonite) versus mean Fa contents of olivine for all chondrules selected for this study. Again, for Kainsaz type I chondrules, the lowest measured Fa and Fs contents are plotted. Chondrules that do not contain any low-Ca pyroxene or olivine are plotted below the x axis or left of the y axis, respectively. When significant zoning is present, data points represent the weighted mean Fa and/or Fs based on modal analysis and the range of measured compositions is indicated. For olivine- and pyroxene-bearing chondrules in MET 00526 (L) and MET 00426 (CR), data points plot along the 1:1 line (**Fig. 1.3a,b**), while type I chondrules in Kainsaz are shifted significantly to the right of the 1:1 line (**Fig. 1.3c**).

An Fe/(Fe+Mg) atomic ratio of 10% for olivine and low-Ca pyroxene compositions has generally been used in the literature to distinguish between type I and type II chondrules (e.g., Jones et al. 2005). This value fits very well with our textural observations and is exemplified by a hiatus between 5% and 10% in the data for the L and CR chondrite (**Fig. 1.3a,b**). While we feel confident that we did not use any sample selection criteria that would have resulted in excluding these compositions, it appears that there is no such gap in previously published data for ordinary chondrites, such as Semarkona (LL3.0) (e.g., Takagi et al. 2004). The lowest measured Fe/(Fe+Mg) atomic ratios in Kainsaz type I chondrules are ≤6%, except for one chondrule (K2-Ch14), in which the lowest measured Fa content of olivine was 13.2 mol% (**Table 1.4**). However, the lowest measured Fs content of low-Ca pyroxene in this chondrule was 1.5 mol% and the metal-rich nature of this chondrule clearly required a classification as type I. Type II chondrules in all three chondrites studied have mean olivine (and low-Ca pyroxene) compositions with an Fe/(Fe+Mg) atomic ratio >10% (**Fig. 1.3**). They frequently show zoning (e.g., **Fig. 1.2d,e**) and therefore also large compositional ranges (**Fig. 1.3**). The cores of some olivine grains in certain type II chondrules have Fa contents below 10 mol% (see ranges of Fa contents given in **Table 1.2** and **1.4**, **Fig. 1.3a,c**), but most likely crystallized from the host chondrule melt (see Chapter 2).

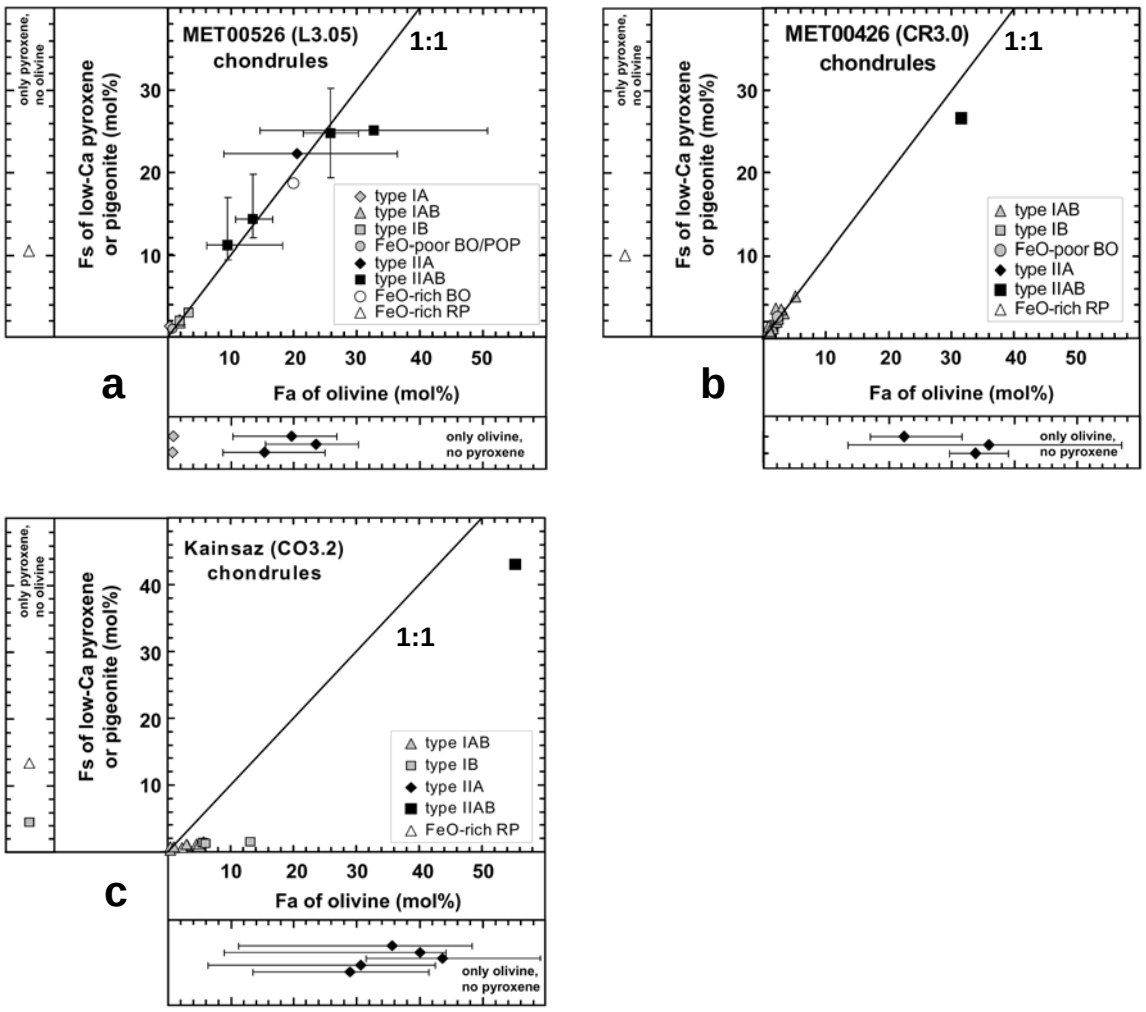

Fig. 1.3. Fs content of low-Ca pyroxene (or pigeonite) vs. Fa content of olivine in chondrules from a) MET 00526 (L3.05), b) MET 00426 (CR3), and c) Kainsaz (CO3.2). Chondrules that do not contain any low-Ca pyroxene/pigeonite or olivine are plotted below the x axis or left of the y axis, respectively. For type I chondrules in MET 00526 and MET 00426, Fa contents of olivine and Fs contents of low-Ca pyroxene (or pigeonite) represent mean values for each chondrule. For Kainsaz type I chondrules, the lowest measured Fa and Fs contents are plotted. The range of measured compositions is indicated for type II chondrules and data points represent the weighted mean Fa (and Fs) based on modal analysis.

Type I and type II chondrules not only have significantly different textures and distinct mean Fa and Fs contents, but their silicates also show some differences in minor element compositions (e.g., Scott and Taylor 1983; Jones and Scott 1989; Jones 1990, 1994, 1996a). **Figure 1.4** shows MnO (wt%) versus FeO (wt%), **Figure 1.5** shows CaO (wt%) versus FeO (wt%) and **Figure 1.6** shows Cr_2O_3 (wt%) versus FeO (wt%) of

individual olivine analyses, comparing FeO-poor and FeO-rich chondrules from MET 00526 (L), MET 00426 (CR) and Kainsaz (CO). The number of individual olivine analyses per chondrule is between 2 and 10 and number of chondrules per textural type plotted is given in brackets in the legend. Chondrule textures other than porphyritic are included in these plots as well. To distinguish between FeO-poor and FeO-rich non-porphyritic chondrules, we use the same cutoff value (Fe/(Fe+Mg) atomic ratio = 10%) as for porphyritic chondrules.

MnO contents of olivines in FeO-poor chondrules are typically <0.6 wt% (most of them <0.3 wt%, **Fig. 1.4a,c,e**), while olivines in FeO-rich chondrules show MnO contents up to 1 wt% (**Fig. 1.4b,d,f**). In fact, type IIA chondrule olivines in all three chondrites show significant positive correlations between MnO and FeO (**Fig. 1.4b,d,f**). This general trend has been observed before (e.g., Brearley and Jones 1998; McSween 1977a,c). However, it seems significant that the type IIA trends have distinct slopes in the different chondrites (steepest in MET 00526 (L), intermediate in MET 00426 (CR) and shallowest in Kainsaz (CO); **Fig. 1.4b,d,f**), which will be discussed in detail in Chapter 2. Olivines in type IIAB chondrules in MET 00526 show more scatter than those in type IIA chondrules (**Fig. 1.4b**). High Mn contents (0.76–0.90 wt%) in olivine were observed in the FeO-rich BO chondrule in MET 00526 (L-Ch19, **Fig. 1.2j**).

In contrast to type IIA chondrules, olivine analyses from the two chondrules in MET 00526 (L-Ch20 and L-Ch14) that show evidence for reduction (**Fig. 1.2g,h**) exhibit negative trends in the MnO (wt%) vs. FeO (wt%) diagram (**Fig. 1.4b**), which correspond to their zoning behavior (FeO-rich cores and FeO-poor edges). Negative trends are also observed in CaO versus FeO (**Fig. 1.5b**) and Cr_2O_3 versus FeO (**Fig. 1.6b**).

Olivines in type IA chondrules in MET 00526 (L) have the lowest MnO contents (all except one analysis are below the EMP detection limit of 0.02 wt%; **Fig. 1.4a**), but they have high CaO contents between 0.31 and 0.74 wt% (**Fig. 1.5a**). It is characteristic for type IA chondrule olivines to show steep negative correlations between CaO and FeO (e.g., Scott and Taylor 1983). Olivines in type IAB chondrules in Kainsaz (**Fig. 1.5e**) and MET 00426 (**Fig. 1.5c**) as well as type IB chondrules in MET 00526 (**Fig. 1.5a**) show shallower negative trends than type IA and IAB chondrules in MET 00526 (**Fig. 1.5a**), while the slope of the trend for type IB chondrules in Kainsaz is slightly positive (**Fig.**

1.5e). Olivine in one type IAB chondrule (CR-Ch19) in MET 00426 (CR), which shows unusually high MnO contents (0.9–1.1 wt%; **Fig. 1.4c**), has CaO contents within the normal range observed for type IAB chondrules in MET 00426 (**Fig. 1.5c**). In type II chondrule olivine, the correlation between CaO and FeO, when present, is positive (e.g., Scott and Taylor 1983). **Figure 1.5b** and **1.5d** show that this is the case for type II chondrules in MET 00526 (L) and MET 00426 (CR), but olivines in Kainsaz (CO) type II chondrules have very variable CaO contents (**Fig. 1.5f**).

The behavior of Cr_2O_3 in olivine (**Fig. 1.6**) is, in general, similar to that of MnO (**Fig. 1.4**). However, Cr_2O_3 contents tend to be somewhat higher than MnO contents of olivine in FeO-poor chondrules in MET 00526 (L) and MET 00426 (CR) (**Fig. 1.6a,c** versus **Fig. 1.4a,c**). Type IIA chondrule olivines in MET 00526 (L) and MET 00426 (CR) show positive trends, but at FeO contents higher than 22 wt% and 28 wt%, respectively, Cr_2O_3 contents decrease (**Fig. 1.6b,d**). In Kainsaz type I and type II chondrules, Cr_2O_3 contents are very low (mostly below 0.2 wt%) over a wide range of FeO contents (**Fig. 1.6e,f**).

We found no significant differences in the behavior of minor elements (Mn, Ca, Cr) in low-Ca pyroxene in type I chondrules in MET 00526 (L), MET 00426 (CR) and Kainsaz (CO). The composition of Ca-rich pyroxene is quite variable in type I chondrules in MET 00526 ($Fs_{0.7\text{-}5.7}$, $Wo_{35.9\text{-}55.9}$), MET 00426 ($Fs_{0.85\text{-}6.42}$, $Wo_{26.8\text{-}49.1}$) and Kainsaz ($Fs_{0.25\text{-}10.43}$, $Wo_{28.0\text{-}46.9}$), but minor elements also behave very similarly.

Our few analyses of low-Ca pyroxene in 4 type IIAB chondrules in MET 00526 (L), 1 type IIAB chondrule in MET 00426 (CR) and 1 type IIAB chondrule in Kainsaz (CO) show the same general trends for MnO vs. FeO as olivine in these chondrules (refer to **Fig. 1.4b,d,f**). The same is true for Ca-rich pyroxene in type IIA and type IIAB chondrules. The Fs and Wo contents of Ca-rich pyroxene in type II chondrules are $Fs_{7.3\text{-}24.4}$ and $Wo_{25.1\text{-}43.5}$ in MET 00526 (L), $Fs_{18.8\text{-}40.7}$, $Wo_{29.9\text{-}49.4}$ in MET 00426 (CR) and $Fs_{17.5\text{-}30.0}$, $Wo_{36.2\text{-}47.3}$ in Kainsaz (CO).

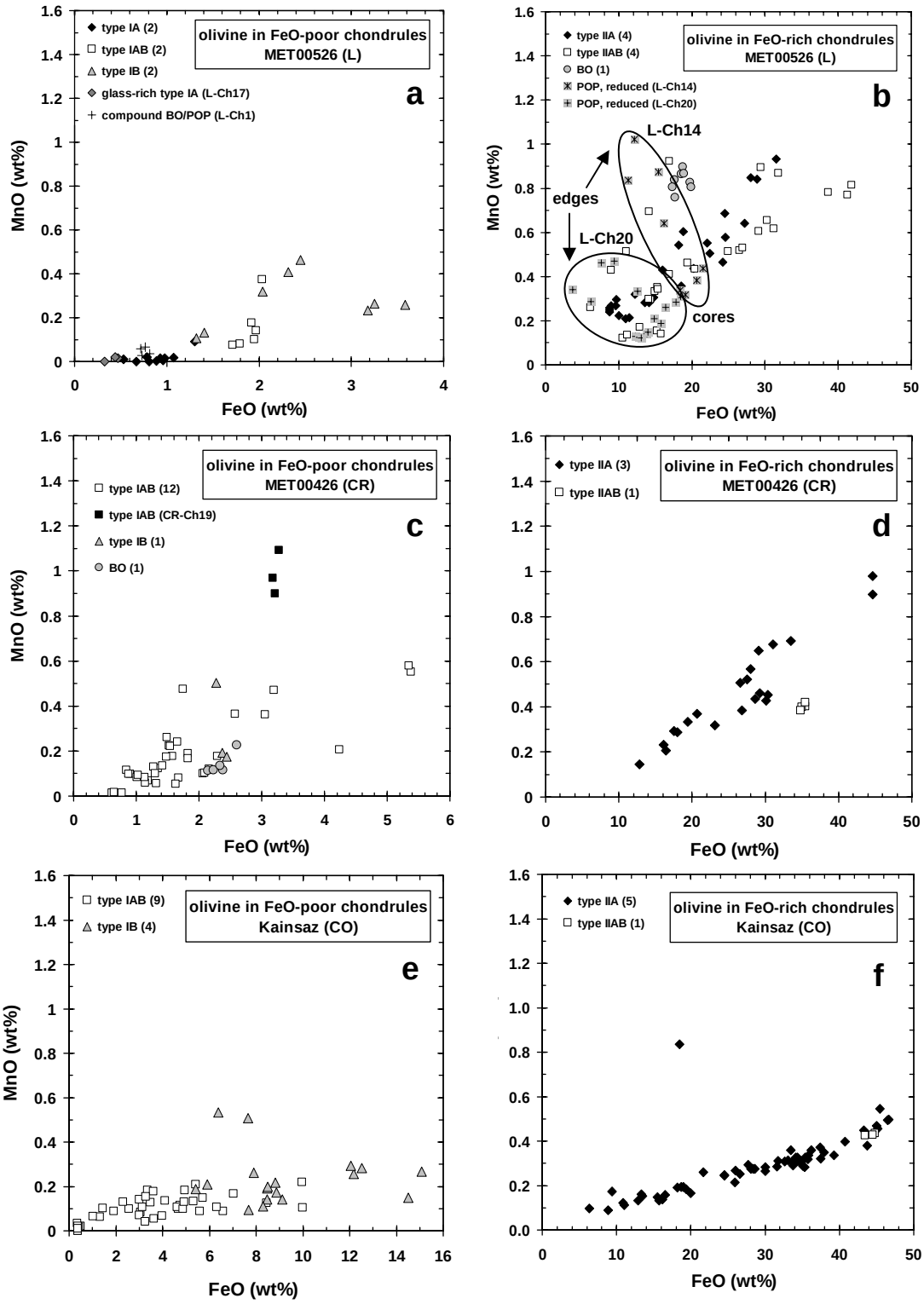

Fig. 1.4. MnO (wt%) vs. FeO (wt%) of individual olivine analyses in FeO-poor and FeO-rich chondrules in a) and b) MET 00526 (L), c) and d) MET 00426 (CR), e and f) Kainsaz (CO). The number of chondrules plotted (or chondrule label) is given in brackets in the legend. Between 2 and 10 analyses were obtained per chondrule.

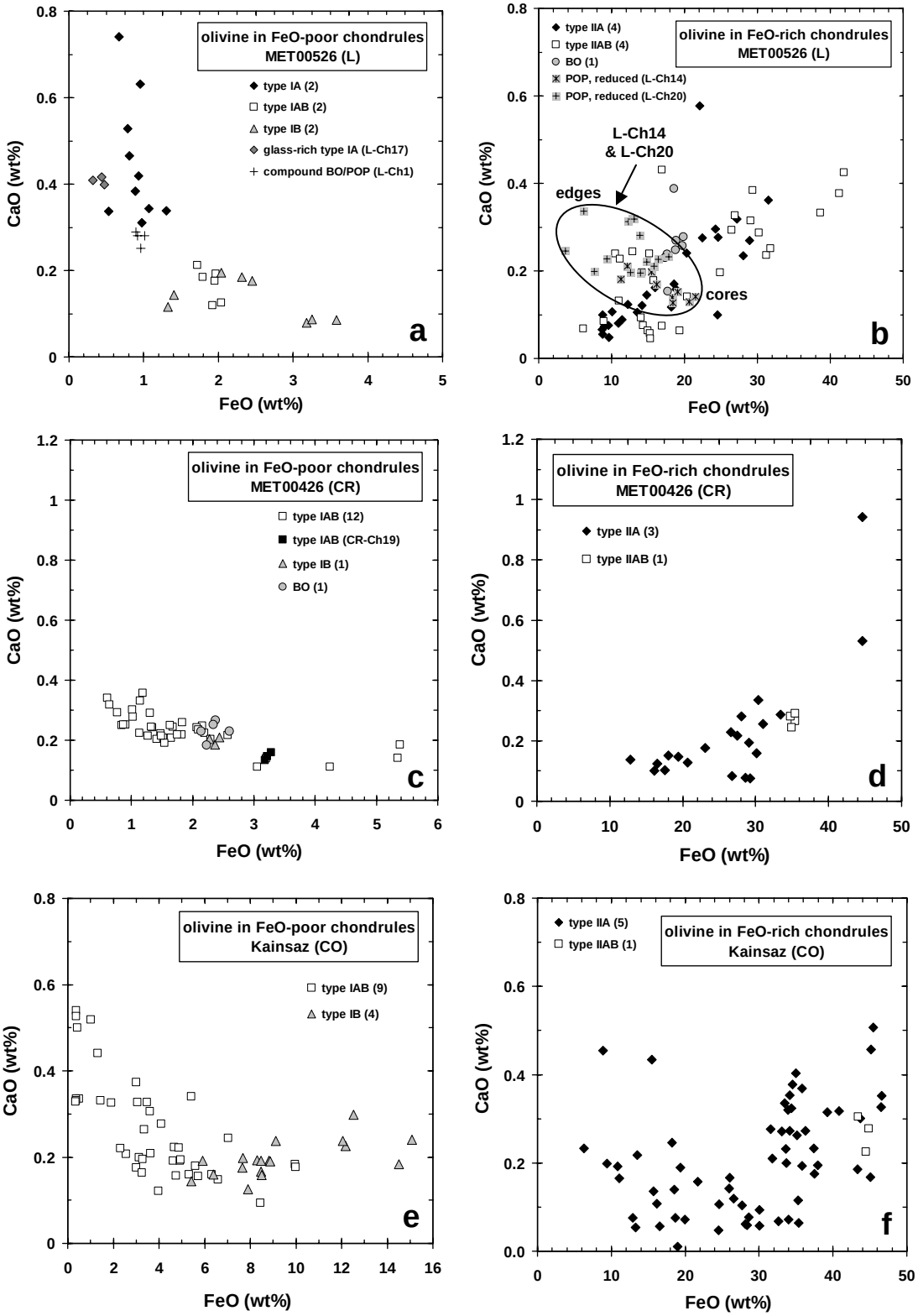

Fig. 1.5. CaO (wt%) vs. FeO (wt%) of individual olivine analyses in FeO-poor and FeO-rich chondrules in a) and b) MET 00526 (L), c) and d) MET 00426 (CR), e and f) Kainsaz (CO). The number of chondrules plotted (or chondrule label) is given in brackets in the legend. Between 2 and 10 analyses were obtained per chondrule.

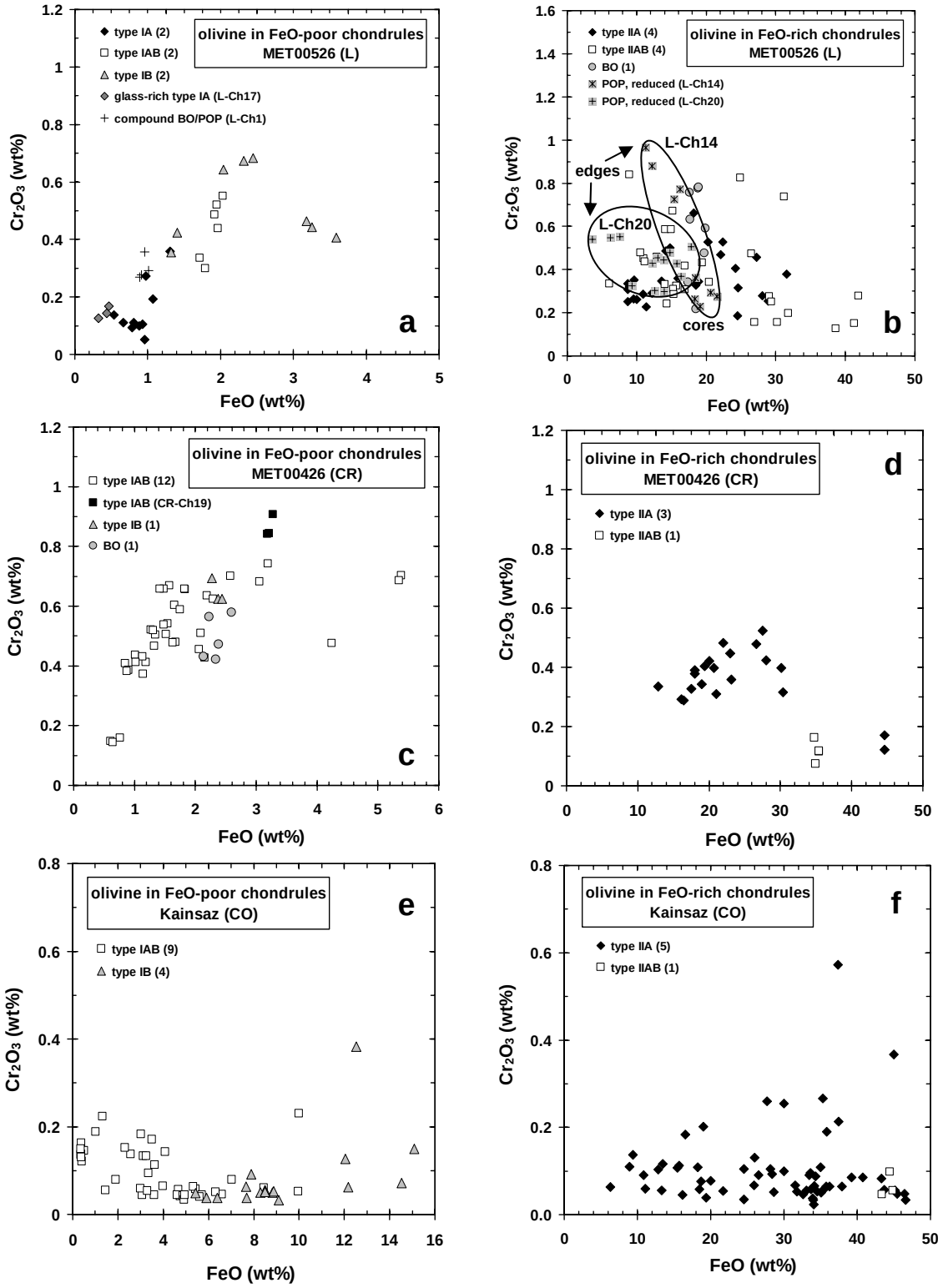

Fig. 1.6. Cr_2O_3 (wt%) vs. FeO (wt%) of individual olivine analyses in FeO-poor and FeO-rich chondrules in a) and b) MET 00526 (L), c) and d) MET 00426 (CR), e and f) Kainsaz (CO). The number of chondrules plotted (or chondrule label) is given in brackets in the legend. Between 2 and 10 analyses were obtained per chondrule.

Mesostasis

Individual analyses and average mesostasis compositions for each chondrule are given in the Microsoft® Office Excel files on the supplementary CD. Mesostasis compositions in both type I and type II chondrules cover a wide range of SiO_2 contents (42–75 wt%). Brearley and Jones (1998) showed that CaO and Al_2O_3 are negatively correlated with SiO_2 in the mesostasis of type I and type II chondrules in unequilibrated ordinary chondrites, while data for CO chondrule mesostasis did not show a clear trend. **Figure 1.7** shows Al_2O_3 (wt%) versus SiO_2 (wt%) and CaO (wt%) versus SiO_2 (wt%) for our data of individual mesostasis analyses in type I and type II chondrules in MET 00526 (L), MET 00426 (CR) and Kainsaz (CO). Type I chondrule mesostases in all three chondrites show negative trends between Al_2O_3 and SiO_2 (**Fig. 1.7a**) as well as between CaO and SiO_2 (**Fig. 1.7c**), whereas the data for type II chondrule mesostases are more complex (**Fig. 1.7b,d**). Most type II chondrules in MET 00526 (L) have mesostasis with somewhat higher SiO_2 contents than type II chondrules in MET 00426 (CR) and Kainsaz (CO). However, the mesostasis in one type IIAB chondrule (L-Ch3) in MET 00526 has high CaO and Al_2O_3 contents, while having low SiO_2 contents (**Fig. 1.7b,d**), producing negative trends for Al_2O_3 and CaO versus SiO_2 in the type II data for MET 00526 (L). The trends are also negative for mesostasis in CR type II chondrules, but our data for Kainsaz type II chondrules show positive trends (**Fig. 1.7b,d**).

All of the type I chondrules we studied in the CR3.0 chondrite MET 00426 have unaltered mesostasis that is clear and glassy. In several of our CR type I chondrules (CR-Ch1, 3, 8, 9, 10, 20), mesostasis glass located in the center is more Ca- and Al-rich, whereas the glass found in the outer parts (which we refer to as "2nd glass") is more Si- (**Fig. 1.7a,c**) and Na-rich and frequently also more K- and Mn-rich. This is very similar to the zoned mesostasis that has been observed in some Semarkona type I chondrules (Matsunami et al. 1993; Libourel et al. 2006; Nagahara et al. 2008; e.g., Alexander and Grossman 2005; Grossman et al. 2002) as well as in type I chondrules in several CR2 chondrites (e.g., Libourel et al. 2006).

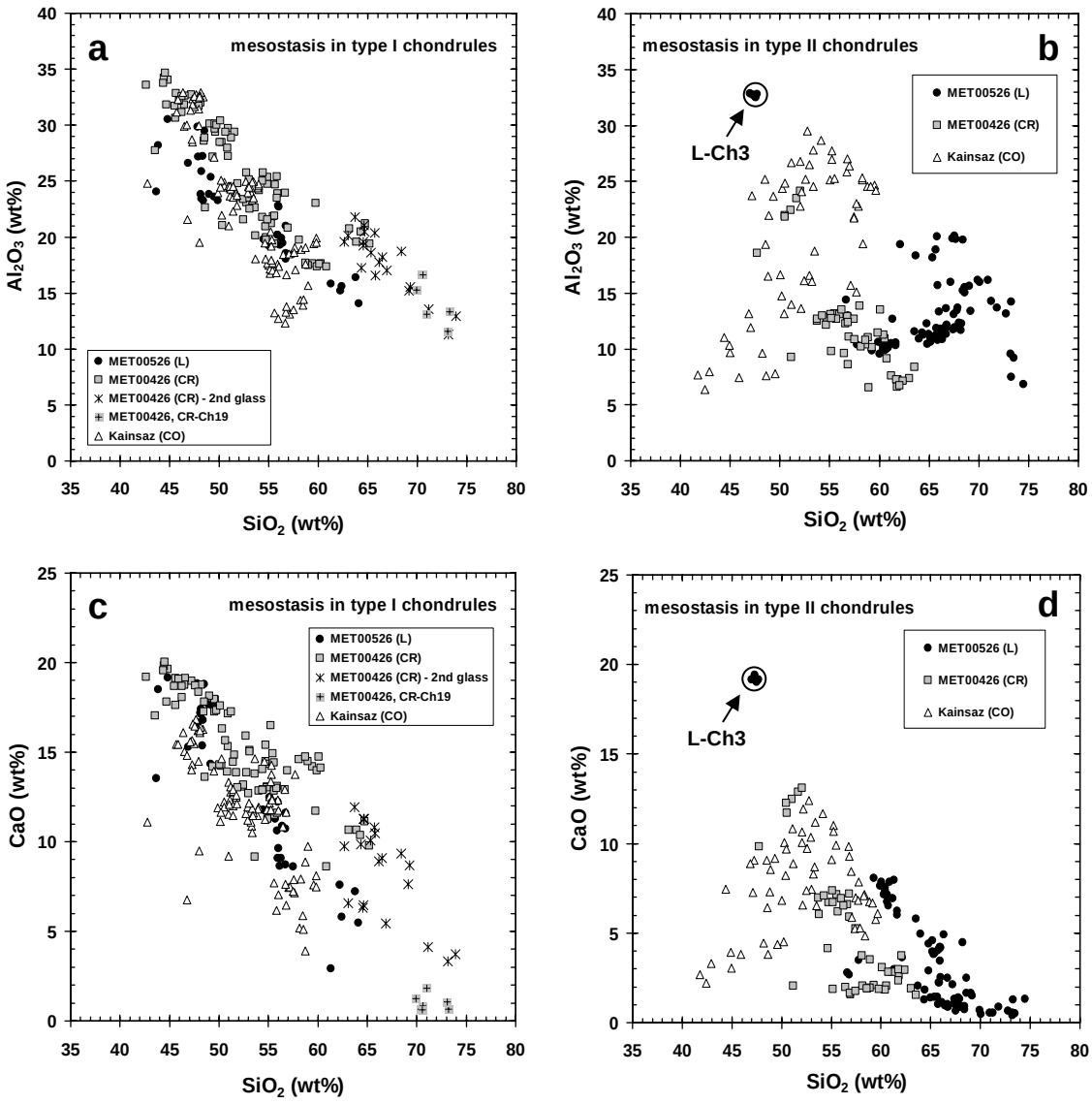

Fig. 1.7. a),b) Al_2O_3 (wt%) vs. SiO_2 (wt%) and c),d) CaO (wt%) vs. SiO_2 (wt%) for individual analyses of mesostasis glass in type I (a,c) and type II (b,d) chondrules from MET 00526 (L), MET 00426 (CR), and Kainsaz (CO).

In contrast to these previous studies, we frequently observed two distinct glass compositions. To demonstrate this, a plot of $(Na_2O+K_2O+MnO)/Al_2O_3$ versus CaO/SiO_2 for individual mesostasis analyses is shown in **Figure 1.8a**. Only the mesostasis in chondrule CR-Ch1 seems to be continuously zoned, although the glass in the outer part of this chondrule is actually present in small patches that are not necessarily interconnected (**Fig. 1.1c,d**). Nevertheless, in the other CR chondrules the modal abundance of the volatile-rich "2nd glass" is actually much lower than in chondrule CR-Ch1 (**Fig. 1.1c,d**). In order to determine the bulk chondrule composition of chondrule CR-Ch1, we used two average mesostasis compositions in our modal recombination analysis (**Fig. 1.1c,d**) as we did for the other chondrules in which the two mesostasis compositions were more distinct. In **Figure 1.8a**, we also plotted individual analyses of mesostasis in the BO chondrule CR-Ch11 and of the glass found within the igneous rim around this chondrule (see also **Fig. 1.2l**) – these two distinct glass compositions are very similar to those observed within the type I chondrules. The mesostasis in chondrule CR-Ch19 is not zoned, but quite unusual in composition as it is very volatile-rich and similar to the 2nd glass compositions that are observed at the edges of other type I chondrules (**Fig. 1.8a**). In one chondrule (CR-Ch2), the 2nd glass composition was found as small patches in the center of the chondrule, however, this might also simply be due to the way the chondrule is exposed in the thin section.

Figure 1.8b shows mesostasis compositions of three chondrules in the L3.05 chondrite MET 00526 that exhibit compositional trends similar to those observed in the CR (MET 00426) chondrules shown in **Figure 8a**. The trend seems to be fairly continuous for chondrule L-Ch1, a compound chondrule consisting of a BO chondrule in the center and an enveloping POP chondrule (see **Fig. 1.2i**). The glass becomes more volatile-rich towards the edges of this compound chondrule. The glass found within an igneous rim around chondrule L-Ch16 (shown in **Fig. 1.2c**) is also more volatile-rich than the glass in the center of the chondrule (**Fig. 1.8b**). Even though the third chondrule (L-Ch17) is a very glass-rich type IA chondrule (**Fig. 1.2f**), the 2nd glass composition is only found at the very edge of this chondrule and the two compositions seem to be very distinct (**Fig. 1.8b**).

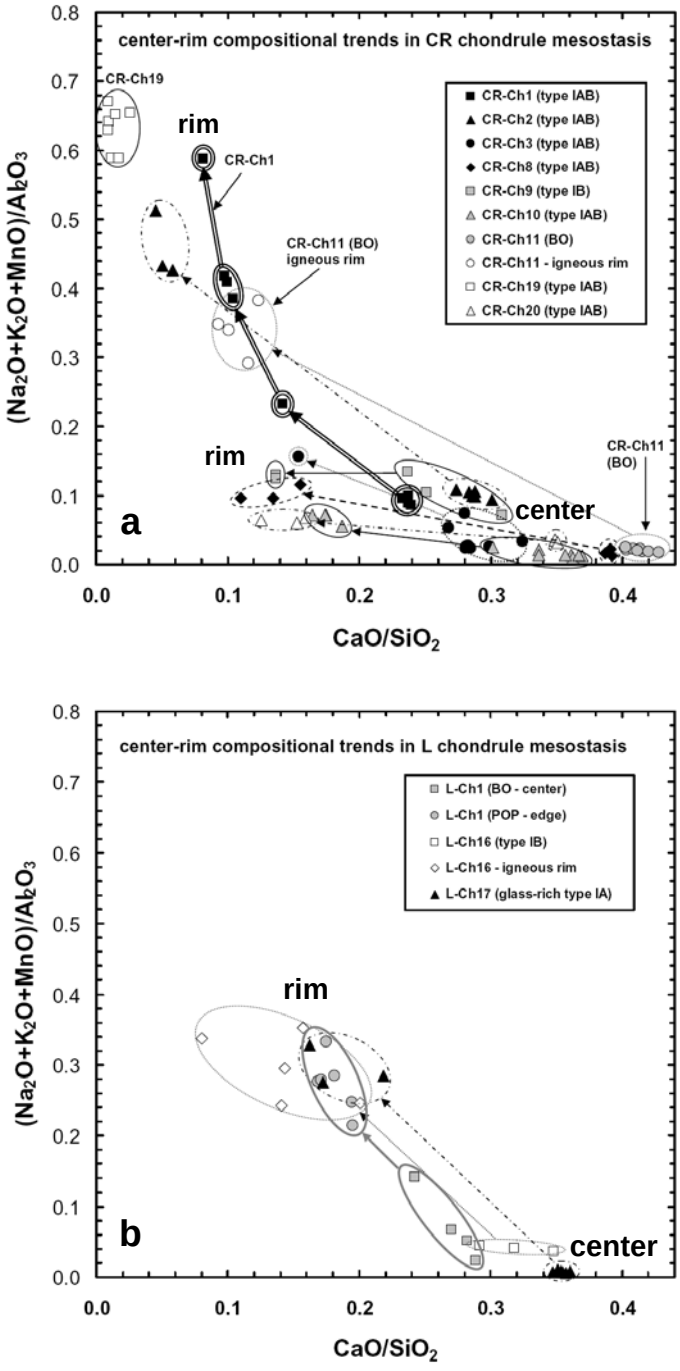

Fig. 1.8. $(Na_2O+K_2O+MnO)/Al_2O_3$ versus CaO/SiO_2 for individual mesostasis analyses in a) MET 00426 (CR) chondrules and b) MET 00526 (L) chondrules that show compositional differences between the glass located in the center versus a 2nd glass located in the outer parts of the chondrule (in some cases within igneous rims).

K/Al vs. Na/Al (relative to CI) plots for individual mesostasis analyses in all FeO-poor and FeO-rich chondrules in MET 00526 (L), MET 00426 (CR) and Kainsaz (CO) are shown in **Figure 1.9**. In unequilibrated ordinary chondrites, it has been observed that mesostasis compositions of type I and type II chondrules follow distinct trends in this kind of diagram (e.g., Grossman and Brearley 2005). Most of our analyses of type I chondrule mesostases in MET 00526 (Fig. 9a), MET 00426 (**Fig. 1.9c**) and Kainsaz (**Fig. 1.9e**) follow the typical trend and plot below the CI trendline, having Na/Al > K/Al. Type II chondrule mesostases in MET 00526 (**Fig. 1.9b**) and MET 00426 (**Fig. 1.9d**) exhibit characteristic trends towards higher K/Al ratios and frequently plot above the CI trendline, having K/Al > Na/Al. However, mesostasis compositions in Kainsaz type II chondrules (**Fig. 1.9f**) do not follow the typical trend and have Na/Al > K/Al similar to mesostasis in type I chondrules in Kainsaz (**Fig. 1.9e**).

The 2nd glass compositions found at the edges of many CR type I chondrules mentioned above, have higher Na/Al ratios and frequently also higher K/Al ratios than the glass found in the center of these chondrules (**Fig. 1.9c**). The glass-rich type IA chondrule L-Ch17 in the L chondrite MET 00526 again shows two very different glass compositions (**Fig. 1.9a**) with higher Na/Al and higher K/Al ratios at the edges, whereas the mesostasis analyses of the compound BO/POP chondrule L-Ch1 show more of a continuous trend towards higher Na/Al and K/Al ratios (**Fig. 1.9a**). Mesostasis in chondrule CR-Ch19 is clearly different from the mesostasis found in the center of other type I chondrules in MET 00426; it is the most volatile-rich and has the highest observed K/Al and Na/Al ratios (**Fig. 1.9c**). This chondrule contains olivines with very high MnO contents (**Fig. 1.4c**). The opposite is observed in type IA chondrules in MET 00526 (L), which have very low MnO contents in their olivines (**Fig. 1.4a**) and very low Na and K contents in their mesostases (**Fig. 1.9a**). Mesostasis compositions of Kainsaz type IB chondrules have higher Na/Al ratios than those in type IAB chondrules (**Fig. 1.9e**). Almost all of our individual mesostasis analyses in Kainsaz type IAB chondrule K2-Ch8 (shown in **Fig. 1.1e,f**) and several analyses in type IAB chondrule K1-Ch10 are close to plagioclase in composition and stoichiometry (~An_{77} and ~An_{76}, respectively).

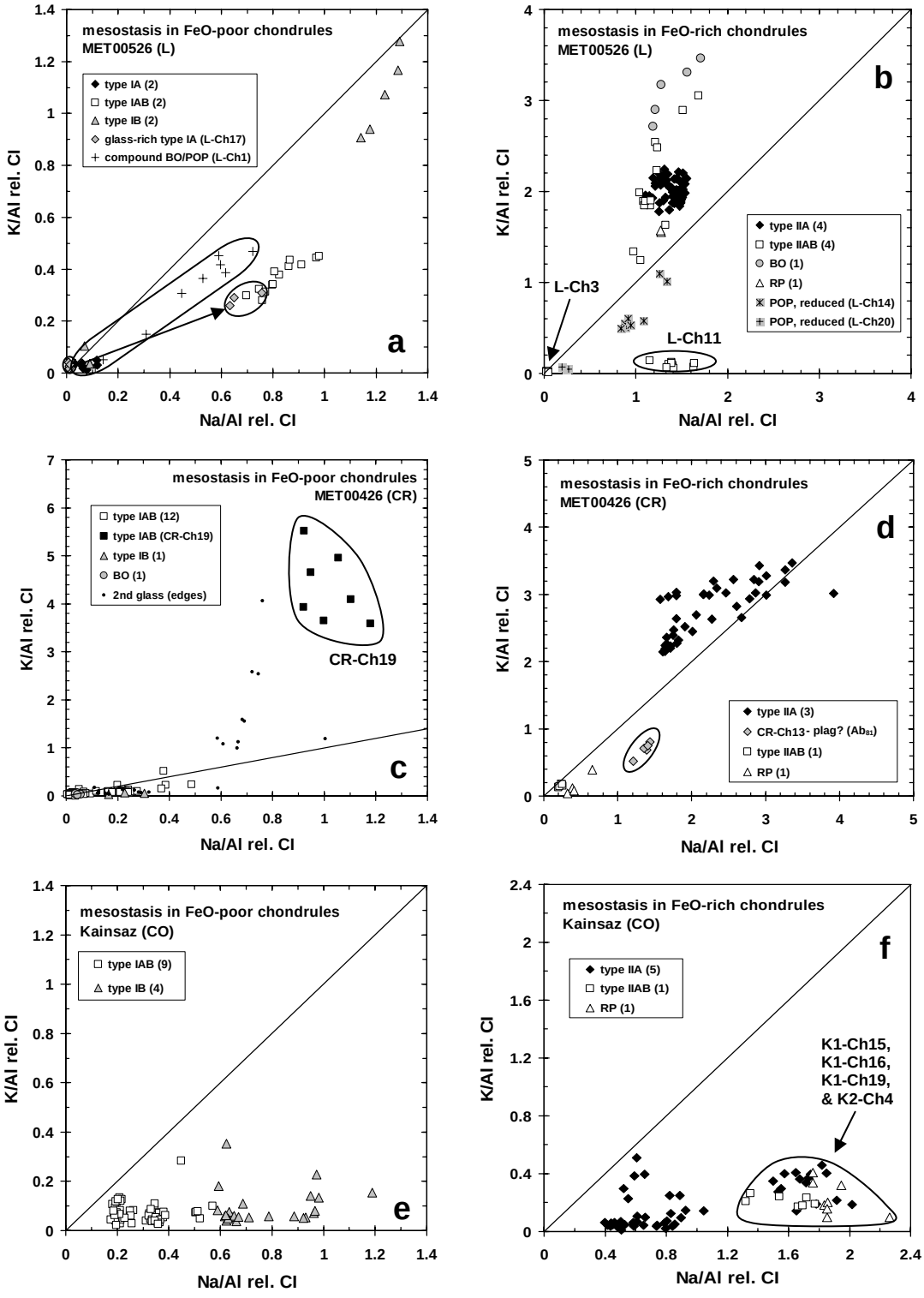

Fig. 1.9. K/Al vs. Na/Al (relative to CI) for individual analyses of mesostasis glass in FeO-poor and FeO-rich chondrules in a) and b) MET 00526 (L), c) and d) MET 00426 (CR), and e) and f) Kainsaz (CO).

A few FeO-rich chondrules have glass compositions with low K/Al but Na/Al ratios >1 (**Fig. 1.9b**: L-Ch11; **Fig. 1.9f**: K1-Ch15, K1-Ch16, K1-Ch19 and K2-Ch4). According to Grossman and Brearley (2005), this is indicative of the crystallization of albite. A distinct phase that is close to plagioclase in composition and stoichiometry (~Ab_{81}) was observed in chondrule CR-Ch13 in MET 00426 (**Fig. 1.9d**), but not in any other type II chondrules. The two reduced MET 00526 chondrules L-Ch14 and L-Ch20 (**Fig. 1.9b**) show glass compositions similar to some of the type I chondrules (**Fig. 1.9a**). The mesostasis in type IIAB chondrule L-Ch3, which also has the highest observed Al_2O_3 and SiO_2 contents among the type II chondrules in MET 00526 (**Fig. 1.7b,d**), has very low K and Na contents (**Fig. 1.9b**). The mesostasis compositions of the FeO-rich RP chondrules in MET 00526 (L), MET 00426 (CR) and Kainsaz (CO) plot in very different regions of the diagram (**Fig. 1.9b,d,f**).

Opaque minerals

The metal content we observed in FeO-poor chondrules from MET 00526 (L), MET 00426 (CR) and Kainsaz (CO) is quite variable. To some extent this depends on how a chondrule is exposed in the thin section (e.g., Ebel et al. 2008). Type I chondrules in Kainsaz frequently contain abundant round or elongated metal blebs in their interiors as is typical for CO chondrites (e.g., Rubin and Wasson 2005), while it is characteristic for MET 00426 and other CR type I chondrules to have a continuous or discontinuous layer of metal grains around the periphery in addition to some interior metal (e.g., Weisberg et al. 1993a; Connolly et al. 2001).

FeO-poor chondrules in the CR chondrite MET 00426 contain only Fe,Ni metal, but no sulfides. The compositional range of metal in FeO-poor chondrules in MET 00426 (CR) is 3.7–16.6 wt% Ni, 0.21–0.56 wt% Co, 0.11–0.79 wt% Cr and 0.17–0.99 wt% P, which is very similar to what has been observed in other CR chondrites (e.g., Weisberg et al. 1993a). Some of the metal in MET 00426 (CR) is weathered to an Fe-hydroxide, which contains varying amounts of Ni (1.2–7.4 wt%), S (0.2–1.9 wt%) and P_2O_5 (0.1–1.2 wt%).

FeO-poor chondrules in MET 00526 (L) and Kainsaz (CO) contain kamacite, taenite and/or troilite/monosulfide solid solution (MSS). The typical compositional range of

kamacite in FeO-poor chondrules in MET 00526 (L) is 1.1–4.5 wt% Ni, 0.15–0.55 wt% Co, 0.08–0.48 wt% Cr and up to 0.38 wt% P. Kamacite in FeO-poor chondrules in Kainsaz has 2.3–6.6 wt% Ni, 0.33–0.96 wt% Co, up to 0.97 wt% Cr and P is mostly below the EMP detection limit of 0.04 wt%. Many type I chondrules in Kainsaz contain taenite with low Co contents (<0.15 wt%), while taenite in MET 00526 (L), although only found in one type IA chondrule, has higher Co contents (up to 1.1 wt%). Monosulfide solid solution (MSS) in FeO-poor chondrules in both Kainsaz (CO) and MET 00526 (L) has Ni contents up to 0.3 wt%. Some of the metal in MET 00526 (L) has been replaced by magnetite. Furthermore, many terrestrial alteration veins are present.

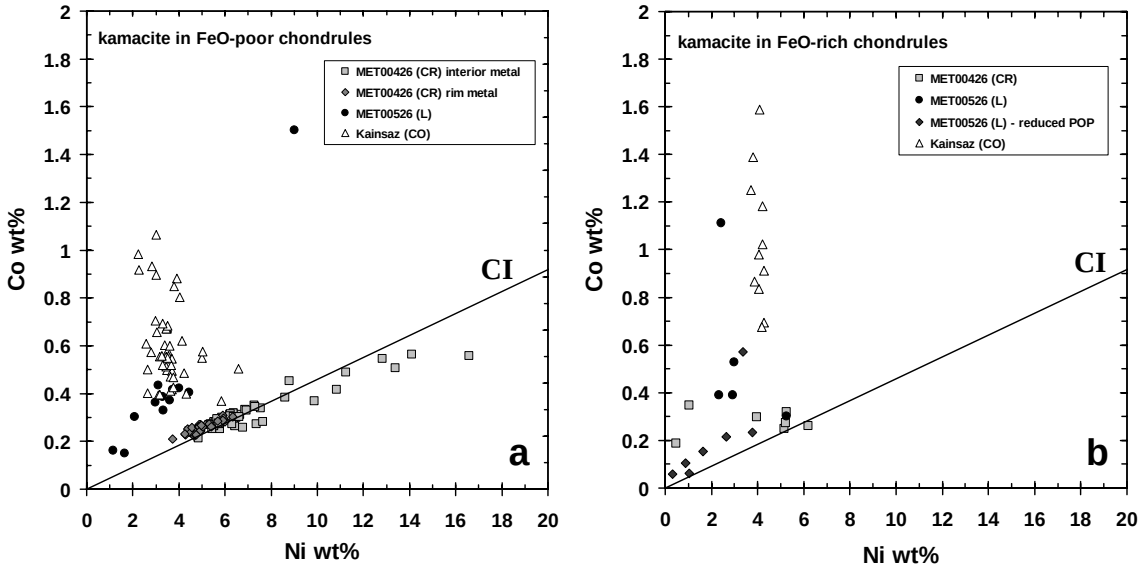

Fig. 1.10. a) Co (wt%) vs. Ni (wt%) of individual Fe,Ni metal grains (between 1 and 10 analyses per chondrule) in FeO-poor chondrules in MET 00426 (CR), MET 00526 (L) and Kainsaz (CO). Metal compositions in FeO-poor chondrules in MET 00426 (CR) correlate along the CI ratio. Some metal grains found in the interior of FeO-poor CR chondrules have high Ni contents (up to 17 wt%), whereas kamacite grains along the periphery have lower Ni and Co contents (see also Weisberg et al. 1993a; Connolly et al. 2001). Kamacite grains in FeO-poor chondrules in Kainsaz (CO) and MET 00526 (L) have lower Ni and higher Co contents than CR chondrule metal. b) Co (wt%) vs. Ni (wt%) of individual kamacite analyses (between 1 and 5 analyses per chondrule) in FeO-rich chondrules in MET 00426 (CR), MET 00526 (L) and Kainsaz (CO). The modal abundance of kamacite is much lower in FeO-rich chondrules, which is why the number of analyses plotted is much smaller. However, the behavior of Co and Ni in kamacite in FeO-rich chondrules is actually quite similar to that of kamacite in FeO-poor chondrules in each chondrite, except for somewhat higher Co contents in FeO-rich CO chondrules and lower Ni contents in FeO-rich CR chondrules (see text).

Figure 1.10a shows Co (wt%) versus Ni (wt%) for individual Fe,Ni metal analyses in FeO-poor chondrules in MET 00426 (CR), MET 00526 (L) and Kainsaz (CO). Cobalt and Ni contents of metal in FeO-poor chondrules in MET 00426 (CR) show a positive correlation with most analyses lying close to the CI ratio, similar to what has been observed in other CR chondrites (e.g., Weisberg et al. 1993a; Connolly et al. 2001). The metal compositions are frequently more Ni-rich (up to 16.6 wt% Ni) in the center of FeO-poor MET 00426 (CR) chondrules, while lower Ni contents are found in metal grains at the chondrule rims (**Fig. 1.10a**). Fe,Ni metal grains in FeO-poor chondrules in Kainsaz (CO) and MET 00526 (L) have lower Ni and higher Co contents than metal in FeO-poor CR chondrules (**Fig. 1.10a**). One metal grain in MET 00526 (L) type IA chondrule L-Ch13 has a higher Ni (9.0 wt%) and Co content (1.5 wt%) than what was typically observed (**Fig. 1.10a**). Co and Ni show a slightly negative trend in metal in FeO-poor Kainsaz (CO) chondrules (**Fig. 1.10a**).

Compared to FeO-poor chondrules, the modal abundances of metals and sulfides in FeO-rich chondrules is typically very low (<3 vol%) in all three chondrites studied. However, some of the type IIAB chondrules in MET 00526 (L) show high sulfide contents, up to 15 vol%. FeO-rich chondrules in MET 00526 (L) and Kainsaz (CO) contain the same type of opaque minerals as FeO-poor chondrules in these meteorites: kamacite, taenite and/or troilite/MSS. In contrast, FeO-rich chondrules in MET 00426 (CR) show more of a variety of opaque minerals than FeO-poor chondrules in CR chondrites, including kamacite, taenite, troilite/MSS and pentlandite (see also Schrader et al. 2008).

Figure 1.10b shows Co (wt%) versus Ni (wt%) for individual kamacite analyses in FeO-rich chondrules in MET 00426 (CR), MET 00526 (L) and Kainsaz (CO). The number of analyses (between 1 and 5 analyses per chondrule when kamacite was present) is smaller than for the FeO-poor chondrules shown in **Figure 1.10a** (between 1 and 10 analyses per chondrule), because the modal abundance of kamacite is much lower in FeO-rich chondrules. The behavior of Co and Ni in kamacite in FeO-rich chondrules is in general quite similar to that of kamacite in FeO-poor chondrules in each chondrite: several kamacite analyses in FeO-rich chondrules from MET 00426 (CR) cluster around the Co/Ni ratio of CI chondrites, while kamacite grains in FeO-rich chondrules in

Kainsaz (CO) and MET 00526 (L) have lower Ni and higher Co contents (**Fig. 1.10b**). However, there are some differences as well. The range of Ni contents observed in kamacite of FeO-rich chondrules in MET 00426 (CR) is more limited than in FeO-poor chondrules in MET 00426 (CR), with a few analyses having much lower Ni contents and plotting above the CI line. Kamacite in FeO-rich chondrules in Kainsaz (CO) shows somewhat higher Co contents (up to 1.6 wt%) and also a more limited range of Ni contents (3.7–4.3 wt% Ni) than in FeO-poor chondrules in Kainsaz (CO). Metal in two reduced chondrules in MET 00526 (L-Ch14 and L-Ch20, **Fig. 1.2g,h**) have higher Co/Ni ratios than CI, but show a trend parallel to the CI line.

Bulk chondrule compositions

Individual bulk chondrule compositions for the 20 chondrules studied in each chondrite are given (as element wt%) in **Table 1.5** (MET 00526 – L), **Table 1.6** (MET 00426 – CR) and **Table 1.7** (Kainsaz – CO). The supplementary CD contains Microsoft Office Excel® files with the collected and generated data for each chondrule (EMP data, BSE image, corresponding phase image and details of the modal recombination analysis). Metal grains along the periphery of CR type I chondrules were included in the bulk chondrule compositions, as they are thought to belong to the chondrule (e.g., Connolly et al. 2001). The bulk compositions of igneous rims found around two chondrules (L-Ch16 and CR-Ch11) were calculated separately (see **Tables 1.5** and **1.6**). For Kainsaz type I chondrules, we used the olivine analysis with the lowest measured Fa content and the low-Ca pyroxene analysis with the lowest measured Fs content to calculate the bulk chondrule composition, which will be further explained in the discussion below.

Table 1.5. Bulk chemical compositions of individual MET 00526 (L3.05) chondrules.

Chondrule	Textural type	Density (g/cm^3)	Si	Ti	Al	Cr	Fe	Mn	Mg	Ca	Na	K	Ni	Co	P	S
FeO-poor chondrules																
L-Ch13	PO	3.4	17.9	0.10	1.8	0.13	12.7	<0.02	24.6	2.5	0.08	<0.02	1.0	0.09	<0.02	<0.02
L-Ch8	PO	3.9	12.0	0.04	1.6	0.10	33.8	<0.02	16.9	1.7	0.05	<0.02	0.73	0.08	0.03	6.0
L-Ch17	PO, glass-rich	3.0	20.7	0.31	6.0	0.18	4.9	0.03	17.3	5.7	0.47	0.04	0.13	<0.02	<0.02	0.96
L-Ch12	POP	3.3	23.3	0.09	1.4	0.36	7.2	0.21	21.7	1.5	0.54	0.04	0.20	<0.02	<0.02	0.41
L-Ch6	POP	3.2	25.2	0.09	1.1	0.42	3.1	0.17	22.7	1.4	0.35	0.03	0.07	<0.02	<0.02	0.19
L-Ch16	PP	3.4	25.6	<0.02	0.11	0.26	7.0	0.06	22.2	0.10	<0.02	<0.02	0.15	<0.02	<0.02	0.22
L-Ch16 – igneous rim		4.6	11.4	<0.02	0.48	0.34	54.7	0.03	8.7	0.32	0.15	0.03	0.78	0.05	0.13	3.3
L-Ch15	PP	3.3	25.8	0.07	0.87	0.45	7.0	0.27	19.2	1.3	0.45	0.06	0.22	<0.02	<0.02	0.34
L-Ch1	BO/POP	3.0	22.5	0.23	4.0	0.33	2.5	0.10	19.6	4.3	0.83	0.07	<0.03	<0.02	<0.02	1.1
FeO-rich chondrules																
L-Ch4	PO	3.3	19.6	0.05	0.85	0.29	13.9	0.28	21.4	1.0	0.73	0.13	<0.03	<0.02	0.14	0.54
L-Ch7	PO	3.3	20.8	0.09	1.3	0.43	15.0	0.34	18.1	1.3	1.0	0.17	0.08	<0.02	0.06	0.46
L-Ch9	PO	3.4	19.1	0.04	0.57	0.36	12.9	0.27	23.3	0.79	0.45	0.09	0.04	<0.02	0.04	1.6
L-Ch2	PO	3.3	20.0	0.05	1.0	0.25	16.6	0.37	18.8	0.30	0.73	0.14	<0.03	<0.02	<0.02	2.7
L-Ch11	POP	3.6	16.4	0.04	1.1	0.25	27.2	0.32	12.5	1.3	0.86	<0.02	0.76	<0.02	0.06	7.2
L-Ch10	POP	3.2	21.6	0.09	1.5	0.45	13.7	0.29	15.9	2.1	1.0	0.19	0.09	<0.02	<0.02	3.9
L-Ch18	POP	3.3	23.4	0.05	0.88	0.45	14.3	0.45	16.1	0.82	0.62	0.12	<0.03	<0.02	<0.02	0.89
L-Ch3	POP	3.3	24.6	0.03	0.78	0.46	8.1	0.10	20.6	0.94	<0.02	<0.02	0.10	<0.02	<0.02	0.07
L-Ch14	POP, reduced	3.6	18.3	0.10	1.4	1.0	23.6	0.45	15.6	1.4	0.60	0.06	0.66	0.06	<0.02	1.5
L-Ch20	POP, reduced	3.5	21.7	0.04	0.58	0.41	14.3	0.14	20.8	0.80	0.04	<0.02	0.13	<0.02	<0.02	0.14
L-Ch19	BO	3.2	20.9	0.06	1.2	0.29	17.6	0.44	15.2	0.50	0.96	0.25	0.08	<0.02	<0.02	4.7
L-Ch5	RP	3.3	24.6	0.05	0.85	0.61	11.0	0.43	16.2	0.88	0.43	0.08	<0.03	<0.02	<0.02	2.8

Table 1.6. Bulk chemical compositions of individual MET 00426 (CR3.0) chondrules.

Chondrule	Textural type	Density (g/cm^3)	Si	Ti	Al	Cr	Fe	Mn	Mg	Ca	Na	K	Ni	Co	P	S
FeO-poor chondrules																
CR-Ch12	POP	3.1	22.5	0.16	3.7	0.46	2.3	0.16	21.2	3.8	0.43	0.03	0.09	<0.02	<0.02	<0.02
CR-Ch14	POP	3.2	22.3	0.13	2.1	0.24	3.6	0.04	23.6	2.6	0.06	<0.02	0.30	<0.02	0.03	<0.02
CR-Ch2	POP	3.1	22.6	0.12	4.3	0.45	3.2	0.38	19.0	4.1	0.54	0.05	<0.03	<0.02	<0.02	<0.02
CR-Ch3	POP	3.7	17.2	0.07	1.3	0.45	25.1	0.09	18.6	1.4	0.07	<0.02	1.6	0.08	0.08	<0.02
CR-Ch5	POP	3.7	17.8	0.06	1.1	0.34	21.4	0.08	20.0	1.1	0.13	<0.02	1.9	0.08	0.10	<0.02
CR-Ch10	POP	3.6	19.2	0.08	1.2	0.45	19.0	0.09	19.8	1.7	0.03	<0.02	1.1	0.06	0.06	<0.02
CR-Ch8	POP	4.2	14.6	0.06	0.92	0.40	38.0	0.09	14.3	1.1	0.03	<0.02	2.5	0.13	0.14	<0.02
CR-Ch15	POP	4.2	13.9	0.07	2.4	0.35	39.1	0.07	11.2	2.8	<0.02	<0.02	2.6	0.12	0.17	<0.02
CR-Ch19	POP	3.2	24.4	0.08	1.2	0.96	6.8	1.1	18.9	1.7	0.53	0.24	0.25	<0.02	<0.02	<0.02
CR-Ch18	POP	3.4	22.9	0.05	0.98	0.51	16.3	0.23	17.1	0.84	0.13	<0.02	0.90	0.04	0.05	<0.02
CR-Ch1	POP	3.4	22.9	0.06	0.94	0.50	11.1	0.19	20.7	1.1	0.13	0.03	0.52	0.03	0.05	<0.02
CR-Ch7	POP	4.0	16.5	0.06	1.5	0.44	33.4	0.05	14.1	1.4	<0.02	<0.02	2.0	0.10	0.15	<0.02
CR-Ch20	POP	3.4	21.3	0.16	3.3	0.39	15.6	0.07	14.4	4.3	0.12	<0.02	0.98	0.05	0.06	<0.02
CR-Ch9	PP	4.1	16.8	0.04	0.62	0.36	36.8	0.08	13.1	0.66	0.07	<0.02	2.2	0.11	0.11	<0.02
CR-Ch11	BO	3.3	21.5	0.11	2.0	0.38	4.7	0.11	24.1	2.9	0.05	<0.02	0.18	<0.02	<0.02	<0.02
CR-Ch11 – igneous rim		5.1	9.9	0.06	0.29	0.33	59.1	0.06	8.1	0.86	0.05	<0.02	3.2	0.16	0.21	<0.02
FeO-rich chondrules																
CR-Ch6	PO	3.4	18.5	<0.02	0.26	0.28	15.7	0.28	23.3	0.17	0.33	0.06	<0.03	<0.02	0.03	<0.02
CR-Ch13	PO	3.5	18.2	0.08	1.4	0.34	22.2	0.32	14.3	1.5	1.3	0.20	0.31	<0.02	0.18	1.3
CR-Ch16	PO	3.3	20.3	0.06	1.2	0.79	19.7	0.37	13.9	0.85	1.9	0.24	<0.03	<0.02	0.12	0.20
CR-Ch4	POP	3.4	21.6	0.09	1.7	0.55	15.7	0.28	15.8	2.0	0.09	0.03	<0.03	<0.02	0.03	<0.02
CR-Ch17	RP	3.1	29.5	0.04	0.59	0.56	6.1	0.43	14.6	1.0	0.10	0.03	<0.03	<0.02	<0.02	<0.02

Table 1.7. Bulk chemical compositions of individual Kainsaz (CO3.2) chondrules.

Chondrule	Textural type	Density (g/cm^3)	Si	Ti	Al	Cr	Fe	Mn	Mg	Ca	Na	K	Ni	Co	P	S
FeO-poor chondrules																
K2-Ch9	POP	3.2	19.3	0.10	1.6	0.16	12.4	0.03	21.5	1.8	0.42	<0.02	0.57	0.03	<0.02	2.7
K1-Ch9	POP	3.5	19.0	0.09	2.2	0.23	15.6	0.07	19.3	2.2	0.33	<0.02	0.44	0.06	<0.02	2.9
K1-Ch21	POP	3.6	19.4	0.06	0.82	0.18	16.6	0.06	22.3	0.73	0.08	<0.02	1.8	0.06	<0.02	0.09
K2-Ch8	POP	3.2	22.4	0.08	1.9	0.22	4.0	0.06	23.9	2.0	0.19	<0.02	0.45	<0.02	<0.02	0.27
K1-Ch12	POP	3.4	21.9	0.04	0.37	0.20	8.4	0.04	25.0	0.45	<0.02	<0.02	0.41	0.05	<0.02	0.59
K1-Ch1	POP	3.6	17.4	0.12	2.4	0.33	20.4	0.10	17.4	1.7	0.16	<0.02	1.7	0.07	<0.02	3.5
K1-Ch10	POP	3.9	17.1	0.06	1.5	0.19	28.7	0.06	15.7	1.8	0.15	<0.02	1.5	0.14	<0.02	0.71
K1-Ch13	POP	3.7	19.1	0.08	0.43	0.30	22.3	0.05	18.6	0.62	<0.02	<0.02	1.9	0.12	<0.02	1.3
K1-Ch14	POP	3.5	21.6	0.06	0.39	0.24	14.0	0.04	19.9	0.36	<0.02	<0.02	0.12	0.05	0.04	4.6
K1-Ch11	PP	3.7	18.7	0.07	1.8	0.36	26.5	0.10	12.0	2.5	0.58	<0.02	1.8	0.10	<0.02	2.7
K2-Ch14	PP	3.8	19.6	0.06	0.55	0.35	25.1	0.11	16.1	0.89	0.08	<0.02	0.75	0.11	0.04	2.0
K1-Ch17	PP	3.9	18.7	0.08	0.83	0.32	28.3	0.07	14.5	1.4	0.32	<0.02	1.6	0.11	<0.02	0.61
K1-Ch20	PP	3.1	26.8	0.11	2.0	0.51	2.9	0.45	15.4	4.2	1.7	0.04	<0.03	<0.02	<0.02	<0.02
FeO-rich chondrules																
K1-Ch7	PO	3.5	17.6	0.06	0.94	0.53	22.6	0.20	16.4	1.3	0.29	0.03	0.08	<0.02	<0.02	0.25
K1-Ch8	PO	3.8	15.9	<0.02	0.85	0.10	30.2	0.21	14.2	1.1	0.27	<0.02	0.81	0.07	<0.02	1.4
K1-Ch16	PO	3.7	17.0	<0.02	0.27	0.06	27.9	0.26	15.7	0.29	0.27	<0.02	0.15	<0.02	<0.02	0.05
K2-Ch4	PO	3.4	18.5	0.11	2.1	0.09	18.7	0.14	15.8	1.3	2.0	0.06	<0.03	<0.02	0.05	1.4
K2-Ch7	PO	3.5	18.5	0.07	1.7	0.10	20.2	0.17	16.7	1.6	0.86	0.03	0.29	0.04	<0.02	0.56
K1-Ch15	POP	3.7	20.8	<0.02	0.19	0.28	27.2	0.29	11.4	0.42	0.12	<0.02	0.09	<0.02	<0.02	<0.02
K1-Ch19	RP	3.3	26.2	0.03	0.66	0.45	8.5	0.40	17.3	0.77	0.66	<0.02	0.19	<0.02	<0.02	0.40

Element abundance patterns (normalized to CI chondrites) of individual chondrules from MET 00526 (L), MET 00426 (CR) and Kainsaz (CO) are shown in **Figure 1.11**, with FeO-poor chondrules on the left-hand side (**Fig. 1.11a,c,e**) and FeO-rich chondrules on the right-hand side (**Fig. 1.11b,d,f**). Lithophile elements are plotted as a function of increasing volatility according to Lodders (2003) and this is followed with siderophile elements. Phosphorus behaves as a siderophile element in FeO-poor chondrules and is plotted as such in **Figures 1.11a,c,e**, while it behaves rather lithophile in FeO-rich chondrules (**Fig. 1.11b,d,f**) (e.g., Lauretta et al. 2001; Jones 1990).

FeO-poor chondrules in MET 00426 (CR) have refractory element (Al, Ca, Ti) abundances that are not fractionated relative to one another and minimally fractionated from Mg and Si (**Fig. 1.11c**), whereas FeO-poor chondrules in MET 00526 (L) and Kainsaz (CO) show more fractionations between these elements (**Fig. 1.11a,e**). Two FeO-poor chondrules (L-Ch17 and L-Ch1) in MET 00526 (L) show an enrichment in Al, Ca and Ti relative to Mg and Si (**Fig. 1.11a**), which is related to the fact that these chondrules have high modal abundances of mesostasis glass in the thin section studied (**Fig. 1.2f,i**). In contrast, chondrule L-Ch16 in MET 00526 (L) is depleted in Al, Ca and Ti (**Fig. 1.11a**), consistent with the exposed modal abundance of mesostasis in this chondrule (**Fig. 1.2c**). In Kainsaz (CO) type I chondrules, Ti is relatively unfractionated with respect to Mg and Si (**Fig. 1.11e**). Nonetheless, four Kainsaz type I chondrules (K1-Ch12, K1-Ch13, K1-Ch14 and K1-Ch21) that have very little mesostasis exposed in the thin section show depletions in Al and Ca (**Fig. 1.11e**). These four chondrules also have the lowest Na contents (**Fig. 1.11e**).

In FeO-poor chondrules in MET 00426 (CR), which contain abundant Fe,Ni metal but no sulfides, siderophile elements (Fe, Ni, Co, P) are not fractionated relative to one another and S is considerably depleted (**Fig. 1.11c**). FeO-poor chondrules in MET 00526 (L) and Kainsaz (CO) show more variability in Fe, Ni, Co, P and S (**Fig. 1.11a,e**). Chondrules CR-Ch19 in MET 00426 (CR) and K1-Ch20 in Kainsaz (CO) show element abundance patterns distinct from other FeO-poor chondrules in these chondrites, with higher abundances of Cr, Mn and K in MET 00426 chondrule CR-Ch19 (**Fig. 1.11c**) and higher abundances of Ca, Cr, Mn and Na in Kainsaz chondrule K1-Ch20 (**Fig. 1.11e**).

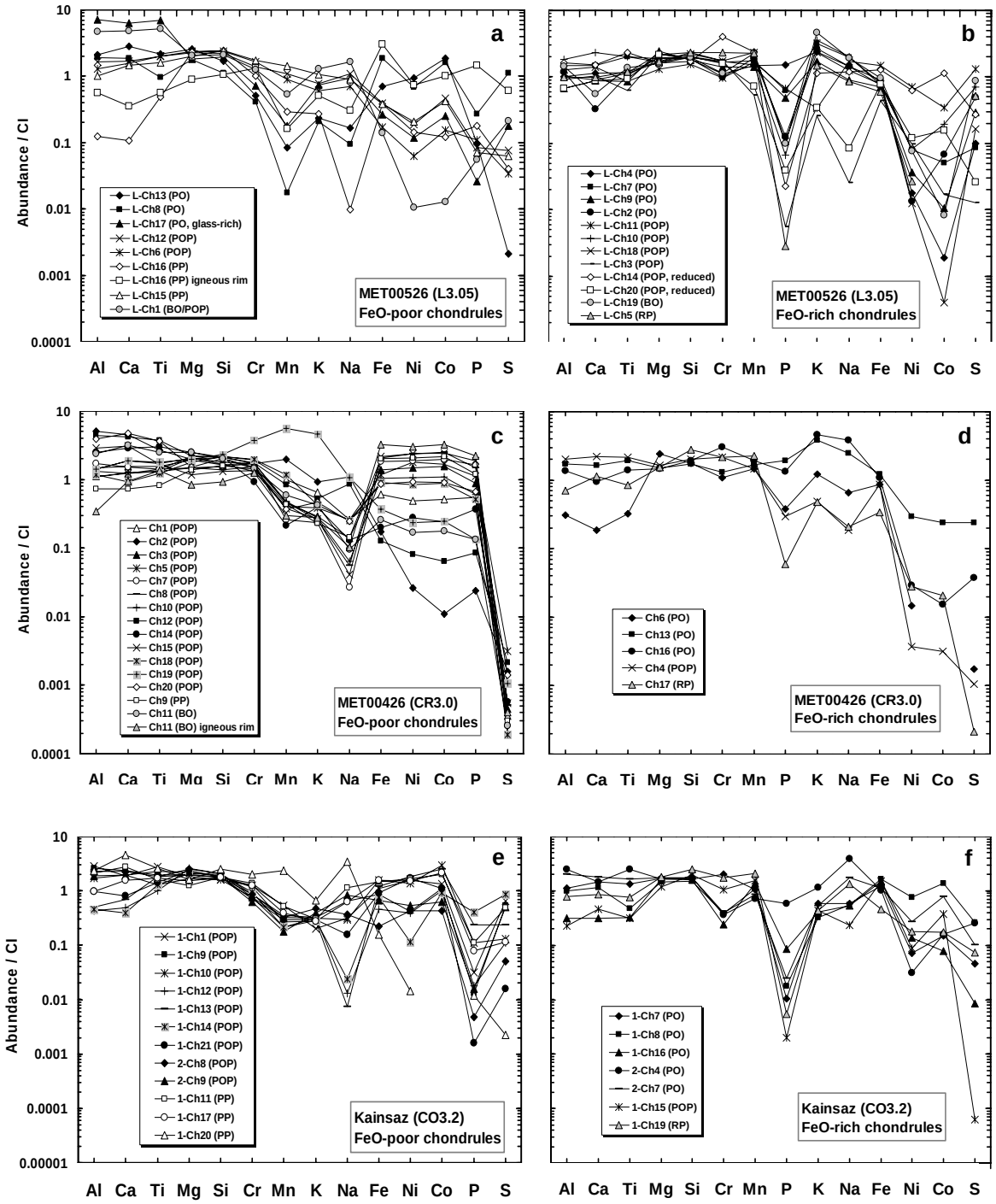

Fig. 1.11. Bulk chemical compositions of individual chondrules in MET 00526 (L), MET 00426 (CR) and Kainsaz (CO) determined by modal recombination analysis. FeO-poor chondrules are shown on the left-hand side (a, c, e), FeO-rich chondrules on the right-hand side (b, d, f). Elemental abundances are normalized to CI chondrite abundances (Lodders 2003). Elements on the ordinate are arranged in order of increasing volatility; siderophile elements are plotted last. Phosphorus was treated as siderophile in type I chondrules, but as lithophile in type II chondrules (e.g., Lauretta et al. 2001; Jones 1990).

In contrast to FeO-poor chondrules in MET 00526 (L), MET 00426 (CR) and Kainsaz (CO), which show a general drop in element abundances between Si and Mn, the element abundance patterns of FeO-rich chondrules are relatively unfractionated for elements between Al and Mn (**Fig. 1.11b,d,f**). However, FeO-rich chondrules with little mesostasis exposed in the thin section show depletions of Al, Ca, and Ti relative to Mg and Si (e.g., **Fig. 1.11d:** CR-Ch6, **Fig. 1.11f:** K1-Ch15 and K1-Ch16), similar to what we observed in FeO-poor chondrules. A few FeO-rich chondrules in Kainsaz show a depletion in Cr (**Fig. 1.11f**). Siderophile elements and S generally show a stronger depletion in FeO-rich chondrules in MET 00426 (CR) than in MET 00526 (L) and Kainsaz (CO). Enrichment of Co relative to Ni in many FeO-rich chondrules in Kainsaz (**Fig. 1.11f**) is consistent with our observations of high Co and low Ni contents in kamacite (**Fig. 1.10b**).

Figures 1.12a,c,e show individual bulk compositions of chondrules in MET 00526 (L), MET 00426 (CR) and Kainsaz (CO) in Fe-Mg-Si (wt% element) ternary diagrams and **Figures 1.12b,d,f** show individual chondrule data in FeO-MgO-SiO_2 (wt% oxide) ternary diagrams, for the silicate portions only. In all three chondrites, the compositions of type I and type II chondrules are clearly distinct when only the silicate portion is considered (**Fig. 1.12b,d,f**). However, when the metal is included in the bulk compositions (**Fig. 1.12a,c,e**), type I chondrules show a general trend from Fe-poor to Fe-rich compositions and some of them overlap with type II chondrules. FeO contents of the silicate portions of type II chondrules show a general increase from L to CR to CO (**Fig. 1.12b,d,f**).

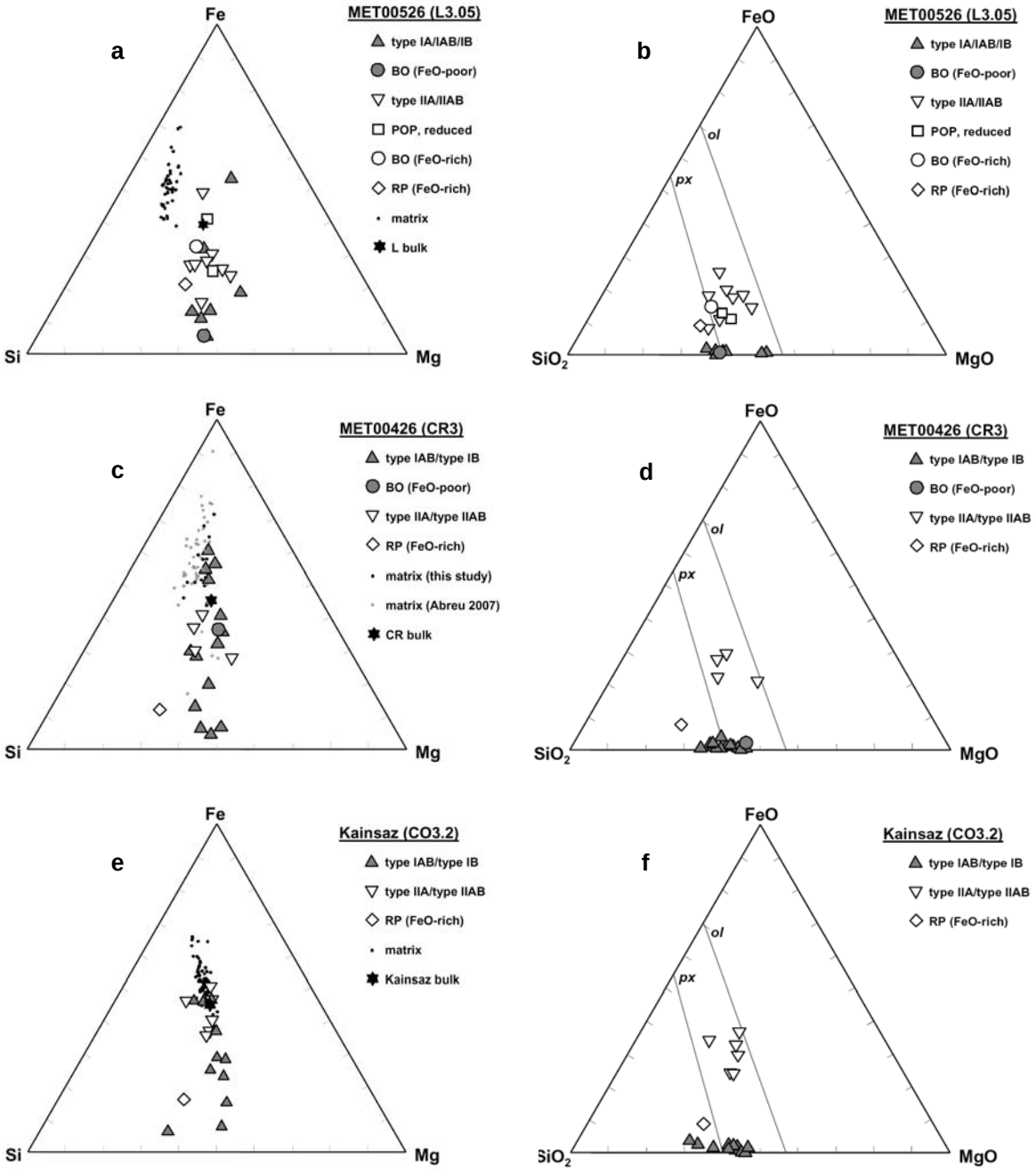

Fig. 1.12. a,c,e) Fe-Mg-Si ternaries (element wt%) for bulk chondrule, matrix and bulk chondrite compositions and b,d,f) FeO-MgO-SiO_2 ternaries (oxide wt%) for the silicate portions of chondrules in a,b) MET 00526 (L), c,d) MET 00426 (CR) and e,f) Kainsaz (CO). L and CR bulk data are from Lodders and Fegley (1998). Kainsaz bulk is from Ahrens et al. (1973).

Bulk matrix compositions

Bulk matrix compositions in MET 00526 (L), MET 00426 (CR) and Kainsaz (CO) were obtained by EMP defocused beam analyses (10 μm beam diameter). In **Table 1.8**, average matrix compositions determined in this work are compared to literature data. Matrix compositions in Fe-Mg-Si (element wt%) ternary diagrams are shown in **Figures 1.12a,c,e**. In MET 00526 (L), matrix compositions are more Si-rich than in MET 00426 (CR) and Kainsaz (CO). Average Mg contents of matrix increase from L to CR to CO, while average Fe contents are fairly comparable (**Table 1.8**).

Table 1.8. Average matrix compositions (element wt%) of MET 00526 (L), MET 00426 (CR), and Kainsaz (CO) compared to literature data.

	MET 00526 (L3.05)	MET 00526 (L3.05) GB05	Semar-kona (LL3.0) GB05	MET 00426 (CR3.0)	MET 00426 (CR3.0) A07	Kainsaz (CO3.2)	Kainsaz (CO3.2) GB05	ALHA 77307 (CO3.0) B93
# ana-lyses	40	11	20	15	47	72	10	31
Si	18.5	18.7	16.0	12.0	12.5	13.9	14.1	14.2
Ti	0.03	0.04	0.03	0.04	0.03	0.04	0.05	0.04
Al	2.2	2.2	1.5	0.79	0.92	1.0	1.3	2.4
Cr	0.17	0.18	0.16	0.25	0.18	0.23	0.25	0.24
Fe	26.1	26.6	23.5	26.9	27.3	27.5	26.8	25.0
Mn	0.15	0.18	0.15	0.23	0.14	0.27	0.33	0.18
Mg	6.2	6.8	6.7	8.8	7.9	10.4	10.2	8.9
Ca	0.65	0.61	0.56	0.85	0.66	0.44	0.53	0.76
Na	1.6	1.4	1.6	0.22	0.16	0.45	0.50	0.18
K	0.36	0.32	0.31	0.09	0.15	0.10	0.13	0.10
Ni	1.4	0.96	0.96	1.3	1.4	0.40	0.72	2.6
P	0.03	0.00	0.00	0.11	0.11	0.10	0.07	0.11
S	0.52	0.43	1.2	2.9	2.0	0.14	0.15	1.1

GB05 = Grossman and Brearley (2005)
A07 = Abreu (2007)
B93 = Brearley (1993)

DISCUSSION

Our detailed study of chondrules provides a self-consistent dataset that combines chondrule textures with mineralogy and bulk chemical compositions for not only one chondrite, but three fairly pristine members (MET 00526, MET 00426 and Kainsaz) of different chondrite groups (L, CR and CO). These data allow us to compare the mineralogy and bulk compositions of chondrules with the same texture in different chondrites and to examine the compositional relationship between different chondrule types (e.g., type I versus type II) within a chondrite group. This information can be used to improve our understanding of the nature and variability of chondrule precursor materials, nebular heterogeneities, conditions during chondrule formation such as varying oxygen fugacity, and reheating/recycling of material (e.g., Grossman et al. 1988; Jones et al. 2005).

We currently have a limited understanding as to how chondrules of the same textural type compare between the different chondrite groups (e.g., Scott and Taylor 1983). This is mostly due to the fact that many studies of chondrules have focused on just one chondrite (or one chondrite group). In addition, many literature data are compromised by the fact that the chondrites studied have been affected by secondary processes (see review in Jones 2005 and references therein). It has been recognized that oxygen isotopic compositions of chondrules from different chondrite groups are significantly different (e.g., Clayton 2003; Krot et al. 2006; Yurimoto et al. 2008). However, we do not know if the differences in oxygen isotopic composition are reflected in the mineral and bulk chondrule compositions. Furthermore, available datasets for bulk chondrule compositions of members from the same chondrite group (e.g., CO chondrites) show some discrepancies, even for major elements (e.g., Jones et al. 2005). Our Kainsaz (CO3.2) bulk chondrule data obtained by modal recombination via EMP allow us to resolve some of the confusion with these previous datasets.

We also obtained bulk compositional data for fine-grained matrix in the three chondrites studied. These data could potentially help to address fundamental questions that are important for chondrule formation models – for example, whether chondrules and matrix formed in the same or in different regions of the solar nebula.

It is extremely important to study the least processed chondrites in order to avoid ambiguity in the data sets (see also Huss et al. 2005). For that reason, we first address how parent body processes (i.e., thermal metamorphism, aqueous alteration) and/or terrestrial alteration may have modified the primary nebular record in the chondrites included in this study.

Effects of secondary alteration on mineralogy and bulk composition of chondrules

Thermal metamorphism

MET 00426 (CR3.0) is one of the few most pristine chondrites found to date (Abreu 2007; Abreu and Brearley, Forthcoming) and MET 00526 (L3.05) has not been metamorphosed significantly (Grossman and Brearley 2005). However, we need to carefully consider possible effects of thermal metamorphism that may have affected our Kainsaz data. Based on petrographic and mineralogic characteristics, Kainsaz was first classified as a petrologic type 3.1 (Scott and Jones 1990) and later as 3.2 (e.g., Chizmadia et al. 2002; Grossman and Brearley 2005). In contrast, a study of the structural grade of organic matter in Kainsaz by Bonal et al. (2007) resulted in a classification as petrologic type 3.6.

As a result of thermal metamorphism, many type I chondrule olivines in Kainsaz have developed compositional zoning with thin FeO-rich rims (e.g., **Fig. 1.1e**) due to Fe-Mg exchange with the surrounding FeO-rich matrix (e.g., Scott and Jones 1990). Iron-magnesium diffusion is much faster in olivine than in pyroxene (e.g., Freer 1981), but to be cautious we used the olivine and low-Ca pyroxene compositions with the lowest measured Fa and Fs contents, instead of average compositions, for calculating the bulk compositions of type I chondrules in Kainsaz. **Figure 1.3c** indicates that even the lowest measured Fa contents in Kainsaz type I chondrule olivines are probably somewhat higher than their original Fa contents before thermal metamorphism occurred, because Kainsaz type I chondrules do not plot on the 1:1 line like type I chondrules in the other two more pristine chondrites (**Fig. 1.3a,b**). However, this does not seem to have much of an effect when the FeO contents of the silicate portion are calculated, as the FeO contents of Kainsaz type I chondrules are not significantly higher than those of type I chondrules in

MET 00526 and MET 00426 (**Fig. 1.12f** vs. **Fig. 1.12b,d**). Therefore, we feel confident that our bulk compositional data for Kainsaz type I chondrules are fairly close to their initial compositions (with respect to Fe and Mg) before thermal metamorphism occurred.

Iron-magnesium exchange between type II chondrule olivines and matrix in Kainsaz was probably not very significant, assuming that the initial Fa contents of matrix olivines in Kainsaz were comparable to those found in ALHA 77307 (CO3.0), which mainly range from Fa_{18} to Fa_{72} (Brearley 1993). However, an issue of concern for type II bulk chondrule compositions in Kainsaz is the behavior of Cr during thermal metamorphism. At the onset of thermal metamorphism (petrologic type 3.0 to 3.2), Cr contents of olivine decrease significantly due to the exsolution of a Cr-rich phase, probably chromite (Jones and Lofgren 1993; Grossman and Brearley 2005). Cr_2O_3 contents in type II chondrule olivines in Kainsaz are much lower (mostly below 0.2 wt% Cr_2O_3; **Fig. 1.6f**) than in more primitive CO chondrites like ALHA 77307 (0.2–0.6 wt% Cr_2O_3, Grossman and Brearley 2005) indicating secondary chromite crystallization. It is nearly impossible to obtain reasonably good EMP analyses on the exsolved chromites at the edges of olivine grains. Therefore, it is likely that we underestimated the bulk Cr contents in some of the type II chondrules in Kainsaz – probably in chondrules K1-Ch8, K1-Ch16, K2-Ch4 and K2-Ch7, which show the lowest bulk Cr contents in **Figure 1.11f**. Chondrule K1-Ch7 has the highest bulk Cr content of all the type II chondrules studied in Kainsaz, which can be related to the fact that several chromite grains are exposed in the thin section. These chromite grains seem to have crystallized from the chondrule melt rather than being the product of thermal metamorphism.

Phosphorus contents of kamacite in Kainsaz type I chondrules are below the EMP detection limit of 0.04 wt%, which is consistent with the findings by Scott and Jones (1990) for other metamorphosed CO chondrites. Only kamacite in the very least metamorphosed CO chondrites contains high levels of P (0.23 wt% P in CO3.0 chondrite ALHA 77307: Scott and Jones 1990). It is known from observations in other chondrite groups, that P leaves the metal during the onset of thermal metamorphism to form larger phosphate grains (>20 μm), which are observed in the matrix of chondrites with petrologic types higher than 3.5 (e.g., Huss et al. 2006). However, Lauretta et al. (2001) and Lauretta and Buseck (2003) observed tiny grains (≤3 μm) of maricite ($FeNaPO_4$) at

the edges of kamacite grains and other phosphates with variable compositions as thin rims around metal grains in Bishunpur (LL3.1) type I chondrules. Similar observations were made by Rubin and Grossman (1985). Because we did not obtain WDS element maps for P, we might have missed accessory phosphate phases. Hence, our bulk P contents for CO type I chondrules may be a bit low (**Fig. 1.11e**). Other effects that might be related to thermal metamorphism in Kainsaz are discussed along with the data below.

Aqueous alteration

Most CR chondrites found to date are highly aqueously altered (Weisberg et al. 1993a; Weisberg et al. 1995; Krot et al. 2002; Weisberg and Huber 2007). However, MET 00426 has been recognized as one of the most pristine CR chondrites (petrologic type 3.0). Its fine-grained matrix mainly consists of amorphous material and nano-sulfides (Abreu 2007; Abreu and Brearley, Forthcoming). Minerals indicative of aqueous alteration which are characteristic for other CR chondrites (e.g., Renazzo, Al Rais), such as phyllosilicates, calcite and magnetite are very rare in MET 00426 (Abreu 2007; Abreu and Brearley, Forthcoming). The mesostasis glass in type IIA chondrules in MET 00426 (CR) has high Na_2O and K_2O contents (**Fig. 1.9d**), further suggesting that aqueous alteration must have been very limited, as these elements would easily be mobilized and enter the matrix (Burger 2005).

All of the type I chondrules we studied in MET 00426 have unaltered mesostasis that is clear and glassy. In several chondrules we found that the glass is more Na- and Si-rich (sometimes also more K- and Mn-rich) towards the chondrule edges (**Fig. 1.8a**). This is very similar to what has been observed in some Semarkona type I chondrules (e.g., Matsunami et al. 1993; Grossman et al. 2002; Libourel et al. 2006; Nagahara et al. 2008) as well as in other CR chondrites (e.g., Libourel et al. 2006). However, currently there is no consensus whether these compositional trends are due to aqueous alteration on the parent asteroid (Grossman et al. 2002), recondensation of elements lost during chondrule formation (e.g., Matsunami et al. 1993; Nagahara et al. 2008) or gas-melt interactions (e.g., Libourel et al. 2006). This is discussed further below.

Evidence for aqueous alteration has also been described in low petrologic type ordinary chondrites (e.g., Hutchison et al. 1987; Alexander et al. 1989a; Sears et al. 1995;

Grossman et al. 2000), but currently nothing is known about aqueous alteration in MET 00526 (L). Some of the Fe,Ni metal in MET 00526 (L) has been replaced by magnetite, which suggests that minor aqueous alteration occurred on the parent asteroid (e.g., Krot et al. 1997; Choi et al. 1998). Nevertheless, the fact that chondrule mesostases are unaltered and that Na_2O and K_2O contents are high in type IIA chondrule mesostases (**Fig. 1.9b**) indicates that aqueous alteration must have been very minor in MET 00526 (L).

Terrestrial weathering (MET 00426 [CR3.0] and MET 00526 [L3.05])

MET 00426 (CR) and MET 00526 (L) are Antarctic meteorites and experienced some terrestrial weathering. The presence of terrestrial water and/or ice affects Fe,Ni metal first as it is oxidized, hydrated and partially replaced by Fe oxides and Fe hydroxides (e.g., Ikeda and Kojima 1991; Lee and Bland 2004). Such reddish-brown alteration products occur around metal grains and as veins along grain boundaries, cracks and fractures in both MET 00426 and MET 00526. However, they seem to be slightly more common in MET 00526 (L) than in MET 00426 (CR), supporting the higher degree of terrestrial weathering B/C that has been assigned to MET 00526 (Connolly et al. 2007b), compared to grade B assigned to MET 00426 (Russell et al. 2002).

Areas in MET 00426 (CR) and MET 00526 (L) chondrules that are occupied by alteration products were counted as kamacite when determining bulk chondrule compositions, because terrestrial alteration is much faster for kamacite than for taenite (e.g., Ikeda and Kojima 1991). Areas occupied by larger veins of Fe hydroxides were excluded and not taken into account for bulk chondrule compositions.

Comparison of chondrules with the same texture in different chondrite groups

Chondrules in CO chondrites are much smaller (mean diameter 0.15 mm) than chondrules in CR (0.7 mm) and ordinary (0.3 – 0.9 mm) chondrites (e.g., Brearley and Jones 1998), but they show the same general characteristics and textural types. Currently, there are only very few studies/reviews available in the literature describing the similarities and differences of chondrules in different chondrite groups or comparing their compositional diversity (e.g., Scott and Taylor 1983; Grossman and Wasson 1983a;

Grossman et al. 1988; Jones et al. 2005). Many datasets reviewed in these publications are compromised by varying degrees of secondary processing. Chondrules from CR chondrites have not yet been compared comprehensively to those in other chondrite groups, probably because most CR chondrites are typically highly aqueously altered (e.g., Weisberg et al. 1993a, 1995; Krot et al. 2002). Unaltered type 3 CR chondrites have only been recognized very recently (Weisberg 2001; Abreu 2007; Abreu and Brearley, Forthcoming).

Table 1.1 shows the relative proportions of textural types of the chondrules selected for detailed analysis in MET 00526 (L), MET 00426 (CR) and Kainsaz (CO) compared to the observed relative proportions in their respective chondrite groups. FeO-poor porphyritic (type I) chondrules are the most common chondrule type in all three chondrite groups (**Table 1.1**). FeO-rich porphyritic (type II) chondrules are most abundant in ordinary chondrites (10-50%; Grossman et al. 1988), much less abundant in CO chondrites (3%; Grossman et al. 1988) and rare in CR chondrites (<1%; Weisberg et al. 1993a). We selected a higher than representative proportion of type II chondrules in Kainsaz (CO) and MET 00426 (CR), so that we had sufficient information on this type of chondrules.

FeO-poor porphyritic (type I) chondrules

Textural characteristics

Scott and Taylor (1983) observed that type I chondrules in CO, CM, CV and type 3 ordinary chondrites are usually quite round, contain relatively small olivine crystals, abundant Fe,Ni metal and clear mesostasis. Scott and Taylor (1983) also described a textural continuum from type IA to IAB to IB chondrules, which is associated with an increase in the modal abundance of low-Ca pyroxene. In type IA chondrules, minor low-Ca pyroxene may be present as phenocrysts along the edges. In type IAB chondrules, low-Ca pyroxene often forms an outer layer, poikilitically enclosing olivines (see **Fig. 1.1**). In type IB chondrules, olivine is often only present as small chadacrysts that show resorbed edges. Type I chondrules in CR chondrites exhibit the same general features, but tend to show more layering with olivine and mesostasis in the core, an outer layer of low-

Ca pyroxene, and a continuous or discontinuous layer of metal grains (e.g., Weisberg et al. 1993a). In the more pristine CR chondrites, silica-rich outer layers may be present as well, while the absence of silica rims in aqueously altered CR chondrites could be the result of its replacement by phyllosilicates (e.g., Krot et al. 2002). Our dataset for MET 00426 (CR3.0) includes two type I chondrules with a silica-rich outer layer (CR-Ch10 and CR-Ch19) and a type I chondrule that contains silica in the interior (CR-Ch18).

Olivine and pyroxene

The minor element chemistry of olivine, low-Ca pyroxene and Ca-rich pyroxene in type I chondrules is essentially very similar in MET 00526 (L), MET 00426 (CR) and Kainsaz (CO). One exception is Cr_2O_3 in olivine, which is lower in type I chondrules in Kainsaz (CO3.2) (**Fig. 1.6e**) than in MET 00526 (L3.05) (**Fig. 1.6a**) and MET 00426 (CR3.0) (**Fig. 1.6c**). It is likely that this is an effect related to thermal metamorphism as discussed for type II chondrules above (e.g., Brearley and Jones 1998).

Experimental studies predict a positive correlation between CaO and FeO in forsteritic olivine that crystallized from a melt (e.g., Jurewicz and Watson 1988; Libourel 1999; Pack and Palme 2003). However, a negative correlation has been observed in type I chondrule olivine in CO, CM, CV and ordinary chondrites (e.g., McSween 1977c; Scott and Taylor 1983; Jones and Scott 1989; Jones 1992; Scott et al. 1994) and its origin remains enigmatic (e.g., Jones and Scott 1989; Libourel 1999; Pack and Palme 2003). Our data for type I chondrule olivines also show negative correlations between CaO and FeO (**Fig. 1.5a,c,e**), although the trend is quite shallow in the MET 00426 (CR) data (**Fig. 1.5c**).

Mesostasis

Mesostasis compositions of type I chondrules show negative trends in Al_2O_3 (wt%) vs. SiO_2 (wt%) and CaO (wt%) vs. SiO_2 (wt%) diagrams (**Fig. 1.7a,c**), consistent with previously published data (e.g., Brearley and Jones 1998). Our data for Kainsaz (CO), MET 00426 (CR) and MET 00526 (L) type I chondrule mesostases show significant overlap in such diagrams (**Fig. 1.7a,c**), indicating a similar crystallization history.

Mesostasis in most of the type I chondrules in MET 00526 (L) and Kainsaz (CO) has low K and variable Na contents (**Fig. 1.9a,c,e**), as is typical for type I chondrules in ordinary and carbonaceous chondrites (e.g., Hewins 1991; Grossman and Brearley 2005). In contrast, mesostasis in type I chondrules in the CR chondrite MET 00426 frequently shows two different compositions (**Figs. 1.8a** and **1.9c**) with one having higher than typical abundances of volatiles (Na, K, Mn, Si). This 2nd glass is located in the outer parts of the chondrules, whereas the glass located in the center is more Ca- and Al-rich. A few chondrules in the L chondrite MET 00526 show similar features, but the 2nd glass is not as volatile-rich as in the CR chondrules (**Figs. 1.8a,b** and **1.9a,c**).

Several authors have made observations comparable to ours in mesostasis glass in type I chondrules in Semarkona (Matsunami et al. 1993; Grossman et al. 2002; Libourel et al. 2006; Nagahara et al. 2008) and in CR2 chondrites (Libourel et al. 2006), although compositional zoning was observed rather than two distinct glass compositions. Libourel et al. (2006) argued that the zoning was caused by gas-melt interactions as the chondrules cooled in the nebula. On the other hand, Grossman et al. (2002) suggested that both high- and low-temperature processes were involved in the formation of zoned chondrules and presented evidence (from H_2O contents and D/H ratios) that hydration of chondrule glass during aqueous alteration on the parent asteroid must have played a major role in producing zoning in the mesostasis. The CR2 chondrites studied by Libourel et al. (2006) experienced aqueous alteration on their parent body (e.g., Weisberg et al. 1993a, 1995; Krot et al. 2002), as did Semarkona (e.g., Alexander et al. 1989a; Grossman et al. 2000). The CR chondrite we studied (MET 00426) is one of the most pristine CR chondrites (CR3.0) found to date. In fact, MET 00426 is much less altered than Semarkona (Abreu 2007; Abreu and Brearley, Forthcoming). Of all the meteorites in which compositional trends have been observed in type I chondrule mesostasis, MET 00426 is the most pristine and therefore, the origin of the different glass compositions is more likely nebular than a product of secondary asteroidal alteration.

Metal and sulfides

Ni and Co contents of Fe,Ni metal in type I chondrules in MET 00426 (CR) lie along the CI line (**Fig. 1.10a**), which is consistent with previous studies of metal in CR

chondrites (e.g., Weisberg et al. 1993a; Weisberg et al. 1995; Connolly et al. 2001). The precursor material of CR type I chondrules probably contained metal grains that were the product of direct condensation from a gas of solar bulk composition (Weisberg et al. 1993a, 1995; Krot et al. 2002), so that the metal that crystallized from the chondrule melt retained the solar Co/Ni ratios.

The lower Ni contents of kamacite in MET 00526 (L) and Kainsaz (CO) type I chondrules and the higher Co contents of kamacite in Kainsaz (CO) type I chondrules (**Fig. 1.10a**) are more difficult to explain. Rambaldi and Wasson (1984) observed similarly low Ni contents (~2-4 wt%) in kamacite in Krymka (LL) and Chainpur (LL) chondrules and suggested that such (originally CI-like) kamacite may have been diluted by Fe reduced from the silicates during chondrule formation. However, type I chondrule silicates in MET 00526 (L) and Kainsaz (CO) do not show evidence for reduction. The higher Co contents of the kamacite in Kainsaz (CO) type I chondrules can probably be attributed to thermal metamorphism (e.g., McSween 1977b; Scott and Jones 1990).

We did not observe sulfides in our CR type I chondrules, consistent with Krot et al. (2002). Type I chondrules in MET 00426 (CR3.0) also do not contain any taenite. In contrast, type I chondrules in Kainsaz (CO) contain abundant taenite, troilite and/or monosulfide solid solution (MSS). In MET 00526 (L) type I chondrules, taenite and troilite/MSS are present but are much less abundant than in Kainsaz type I chondrules, probably because they have been affected by terrestrial alteration. Thermodynamic equilibrium calculations predict taenite-FeS assemblages for sulfidization of kamacite at temperatures below 710 K (e.g., Kerridge 1979), but experimental studies have shown that pentlandite and other phases, which we did not observe in Kainsaz and MET 00526 type I chondrules, should also form (e.g., Lauretta et al. 1998). However, the sulfides present in Kainsaz (CO) and MET 00526 (L) type I chondrules could also be primary as they may have crystallized from the chondrule melts (e.g., Rubin et al. 1999). If this were the case, sulfides would have been present in the precursor material of these chondrules. Sulfur isotope studies (e.g., Tachibana and Huss 2005), analyses of rare earth elements (e.g., Kong et al. 2000) and/or other minor and trace elements (e.g., Donnelly and Brearley 2007) would be needed in order to better constrain the origin of sulfides in CO and L type I chondrules. Yu et al. (1996) showed that very short heating times (a minute

or less), high initial cooling rates (at least 5000ºC/hr) and oxygen fugacities near the IW buffer are needed in order to avoid S loss during the chondrule-forming event.

The fact that mesostasis glass in the center of MET 00426 (CR) type I chondrules contains measurable S contents (0.01 to 0.1 wt%) could indicate that sulfides were present in the precursor material of CR type I chondrules, but were volatilized during the chondrule formation process. On the other hand, S could have condensed into the glass along with other volatiles as mentioned above.

Bulk chondrule compositions

Type I chondrules studied in MET 00526 (L), MET 00426 (CR) and Kainsaz (CO) share the common characteristic feature that their silicate portions have very similar FeO, MgO and SiO_2 contents (**Fig. 1.12b,d,f**). However, there are also significant differences in the bulk compositions of type I chondrules in these meteorites. **Figure 1.13** shows Ni/Fe versus S/Fe (element wt% ratios) for bulk compositions of type I chondrules in MET 00526 (L), MET 00426 (CR) and Kainsaz (CO). Because CR type I chondrules contain very little sulfur, they have S/Fe ratios close to zero and do not contain any sulfides. The variable Ni/Fe and S/Fe ratios of CO type I chondrules are probably related to different modal abundances of kamacite, taenite and troilite/MSS. L type I chondrules tend to have lower Ni/Fe ratios than most CO type I chondrules.

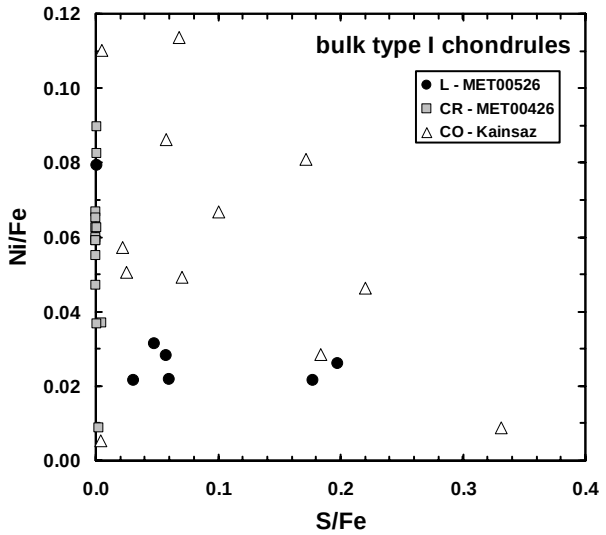

Fig. 1.13. Ni/Fe versus S/Fe (element wt% ratios) for bulk chondrule compositions of type I chondrules in MET 00526 (L), MET 00426 (CR) and Kainsaz (CO).

Another major difference can be found in the bulk chondrule K and Na abundances shown in **Figure 1.14**. Most MET 00526 (L) and MET 00426 (CR) type I chondrules have K/Na ratios that vary around the solar ratio, while Kainsaz (CO) type I chondrules have variable Na but a more limited range of K contents. It is not clear, whether the low K contents of Kainsaz type I chondrules are a primary feature or if they are related to thermal metamorphism.

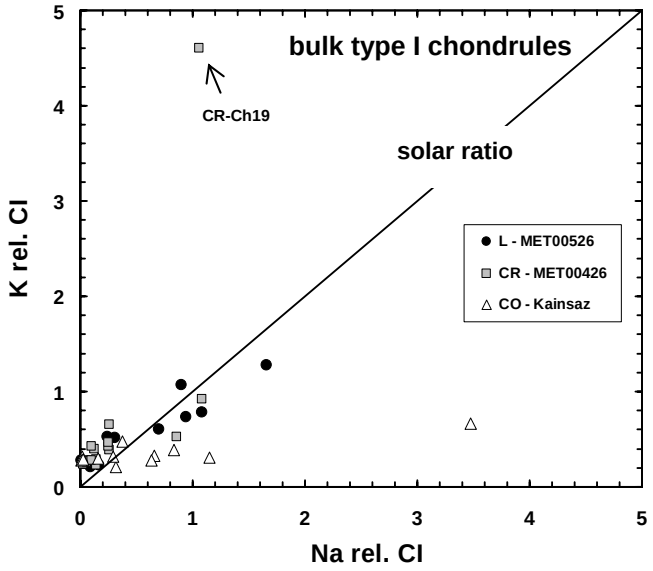

Fig. 1.14. K versus Na (CI-normalized) for bulk chondrule compositions of type I chondrules in MET 00526 (L), MET 00426 (CR) and Kainsaz (CO).

In conclusion, silicates in type I chondrules in MET 00526 (L), MET 00426 (CR) and Kainsaz (CO) show similar minor element chemistry. Major differences can be found in the minor element chemistry of Fe,Ni metal and in the absence of sulfides and taenite in MET 00426 (CR) type I chondrules. The latter also frequently show a 2nd mesostasis glass that is rich in volatile elements (Na, K, Mn and Si).

FeO-rich porphyritic (type II) chondrules

Textural characteristics

Type II chondrules in CO, CM, CV and type 3 ordinary chondrites tend to have irregular shapes and consist of euhedral olivine crystals (that are typically strongly zoned), microcrystalline mesostasis and rare Fe,Ni metal (e.g., Scott and Taylor 1983). The same is true for type II chondrules in CR chondrites, although Weisberg et al. (1993a) and Schrader et al. (2008) found that they are rather fragments than whole chondrules. For Semarkona (LL3.0), Jones (1990, 1996a) described a textural continuum from type IIA to IIAB to IIB chondrules, representing an increase in the modal abundance of low-Ca pyroxene. Low-Ca pyroxene is typically not observed around the edges as in type I chondrules, but rather as large phenocrysts in the interior of type II chondrules (e.g., Jones 1996a). Poikilitic olivine enclosed in pyroxene is rare in type II chondrules (e.g., Jones 1996a). Our observations for type II chondrules in MET 00526 (L3.05), MET 00426 (CR3.0) and Kainsaz (CO3.2) are consistent with these previous studies.

Olivine and pyroxene

One significant difference between type II chondrules in CO, CR and UOC is the mean Fa content of olivine, which decreases in the order CO > CR > UOC (**Fig. 1.3**). Positive correlations between MnO (wt%) and FeO (wt%) have been observed previously in type II chondrule olivine in primitive chondrites (e.g., McSween 1977a,c; Brearley and Jones 1998). However, we noticed that the slopes of the trends (compare **Fig. 1.4b, d** and **f**) are actually significantly different for type IIA chondrule olivine in MET 00526 (L), MET 00426 (CR) and Kainsaz (CO). These Fe-Mn trends in type IIA chondrule olivine and possible explanations for the different slopes observed in unequilibrated ordinary, CR and CO chondrites are the focus of Chapter 2 of this thesis. Fe-Mn trends in olivine are more robust than Fe-Ca and Fe-Cr trends. Although these frequently also show positive trends in type IIA chondrule olivine (e.g., **Fig. 1.5b,d** and **Fig. 1.6b,d**), they are more easily disturbed by thermal metamorphism, as observed in the Kainsaz data (**Fig. 1.5f** and **Fig. 1.6f**). Cr_2O_3 contents in type IIA olivine are also affected by the onset of chromite

crystallization (e.g., Jones 1990), which explains the drop in Cr_2O_3 contents at higher FeO contents (i.e., at the edges of the grains) in **Figures 1.6b** and **1.6d**. It is likely that Fe-Ca and Fe-Cr trends would show similar differences in slope as the Fe-Mn trends in type IIA olivine in L, CR and CO, if these trends were not disturbed by secondary overprints.

The type IIAB chondrules we encountered in Kainsaz (K1-Ch15) and MET 00426 (CR-Ch4) are rather atypical (refer to supplementary xls-files), so that a reasonable comparison to the more characteristic type IIAB chondrules found in MET 00526 (L) is not appropriate. However, the four type IIAB chondrules in MET 00526 (L) show many similarities to the porphyritic pyroxene chondrules described by Jones (1996a) in Semarkona (LL). We also observed four pyroxene minerals (clinoenstatite, orthorhombic enstatite, pigeonite, augite) and complex zoning features.

Mesostasis

In contrast to type I chondrules discussed above, mesostasis compositions in CO, CR and UOC type II chondrules tend to occupy different regions with only little overlap in the Al_2O_3 (wt%) vs. SiO_2 (wt%) and CaO (wt%) vs. SiO_2 (wt%) diagrams shown in **Figure 1.7b,d**. This is probably related to differences observed in bulk chondrule Si contents, as further discussed in Chapter 2 of this thesis for CO, CR and UOC type IIA chondrules.

Type II chondrules typically have mesostasis compositions with higher K_2O and Na_2O contents than type I chondrules (e.g., Hewins 1991; Grossman and Brearley 2005). **Figure 1.9** shows that this is true for mesostasis in type IIA chondrules in MET 00526 (L) and MET 00426 (CR) and some type IIAB chondrules in MET 00526 (L). However, K_2O contents in Kainsaz type IIA and type IIAB chondrule mesostasis (**Fig. 1.9f**) are low and comparable with those observed in Kainsaz type I chondrule mesostasis (**Fig. 1.9e**). It is not clear whether this is a primary or secondary feature.

Metal and sulfides

The modal abundance of opaque phases in type II chondrules in Kainsaz (CO), MET 00426 (CR) and MET 00526 (L) is mostly below 3 vol%. Our limited number of metal analyses in type II chondrules (**Fig. 1.10b**) show, that kamacite grains in Kainsaz type II chondrules tend to have higher Co contents than those in MET 00426 (CR) and MET 00526 (L) type II chondrules. This can probably be attributed to thermal metamorphism (e.g., McSween 1977b; Scott and Jones 1990).

Bulk chondrule compositions

FeO contents of the silicate portion of the type II chondrules studied show a comparable trend to that observed for average Fa contents of type II chondrule olivines, being highest in Kainsaz (CO) (**Fig. 1.12f**), intermediate in MET 00426 (CR) (**Fig. 1.12d**) and lowest in MET 00526 (L) (**Fig. 1.12b**). This general trend is also observed in the bulk Fe content of type II chondrule compositions (**Fig. 1.12a,c,e**) as the modal abundances of opaque minerals are so low.

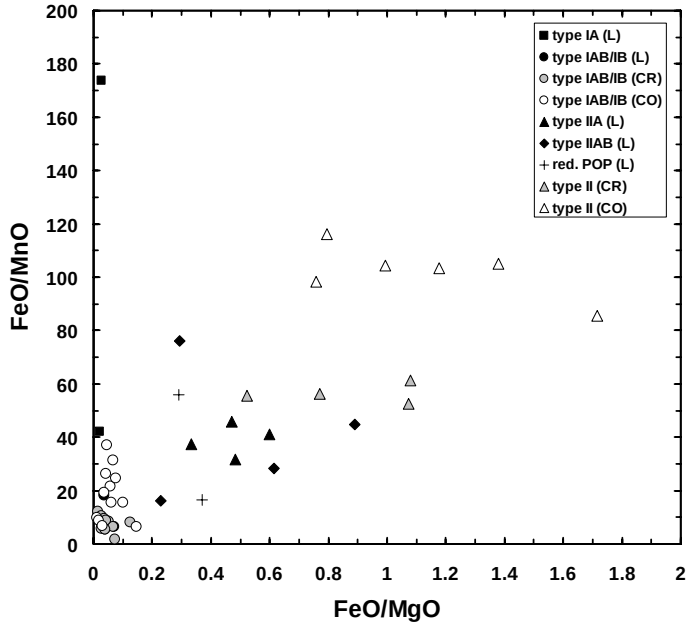

Fig. 1.15. FeO/MnO versus FeO/MgO (oxide wt% ratios) for the silicate portion of type I and type II chondrules in MET 00526 (L), MET 00426 (CR) and Kainsaz (CO). FeO/MnO ratios of type II chondrules (triangles) show a decrease in the order CO>CR>L, which is consistent with the Fe-Mn trends we observed in type II olivine shown in Figure 1.4b,d,f. The two type IA chondrules (black squares) in MET 00526 (L) show the lowest bulk Mn contents which is reflected in their high FeO/MnO ratios.

The bulk compositions of type II chondrules in MET 00526 (L), MET 00426 (CR) and Kainsaz (CO) also reflect the different Fe-Mn trends we observed in type II olivine (**Fig. 1.4b,d,f**). This is shown in **Figure 1.15**, where FeO/MnO versus FeO/MgO (oxide wt% ratios) is plotted for the silicate portions of type II chondrules (as well as of type I chondrules for comparison). FeO/MnO ratios are high in CO type IIA chondrules, intermediate in CR type IIA chondrules and low in L type IIA chondrules, while most type I chondrules cluster around the origin of this diagram.

Bulk K and Na abundances of type II chondrules are shown (relative to CI chondrites) in **Figure 1.16**. Most MET 00526 (L) and MET 00426 (CR) type II chondrules have K contents higher than solar while most Kainsaz (CO) type II chondrules have K contents lower than solar. This is reflected in the mesostasis compositions (**Fig. 1.9b,d,f**) and, as mentioned above, it is not clear whether the low K contents of Kainsaz type II chondrules are a primary feature or if they are related to thermal metamorphism.

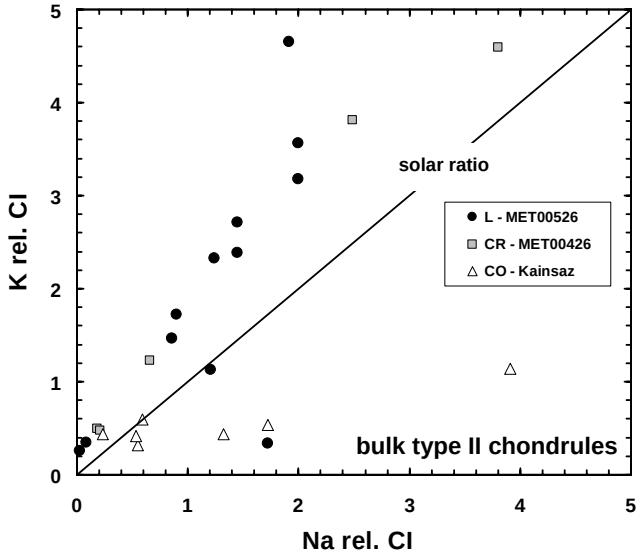

Fig. 1.16. K versus Na (CI-normalized) for bulk chondrule compositions of type II chondrules in MET 00526 (L), MET 00426 (CR) and Kainsaz (CO).

A major conclusion of our work is that type II chondrules in MET 00526 (L), MET 00426 (CR) and Kainsaz (CO) show systematic differences in bulk FeO, MgO and MnO contents that are reflected in their olivine compositions.

Barred olivine (BO) chondrules

The peculiar textures of barred olivine chondrules have promoted several analytical and experimental studies to investigate their properties and formation conditions (e.g., Weisberg 1986, 1987; Lofgren and Lanier 1990; Tsuchiyama et al. 2004; Varela et al. 2006). In experimental studies, BO textures develop when the crystalline precursor is melted at a higher initial temperature than for a PO texture, very close to or slightly above the liquidus, to obtain very few nuclei – ideally only one (e.g., Lofgren and Lanier 1990). Weisberg (1987) suggested that development of the barred olivine texture might be in part controlled by composition, because he found that BO chondrules in ordinary chondrites are enriched in Al_2O_3, Na_2O and K_2O compared to other types of ferromagnesian chondrules. He also observed no significant differences in the average bulk compositions of BO chondrules in type 3 H, L and LL chondrites. Lofgren and Lanier (1990) performed experiments using a starting composition similar to that of Weisberg's (1987) average L3 BO chondrule composition (given in **Table 1.9**) and found that this composition produces BO textures over a greater range of melting temperatures and a wider variation of cooling conditions than others. However, in general, experimental studies have shown that barred textures can be produced over a wide range of compositions – the only restriction is that olivine needs to be on the liquidus (e.g., Tsuchiyama et al. 1980; Lofgren and Lanier 1990; Hewins and Radomsky 1990; Tsuchiyama et al. 2004).

Our study included two FeO-poor and two FeO-rich chondrules that show barred textures (**Fig. 1.2i,j,k,l** and **Fig. 1.12**), one of each in the L chondrite MET 00526 and the CR chondrite MET 00426. The bulk compositions of the silicate portions of these chondrules are shown in **Table 1.9**, compared to bulk compositions of porphyritic chondrules and published data for BO chondrules in ordinary chondrites (Lux et al. 1981; Weisberg 1987) and in Allende (Simon and Haggerty 1980). Our barred olivine chondrule compositions all have lower bulk Al_2O_3 contents than the average BO chondrule compositions determined by Simon and Haggerty (1980) in Allende, by Lux et al. (1981) in H3 chondrites and by Weisberg (1987) in ordinary chondrites. Lux et al. (1981) and Weisberg (1987) obtained their bulk chondrule compositions via defocused beam analyses (DBA) without applying a density correction. Therefore, we suspect that

Table 1.9. Bulk compositions of barred olivine (BO) chondrules compared to porphyritic chondrules and literature data.

	FeO-poor					FeO-rich					
reference	BO[a] (L-Ch1) this study[b]	IA (L-Ch13) this study[b]	BO (CR-Ch11) this study[b]	IAB (CR) this study[b]	BO (Allende) S&H (1980)[d]	BO (H3) Lux et al. (1981)	BO (L3) Weisberg (1987)	BO (L-Ch19) this study[b]	IIAB (L) this study[b]	IIA-BO (CR-Ch16) this study[b]	IIA (CR) this study[b]
method	MRA	MRA	MRA	MRA	MRA	DBA	DBA	MRA	MRA	MRA	MRA
number of chondrules	1	1	1	12[c]	5	7	29	1	4	1	2
SiO_2	45.7	44.0	47.6	51.9	43.9	46.4	45.6	51.2	50.4	43.7	40.1
TiO_2	0.24	0.18	0.19	0.18	0.45	0.26	0.19	0.12	0.10	0.10	0.08
Al_2O_3	4.8	3.9	3.9	4.6	9.1	6.7	5.9	2.7	2.3	2.2	1.7
Cr_2O_3	0.36	0.17	0.56	0.60	0.24	0.3	0.52	0.48	0.64	1.2	0.46
FeO	0.70	1.0	2.0	1.5	2.8	8.4	16.1	14.0	14.3	25.0	23.4
MnO	0.07	<0.03	0.15	0.20	0.09	0.19	0.47	0.65	0.42	0.48	0.40
MgO	43.9	47.0	41.3	36.8	37.5	29.5	26.4	29.0	29.5	23.2	31.6
CaO	4.0	4.1	4.1	3.8	5.5	2.4	2.2	0.80	2.0	1.2	1.2
Na_2O	0.30	0.13	0.07	0.21	1.7	3.0	2.2	1.5	0.97	2.6	1.1
K_2O	<0.03	<0.03	<0.03	<0.03	0.15	0.48	0.35	0.34	0.11	0.29	0.17
NiO	<0.04	<0.04	<0.04	<0.04	n.a.	n.a.	n.a.	0.11	<0.04	<0.04	<0.04
P_2O_5	<0.05	<0.05	<0.05	<0.05	n.a.	0.08	n.a.	<0.05	<0.05	0.28	0.25
SO_3	<0.05	<0.05	<0.05	<0.05	n.a.	n.a.	n.a.	<0.05	<0.05	0.11	<0.05
Total	100.2	100.7	99.9	99.9	101.3	97.7	100.0	100.9	100.8	100.3	100.5

[a]Compound chondrule. This composition is for the part with barred texture only (olivine plus mesostasis in between the bars).
[b]Given bulk chondrule composition corresponds to silicate portion only.
[c]The average composition for CR type IAB chondrules does not include the atypical chondrule CR-Ch19.
[d]S&H (1980) = Simon and Haggerty (1980)

the high Al_2O_3, Na_2O and K_2O contents they report might be an artifact of their analytical method (refer to Appendix A). On the other hand, Simon and Haggerty (1980) obtained their bulk compositions via modal recombination analysis (MRA) and included phase densities, but their Al_2O_3 contents are even higher. However, they also mention that the Allende BO chondrules they studied have high modal proportions of mesostasis. This could be a 2D cutting effect, but provides a simple explanation for the high Al_2O_3 contents.

As can be seen in **Table 1.9**, the bulk compositions of our two FeO-poor BO chondrules, L-Ch1 in MET 00526 (**Fig. 1.2i**) and CR-Ch11 in MET 00426 (**Fig. 1.2l**), are very similar to those of type IA and type IAB chondrules. [Chondrule L-Ch1 (**Fig. 1.2i**) is actually a compound chondrule, but the bulk composition given in **Table 1.9** is only for the olivine bars plus mesostasis in between the bars.] Also, the bulk composition of the FeO-rich BO chondrule L-Ch19 (**Fig. 1.2j**) is very similar to the average type IIAB composition measured in MET 00526 (L) and the bulk composition of the FeO-rich chondrule CR-Ch16, which is texturally intermediate between porphyritic and barred (**Fig. 1.2k**), does not differ much from the average type IIA composition in MET 00426 (CR). Since bulk compositions of our BO chondrules are very similar to those of porphyritic chondrules and we observe FeO-poor as well as FeO-rich compositional extremes (see also **Fig. 1.12**), these observations support the results of experimental studies that show that barred textures can be produced over a wide range of compositions and simply require higher initial temperatures than porphyritic chondrules (e.g., Tsuchiyama et al. 1980; Hewins and Radomsky 1990; Lofgren and Lanier 1990; Tsuchiyama et al. 2004).

The two FeO-rich BO chondrules have lower Al_2O_3, CaO and TiO_2 contents, but higher Na_2O, K_2O and MnO contents than the two FeO-poor BO chondrules. This agrees well with an observation by Matsuda et al. (1990), who showed that BO chondrules in Allende exhibit a positive correlation between the Fa content of olivine and bulk K contents. Lux et al. (1981) and Weisberg (1987) did not distinguish between FeO-poor and FeO-rich BO chondrules in their studies, therefore, their average BO chondrule compositions given in **Table 1.9** include both. Weisberg (1987) did not find very many FeO-poor BO chondrules in type 3 H, L and LL chondrites (6 out of 62), which is why

their average composition has a much higher FeO content than the one by Lux et al. (1981). FeO-poor BO chondrules seem to be more common in CV3 chondrites (e.g., Weisberg 1986) and the BO chondrules studied by Simon and Haggerty (1980) are all FeO-poor. When the average FeO-poor BO chondrule composition from Simon and Haggerty (1980) is compared to Weisberg's (1987) average composition of mostly FeO-rich BO chondrules (**Table 1.9**), the statement from above still holds true: the FeO-poor BO bulk composition has higher Al_2O_3, CaO and TiO_2 contents, but lower Na_2O, K_2O and MnO than the FeO-rich BO bulk composition.

Currently, it is difficult to say whether or not there might be a gap between FeO-poor and FeO-rich BO chondrules. The data obtained by Simon and Haggerty (1980), Lux et al. (1981) and Weisberg (1987) are somewhat compromised by secondary overprints, plus Lux et al. (1981) and Weisberg (1987) combined FeO-poor and FeO-rich BO chondrules to one average composition. There clearly is a wide gap in the FeO contents of our four BO chondrules ($Fa_{0.7}$ and $Fa_{2.3}$ versus Fa_{20} and Fa_{34}) in two of the most primitive chondrites, MET 00526 (L3.05) and MET 00426 (CR3.0), but more data are needed to verify whether this gap is real.

In conclusion, our FeO-poor and FeO-rich BO chondrules show significant differences in their refractory and volatile element contents (**Table 1.9**): the FeO-poor BO bulk compositions have higher Al_2O_3, CaO and TiO_2 contents, but lower Na_2O, K_2O and MnO than FeO-rich BO chondrules. The bulk compositions of our BO chondrules are very similar to those of porphyritic chondrules, which suggests that there is no preferred composition for the BO texture as proposed by Weisberg (1987).

Radial pyroxene (RP) chondrules

Experimental studies have shown that radial pyroxene (RP) chondrules, like BO chondrules, require complete, or nearly complete, melting of precursor dustballs (e.g., Hewins et al. 1981; Lofgren and Russell 1986). On the other hand, Engler et al. (2007) advocate that non-porphyritic pyroxene chondrules may have formed by liquid condensation, as has also been suggested for BO chondrules by Varela et al. (2006). Currently, there is a very limited number of studies available in the literature regarding the characteristics of RP chondrules (Nehru et al. 1988; Engler et al. 2007). Because they

seem to be texturally and compositionally gradational, these studies also include other completely molten chondrule types, such as cryptocrystalline and glassy textures (Nehru et al. 1988). Engler et al. (2007) preferred to distinguish between cryptocrystalline, granular, fibrous and platy textures.

We studied three RP chondrules (**Figs. 1.2m,n**,**o),** one in each of the three chondrites MET 00526 (L3.05), MET 00426 (CR3.0) and Kainsaz (CO3.2). Their bulk compositions (**Table 1.10**, **Fig. 1.12**) are very similar to an average RP composition published by Lux et al. (1981) for H3 chondrites. The RP chondrule in MET 00426 (CR-Ch17) contains silica and has a slightly higher bulk SiO_2 content (63.4 wt%) than the other two RP chondrules (57.2 and 57.6 wt%). In contrast to the BO chondrules discussed above, the bulk FeO contents of our RP chondrules show a very narrow range from 7.5 to 8.5 wt% (**Fig. 1.12b,d,f**). In comparison, the average RP composition by Lux et al. (1981) has 6.7 wt% FeO with one standard deviation of ±4.0 wt%. Bulk compositions published by Engler et al. (2007) for chondrules in Bishunpur (LL3.1) and Krymka (LL3.1) classified as fibrous or platy have FeO contents between 6.4 and 18.8 wt%. Overall, RP chondrules appear to show a more limited compositional range than BO chondrules.

Table 1.10. Bulk compositions (silicate portion) of radial pyroxene chondrules compared to literature data.

	MET 00526 L-Ch5	**MET 00426** CR-Ch17	**Kainsaz** K1-Ch19	**H3 (8 chondrules)** Lux et al. (1981)
SiO_2	57.2	63.4	57.6	55.9
TiO_2	0.10	0.06	0.06	0.10
Al_2O_3	1.7	1.1	1.3	1.9
Cr_2O_3	0.96	0.82	0.67	0.48
FeO	8.5	7.5	8.4	6.7
MnO	0.60	0.55	0.55	0.31
MgO	29.2	24.3	29.6	29.5
CaO	1.3	1.5	1.0	2.0
Na_2O	0.63	0.14	0.90	0.83
K_2O	0.10	<0.03	<0.03	0.13
NiO	<0.04	<0.04	<0.04	n.a.
P_2O_5	<0.05	<0.05	<0.05	0.04
SO_3	<0.05	<0.05	<0.05	n.a.
Total	100.4	99.4	100.1	97.9

Is there a genetic relationship between type I and type II chondrules?

Although type I and type II chondrules record significantly different oxidation states (e.g., review in Jones et al. 2005), it is intriguing that they both occur, though in different modal proportions, in ordinary and many types of carbonaceous chondrites. Scott and Taylor (1983) suggested that type I and type II chondrules may have formed in different regions of the nebula from somewhat different starting materials. On the other hand, Jones (1990) and Sears et al. (1996) proposed that, in ordinary chondrites, type I chondrule compositions could potentially have been derived from type II compositions by reduction, physical loss of metal and evaporation of volatile elements, including Si.

In order to address a potential genetic relationship between type I and type II chondrules, it is important to know how their bulk compositions compare. Several EMP datasets of bulk chondrule compositions available in the literature tend to suggest that type II chondrules are more Fe-rich than type I chondrules (e.g., McSween 1977a; Jones and Scott 1989; Jones 1990), so that physical loss of metal needs to be invoked in the model by Jones (1990) and Sears et al. (1996). However, we found that this is not necessarily true. Below, we first discuss the bulk Fe contents of type I and type II chondrules. Then, we address the question of whether type I and type II chondrules could be genetically related and could have formed within the same region of the solar nebula.

The bulk Fe content of type I and type II chondrules

Jones et al. (2005) recognized that available EMP and INAA datasets for bulk chondrule compositions show significant discrepancies, especially for the major element Fe. The situation is most extreme for CO chondrites. In **Figure 1.17**, the different datasets available in the literature for CO chondrules are shown for comparison with our data. We made an effort to distinguish between type I and type II compositions as this information was provided in the publications and/or in the supplementary materials. Bulk compositions of Ornans (CO3.4) and Kainsaz (CO3.2) chondrules studied by McSween (1977a) via EMP defocused beam analyses show two populations in a Fe-Mg-Si ternary (**Fig. 1.17a,c**) with a hiatus between type I (Fe-poor) and type II (Fe-rich) compositions, whereas data obtained via INAA by Rubin and Wasson (1988) for Ornans (CO3.4) type I

chondrules (**Fig. 1.17b**) have Fe contents similar to the type II bulk compositions determined by McSween (1977a). Rubin and Wasson's (1988) dataset contained only one FeO-rich chondrule (BO), which has the highest Fe content in this dataset. Our bulk chondrule data for Kainsaz type I chondrules (**Fig. 1.17d**) show a continuous trend from Fe-poor to Fe-rich compositions, with some type I compositions overlapping with type II compositions. In our dataset, the bulk Fe content of type I chondrules depends on the modal proportion of metal and sulfides exposed in the thin section, which will be further discussed below.

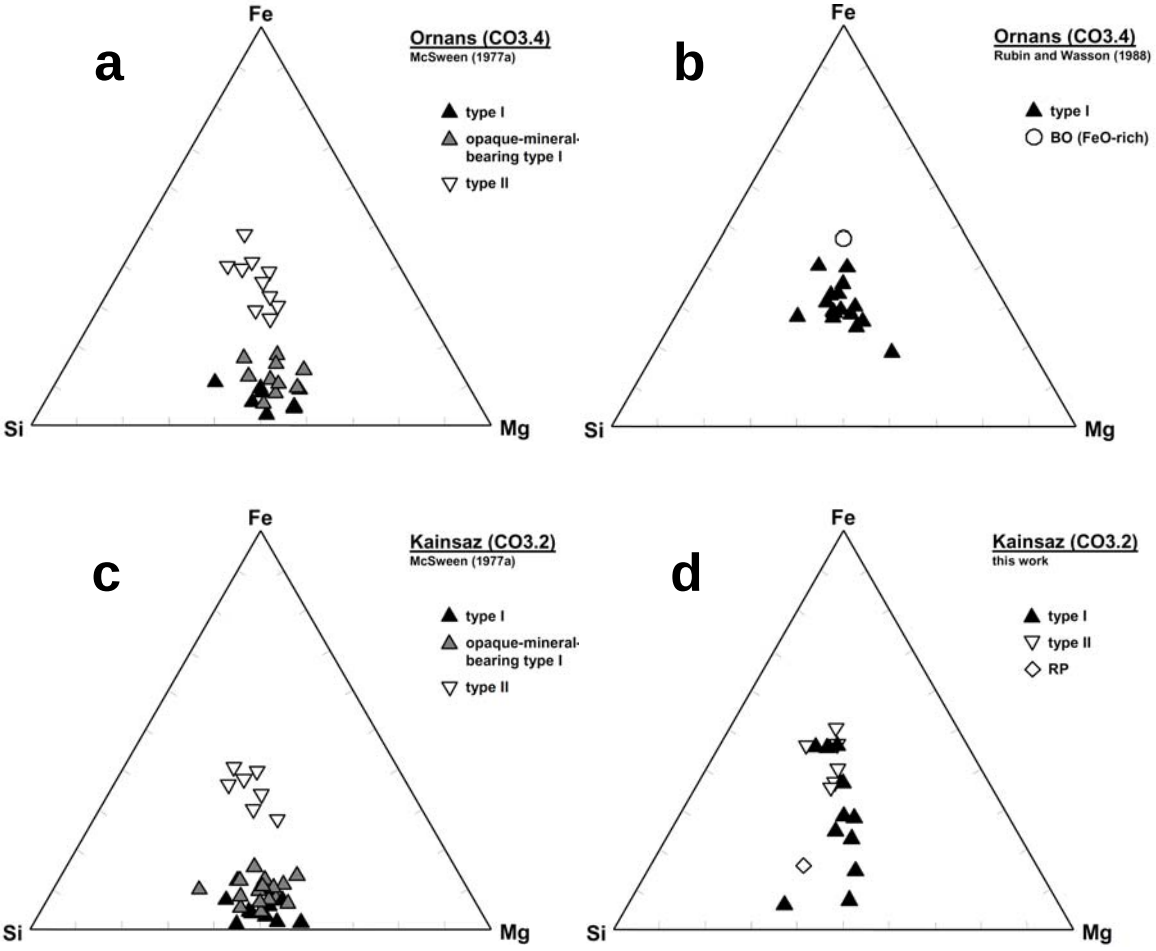

Fig. 1.17. Fe-Mg-Si ternaries (element wt%) for bulk compositions of CO chondrite chondrules from the literature and this work. a) and c) McSween (1977a) determined bulk chondrule composition of Kainsaz (CO3.2) and Ornans (CO3.4) by EMP defocused beam analyses. His data show a gap between Fe-poor (type I) and Fe-rich (type II) compositions. b) Rubin and Wasson (1988) obtained a dataset for Ornans (CO3.4) chondrules via INAA. Most of their type I chondrules show more Fe-rich compositions than those from McSween (1977a). d) Bulk chondrule compositions of Kainsaz obtained in this work via modal recombination. Type I chondrule compositions show a continuous trend towards more Fe-rich compositions depending on how much metal and sulfides are exposed in the thin section. Most of our type I chondrules are also more Fe-rich than those in McSween's (1977a) work.

Even though McSween (1977a) distinguished between type I and opaque-mineral-bearing type I chondrules, the data for his opaque-mineral-bearing type I chondrules show only slightly higher Fe contents than the regular type I chondrules (**Fig. 1.17a,c**). This points to an analytical problem with McSweeen's (1977a) data. McSween (1977a) applied a normative correction (from Bower et al. 1977) to his defocused beam analyses, but the different phase densities were not considered. Because of the much higher densities of kamacite ($\rho = 7.90$ g/cm^3) and taenite ($\rho = 8.01$ g/cm^3) compared to the different silicate phases ($\rho \approx 2.6 - 3.5$ g/cm^3), metal-rich type I chondrules should have much higher Fe contents than metal-poor type I chondrules. This is demonstrated in **Figure 1.18**, which shows the consequences of determining bulk compositions of type I chondrules via EMP (here, via modal recombination analysis) with and without considering phase densities. If phase densities are not taken into account, bulk Fe contents are underestimated by a factor of about 2.

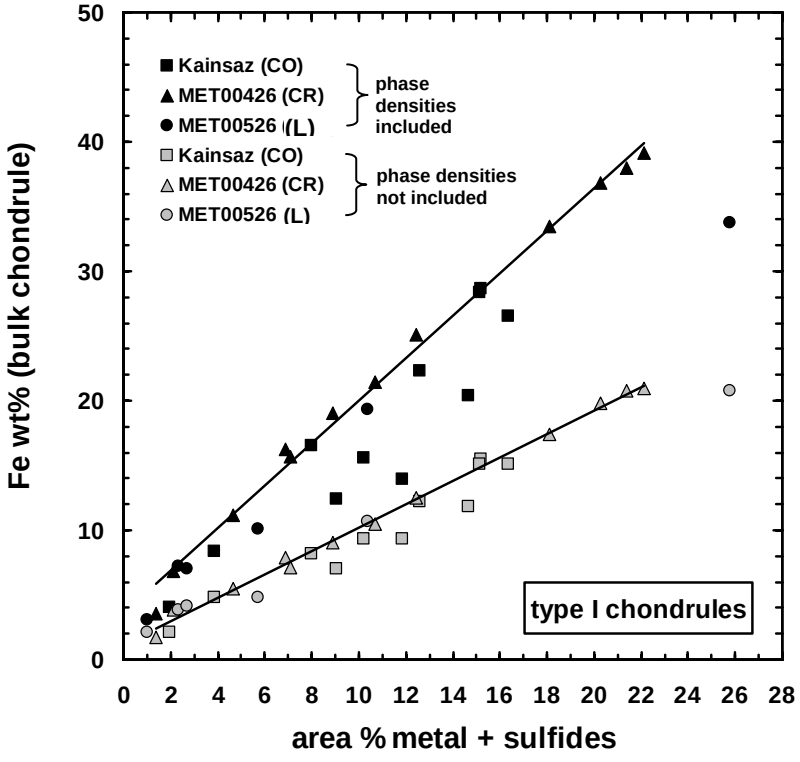

Fig. 1.18. Bulk Fe content (wt%) vs. metal + sulfide modal abundance (area %) in type I chondrules with (black symbols) and without (gray symbols) including phase densities in modal recombination analysis (MRA). Trendlines are shown for MET 00426 (CR) type I chondrules, which do not contain any sulfides, while type I chondrules in Kainsaz (CO) and MET 00526 (L) do. When phase densities are included in MRA, the calculated bulk Fe content is higher by a factor of about two.

In addition to not including phase densities, McSween (1977a) excluded analyses with totals higher than 103 wt%. This must have led to the preferential exclusion of metal/sulfide analyses and mixed metal-silicate analyses, because all Fe was analyzed as FeO. If some of the FeO could have been assigned to a metal/sulfide component and converted to Fe, analysis totals would probably have been acceptable (also see Appendix A for further discussion of problems with EMP defocused beam analyses).

Another possible explanation for the discrepancy in Fe contents of type I chondrules determined in the different studies, could be that the chondrule outlines were chosen differently (i.e., metal along chondrule edges may not have been included in McSween's study). However, metal along the periphery of type I chondrules in CO chondrites is not nearly as common as in CR chondrites for example, so that this cannot be a satisfactory explanation.

Jones et al. (2005) suggested that the higher Fe contents observed for Ornans chondrules in Rubin and Wasson's (1988) study (**Fig. 1.17b**) might be due to the higher degree of thermal metamorphism recorded in Ornans (CO3.4) than in Kainsaz (CO3.2): Fe-Mg exchange between type I chondrules and the surrounding fine-grained matrix resulted in higher FeO contents in Ornans type I chondrule olivine than in Kainsaz type I chondrule olivine (Scott and Jones 1990; Jones and Rubie 1991). However, when comparing McSween's (1977a) Kainsaz and Ornans bulk chondrule data (**Fig. 1.17a,c)**, it appears that the slightly higher FeO contents of Ornans chondrule olivine do not effect the bulk chondrule data by much. We conclude that the higher Fe contents observed in Rubin and Wasson's (1988) Ornans bulk chondrule data (**Fig. 1.17b**) are most likely due to the fact that metal and sulfides were correctly accounted for in their 3D method (INAA), while the Fe contents in McSween's (1977a) data are too low due to problems with the analytical technique (see discussion above).

For all three chondrites studied, our bulk chondrule data of type I chondrules exhibit continuous trends from Fe-poor to Fe-rich compositions in the Fe-Mg-Si ternaries (**Fig. 1.12a,c,e**), which, as shown above (**Fig. 1.18**), depend on the modal abundance of Fe,Ni metal (and sulfides in Kainsaz and MET 00526 (L)) exposed in the thin section. When chondrules are examined in thin sections, there are quite large uncertainties regarding the true 3D modal abundance of metal and sulfides (e.g., Ebel et al. 2008). If for example, a

very large metal grain is exposed in the cross section of a chondrule, this would lead to a significant overestimation of siderophile elements. On the other hand, if only very few metal grains are exposed in the thin section but the 3D object contains a lot more metal, this would lead to a significant underestimation of siderophile elements in the bulk chondrule composition. Type I chondrules that contain small, but homogeneously distributed metal grains are those for which a bulk composition can be determined most accurately in a 2D section. We tried to select type I chondrules that meet this criterion, but we cannot exclude that the bulk Fe content may have been underestimated in some chondrules and overestimated in others. Considering this 2D sectioning effect, our data for CO type I chondrules (**Fig. 1.17d**) are more similar in their bulk Fe content to Rubin and Wasson's (1988) data (**Fig. 1.17b**) than to McSween's (1977a) data (**Fig. 1.17a,c**).

In all three chondrites studied, there are some type I chondrules that overlap significantly with type II compositions in the Fe-Mg-Si ternaries (**Fig. 1.12a,c,e**). Several type I chondrules in MET 00426 (CR) and one type I chondrule in MET 00526 (L) have even higher bulk Fe contents than type II chondrules (**Fig. 1.12a,c**). These are the most metal-rich type I chondrules in the 2D thin sections (also refer to **Fig. 1.18**). We conclude that, if opaque phases and their densities are properly considered when determining bulk chondrule compositions via EMP, there is no gap between the bulk Fe contents of type I and type II chondrules in CO, CR and ordinary chondrites (**Fig. 1.12a,c,e**). Type I chondrules show a continuous trend from Fe-poor to Fe-rich compositions depending on the modal abundance of metal (and sulfides) exposed in the thin section (**Fig. 1.18**). Metal-rich type I chondrules have bulk Fe contents comparable to those of type II chondrules, which indicates that there is not a significant difference in the bulk Fe content between type I and type II chondrules as has been suggested previously.

Did type I and type II chondrules form in the same nebular reservoir(s)?

It has been suggested that certain components of chondrites, for example CAIs and refractory forsterites, may have formed within a common nebular reservoir and were later mixed into the different chondrite groups in different proportions (e.g., Guan et al. 2000; Pack et al. 2004). We can ask whether a similar scenario is likely for type I and type II chondrules in the different chondrite groups. In other words, did UOC, CR and CO type I chondrules form within a single nebular reservoir and did UOC, CR and CO type II chondrules form in a different one?

Above, we showed that chondrules of the same textural type within a certain chondrite are very similar, but there are significant differences in the mineralogy and bulk chemistry of chondrules between the different chondrite groups. Our observations indicate that chondrules of the same textural type in the different chondrite groups cannot have been derived from a common reservoir in the solar nebula. Another line of evidence comes from oxygen isotopic compositions. Chondrules in CO and ordinary chondrites have significantly different oxygen isotopic compositions. Type I and type II chondrules in ordinary chondrites plot above the terrestrial fractionation line (TFL) in a three-isotope diagram, whereas type I and type II chondrules in CO chondrites plot below the terrestrial fractionation line, along the CCAM line (e.g., Kita et al. 2006, 2007; Yurimoto et al. 2008). In both cases, type II chondrules tend to have more ^{16}O-depleted compositions than type I chondrules, but the difference in oxygen isotopic compositions of chondrules of the same textural type in CO and ordinary chondrites is larger than the difference between type I and type II chondrules within the same chondrite. This implies that type I and type II chondrules within the same chondrite group are more closely genetically related to each other than chondrules of the same textural type in different chondrite groups. But how similar are type I and type II bulk chondrule compositions within a certain chondrite and how could type I and type II chondrules be related to each other? Could they have formed within the same nebular reservoir? Below, we address these questions by trying to understand the nature of chondrule precursor material. We consider that chondrules formed from precursor dustballs that consisted of a mixture of fine-grained materials as well as coarser grains that survived chondrule formation as relict grains in porphyritic chondrules (e.g., Jones et al. 2005).

To what extent do bulk compositions of type I and type II chondrules overlap?

Above, we showed that there is considerable overlap for Fe between type I and type II chondrules (**Fig. 1.12a,c,e**). This is also true for Si and Mg, as shown in **Figure 1.19a** and **b**. With decreasing Fe content, both bulk Si and Mg tend to increase. The scatter in the data is mostly due to the different modal proportions of olivine and pyroxene.

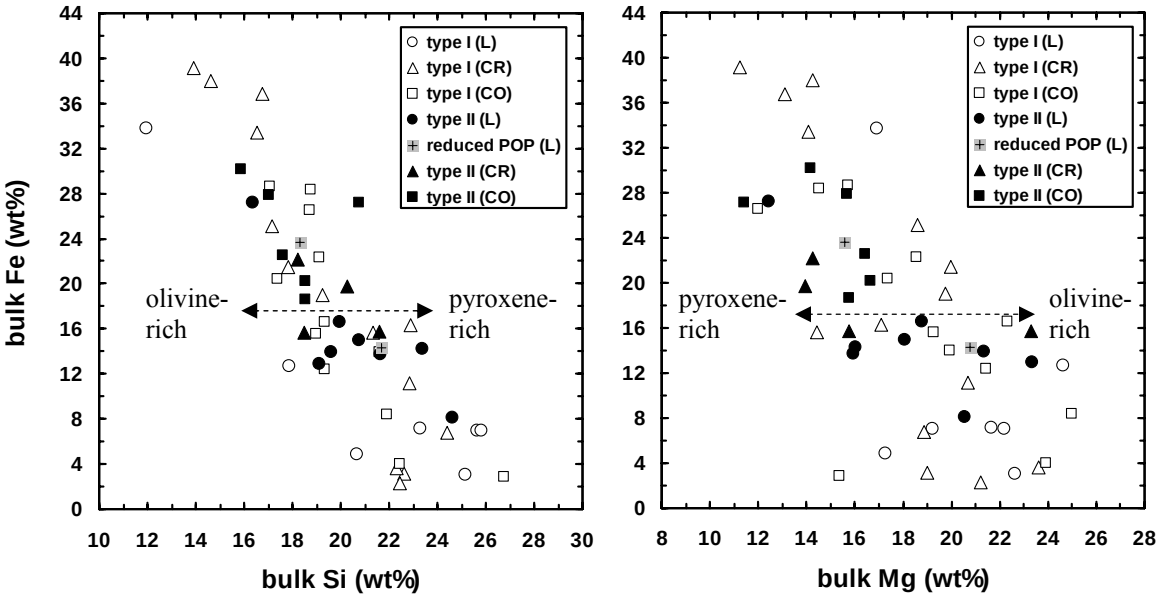

Fig. 1.19. a) Bulk Fe content (wt%) vs. bulk Si content (wt%) and b) bulk Fe content (wt%) vs. bulk Mg content (wt%) for type I and type II chondrules in MET 00526 (L), MET 00426 (CR) and Kainsaz (CO).

We can also look at refractory elements. **Figure 1.20** shows bulk Ca (wt%) versus bulk Al (wt%) and bulk Ti (wt%) versus bulk Al (wt%) for the chondrules in our study. Most type I and type II chondrules in all three chondrites overlap significantly in these plots and show strong positive correlations close to the CI ratio, but there are also some type I chondrules that have significantly higher abundances of Ca, Al and Ti than type II chondrules. Grossman and Wasson (1983a) cautioned that interelement correlations in EMP studies can be caused by sectioning problems. Because the proportions of mesostasis and silicate minerals vary in 2D sections, this would lead to apparent correlations between elements concentrated in each of these two components. However, correlations between refractory lithophile elements, such as those shown in **Figure 1.20**, are also observed in INAA studies (see review in Grossman and Wasson 1983a), therefore it is very likely that the correlations are real.

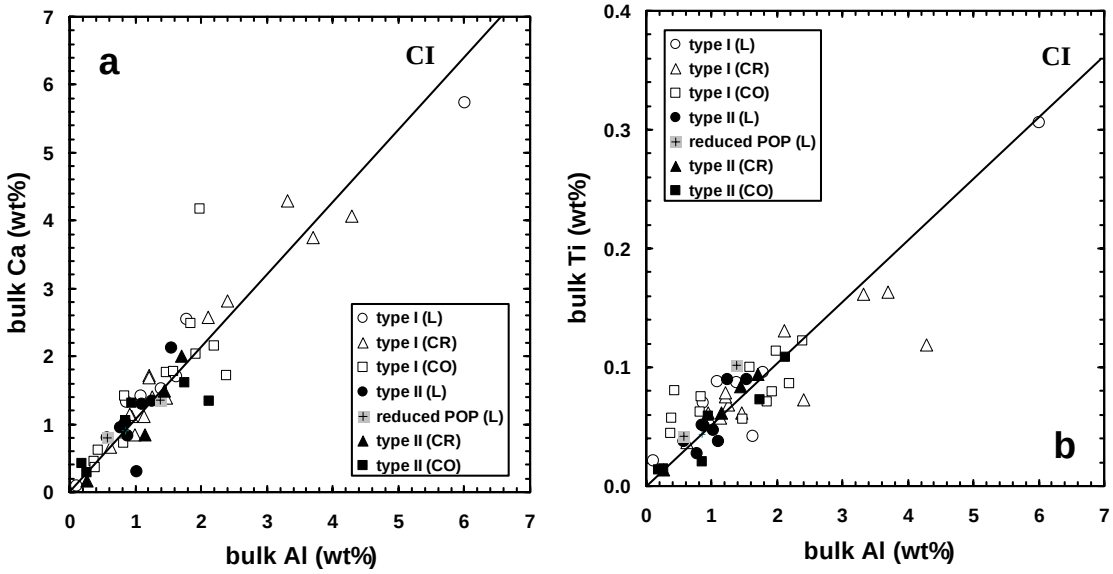

Fig. 1.20. a) Bulk Ca content (wt%) vs. bulk Al content (wt%) and b) bulk Ti content (wt%) vs. bulk Al content (wt%) for type I and type II chondrules in MET 00526 (L), MET 00426 (CR) and Kainsaz (CO).

For Semarkona (LL3.0), Jones (1990) found that refractory lithophile element abundances are typically higher in type I than in type II chondrules. Our data for type I and type II chondrules show considerable overlap (**Fig. 1.20**), but some type I chondrules do have higher refractory element concentrations compared to type II chondrules. It appears that the precursor materials for type I and type II chondrules in all three chondrites studied included an identical refractory component (e.g., CAIs).

A more significant difference between type I and type II chondrules can be found in the bulk volatile element contents. This is shown in **Figure 1.21**, where K is plotted versus Na (both relative to CI chondrites). In MET 00526 (L) and MET 00426 (CR), most type I chondrules (**Fig. 1.21a**) have lower Na and K abundances than type II chondrules (**Fig. 1.21b**). The K/Na ratio of most L and CR type I chondrules varies around the CI ratio, while most L and CR type II chondrules have a K/Na ratio higher than CI. In contrast, type I and type II chondrules in Kainsaz have similar volatile element contents, with variable Na but a limited range of K contents. However, as discussed above, it is not clear whether this is a primary feature or a secondary overprint for Kainsaz.

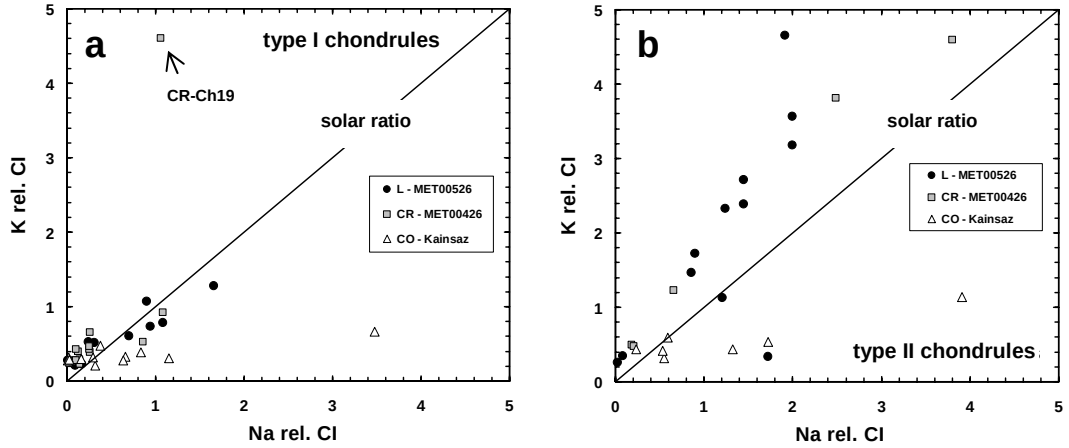

Fig. 1.21. K versus Na (CI-normalized) plot for bulk chondrule compositions of a) type I and b) type II chondrules in MET 00526 (L), MET 00426 (CR) and Kainsaz (CO). Type I and type II chondrules in Kainsaz have similarly low K and variable Na contents.

What explains the different oxidation states of type I and type II chondrules?

Type I and type II chondrules clearly record differences in oxidation state which are manifested in the FeO contents of their silicate portions. As can be seen in **Figures 1.12b**,**d** and **f**, the gap between bulk FeO contents is very small between type I and type II chondrules in MET 00526 (L), intermediate in MET 00426 (CR) and largest in Kainsaz (CO). Based on chemical equilibria between metal and silicates, calculated oxygen fugacities for type I chondrules range between IW-1.5 to IW-5 (e.g, Zanda et al. 1994; Lauretta et al. 2001). Type II chondrules contain minor amounts of Fe,Ni metal (<5 vol%), which restricts the oxygen fugacity recorded in type II chondrules close to the IW buffer. Textures and compositions that resemble type II chondrules in ordinary chondrites have been experimentally reproduced at IW-0.5 (e.g., Lofgren 1989).

Jones (1990) and Sears et al. (1996) suggested that, in ordinary chondrites, type I chondrule compositions could potentially have been derived from type II compositions by reduction of FeO to Fe metal, physical loss of some of the metal and evaporation of volatile elements. Jones (1990) pointed out that Fe loss from type II chondrule compositions should be complemented by significant increases in the concentrations of all other elements, particularly Si and Mg, but because the concentrations of Si are

actually quite similar in type I and type II chondrules, significant evaporation of Si needs to be invoked as well.

Above, we demonstrated that the bulk Fe, Mg and Si contents of type I and type II chondrules overlap significantly, especially when type I chondrules are metal-rich. This implies that Fe does not necessarily need to be physically lost and Si does not need to be evaporated either to produce type I chondrules from type II compositions. However, there is a significant problem with this model. While type I and type II chondrules follow the same trend in a diagram where Fe/Mg is plotted versus bulk Fe (wt%) (**Fig. 1.22a**), they exhibit two different trends when Ni/Mg is plotted versus bulk Fe (wt%) (**Fig. 1.22b)** with type II chondrules having significantly lower Ni/Mg ratios than type I chondrules. The high bulk Ni contents of type I chondrules would not be observed if type I chondrules had formed by the reduction of type II compositions, simply because type II chondrules do not contain enough Ni. Conversely, type II chondrules could also not have formed by the oxidation of type I chondrules combined with volatile gain.

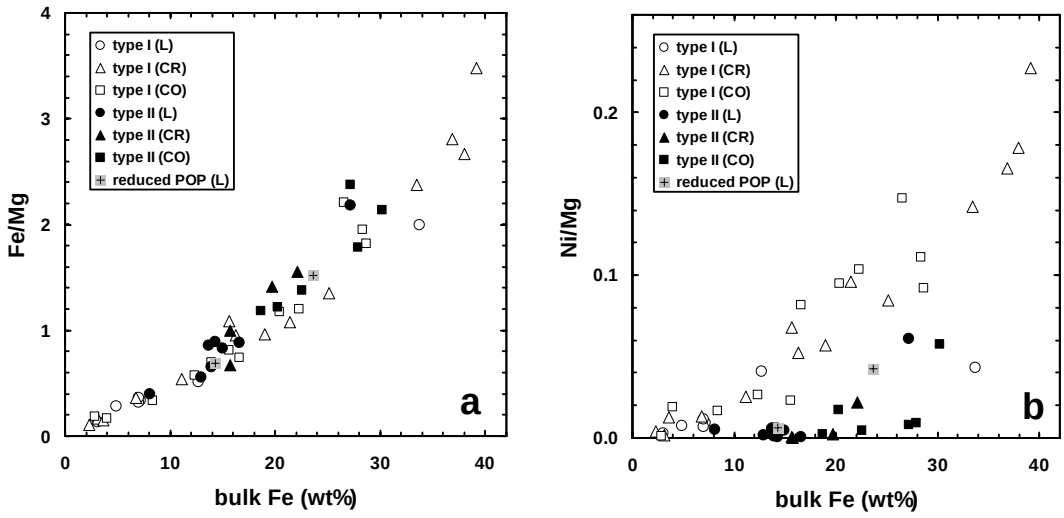

Fig. 1.22. a) Fe/Mg vs. bulk Fe content (wt%), and b) Ni/Mg vs. bulk Fe content (wt%) for type I and type II chondrules in MET 00526 (L), MET 00426 (CR) and Kainsaz (CO).

Nevertheless, there is evidence that some reduction did occur. In MET 00526 (L), we observed dusty olivine relicts (e.g., **Fig. 1.2c**) and also whole chondrules that experienced reduction (**Fig. 1.2g,h**). Experimental studies have shown that reduction of Fe^{2+} (in silicates) to Fe metal requires temperatures above 1100ºC (Boland and Duba 1981; Nagahara 1985, 1986; Connolly et al. 1994; Danielson and Jones 1995; Lemelle et al. 2001, 2001; Leroux et al. 2003). Chondrites of petrologic type 3 did not experience such high temperatures on their parent body, therefore, it seems more likely that these temperatures were reached in the solar nebula, probably during chondrule forming events. However, because of the problem with Ni (**Fig. 1.22**), reduction of type II material during chondrule forming events cannot have been the major process that produced type I chondrules in CO, CR and ordinary chondrites.

Another possible model that suggests a genetic relationship between type I and type II chondrules has been proposed by Cohen et al. (2000). In this model, type I chondrules represent evaporation residues of type II chondrules. Fe is lost as FeO by evaporation, as are SiO_2 and volatile elements. However, the same problem with Ni remains (**Fig. 1.22**), because the high proportions of Fe,Ni metal and the high bulk Ni contents of type I chondrules cannot be reproduced.

The differences in the bulk compositions of type I and type II chondrules (Ni and volatile element abundances) cannot solely be the result of the chondrule forming process, so we may ask the question whether the oxidation state of the precursor material of type I and type II chondrules was already fundamentally different. If this is the case, these materials would probably not have coexisted within the same nebular region, unless the oxygen fugacity of the nebular region changed over time and type I and type II chondrules formed at different times. According to the classical condensation sequence for the canonical solar nebula (e.g., Grossman 1972), it makes sense to suggest that type I chondrules formed first – possibly at somewhat higher temperatures than type II chondrules. The precursor material of type I chondrules probably consisted mostly of high temperature condensates, including a somewhat higher abundance of refractory lithophile elements (e.g., in form of CAIs), a higher abundance of Fe,Ni metal and more Mg-rich silicates than the precursor materials of type II chondrules.

The formation of type II chondrules could have followed somewhat later in time at lower ambient temperatures, as their precursor material may have contained more Fe-bearing silicates, sulfides and a higher abundance of volatiles. Condensation calculations by Wood and Hashimoto (1993) and Ebel and Grossman (2000) show that it is much easier to incorporate significant amounts of Fe^{2+} into silicates in fractionated and/or dust-enriched systems. Another possibility, which is discussed further below, is that ice particles may have been mixed into the type II precursor material due to the inward drift of the snowline into the nebular region over time. Major support for a model, in which type I chondrules form before type II chondrules, comes from Kunihiro et al. (2004) and Kurahashi et al. (2008), who found that in CO chondrites, type II chondrules are significantly younger than type I chondrules (up to 1 My).

Fe-Mn systematics of type II chondrule olivines, which are discussed in detail in Chapter 2, provide evidence that type II chondrules in CO chondrites and type II chondrules in ordinary chondrites originated from significantly different reservoirs, which might correspond to different locations in the solar nebula. Based on differences in the proportions of chondrules that were completely melted, chondrule ages, bulk chondrite volatile contents and elemental fractionations, Wood (2005) argued that the formation region of ordinary chondrites is probably located closer to the Sun than the formation region of CO chondrites. While Wood (2005) suggests that CR chondrites formed further away from the Sun than CO chondrites, our Fe-Mn data of CR type II chondrules appear to imply that CR chondrites could represent a connection between the UOC and CO reservoirs (Chapter 2). We observed at least two populations in the Fe-Mn trends of CR type IIA chondrule olivine, one of which overlaps with the data for type II chondrules in ordinary chondrites, while the other is clearly intermediate between UOC and CO. Further evidence for such a relationship comes from an oxygen isotope study by Connolly et al. (2007a; 2008), who found that oxygen isotopic compositions of CR type II chondrules show three different populations: one that overlaps with CR type I chondrules, one that overlaps with OC chondrules and one that plots on the CCAM line, just below the TFL, close to CO type II chondrules. The fact that type II chondrules typically show somewhat heavier oxygen isotopic compositions than type I chondrules (e.g., Yurimoto et al. 2008) fits well with our suggestion that an ice component may have

been mixed into the precursor material of type II chondrules. The gap in FeO contents between the silicate portions of type I and type II chondrules is much larger in CO chondrites than in CR and ordinary chondrites (**Fig. 1.12b,d,f**). This suggests that the fO_2 conditions between type I and type II chondrule formation changed most dramatically in the CO chondrite formation region. If the formation region of ordinary chondrites was closer to the Sun than that of CO chondrites, it is likely that CO chondrites were affected more significantly by the inward drift of ice particles, such as suggested by Cyr et al. (1998). If the proportion of ice that was mixed into the precursor material of CO type II chondrules was higher than that mixed into CR and ordinary type II chondrule precursor materials, it would provide a simple explanation for the observed differences in bulk FeO contents (**Fig. 1.12b,d,f**), as H_2O reacts as an oxidizing agent, but it would also volatilize during the chondrule forming process and not leave a trace that it was once there.

Jones (1996b) pointed out that the presence of FeO-rich ("dusty") relict grains in type I chondrules indicates that at least some type II chondrules must have formed and disaggregated before type I chondrules formed. The fact that FeO-rich relicts are found in type I chondrules and FeO-poor relicts are found in type II chondrules provides another argument for a close spatial proximity of both chondrule types, but it also implies that the model suggested above is still too simple to explain all observations.

The compositional relationship between chondrules and matrix

In addition to bulk chondrule data, we obtained bulk compositional data for fine-grained matrix in the three chondrites studied, in order to address a fundamental question that is extremely important for chondrule formation models: Did chondrules and matrix form in the same or in different regions of the solar nebula? Before we can attempt to answer this question, we first need to address what is currently known about the nature and origin of fine-grained matrix material in pristine chondrites and about how matrix material is affected by secondary processes.

The nature and origin of matrix in pristine chondrites

Fine-grained matrices are known to be texturally and mineralogically very variable among the different chondrite groups (e.g., Scott et al. 1988; Brearley 1996). However, interpretations of the origin of matrix have been compromised by the fact that matrix is highly reactive because of its very fine grain size, with the result that it is difficult to find chondrites that show no secondary effects in their matrices. More recent studies of matrix in the most pristine chondrites have resulted in an improved understanding of the original pristine material. These chondrites include the CO3.0 chondrite ALHA 77307 (Brearley 1993), the unique carbonaceous chondrite Acfer 094 (Greshake 1997) and the two CR3.0 chondrites, MET 00426 and QUE 99177 (Abreu 2007; Abreu and Brearley, Forthcoming).

Our study includes one of the most pristine chondrites, the CR3.0 chondrite MET 00426. Its fine-grained matrix (<5 μm) shares several characteristics with the other most pristine chondrites mentioned above: they all consist of disequilibrium assemblages and contain high abundances of amorphous silicate material, nanosulfides (<300 nm) and interstellar grains (e.g., Brearley 1993; Greshake 1997; Abreu 2007; Abreu and Brearley, Forthcoming; Floss and Stadermann 2009). Brearley (1993) and Abreu and Brearley (Forthcoming) suggest that the amorphous silicate material formed by disequilibrium condensation from material that underwent evaporation into the gas phase during transient heating events in the solar nebula, possibly those that formed chondrules. Abreu and Brearley (Forthcoming) also conclude that the nanosulfides may have formed by annealing of S-bearing silicate material during chondrule formation events, because they occur intimately associated with the amorphous silicate material. These recent observations imply that a high percentage of the matrix material found in pristine chondrites may represent highly processed residual material left over from chondrule formation (Abreu and Brearley, Forthcoming).

Secondary alteration of matrix

The L chondrite MET 00526 has been classified as petrologic type 3.05 by Grossman and Brearley (2005), but its fine-grained matrix material has not been studied in detail yet. In **Table 1.8**, we compared our EMP matrix data for MET 00526 to matrix

data for Semarkona and MET 00526 from Grossman and Brearley (2005). For most elements, all these analyses are very similar. The one notable difference is that the abundance of S is higher in Semarkona matrix (1.2 wt%) compared to MET 00526 (0.43–0.52 wt%), consistent with observations by Grossman and Brearley (2005) that some mobilization and coarsening of sulfides has occurred in the matrix of MET 00526 due to minor thermal metamorphism. However, we also found phosphates around type IIA chondrules in MET 00526, which suggests that some aqueous alteration probably occurred as well (e.g., Burger 2005; Brearley 2006).

Matrix in Kainsaz (CO3.2) has been affected significantly by thermal metamorphism (Brearley 1994). It is dominated by fine-grained (<0.5 μm) FeO-rich olivines ranging in composition from Fa_{48} to Fa_{72} (Brearley and Jones 1998). Brearley (1993) suggested that FeO-rich olivines probably formed by the recrystallization of amorphous silicate material, such as is found in the matrix of the more pristine CO3.0 chondrite ALHA 77307. Higher S contents are observed in EMP matrix data of ALHA 77307 (1.1 wt%) from Brearley (1993) compared to Kainsaz (0.14–0.15 wt%, **Table 1.8**), indicating that mobilization and coarsening of sulfides has also occurred in Kainsaz (see also Grossman and Brearley 2005).

For MET 00526 (L3.05) and Kainsaz (CO3.2), we need to be careful when discussing the relationship between chondrules and matrix, because the matrices in these two chondrites have been affected by secondary processing. However, MET 00426 (CR3.0) represents one of the most pristine chondrites known, which is why we will focus our discussion on this meteorite.

Definition of "complementarity" and literature review

Several authors have previously argued that chondrules and matrix must have formed in the same region of the solar nebula, because their compositions appear to be "complementary" (Wood 1985; Klerner and Palme 1999a,b, 2000; Palme and Klerner 2000; Bland et al. 2005; Hezel and Palme 2008). This means that bulk chondrule and bulk matrix compositions are significantly different, but the composition of both added together in their modal proportions is closer to the solar composition (or the bulk composition of CI chondrites). The X-wind model by Shu et al. (1997, 2001) specifically

predicts that chondrules and matrix are not formed in the same reservoir, which means that if a compositional complementarity between chondrules and matrix indeed exists, this mechanism cannot have been responsible for chondrule formation. On the other hand, local chondrule formation models, such as the shock wave model (e.g., Desch et al. 2005) are supported by compositional complementarity between chondrules and matrix.

The question of whether or not complementarity really does exist remains controversial (e.g., Huss et al. 2005) as it is likely that previous studies were inadequate because secondary overprints in the chondrites studied may have mimicked complementarity. Wood (1985) was the first to suggest a complementary relationship between chondrules and matrix in the CM chondrite Murchison based on Fe/Si ratios. Scott et al. (1982, 1984), Scott and Taylor (1983) and Taylor (2001) demonstrated complementarity between matrix and the silicate portion of chondrules in several ordinary and carbonaceous chondrites using MgO-FeO-SiO_2 ternaries. The discussion about complementarity intensified after Klerner and Palme (1999a,b, 2000) showed large fractionations between chondrule and matrix compositions in diagrams like Si vs. Mg (wt%), Cr vs. Fe (wt%) and Ti/Al vs. Al (wt%) for Renazzo (CR) and Allende (CV). Brearley (1996) and Huss et al. (2005) pointed out that complementary compositions could either represent different fractions of a single bulk material reservoir, or they could reflect transfer of material from chondrules to matrix such as evaporation of volatiles from chondrules during chondrule formation and recondensation of these elements onto matrix grains. However, a first order problem is that most of the chondrites that have been studied to date are now recognized to have undergone extensive secondary processing, either thermal metamorphism and/or aqueous alteration. Therefore, many of the arguments presented in the earlier studies have to be questionable given that element fractionations could have been caused by the redistribution of elements during secondary alteration. Some authors have argued that the redistribution of elements like Mg, Si, Ti and Al is limited during secondary alteration (see review in Huss et al. 2005). However, studying the most pristine chondrites assures that we can examine the behavior of all elements, even those that are mobile during secondary processes (e.g., Cr and volatiles).

Before we discuss what our chondrule and matrix data show, we address another issue that has been neglected somewhat in the literature: problems with the analytical

method. Even though this is rather a secondary issue, it is important, because if data are plotted in a misleading way or if they are not accurate they tend to show more complementarity than is actually there, as is demonstrated below.

Analytical issues

When discussing complementarity between chondrules and matrix, it has been common practice (Scott et al. 1982, 1984; Scott and Taylor 1983; Taylor 2001; Klerner and Palme 1999a,b, 2000; Hezel and Palme 2008) to use only the silicate portion of chondrules, instead of the true bulk chondrule compositions that include Fe,Ni metal and sulfides. The main argument for doing this has been that the metal-plus-sulfide content of chondrules is highly variable and difficult to determine, especially when bulk chondrule compositions are obtained via EMP in 2D thin sections. However, small sulfide and metal grains (<5 μm) in the matrix are included when bulk compositions of chondrite matrices are determined via EMP defocused beam analyses: typical beam diameters used for DBA of chondrite matrices are ≥10 μm, which makes it difficult to avoid small opaque phases, in particular the nanosulfides that occur in the most pristine chondrite matrices mentioned above. Hence, opaque phases are treated differently in the two materials using this approach. Another problem is that Fe in EMP defocused beam analyses of matrix is usually measured as FeO and that analyses totals may not have been normalized to 100 wt%, taking sulfide and metal phases into account.

One diagram that has typically been used to demonstrate complementarity between chondrules and matrix is Mg (wt%) versus Si (wt%) (e.g., Klerner and Palme 1999b; Huss et al. 2005). On this plot, chondrule and matrix compositions were shown as being significantly different. However, we argue that this is mainly due to the fact that only the silicate portions of chondrules were plotted, as discussed in detail below. The data used by Klerner and Palme (1999b) and Huss et al. (2005) were obtained on the CR2 chondrite Renazzo and details of the analytical method were given in Klerner (2001). She obtained bulk chondrule data by EMP defocused beam analyses (10 μm diameter) along the two major axes of a chondrule exposed in a thin section. It appears that metal grains at chondrule margins (which are frequent in Renazzo) were not included, and that no normative and/or density correction was performed on the defocused beam analyses.

Therefore, these data are probably more representative of the silicate portions of chondrules than of the complete bulk compositions including metals.

To demonstrate how bulk chondrule and matrix data may be affected by such analytical issues, **Figure 1.23** shows Mg (wt%) vs. Si (wt%) for the chondrule and matrix compositions determined in this study. On the left-hand side (**Fig. 1.23a,c,e**), complete bulk chondrule compositions, including opaque minerals, are plotted. For the matrix data, sufficient Fe was combined with all measured S to make troilite and all Ni was attributed to Fe,Ni metal using an Fe/Ni ratio of 4. The resulting matrix data were normalized to 100 wt%. On the right-hand side (**Fig. 1.23b,d,f**), chondrule data are silicate portions only and matrix data are not normalized, while all Fe is attributed to FeO. Complete bulk chondrule compositions, including opaque phases (**Fig. 1.23a,c,e**), tend to be much closer to bulk chondrite compositions than if only the silicate portions are considered (**Fig. 1.23b,d,f**). When only the silicate portion of chondrules is considered, especially the compositions of Kainsaz (CO) and MET 00426 (CR), type I chondrules shift to higher Mg and Si contents. This is not surprising because Fe has basically been subtracted and these chondrules have high modal abundances of opaque phases. Because type II chondrules have much lower modal abundances of metal and sulfides (typically <3 vol%), their compositions do not shift as much. Matrix data normalized to 100 wt%, while taking FeS and FeNi into account, for Kainsaz (CO) and MET 00426 (CR) (**Fig. 1.23a,c**) also lie closer to the bulk chondrite compositions than the matrix data that are not normalized and where all Fe is attributed to FeO (**Fig. 1.23b,d**). The MET 00526 (L) chondrule and matrix data appear to show quite similar Si but very different Mg contents in **Figure 1.23e**. The bulk L chondrite composition does not plot as intermediate between chondrules and matrix in **Figures 1.23e,f** as it probably should**,** which could be related to the fact that this composition represents an average of all L chondrites (Lodders and Fegley 1998) because no bulk compositional data for MET 00526 are currently available.

Overall, **Figure 1.23** shows that when opaque phases are properly taken into account, bulk chondrule and matrix compositions are drawn closer together and are not as distinctly different as previously thought, although there still is little overlap between them. In any case, clearly it is better to use complete chondrule analyses rather than silicate portions only, so this is what we will do to discuss complementarity.

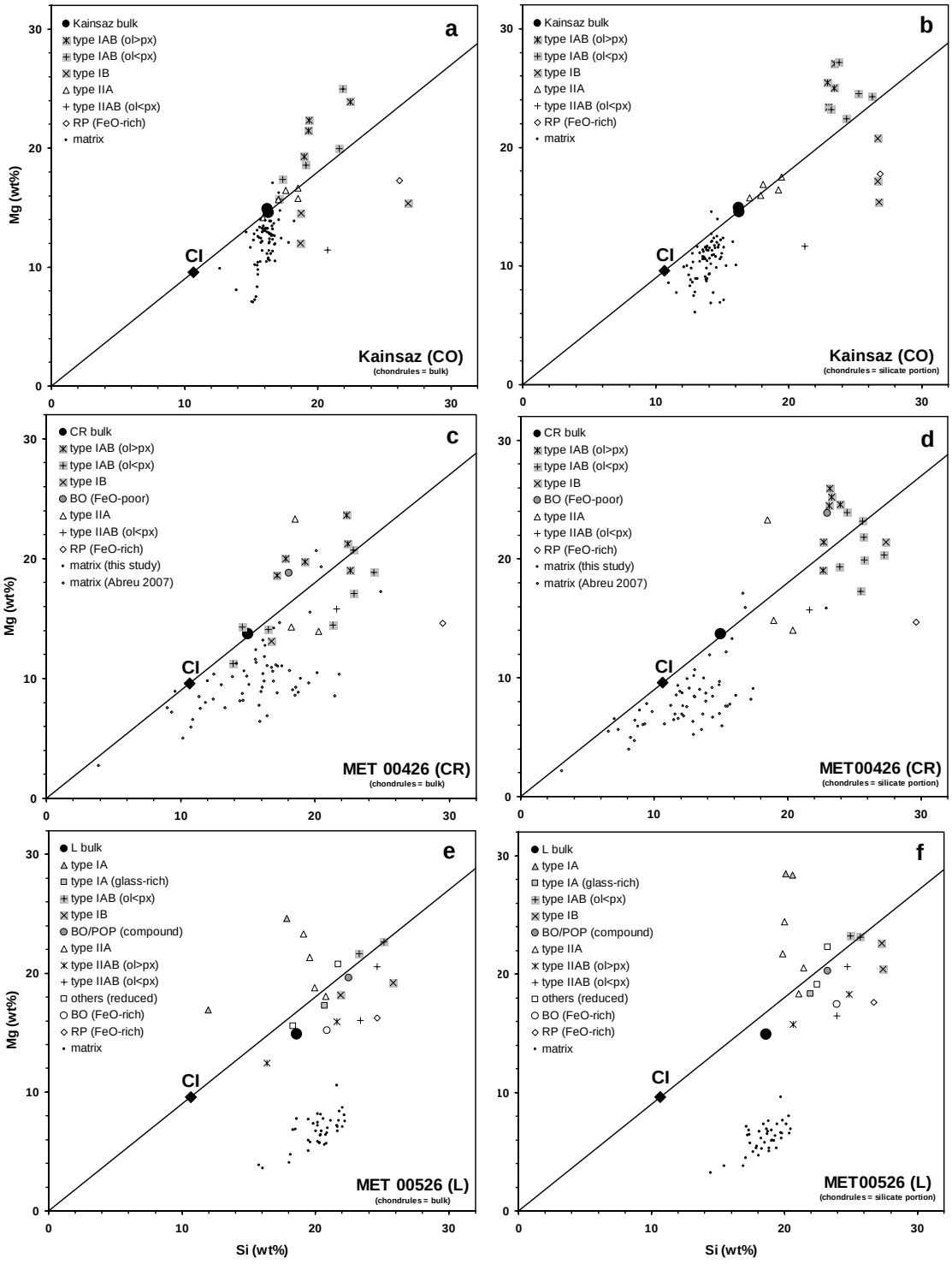

Fig. 1.23. Mg (wt%) vs. Si (wt%) for chondrules, matrix and bulk chondrites in a) and b) Kainsaz, c) and d) MET 00426 (CR), e) and f) MET 00526 (L). a), c), and e) show complete bulk chondrule compositions including opaque phases and matrix data are normalized to 100 wt% while taking FeS and FeNi into account, whereas b), d), and f) show only the silicate portion of chondrules and matrix data are not normalized to 100 wt% (all Fe was attributed to FeO). No bulk chondrite data are available for MET 00526 and MET 00426, so we used L and CR bulk chondrite data from Lodders and Fegley (1998). Kainsaz bulk data are from Ahrens et al. (1973). Matrix analyses were performed with a beam diameter of 10 μm.

Another analytical issue is related to the fact that EMP defocused beam analyses of matrix represent a much smaller scale (in this study 10 μm) than our bulk chondrule analyses (between 100 and 1000 μm). One may ask if we are comparing apples and oranges here, as there is a 2 to 3 orders of magnitude difference in the mass of the samples analyzed. The total mass of matrix analyzed may even be equivalent to the mass of just one chondrule. **Figure 1.24** shows the ranges of bulk chondrule and matrix compositions as well as bulk chondrite compositions normalized to CI for Kainsaz (CO), MET 00426 (CR) and MET 00526 (L). The spread observed in matrix compositions is a reflection of small scale heterogeneities, and if the total mass of matrix analyzed is actually equivalent to that of an individual chondrule, we need to question how we end up with the compositional variability observed in chondrules. If chondrules formed from a fine-grained precursor material similar to matrix, one needs to assume that this material was very heterogeneous also on a larger scale in order to produce the heterogeneity in chondrule compositions. Therefore, fine-grained matrix as it is preserved cannot be representative for the precursor material of chondrules because it is not heterogeneous enough. This bears on Hezel and Palme's (2007) discussion of the fact that if chondrules were formed from fine-grained precursors, they should all be homogeneous in their bulk compositions.

Brearley (1993) observed a remarkably consistent compositional homogeneity on the scale of micrometers in the fine-grained matrix of the pristine CO3.0 chondrite ALHA 77307, suggesting that mixing of fine-grained materials (with different thermal histories) was extremely thorough. On the other hand, matrix data for the pristine CR3.0 chondrite MET 00426 show a large spread that is almost comparable to the range of chondrule compositions (**Fig. 1.24b**). Therefore, the heterogeneity in matrix compositions alone cannot be used as an indication for how pristine a chondrite is. Nevertheless, in the following discussion we exclude Kainsaz (CO3.2) and MET 00526 (L3.05) and focus only on MET 00426 (CR3.0), the most pristine chondrite in our study. We do this in order to avoid interpreting element fractionations as primary, when they could have been caused by the redistribution of elements during thermal metamorphism.

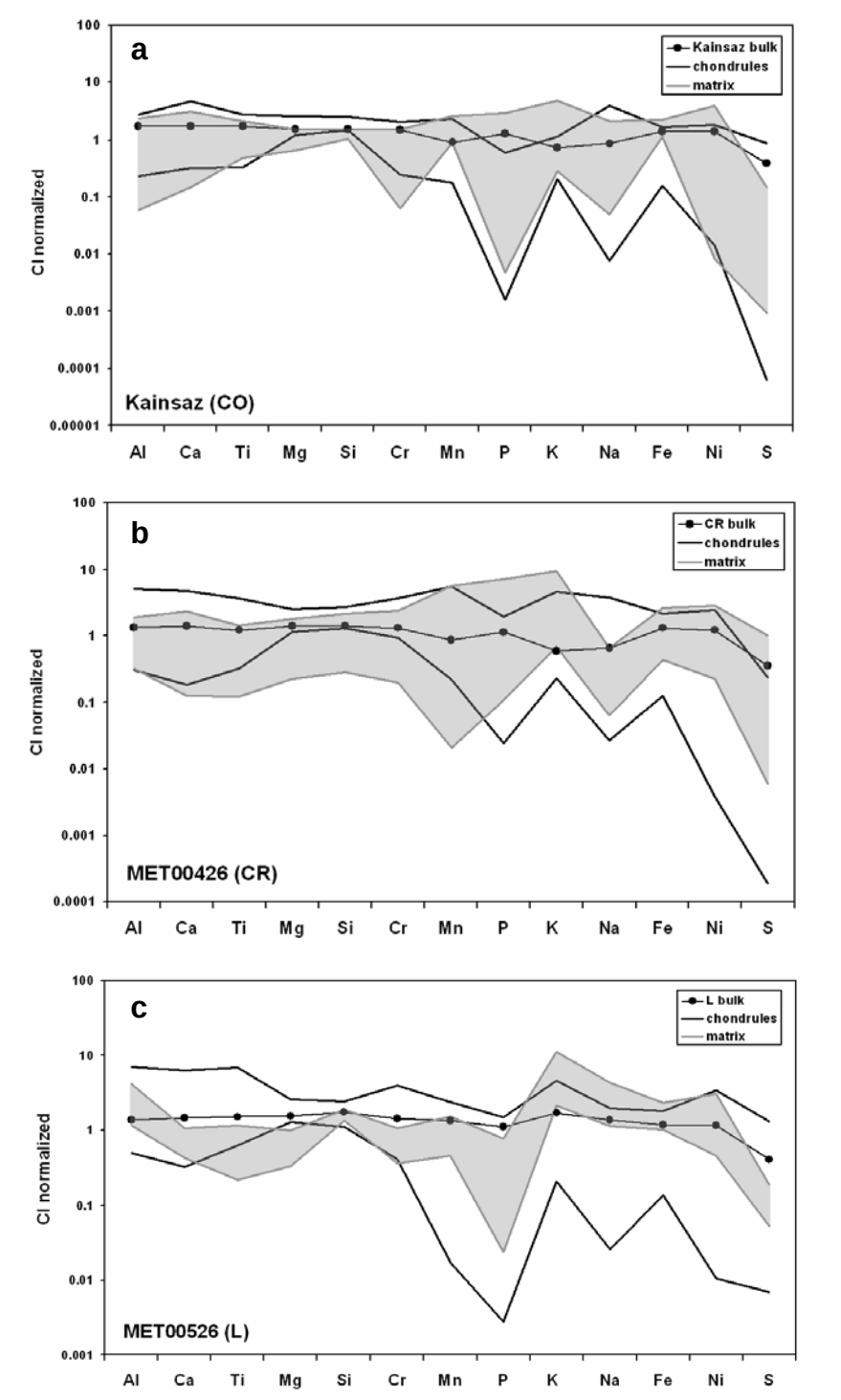

Fig. 1.24. Range of bulk chondrule and matrix compositions compared to bulk chondrite compositions for a) Kainsaz (CO), b) MET 00426 (CR) and c) MET 00526 (L). Matrix data for MET 00426 (CR) include data from Abreu (2007). Data are normalized to CI (Lodders 2003). L and CR bulk data are from Lodders and Fegley (1998). Kainsaz bulk data are from Ahrens et al. (1973).

New insights on the "complementarity" issue gained in this study

The current definition of complementarity (e.g., Huss et al. 2005), which proposes a local chondrule forming process, implies that before chondrule formation occurred, the initial dust had a solar or CI-chondrite composition. However, it is certainly possible that this dust could have already been depleted in moderately volatile elements (e.g., Yin 2005) or simply had a composition different from CI chondrites before chondrules formed. Therefore, we prefer to define complementarity differently: if chondrules and matrix have element patterns that mirror each other, it should be sufficient to indicate a genetic relationship between the two, independent of how the combined (chondrules plus matrix) composition relates to the composition of CI chondrites. In other words, if the element patterns of chondrules and matrix complement each other, it should follow that the chondrule forming process has left the remaining dust with a missing signature that can now be found in the chondrule compositions. Furthermore, complementarity should be observed for all elements, unless an element is affected by a secondary or tertiary process (e.g., terrestrial alteration). If an element is not affected by the chondrule forming mechanism, it should be present in similar abundances in chondrule and matrix compositions. If chondrules and matrix formed in different nebular regions, we would expect to observe random element abundance patterns that are not related to each other in any way.

Figure 1.25 shows all bulk chondrule and matrix data for MET 00426 (CR3.0) as well as the average chondrule and matrix composition. The average chondrule composition represents a weighted mean with 99% type I and 1% type II chondrules. In most chondrules, the abundances of refractory elements, Mg, Si and Cr are higher than in the matrix. The ranges of bulk chondrule and matrix compositions are very similar for Mn. Abundances of elements more volatile than Mn (P, K), siderophile elements and S are higher in the matrix than in most chondrules. Sodium represents an exception to this trend. Abreu and Brearley (Forthcoming) suggested that the low abundance of Na in fine-grained matrix in MET 00426 (CR) is most likely due to terrestrial weathering, probably leaching during residence in the Antarctic ice. Such a depletion of Na is not observed in the matrix of the CR chondrite Renazzo (Zolensky et al. 1993), which is an observed fall.

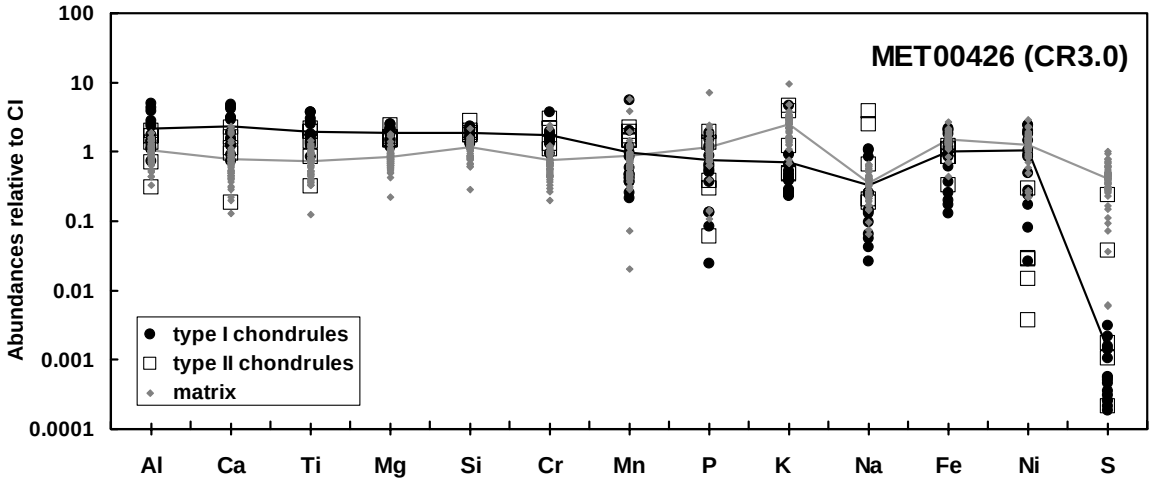

Fig. 1.25. Bulk chondrule and matrix compositions of MET 00426 (CR3.0). Matrix compositions include data from Abreu (2007). The average chondrule composition represents 99% type I and 1% type II chondrules. Elemental abundances are normalized to CI chondrites (Lodders 2003). Elements on the ordinate are arranged in order of increasing volatility; siderophile elements are plotted last.

Since the Na depletion can be accounted for, the element abundance patterns of chondrules and matrix in MET 00426 (CR) appear to mirror each other. According to our definition, we can therefore state that matrix and chondrules are complementary. Our compositional data support previous suggestions by Abreu and Brearley (Forthcoming) that fine-grained matrix represents thermally processed material left over from chondrule formation. It appears to act as a sink for volatile elements that evaporated during the chondrule formation process and recondensed afterwards. Such a close genetic relationship between chondrule and matrix compositions requires that both formed in the same region of the solar nebula, and therefore it supports chondrule formation mechanisms that acted locally, such as shock waves (e.g., Desch et al. 2005).

CONCLUSIONS

A detailed electron microprobe (EMP) study was performed on chondrules of various textural types and matrix in three fairly pristine chondrites: MET 00526 (L3.05), MET 00426 (CR3.0) and Kainsaz (CO3.2). The collected data allowed us to compare mineralogy and bulk compositions of chondrules with the same texture in the three different chondrite groups, to examine the compositional relationship between different

chondrule types (e.g., type I versus type II) within each chondrite group and to address the compositional relationship between chondrules and matrix.

Type I chondrules in MET 00526 (L), MET 00426 (CR) and Kainsaz (CO) show similar silicate chemistry and have comparable FeO, MgO and SiO_2 contents in their silicate portions. Major differences can be found in the minor element chemistry of Fe,Ni metal and in the absence of sulfides and taenite in MET 00426 (CR) type I chondrules. Type II chondrules in MET 00526 (L), MET 00426 (CR), and Kainsaz (CO) show systematic differences in bulk FeO, MgO and MnO contents, which are also reflected in their olivine compositions. This is further discussed in Chapter 2 of this thesis.

Previous EMP datasets of bulk chondrule compositions available in the literature tended to suggest that type II chondrules are more Fe-rich than type I chondrules (e.g., McSween 1977a,b; Jones and Scott 1989; Jones 1990). However, our dataset shows that the Fe contents of type I and type II chondrules are very similar when Fe,Ni metal and sulfides are properly included in the bulk chondrule compositions.

Jones (1990) and Sears et al. (1996) proposed that type I chondrule compositions could potentially have been derived from type II compositions by reduction, physical loss of metal and evaporation of volatile elements. Our new data show that reduction cannot have been the major process that produced type I chondrules from type II compositions. The main reason for this is the low bulk Ni content of type II chondrules (**Fig. 1.22**). It seems more likely that type II chondrules formed after type I chondrules at higher oxygen fugacities, which may have been caused by an increase in the dust/gas ratio and/or inward migration of the snowline and evaporation of water-ice during type II chondrule formation.

In MET 00426 (CR3.0), we observed a strong complementary relationship between chondrules and matrix, indicating that they most likely formed within the same nebular reservoir. A local chondrule forming mechanism, such as shock waves (Desch et al. 2005), is further supported by the fact that there are systematic differences in the chemistry of chondrules from different chondrite groups.

CHAPTER 2 - A COMPARISON OF TYPE IIA CHONDRULES IN ORDINARY AND CARBONACEOUS CHONDRITES: EVIDENCE FOR DIFFERENT NEBULAR RESERVOIRS?

ABSTRACT

In this study, we examined Fe/Mn systematics of type IIA chondrules in some of the most unequilibrated CO, CR and ordinary chondrites. Mean Fa contents of type IIA chondrule olivines increase in the order UOC < CR < CO. Olivines from type IIA chondrules in CO and unequilibrated ordinary chondrites (UOC) have significantly different Fe/Mn ratios (mean molar Fe/Mn = 99 and 44, respectively) and show distinct trends in Mn (afu) vs. Fe (afu) and molar Fe/Mn vs. Fe/Mg diagrams. CR type IIA chondrule olivines show two populations. One population overlaps somewhat with UOC compositions, while the other has properties intermediate between unequilibrated ordinary and CO chondrites.

The observed Fe/Mn trends in type IIA chondrule olivines in unequilibrated CO, CR and ordinary chondrites are difficult to reconcile with inherited moderately volatile element depletions from the precursor materials. Instead, we suggest that significant differences in the modal proportions of silicate and sulfides/(metal) in the precursor material and open system behavior during chondrule formation were responsible for establishing the different Fe/Mn trends. We further demonstrate that relict grains can be identified in type IIA chondrules, based on their distinct Fe-Mn-Mg systematics and discuss the origin of these grains.

INTRODUCTION

Chondrules, the major constituent of most chondritic meteorites, are (sub)-millimeter-sized spherules that were partly or completely melted by a transient heating event in the solar nebula before they accreted into asteroidal bodies. A number of different models have been suggested for chondrule formation, but the mechanism is still actively debated even after several decades of research (e.g., Boss 1996; Ciesla 2005). Chondrules exhibit diverse textures (e.g., porphyritic, barred, radial, or cryptocrystalline)

and the same textural types occur in chondrites of different chondrite groups. Differences in texture are thought to be the result of several factors, such as the number of viable nuclei surviving at the peak temperature, different cooling rates, bulk compositions of the precursor material and maximum temperatures reached in relation to their liquidus (e.g., Lofgren 1989; Hewins et al. 2005). We currently have only a limited understanding as to how chondrules of the same textural type compare between different chondrite groups (e.g., Scott and Taylor 1983). Several studies have shown that oxygen isotopic compositions of chondrules from different chondrite groups are significantly different (e.g., Clayton 2003; Yurimoto et al. 2008). However, we do not yet know if the differences in oxygen isotopic composition are reflected in mineral compositions and bulk chondrule compositions. Systematic differences between chondrules of similar textural types in different chondrite groups could be related to varying chondrule precursor materials, varying oxygen fugacity of separate formation regions in the solar nebula, or to other processes that affected the chondrule populations before they were incorporated into their individual parent bodies. Any such differences could potentially help to interpret oxygen isotopic heterogeneity. The main objective of the work presented in this paper is to investigate the characteristics of chondrule formation regions for each chondrite group by comparing mineral and bulk compositions of FeO-rich porphyritic olivine (type IIA) chondrules from unequilibrated ordinary, CR and CO chondrites.

Our study focuses on the elements Fe and Mn because they are commonly strongly correlated in various types of planetary materials and the Fe/Mn ratio in silicate minerals such as olivine and pyroxene is a very sensitive indicator for redox conditions and volatility (e.g., Miyamoto et al. 1993; Goodrich and Delaney 2000; Papike et al. 2003). In fact, Fe/Mn is such a useful ratio that it can be utilized to classify achondrites and basaltic meteorites (e.g., Goodrich and Delaney 2000; Mittlefehldt 2008). Olivines and pyroxenes in basalts from different asteroids and planets have significantly different Fe/Mn ratios and therefore, different slopes in Mn versus Fe plots (e.g., Schmitt and Laul 1973; Dymek et al. 1976; Karner et al. 2003; Papike et al. 2003). Papike et al. (2003) attributed this observation to the volatility of Mn and the distance of each parent body from the Sun. Type IIA chondrules are small-scale igneous systems (e.g., Jones 1990) and their oxidized nature assures high MnO and FeO contents. In this study, we show that type IIA

chondrules from ordinary and carbonaceous chondrites exhibit distinct Fe/Mn trends and discuss possible reasons for these differences. We also found that Fe/Mn systematics can be useful for identifying relict grains in type IIA chondrules.

SAMPLES AND ANALYTICAL CONDITIONS

In order to be able to explore the pristine nebular record contained in chondrules, we tried to select chondrites for this study that experienced minimal secondary processing, such as thermal metamorphism and/or aqueous alteration. Terrestrial weathering was another issue of concern. As it is basically impossible to come across a meteorite that is entirely unaltered, we account for secondary overprints in the discussion of our data below. The samples examined in this study include two thin sections of the CO chondrite Kainsaz (UNM 1050 and USNM 2486-5), two thin sections of the CR chondrite MET 00426 (JSC–,16-1 and JSC–,16-2), one thin section of the L chondrite MET 00526 (JSC–,25) and one thin section of the L chondrite QUE 97008 (JSC–,35). Kainsaz is an observed fall and has been classified as petrologic type 3.2 (e.g., Chizmadia et al. 2002; Grossman and Brearley 2005) and 3.6 (Bonal et al. 2007). Abreu (2007) recognized MET 00426 as one of the most pristine CR chondrites (type 3.0) that has experienced very minimal aqueous alteration. Floss and Stadermann (2009) have further shown that MET 00426 has high interstellar grain abundances comparable to ALHA 77307 and Acfer 094, supporting the classification of MET 00426 as a very pristine chondrite. Its weathering grade is B (Russell et al. 2002). MET 00526 was originally classified as H3.2 (Grady 2000; Connolly et al. 2007b), however, Grossman and Brearley (2005) suggested a petrologic type 3.05 and found that chondrule sizes may indicate an L or LL group classification. The L3.0 classification of this meteorite has been confirmed by Righter (2007). The weathering grade of MET 00526 is B/C (Connolly et al. 2007b). QUE 97008 was originally classified as L3.4 with a weathering grad of A (Grossman 1999). Benoit et al. (2002) recommended a petrologic type 3.0 for QUE 97008 based on thermoluminescence properties, while Grossman and Brearley (2005) suggested a petrologic type of 3.05 based on petrographic characteristics.

Scanning electron microscope imaging (backscattered electron, or BSE imaging), X-ray mapping and quantitative analyses were obtained on a JEOL 8200 electron microprobe at the University of New Mexico. Bulk chemical compositions of 5 type IIA chondrules in Kainsaz (CO), 2 type IIA chondrules in MET 00426 (CR) and 3 type IIA chondrules in MET 00526 (L) were determined by modal recombination analysis (MRA). These chondrules are part of a larger dataset of bulk chondrule compositions (Chapter 1), for which 20 chondrules with different textures were randomly selected per chondrite. Quantitative analyses were obtained on all phases present in a chondrule and were then combined with their weighted modal proportions to obtain the bulk composition (Berlin et al. 2008b, Appendix A). WDS element maps were used to identify the different phases present. In order to avoid Na loss as discussed in Grossman and Brearley (2005), mesostasis analyses were obtained (5 μm beam diameter, 10 nA beam current) before element maps were collected. The chondrules were mapped with a beam current of 30 nA and a pixel-size between 0.5 and 1.5 μm (depending on chondrule size) for a suite of 5 elements (Al, Ca, Mg, Fe, S). Silicates were analyzed with a focused beam, an accelerating voltage of 15 keV and a beam current of 20 nA. Metals and sulfides were analyzed with a focused beam at 20 keV and a beam current of 40 nA. The number of analyses obtained on a certain mineral phase was between 1 and 15, depending on its modal abundance.

Figure 2.1 shows BSE images of three chondrules and their corresponding phase images that were assembled with the phase tool in Lispix Lx133P (public domain image analysis program for Windows, written and maintained by David Bright, National Institute of Standards and Technology) and/or Adobe Photoshop® based on the collected X-ray maps. Modal abundances of the different phases present were determined with Lispix or with Scion Image®. Refer to Appendix B for a comparison of the two methods. Each color in a phase image represents a certain mineral phase (refer to legends in **Fig. 2.1b,d,f**). In order to take the zoning of olivine crystals into account, a range of olivine compositions was binned into one color (i.e., one shade of green in **Fig. 2.1b,d,f**) based on the collected WDS element map for Mg and the average composition of all analyses obtained in this area was used for the bin range. In each chondrule we defined 3 or 4 bins.

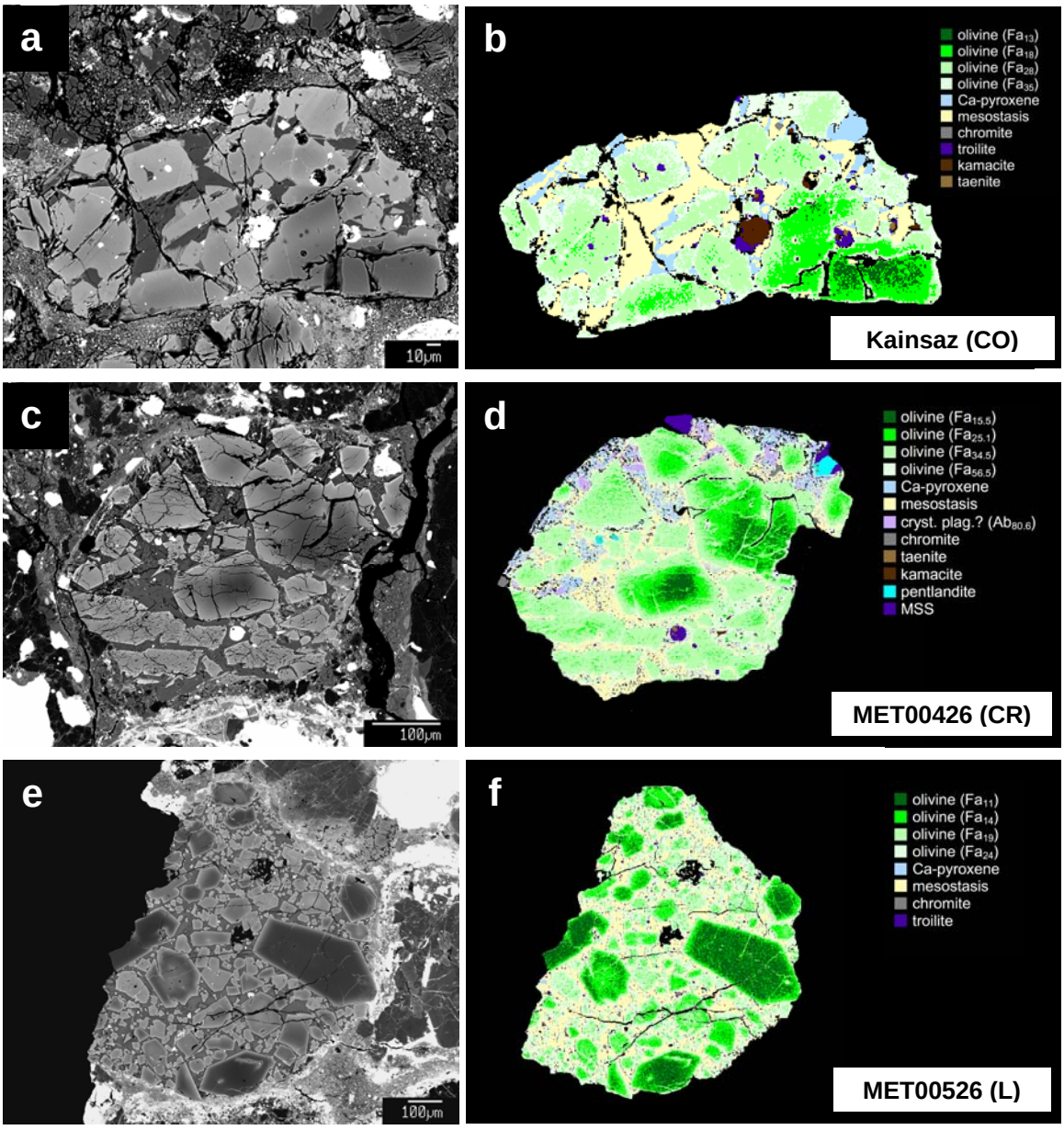

Fig. 2.1. Backscattered electron (BSE) images of type IIA chondrules and their corresponding phase images used for modal analysis. a) and b) Kainsaz (CO) chondrule K2-Ch7. c) and d) MET 00426 (CR) chondrule CR-Ch13. e) and f) MET 00526 (L) chondrule L-Ch4.

RESULTS

Olivine compositions

As is typical for ordinary and most carbonaceous chondrites, two distinct populations of porphyritic chondrules are present in the meteorites examined in this study: FeO-poor (type I) and FeO-rich (type II) chondrules (e.g., Jones et al. 2005). These two types show some textural differences, such as higher amounts of Fe,Ni metal in type I chondrules and larger olivine phenocrysts in type II chondrules (e.g., Scott and Taylor 1983), but the main differences are in their olivine and low-Ca pyroxene compositions. **Figure 2.2** shows histograms for the Fa contents of olivines in porphyritic chondrules in Kainsaz (CO3.2), MET 00426 (CR3.0), MET 00526 (L3.05) and QUE 97008 (L3.05). The histograms do not represent completely random surveys, because only a limited number of chondrules were chosen. As described in Chapter 1, we found that type I chondrules in the two pristine chondrites MET 00426 (CR) and MET 00526 (L) typically have mean olivine and low-Ca pyroxene compositions with an Fe/(Fe+Mg) atomic ratio <5%. The range of olivine compositions in Kainsaz type I chondrules extends to Fa contents >5%. This difference, which is attributable to minor thermal metamorphism in Kainsaz, will be addressed in the Discussion. Type II chondrules in all chondrites studied have mean olivine (and low-Ca pyroxene) compositions with an Fe/(Fe+Mg) atomic ratio >10%, which is the cut-off value that has generally been used to distinguish between type I and type II chondrules (e.g., Jones et al. 2005). In MET 00426 (CR), the gap in Fa contents between type I and type II chondrules appears to be larger and more significant than in MET 00526 (L) (**Fig. 2.2b** vs. **Fig. 2.2c)** and other ordinary chondrites (e.g. Takagi et al. 2004).

Type II chondrule olivines have large compositional ranges, and mean Fa contents calculated using all the type II chondrule olivine analyses from each chondrite decrease from CO (Fa_{34}) > CR (Fa_{29}) > L ($Fa_{19\text{-}20}$). The means for type II chondrules exclude relict forsterite cores of olivine grains, which were also not included in **Figure 2.2**. However, the histograms do include some compositions with Fa<10 (**Fig. 2.2**) that we think crystallized from the host chondrule melt (see Bulk Chondrule Compositions section below).

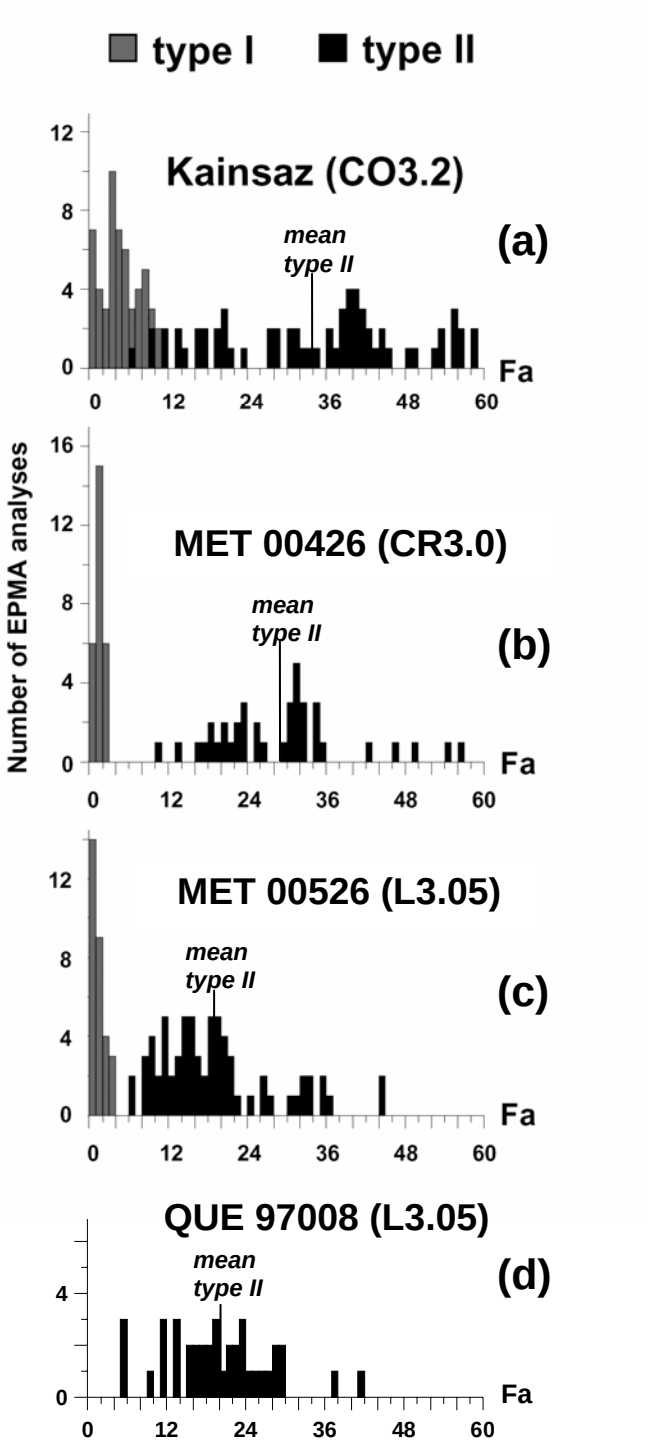

Fig. 2.2. Histograms of olivine compositions in porphyritic chondrules (3 to 10 analyses per chondrule). a) Kainsaz: 11 type IA/AB and 6 type IIA/AB chondrules, b) MET 00426: 9 type IA/AB and 2 type IIA chondrules plus several type II chondrule fragments, c) MET 00526: 7 type IA/AB and 8 type IIA/AB chondrules and d) QUE 97008: 6 type IIA chondrules. No type I chondrules were analyzed in QUE 97008. Fa contents of type I chondrule olivines in Kainsaz are somewhat higher than in the more primitive CR and L chondrite because of Fe-Mg exchange with the surrounding FeO-rich matrix (e.g., Scott and Jones 1990). Mean Fa contents of type II chondrules decrease from CO > CR > L. Forsteritic relict grains in type II chondrules were omitted from this figure. The lowest Fa contents of olivine in type II chondrules represent cores of large zoned grains that crystallized from the chondrule melt (refer to Table 2.4).

Representative type IIA olivine compositions from the different chondrites are given in **Table 2.1**, which compares individual microprobe analyses with approximately the same Fa content (~Fa_{17}). In these specific examples, MnO, Cr_2O_3 and CaO contents increase from CO to CR to UOC chondrites.

Table 2.1. Representative type IIA chondrule olivine compositions (at ~Fa_{17}).

	Kainsaz (CO) this work	MET 00426 (CR) this work	MET 00526 (L) this work	QUE 97008 (L) this work	Semarkona (LL) Jones (1990)
SiO_2	39.9	39.7	39.7	39.5	39.4
TiO_2	<0.04	<0.04	<0.04	<0.04	<0.04
Al_2O_3	0.10	<0.03	<0.03	<0.03	<0.03
Cr_2O_3	0.18	0.29	0.34	0.44	0.40
FeO	16.6	16.1	16.6	16.2	16.1
MnO	0.16	0.23	0.34	0.32	0.34
MgO	43.7	44.2	44.6	44.3	44.1
CaO	0.06	0.10	0.13	0.12	0.13
NiO	<0.03	0.04	<0.03	<0.03	0.04
Total	100.7	100.7	101.7	100.9	100.5
Cations based on 4 oxygens:					
Si	1.000	0.996	0.987	0.990	0.991
Ti	0.001	0.000	0.000	0.000	0.001
Al	0.003	0.001	0.001	0.001	0.000
Cr	0.004	0.006	0.007	0.009	0.008
Fe	0.348	0.338	0.346	0.340	0.339
Mn	0.003	0.005	0.007	0.007	0.007
Mg	1.636	1.652	1.654	1.654	1.654
Ca	0.002	0.003	0.004	0.003	0.004
Ni	0.000	0.001	0.000	0.000	0.001
Total	2.997	3.002	3.006	3.004	3.004
Fa	17.5	17.0	17.3	17.1	17.0
Fe/Mn	104	69	49	51	47

However, the picture becomes more complicated, especially for Cr_2O_3 and CaO, when more data are taken into account. **Figure 2.3** shows minor element data, in afu (atomic formula units) based on four oxygen atoms, for type IIA chondrule olivines from several different chondrites. Data from this study include 5 chondrules in Kainsaz (CO3.2), 2 chondrules and several chondrule fragments in MET 00426 (CR3.0), as well as 6 chondrules each in MET 00526 (L3.05) and QUE 97008 (L3.05). Literature data include 4 chondrules in the CO3.0 chondrite ALHA 77307 (Jones 1992), data from zoning profiles of olivines in 8 chondrules in the LL3.00 chondrite Semarkona (Jones 1990), as well as 2 chondrules in the CR2 chondrite EET 92105 and 1 chondrule in the CR2 chondrite EET 87770 (Burger 2005). In **Figure 2.3a** (Cr vs. Fe), most analyses of type IIA chondrule olivines in the pristine ordinary chondrites (MET 00526, QUE 97008 and Semarkona) show higher Cr contents at a specific Fe content than in CR and CO chondrites. Type IIA olivines in MET 00426 (CR3) and in ALHA 77307 (CO3.0) have

higher Cr contents than olivines in the less pristine CR and CO chondrites. **Figure 2.3b** (Ca vs. Fe) shows that there are no systematic differences in Ca content between the UOC, CR and CO groups. In most type IIA chondrule olivines, Ni is below the detection limit of 0.03 wt% NiO.

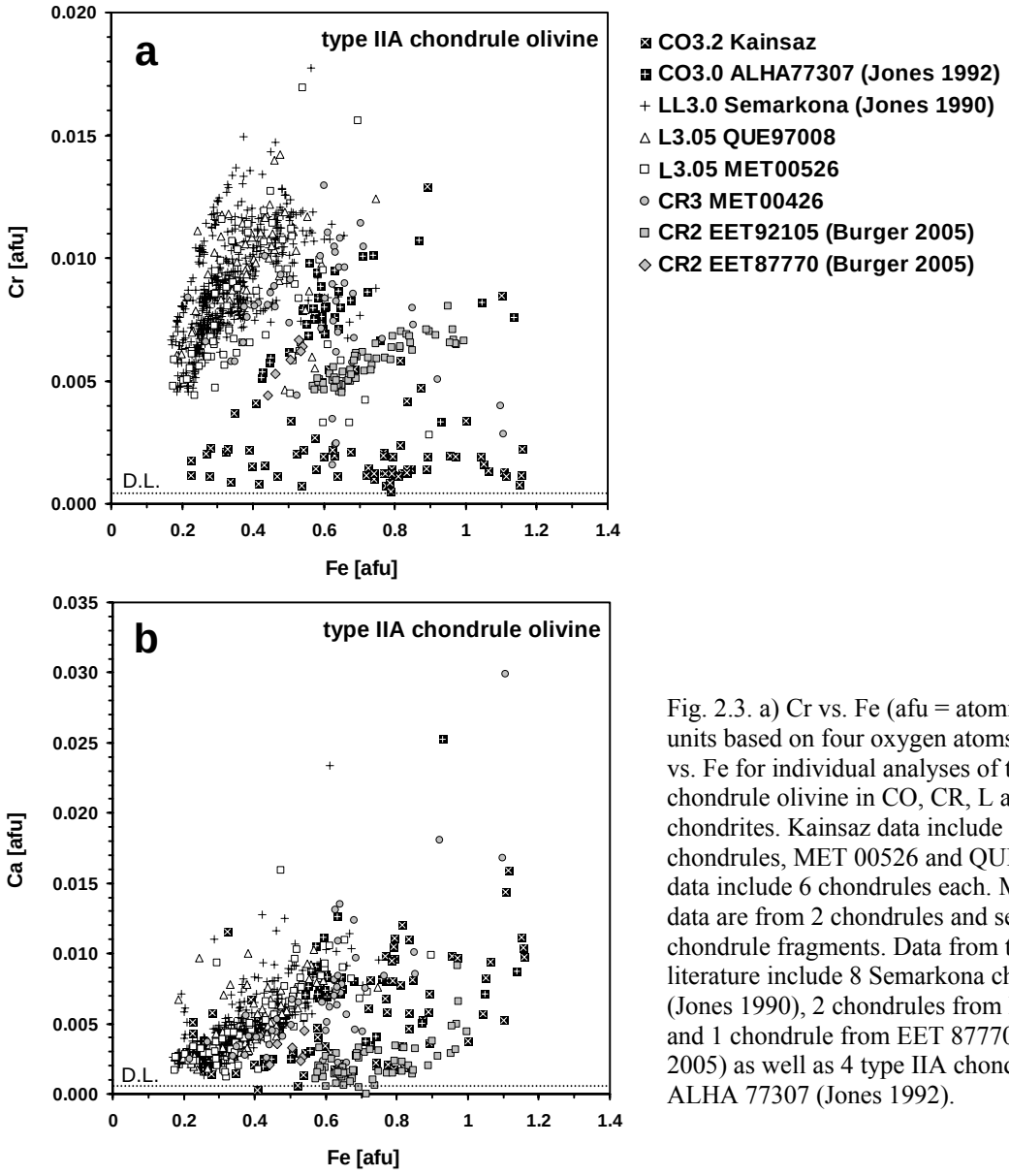

Fig. 2.3. a) Cr vs. Fe (afu = atomic formula units based on four oxygen atoms) and b) Ca vs. Fe for individual analyses of type IIA chondrule olivine in CO, CR, L and LL chondrites. Kainsaz data include 5 chondrules, MET 00526 and QUE 97008 data include 6 chondrules each. MET 00426 data are from 2 chondrules and several chondrule fragments. Data from the literature include 8 Semarkona chondrules (Jones 1990), 2 chondrules from EET 92105 and 1 chondrule from EET 87770 (Burger 2005) as well as 4 type IIA chondrules from ALHA 77307 (Jones 1992).

Figure 2.4 compares Fe-Mn systematics of type IIA chondrule olivine in different chondrites. On a plot of Mn (afu) vs. Fe (afu) (**Fig. 2.4a**), type IIA chondrule olivines in CO and ordinary chondrites (UOC) exhibit distinct trends: best-fit linear regressions for all data have slopes of 0.010 and 0.023, respectively. Our Kainsaz data closely overlap the ALHA 77307 data from Jones (1992). Fe/Mn ratios of type IIA chondrule olivines of L and LL chondrites are indistinguishable. **Figure 2.4b** shows Mn (afu) vs. Fe (afu) for type IIA chondrule olivines in CR chondrites. Two populations can be identified – one that plots distinctly between CO and ordinary chondrites (2 chondrules in EET 92150 and 1 chondrule [Ch13] in MET 00426) and another that overlaps somewhat with ordinary chondrites (1 chondrule in EET 87770 and 1 chondrule [Ch6] in MET 00426). **Figure 2.4c** shows molar Fe/Mn vs. molar Fe/Mg for type IIA chondrule olivines in CO and unequilibrated ordinary chondrites. On this plot, CO chondrule olivines plot in an array fairly parallel to the x-axis (mean Fe/Mn = 99). The large range in Fe/Mn ratios for CO chondrule olivine is mainly due to the fact that MnO contents are low and variable due to the precision/statistical variation of microprobe analyses and that a large number (Fe) is divided by a small number (Mn). The data for type IIA chondrule olivines in UOC show a much smaller range in Fe/Mg ratios, but also a large range in Fe/Mn ratios (mean Fe/Mn = 44). Since MnO contents are higher and FeO contents are lower than in CO chondrule olivine, the errors related to the values of Fe/Mn ratios for UOC are somewhat smaller than for CO chondrule olivine. Therefore, the range in Fe/Mn ratios is better constrained for UOC than for CO type IIA chondrule olivine. **Figure 2.4d** shows molar Fe/Mn vs. molar Fe/Mg for type IIA chondrule olivines in CR chondrites. In general, Fe/Mn ratios decrease as Fe/Mg ratios increase. The same two populations can be observed as in **Figure 2.4b**.

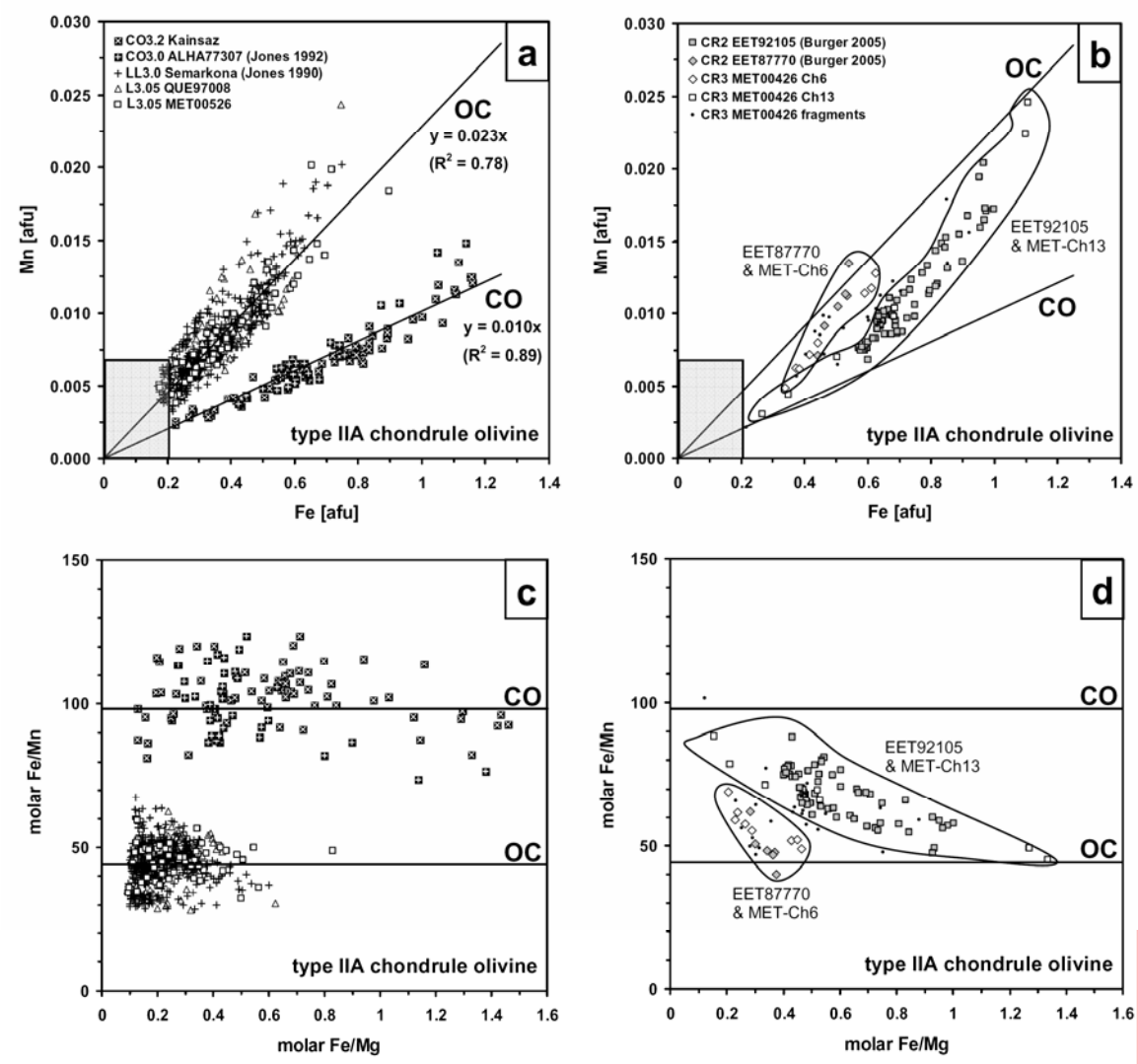

Fig. 2.4. a) Mn (afu) vs. Fe (afu) for individual analyses of type IIA chondrule olivine in CO and ordinary chondrites (OC). Trendlines are best-fit linear regressions forced through the origin. b) Mn (afu) vs. Fe (afu) for type IIA chondrule olivines in CR chondrites. Shaded box in (a) and (b) indicates type I chondrule olivine compositions from all chondrites studied. c) and d) Molar Fe/Mn vs. molar Fe/Mg. Symbols as for (a) and (b). Data sources and number of chondrules as in Figure 2.3.

Fe-Mn data for olivines in Semarkona (from Jones 1990) are shown in more detail in **Figure 2.5**. Each chondrule, represented by zoning profiles across several grains, has a slightly different slope in the Mn vs. Fe plot (**Fig. 2.5a**), which accounts for much of the scatter in the UOC data in **Figure 2.4a**. The two linear regressions bracket the range of data: for chondrule C131 the slope is 0.031 and for C71 the slope is 0.019. In the molar Fe/Mn vs. molar Fe/Mg plot (**Fig. 2.5b**), it is apparent that for most chondrules Fe/Mn ratios tend to decrease slightly as Fe/Mg ratios increase. Two chondrules, A21 and C11, show somewhat steeper negative trends.

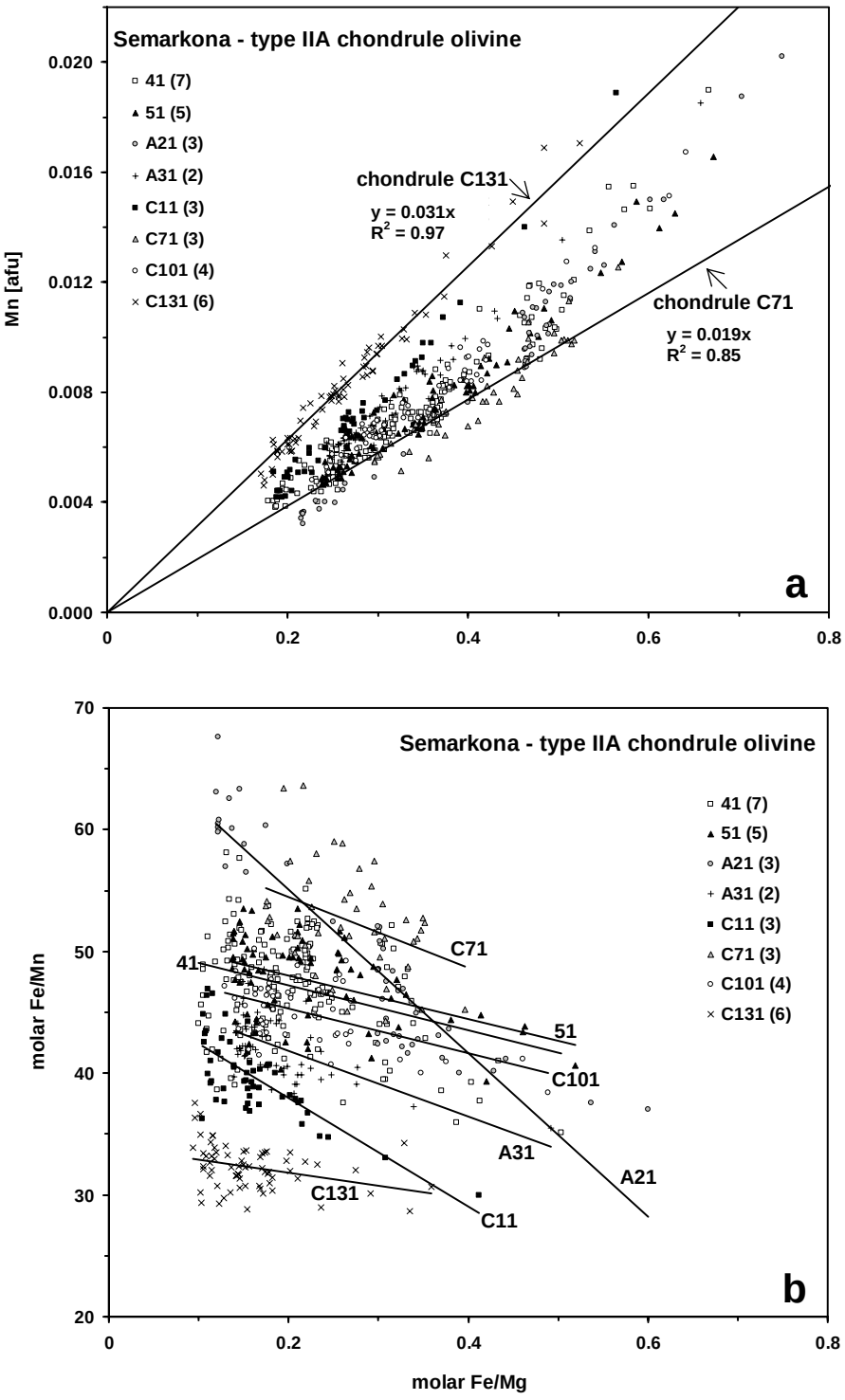

Fig. 2.5. a) Mn vs. Fe for zoning profiles of olivines in type IIA chondrules from Semarkona. Data are from Jones (1990). Each symbol represents one chondrule. The number of olivine grains per chondrule is given in brackets in the legend. Trendlines are best-fit linear regressions forced through the origin. b) Molar Fe/Mn vs. molar Fe/Mg for the same dataset as in (a). Trendlines are linear regressions for each chondrule.

Relict grains

This study has allowed us to identify several relict grains on the basis of Fe-Mn-Mg relationships, as discussed below. Representative microprobe analyses of cores of grains we consider to be relict are given in **Table 2.2**. Analyses of these grains were not included in **Figures 2.4 and 2.5**.

Table 2.2. Microprobe analyses of relict olivine cores.

	Kainsaz, K1-Ch8 Relict 1	Kainsaz, K1-Ch8 Relict 2	Semarkona, 51 Grain 51E
SiO_2	39.5	41.2	40.0
TiO_2	<0.04	<0.04	<0.04
Al_2O_3	0.04	<0.03	<0.03
Cr_2O_3	0.15	0.03	0.34
FeO	18.7	10.1	16.4
MnO	0.89	0.23	0.10
MgO	41.7	49.3	42.9
CaO	0.18	0.19	0.13
NiO	<0.03	<0.03	n.a.
Total	101.2	101.1	99.9
Cations based on 4 oxygens:			
Si	1.000	0.999	1.010
Ti	0.000	0.000	0.000
Al	0.001	0.000	0.000
Cr	0.003	0.001	0.007
Fe	0.395	0.205	0.347
Mn	0.019	0.005	0.002
Mg	1.574	1.785	1.616
Ca	0.005	0.005	0.004
Ni	0.000	0.001	0.000
Total	2.997	3.001	2.986
Fa	20.1	10.3	17.7
Fe/Mn	21	43	162

In Kainsaz chondrule K1-Ch8 (**Fig. 2.6a**), we found that the relict core of Grain 1 (**Fig. 2.6a,b**) has an unusually high Mn content while the host chondrule olivines plot along the CO line (slope 0.010) in the Mn vs. Fe diagram (**Fig. 2.6d**). The relict core of another grain in the same chondrule (Grain 2, **Fig. 2.6a,c**) has a higher Mn content than typical CO type IIA chondrule olivines (**Fig. 2.6d**). Close-up images of these grains (**Fig. 2.6b,c**) reveal the presence of tiny metal blebs (<1 μm). In the molar Fe/Mn vs. molar Fe/Mg diagram (**Fig. 2.6e**), the host chondrule olivines exhibit a trend parallel to the x-

axis (mean Fe/Mn = 105), while the relict cores have much lower Fe/Mn ratios. The Fe/Mn ratio of the relict core of Grain 1 (~21) is lower than the range observed for UOC type IIA chondrule olivine (28-68; mean Fe/Mn = 44). Fe/Mn ratios are higher towards the edge of the grain, approaching the mean value for the host chondrule olivines. The Fe/Mn ratio of the relict core of Grain 2 (~43) falls within the UOC range.

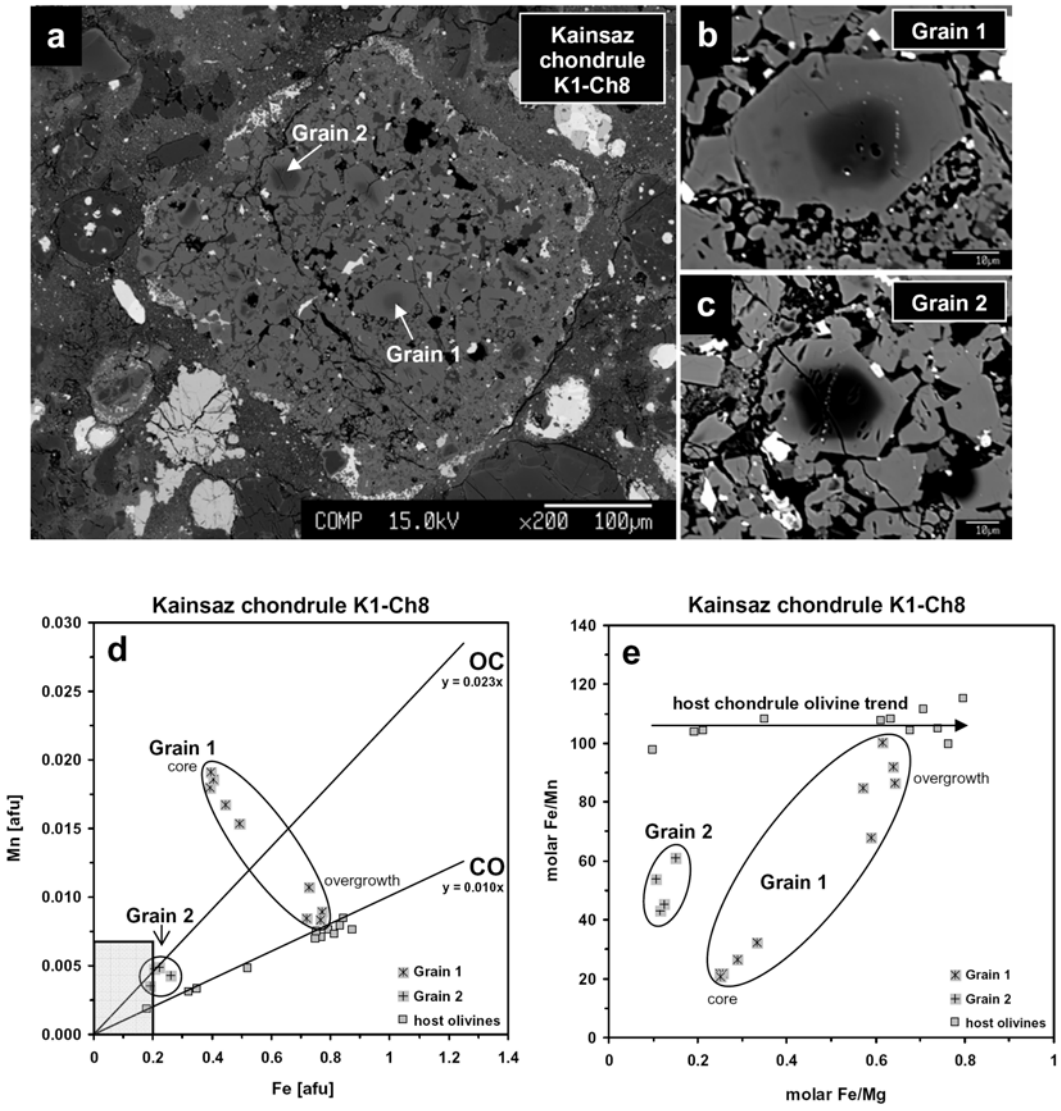

Fig. 2.6. a) BSE image of Kainsaz chondrule K1-Ch8. The two grains that have relict cores with Mn contents higher than the host chondrule olivines are indicated and shown in b) and c). d) Mn vs. Fe and e) molar Fe/Mn vs. molar Fe/Mg of olivines from the chondrule shown in (a). Shaded box in (d) indicates type I chondrule olivine compositions from all chondrites studied.

We also identified a relict grain in Semarkona chondrule 51 (see Jones 1990). An elongated olivine grain (51E) in the center of the chondrule (**Fig. 2.7a**) has an unusually low Mn content compared to all other UOC data (**Fig. 2.7b**), with a composition that lies close to the CO line (slope 0.010). The core of this relict grain has an Fe/Mn ratio as high as 162 (**Fig. 2.7c**), which is significantly above the CO range (74-124; mean Fe/Mn = 99).

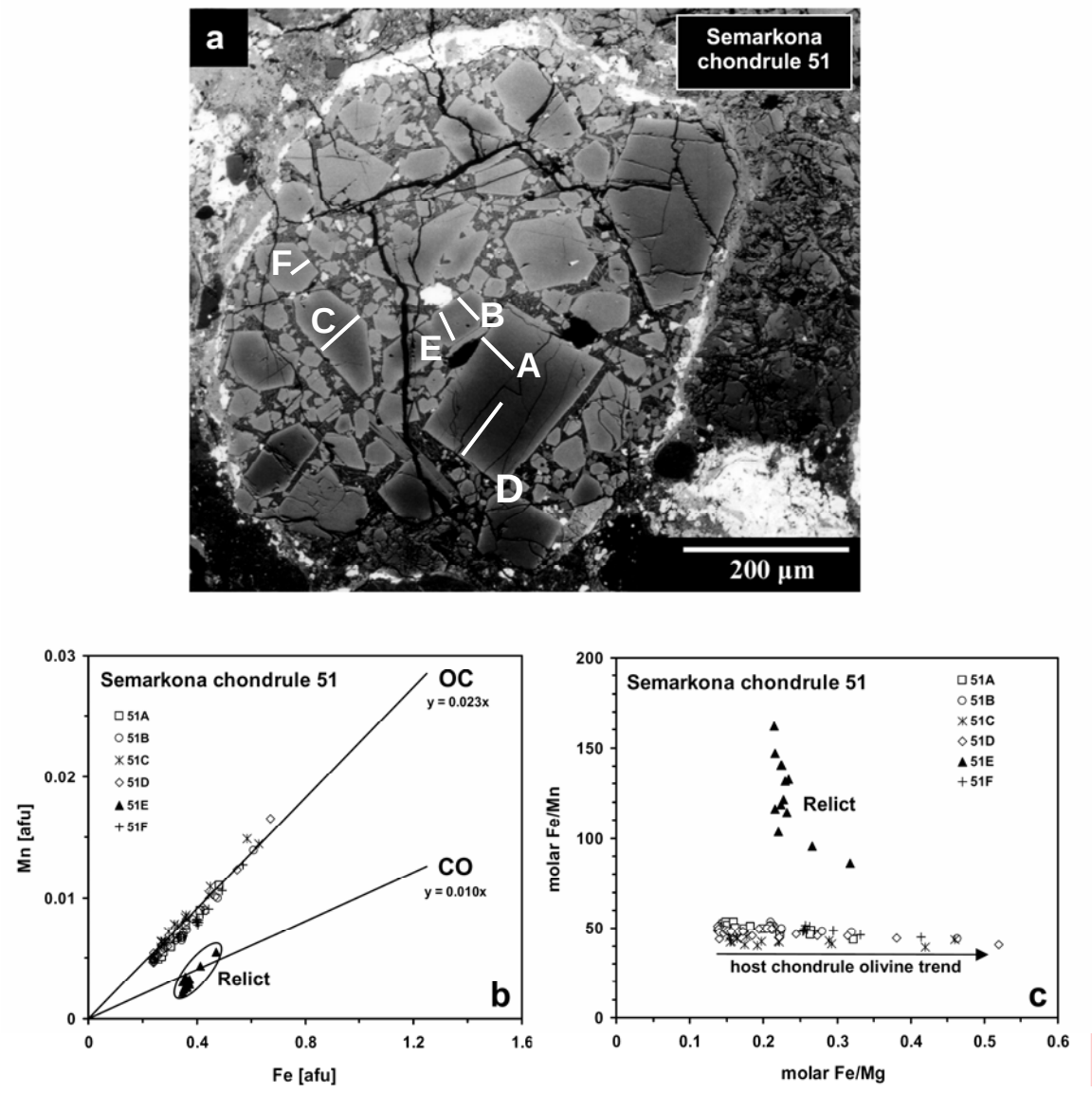

Fig. 2.7. a) BSE image of Semarkona chondrule 51 (Jones 1990). Zoning profiles are indicated. b) Mn vs. Fe and c) molar Fe/Mn vs. molar Fe/Mg of olivines from the chondrule shown in (a). Zoning profile 51E belongs to a relict core that has a much lower Mn content and a higher Fe/Mn ratio than its overgrowth (zoning profile B) and than other olivine grains in this chondrule.

Mesostasis compositions

Average mesostasis compositions for several type IIA chondrules in MET 00526 (L), MET 00426 (CR) and Kainsaz (CO) are given in **Table 2.3** together with the mean mesostasis composition for type IIA chondrules from Semarkona (Jones 1990). SiO_2 contents of type IIA chondrule mesostases in UOCs are higher than in the CO and the CR chondrites. P_2O_5 and K_2O contents are significantly higher in ordinary chondrites and in the CR chondrite than in Kainsaz.

Table 2.3. Average mesostasis compositions of type IIA chondrules.

	MET 00526 (L3.05)			Semarkona (LL3.0)	MET 00426 (CR3)		Kainsaz (CO3.2)				
	L-Ch4	L-Ch7	L-Ch9	Mean[a] Jones (1990)	CR-Ch6	CR-Ch13	K1-Ch7	K1-Ch8	K1-Ch16	K2-Ch4	K2-Ch7
SiO_2	60.6	66.6	65.3	62.6	57.5	56.0	52.6	52.9	50.7	53.7	58.9
TiO_2	0.47	0.49	0.48	0.45	0.40	0.52	0.15	0.06	0.48	0.64	0.07
Al_2O_3	10.2	12.0	11.4	11.2	10.6	12.9	24.3	25.6	13.2	17.2	24.2
Cr_2O_3	0.11	0.13	0.12	0.30	0.03	0.04	0.30	0.14	0.58	0.10	0.20
FeO	9.5	9.0	7.7	7.8	9.7	11.2	4.7	4.2	11.8	4.5	1.9
MnO	0.30	0.30	0.27	0.28	0.38	0.19	<0.03	<0.03	0.08	0.05	<0.03
MgO	2.5	2.5	2.3	4.5	5.3	1.2	2.3	2.1	6.9	4.7	0.62
CaO	7.2	1.1	4.1	7.2	2.0	6.2	9.6	9.8	7.0	7.1	6.5
Na_2O	6.2	6.6	6.7	4.1	10.5	9.3	5.9	5.5	9.3	11.0	8.2
K_2O	0.80	0.98	0.96	0.58	1.3	1.3	0.17	0.05	0.16	0.25	0.06
NiO	<0.03	0.22	0.08	n.a.	0.05	0.08	<0.03	<0.03	<0.03	<0.03	<0.03
P_2O_5	2.0	0.73	1.2	1.3	1.9	1.3	<0.04	0.05	0.51	0.72	0.05
S	0.12	0.09	0.13	n.a.	0.21	0.12	0.05	<0.03	0.23	0.13	<0.03
Total	100.1	100.8	100.7	100.3	99.7	100.3	100.1	100.4	100.9	100.4	100.7

n.a. = not analyzed
[a]mean of 10 chondrules

Figure 2.8a shows Al_2O_3 versus SiO_2 for individual mesostasis analyses of each chondrule from this study. Al_2O_3 and SiO_2 contents show a wide range within a single chondrule (e.g., K1-Ch7, K1-Ch8, K1-Ch16) when mesostasis is present in small pockets rather than being interconnected. Three Kainsaz chondrules (K1-Ch7, K1-Ch8, K2-Ch7) have higher Al_2O_3 contents in their mesostasis than the other chondrules. They also have lower TiO_2, P_2O_5 and S contents (**Table 2.3**).

Figure 2.8b shows alkali contents of mesostases relative to Al and CI chondrites. Mesostases in CR and UOC have K/Al > Na/Al (relative to CI chondrites), whereas in CO, Na/Al > K/Al. CR and CO type IIA chondrule mesostases show a large spread in Na/Al ratios in comparison to mesostases in type IIA chondrules in UOC. The three Kainsaz chondrules that have the highest Al_2O_3 contents in their mesostasis have Na/Al<1, whereas the mesostasis in the other two Kainsaz chondrules have Na/Al ratios closer to 2.

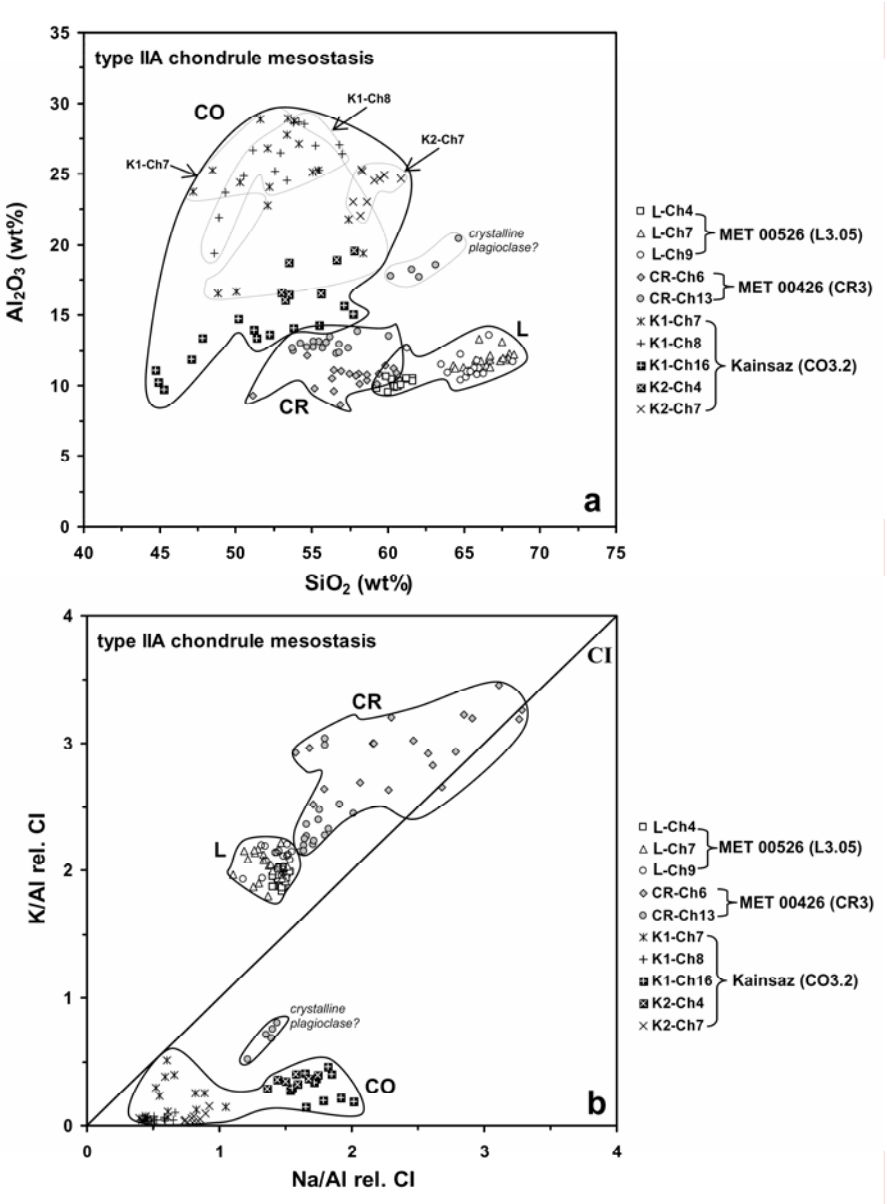

Fig. 2.8. a) Al_2O_3 vs. SiO_2 (wt%) and b) K/Al vs. Na/Al (elemental weight ratios, relative to CI chondrite) for individual mesostasis analyses from 10 type IIA chondrules (3 chondrules from the L chondrite MET 00526, 2 chondrules from the CR chondrite MET 00426 and 5 chondrules from Kainsaz).

One chondrule in the CR chondrite MET 00426 (CR-Ch13, also refer to **Fig. 2.1c,d**) contains a distinct phase that is close to plagioclase in composition (~Ab_{81}) and stoichiometry. It has higher Al_2O_3 and SiO_2 contents than the mesostasis in chondrule CR-Ch13 (**Fig. 2.8a**). In **Figure 2.8b**, it plots near to the mesostasis compositions of Kainsaz chondrules. All individual analyses of the putative plagioclase in CR-Ch13 have MgO contents below 1 wt%, as do several individual mesostasis analyses in Kainsaz chondrules K1-Ch7, K1-Ch8, and K2-Ch7 (refer to supplementary CD).

Bulk chondrule compositions

Bulk compositions of type IIA chondrules in MET 00526 (L), MET 00426 (CR) and Kainsaz (CO) are given in **Table 2.4**. Element abundance patterns for individual type IIA chondrules and mean type IIA bulk compositions, including Semarkona data from Jones (1990) are shown in **Figures 2.9a** and **2.9b**, respectively. Mean bulk Fe contents in type IIA chondrules increase from UOC to CR to CO, while Si and Mg contents decrease slightly. Moderately volatile elements (Cr, Mn, P, and K) are depleted in CO type IIA chondrules relative to type IIA chondrules in CR and UOCs, and Cr, P and K are depleted in CO type IIA chondrules relative to bulk CI chondrites. Bulk molar Fe/Mn ratios increase with increasing bulk Fe content (**Fig. 2.10a**) and decrease with increasing bulk Si content (**Fig. 2.10b**).

Liquidus temperatures for the different bulk chondrule compositions and Fa contents of the first olivine grains to crystallize are also given in **Table 2.4**. These parameters were calculated with MELTS (http://melts.ofm-research.org/) at 1 bar, using the composition of the silicate portion of the chondrule. Most liquidus temperatures were determined at the IW buffer, as this appears to be a reasonable oxygen fugacity for the formation conditions of type II chondrules (e.g., Lofgren 1989). However, for some compositions, calculations at the IW buffer resulted in unreasonably high temperatures or even failed, but were acceptable when calculated at FMQ+0.5 (see **Table 2.4**): this is an artifact of MELTS and does not necessarily mean that the chondrules concerned formed at a much higher oxygen fugacity. Lower liquidus temperatures were observed for CO type IIA chondrules (1609-1632ºC), whereas two of the three L chondrules and CR-Ch6 have liquidi above 1700ºC. Calculated fayalite contents of the first olivine grains that

crystallize from a given bulk composition range from 4 to 6 mol% for type IIA chondrules in the L chondrite and from 7 to 10 mol% for those in Kainsaz. Calculated initial Fa contents for olivines in Kainsaz chondrules K1-Ch8 and K2-Ch4 are very close to the lowest Fa contents measured at the cores of large olivine grains (**Table 2.4**).

Table 2.4. Bulk compositions (element wt%) and liquidus phase relationships of type IIA chondrules.

	MET 00526 (L3.05)				MET 00426 (CR3)			Kainsaz (CO3.2)					
	L-Ch4	L-Ch7	L-Ch9	*mean*	CR-Ch6	CR-Ch13	*mean*	K1-Ch7	K1-Ch8	K1-Ch16	K2-Ch4	K2-Ch7	*mean*
Si	19.6	20.8	19.2	*19.9*	18.5	18.2	*18.3*	17.6	15.9	17.0	18.5	18.5	*17.5*
Ti	0.05	0.09	0.04	*0.06*	0.01	0.08	*0.05*	0.06	0.02	0.01	0.11	0.07	*0.05*
Al	0.88	1.3	0.54	*0.90*	0.27	1.4	*0.86*	0.94	0.85	0.27	2.1	1.7	*1.2*
Cr	0.28	0.42	0.32	*0.34*	0.28	0.33	*0.31*	0.53	0.10	0.06	0.09	0.10	*0.18*
Fe	13.9	14.8	12.8	*13.8*	15.6	22.3	*19.0*	22.6	30.2	27.9	18.7	20.2	*23.9*
Mn	0.28	0.34	0.27	*0.30*	0.28	0.33	*0.31*	0.20	0.21	0.27	0.15	0.17	*0.20*
Mg	21.3	18.0	23.3	*20.8*	23.2	14.4	*18.8*	16.4	14.2	15.7	15.8	16.7	*15.7*
Ca	1.0	1.3	0.75	*1.0*	0.17	1.3	*0.75*	1.3	1.1	0.29	1.3	1.6	*1.1*
Na	0.75	1.0	0.46	*0.74*	0.36	1.2	*0.80*	0.29	0.27	0.27	2.0	0.86	*0.73*
K	0.13	0.17	0.09	*0.13*	0.07	0.20	*0.13*	0.03	0.02	0.02	0.06	0.03	*0.03*
Ni	0.02	0.09	0.03	*0.04*	0.02	0.20	*0.11*	0.08	0.81	0.15	0.03	0.29	*0.27*
P	0.14	0.06	0.04	*0.08*	0.04	0.12	*0.08*	0.00	0.00	0.01	0.05	0.00	*0.01*
S	0.55	0.47	1.6	*0.89*	0.01	1.3	*0.66*	0.25	1.4	0.05	1.4	0.56	*0.73*
molar Fe/Mn	49	43	47	*46*	55	67	*61*	109	143	104	132	121	*122*
(a)	1717	1640	1765			1585					1623	1632	
(b)					1770			1630	1609	1631			
(c)	5	6	4		5	9		8	10	10	7	7	
(d)	10.2	14.7	8.8		18.6	13.5		11.3	9.0	31.5	6.4	13.5	

(a) Liquidus temperature (ºC) calculated using MELTS, at IW buffer.
(b) Liquidus temperature (ºC) calculated using MELTS, at FMQ+0.5.
(c) Fa content of the first olivine that crystallizes from the melt, calculated with MELTS.
(d) Observed Fa content of the most Mg-rich olivine present in the chondrule.

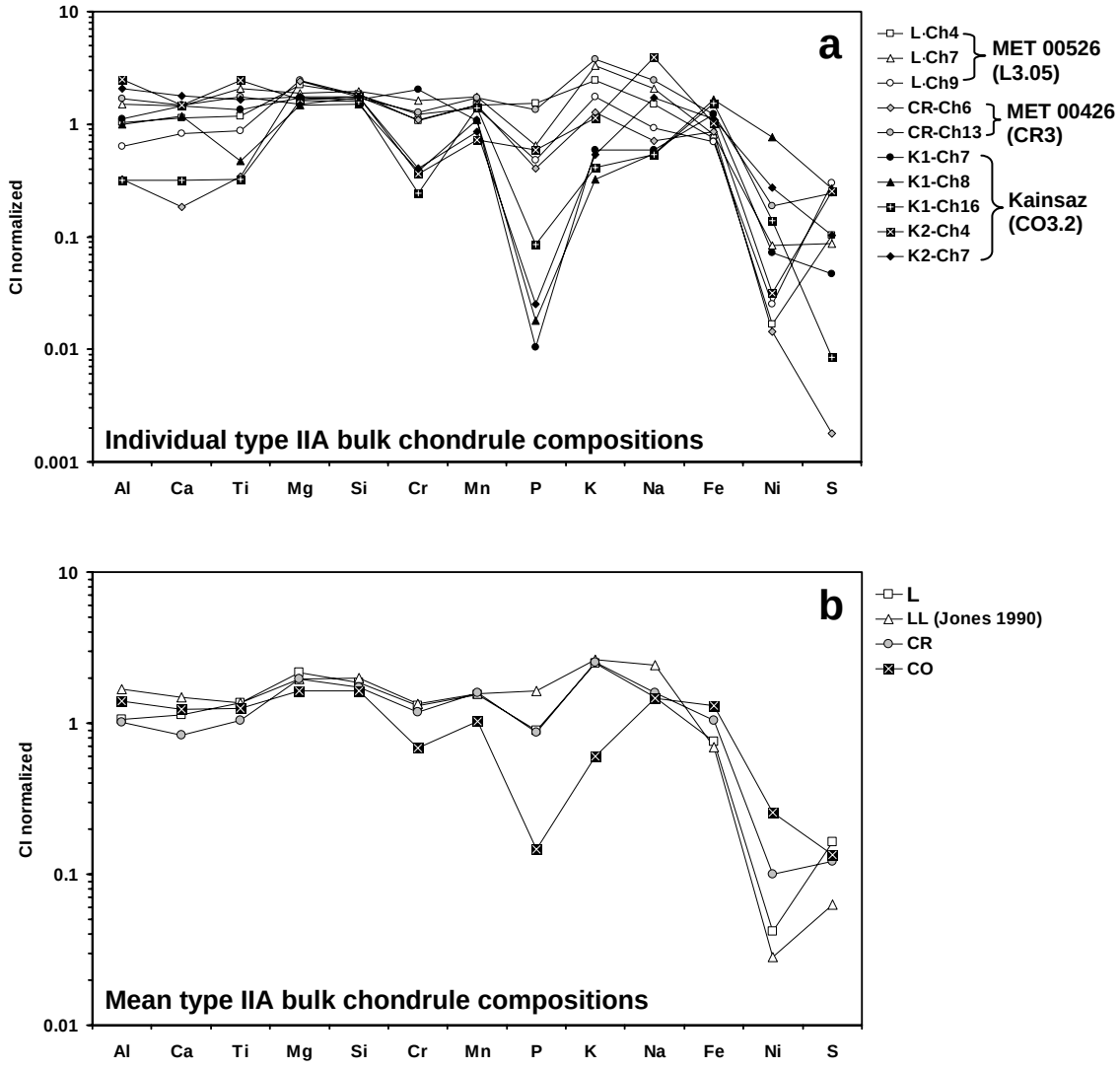

Fig. 2.9. a) Bulk chemical compositions of individual type IIA chondrules in MET 00526 (L3.05), MET 00426 (CR3) and Kainsaz (CO3.2) determined by modal recombination analysis in this study. Elemental abundances are normalized to CI chondrite abundances (Lodders 2003). Elements on the ordinate are arranged in order of increasing volatility; siderophile elements are plotted last. b) Mean bulk chemical compositions of type IIA chondrules for each meteorite shown in (a). LL chondrite data are the mean of 11 type IIA Semarkona chondrules from Jones (1990).

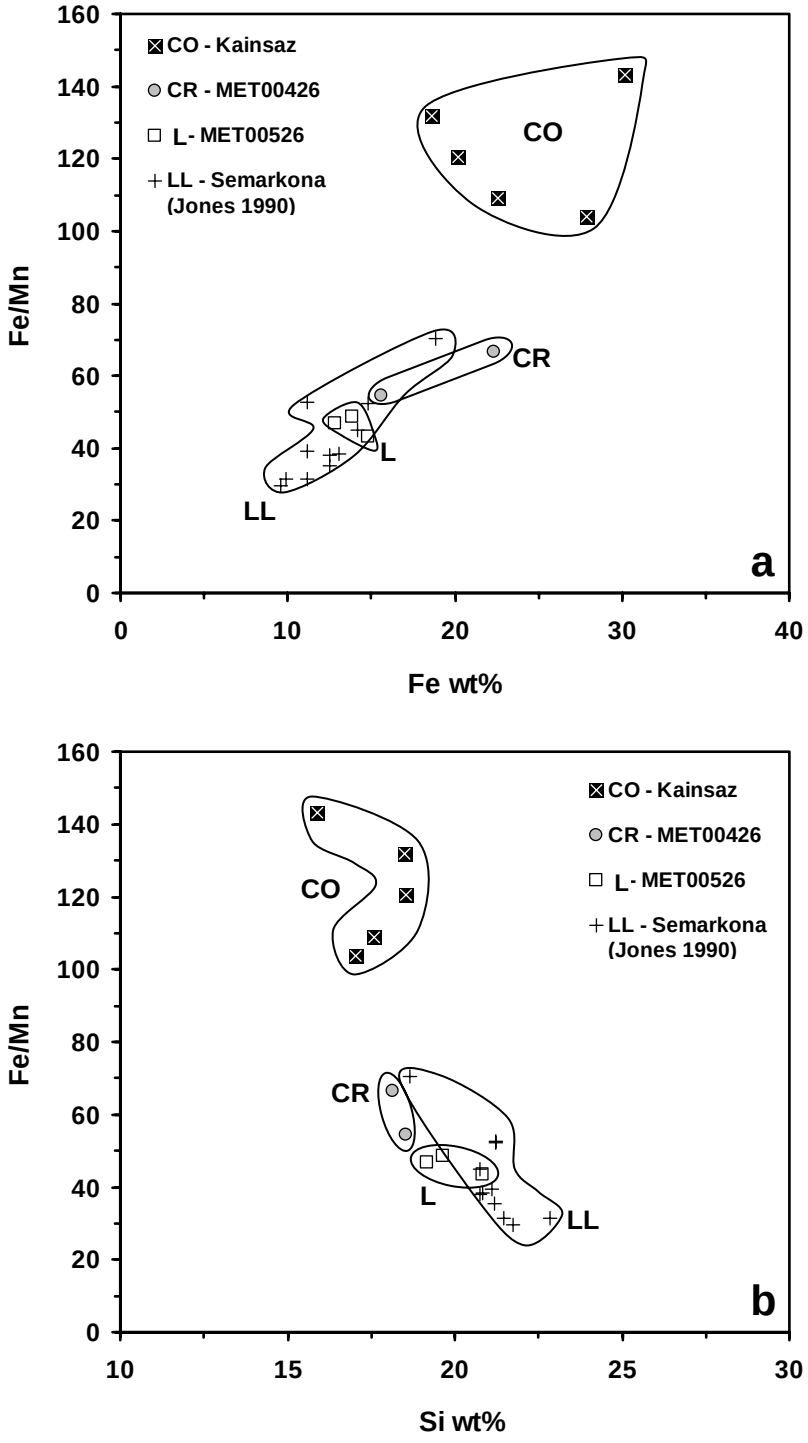

Fig. 2.10. a) Molar Fe/Mn vs. Fe (wt%) of bulk type IIA chondrule compositions in Kainsaz (CO), MET 00426 (CR) and MET 00526 (L). Data for type IIA chondrules from LL chondrite Semarkona are from Jones (1990). Fe/Mn ratios decrease with decreasing bulk Fe content. b) Molar Fe/Mn vs. Si (wt%) of bulk type IIA chondrule compositions. Fe/Mn ratios decrease with increasing bulk Si content.

DISCUSSION

It is generally assumed that similar textural and chemical properties of chondrules indicate that they formed by the same process, but because properties are not identical they must have formed in different locations in the solar nebula (e.g., Scott and Taylor 1983). However, we currently have a very limited knowledge of the mineralogical and compositional differences between chondrules with the same texture from primitive chondrites in different chondrite groups. The main objective of the work presented in this paper is to determine if there are fundamental differences between type IIA chondrules in pristine (i.e., unmetamorphosed) ordinary, CR and CO chondrites and then use this information to make inferences about the reservoirs of material from which these chondrules formed.

In order to look at the pristine nebular record contained in chondrules, we first need to understand how secondary processing, such as thermal metamorphism and/or aqueous alteration, may have affected the individual chondrites. Below we discuss possible secondary modification of Fe/Mn systematics of olivine, and volatile element contents of mesostasis compositions. Mesostasis volatile element contents (notably Na and K) are important for constraining whether Fe/Mn trends in olivine could be related to the volatilization or gain of Mn during chondrule formation, or if chondrules inherited moderately volatile element depletions from their precursors. It is therefore important to establish whether chondrules preserve their nebular content of volatile elements or whether these elements were mobilized during parent body processes.

We then discuss several possible explanations for the different Fe/Mn trends we observed in type IIA chondrules and evaluate whether these distinct trends might be related to fundamental differences in the precursor materials of chondrules, to volatile loss or gain during chondrule formation, to oxidation or reduction before or during chondrule formation and/or to differences in cooling rates. Finally, we discuss the origin of several new relict grains that we identified based on their Fe/Mn systematics.

Secondary alteration

All of the chondrites examined in this study are fairly pristine, except for Kainsaz. Based on petrography and mineralogical characteristics, Kainsaz was first classified as petrologic subtype 3.1 (Scott and Jones 1990) and later as 3.2 (e.g., Chizmadia et al. 2002; Grossman and Brearley 2005), based on a number of different petrographic criteria. However, a study of the structural state of organic (graphitic) matter in Kainsaz by Bonal et al. (2007) resulted in a classification as petrologic type 3.6, indicating a much higher degree of thermal metamorphism. Hence, we need to consider carefully the possible effects of thermal metamorphism on our Kainsaz data.

We have also included literature data for olivine from type IIA chondrules in two CR2 chondrites (Burger 2005) in our study. We briefly evaluate if aqueous alteration could have altered Fe-Mn-Mg systematics in these chondrules.

Olivine compositions

In MET 00426 (CR3.0) and MET 00526 (L3.05), type I chondrule olivines typically have Fa contents <5 mol% (**Fig. 2.2b,c**), consistent with their very low subtype classifications. In contrast, olivines in Kainsaz type I chondrules extend to more Fa-rich compositions (**Fig. 2.2a**). During the onset of thermal metamorphism, these olivine grains developed compositional zoning, with Fo-rich core compositions and Fa-rich rims, as a consequence of Fe-Mg exchange with the surrounding FeO-rich matrix (e.g., Scott and Jones 1990). Matrix olivines in Kainsaz have a fairly wide range of Fa contents, between 48 and 72 mol% (Brearley and Jones 1998). Because type II chondrules are FeO-rich and are more similar in composition to the matrix than type I chondrules, Fe-Mg exchange with matrix is much more limited (e.g., Jones and Rubie 1991). If significant Fe-Mg exchange had occurred between type IIA olivine and matrix in Kainsaz, we would expect the Fe-Mn trends for ALHA 77307 (CO3.0) and Kainsaz (CO3.2) shown in **Figure 2.4a** to be quite different, but this is not the case.

Jones and Lofgren (1993) and Grossman and Brearley (2005) showed that Cr contents of type II olivine decrease significantly at the onset of thermal metamorphism (from petrologic type 3.0 to 3.2) due to the exsolution of a Cr-rich phase, probably chromite. Chromium contents in type IIA chondrule olivines in Kainsaz are lower than

those of the more pristine CO3.0 chondrite ALHA 77307 (**Fig. 2.3a**), consistent with a higher degree of thermal metamorphism for Kainsaz. Since it was nearly impossible to obtain good EMP analyses on exsolved chromites at the edges of olivine grains, we might have underestimated the bulk Cr content of type IIA chondrules in Kainsaz.

While Cr contents in Kainsaz type IIA olivines are lower than in ALHA 77307, in the Mn (afu) vs. Fe (afu) diagram in **Figure 2.4a**, olivine data for Kainsaz and ALHA 77307 show the same trend, indicating that Fe-Mn-Mg relationships were not disturbed significantly in type IIA chondrule olivine in Kainsaz. In ordinary chondrites, Mn contents in type II chondrule olivines equilibrate between petrologic type 3.4 and 3.8 (DeHart et al. 1992). The undisturbed Fe-Mn-Mg relationships in type IIA chondrules and the wide range of matrix compositions in Kainsaz compared to CO chondrites of higher petrologic types (e.g., Brearley and Jones 1998) are more consistent with a petrologic type 3.2 than with the classification of petrologic type 3.6 by Bonal et al. (2007).

The CR2 chondrites EET 87770 and EET 92105 have experienced minimal aqueous alteration, as indicated by the fact that mesostasis glass is only altered around its periphery (Burger 2005). Our olivine data for a more primitive CR3.0 chondrite, MET 00426, show the same general trends in the Mn vs. Fe diagram (**Fig. 2.4b**), indicating that Fe-Mn-Mg systematics of type IIA chondrule olivines in the CR2 chondrites are probably undisturbed.

Mesostasis compositions

Alkali elements are easily redistributed between chondrule mesostases and matrix during thermal metamorphism (e.g., Grossman and Brearley 2005) and this is a concern for our Kainsaz data. Compared to type IIA chondrules in MET 00526 (L) and MET 00426 (CR), mesostasis glass in Kainsaz type IIA chondrules has very low K_2O contents (below 0.5 wt% K_2O, **Fig. 2.8b** and **Table 2.3**). Low K_2O contents in mesostases could also be due to shock metamorphism, but Kainsaz is classified as S1 (Grady 2000) which is effectively unshocked (e.g., Stöffler et al. 1991). Another possible explanation for the low K_2O contents in Kainsaz type IIA chondrules could be crystallization of albite (e.g., Grossman and Brearley 2005). A few individual analyses of mesostasis in three Kainsaz

chondrules (K1-Ch7, K1-Ch8, and K2-Ch7) show MgO contents below 1 wt%, but we did not actually observe a separate phase that could be crystalline plagioclase such as in MET 00426 chondrule CR-Ch13 (**Fig. 2.1c,d**).

K_2O contents in Kainsaz are not only low in type II, but also in type I chondrule mesostases (below 0.3 wt %, Chapter 1) and in the matrix (below 0.3 wt %, Chapter 1). This is in contrast to Na_2O contents, which are highly variable in type II (4.6–11.6 wt%) and in type I chondrules (2.0–12.8 wt%), but low in the matrix (below 1.4 wt%). If alkalis were redistributed between chondrules and matrix during thermal metamorphism, we would expect to see similar behavior for Na and K. We were not able to find mesostasis analyses for type IIA chondrules from a more pristine CO chondrite in the literature, but analyses published as plagioclase for Y-81020 type IIA chondrules by Kunihiro et al. (2004) have low K_2O contents as well (≤0.3 wt%). We conclude that it is possible that low K_2O contents in type IIA chondrule mesostases in CO chondrites are a primary feature, but further investigation is very much needed.

During aqueous alteration, mesostasis glass is easily converted into clay minerals (e.g., Brearley 2006), but when minute amounts of water are present, certain elements might also be leached from the glass without devitrification (e.g., Grossman et al. 2002). Mesostasis glass in the two type IIA chondrules from the CR3 chondrite MET 00426 has high Na_2O and K_2O contents (**Fig. 2.8b**, **Table 2.3**). In the CR2 chondrites studied by Burger (2005), these elements were mobilized by aqueous alteration and entered the matrix, which is why available mesostasis data for the type IIA chondrules from these two meteorites (EET87770 and EET92105) were not included in this study.

Fe/Mn trends in type IIA chondrule olivine

At a given FeO content, type IIA chondrule olivines in UOCs have a higher Mn content than type IIA chondrule olivines in CO chondrites. In a Mn (afu) vs. Fe (afu) diagram (**Fig. 2.4a**), type IIA chondrule olivines from UOC and CO chondrites exhibit trends with different slopes (CO slope = 0.010, UOC slope = 0.023). Our assessment of previously published data of olivine zoning profiles in Semarkona type IIA chondrules (Jones 1990) suggests that all olivine grains which crystallized from the same chondrule melt typically fall on a single trendline in the Mn vs. Fe diagram (**Fig. 2.5a**). However,

olivine data for each chondrule have slightly different slopes (**Fig. 2.5a**), causing the spread in the UOC data in **Fig. 2.4a**. Nevertheless, type IIA chondrule olivines from L and LL chondrites show the same general trend in the Mn vs. Fe diagram. This is consistent with the fact that oxygen isotope compositions of chondrules in L and LL chondrites are similar (e.g., Clayton et al. 1991) and further supports Clayton et al.'s (1991) suggestion that they might be derived from a common reservoir.

Type IIA chondrule olivines in CR chondrites show characteristics intermediate between CO and UOC (**Fig. 2.4b**). The olivine data for type IIA chondrules in CR chondrites shown in **Fig. 2.4b** include data for three different meteorites. The data from Burger (2005) are zoning profiles for one chondrule in EET 87770 and two chondrules in EET 92105, while our data are 7 to 8 random analyses in two type IIA chondrules (Ch6 and Ch13) in MET 00426, plus several type IIA chondrule fragments. Again, the olivine data have a slightly different slope for each chondrule in the Mn vs. Fe diagram (**Fig. 2.4b**). Furthermore, two populations become apparent: EET 87770 and MET 00426-Ch6 show a trend that overlaps somewhat with UOC data, while the chondrules in EET 92105 and MET 00426-Ch13 follow a trend that is intermediate between CO and UOC data. At this point in time, we do not know if the Fe/Mn data correlate with oxygen isotope data. However, Connolly et al. (2008) measured oxygen isotopic compositions of type II chondrule olivines in CR chondrites and found that some of them plot in the UOC region of the three-isotope plot, which is in agreement with our finding that some of our CR type IIA olivine data overlap with the ordinary chondrite data (**Fig. 2.4**).

It is intriguing that the general Fe/Mn trends for type IIA chondrule olivine in unequilibrated ordinary, CR and CO chondrites (**Fig. 2.4a,b**) resemble the Fe/Mn trends observed for olivine from martian (slope 0.0217), terrestrial (slope 0.0134) and lunar (slope 0.0095) basalts (Karner et al. 2003; Papike et al. 2003). Papike et al. (2003) interpreted these trends as being controlled by the volatility of Mn – varying with heliocentric distance from the sun, while oxygen fugacity and metal separation (core formation) appear to have a secondary effect. However, one cannot explain the chondrule trends with a comparable model, as CC chondrules would have to have formed at terrestrial distances from the Sun and UOC chondrules at Mars distances. Also, if

chondrites formed in the asteroid belt between Mars and Jupiter, one would expect that all chondrules would have steeper slopes than the Mars trendline.

Below, we discuss several possible explanations for the different Fe/Mn trends we observe in type IIA chondrules, and evaluate whether these distinct trends might be related to (1) fundamental differences in the precursor materials of chondrules, (2) dynamic processes that occurred during chondrule formation (volatile loss/gain and oxidation/reduction) and/or (3) differences in cooling rates.

Do the Fe/Mn trends relate to fundamental differences in the precursor?

A major topic of discussion in the literature has been whether or not bulk chondrule compositions reflect the composition of the precursor material, i.e. whether chondrules behaved as closed systems (e.g., Grossman and Wasson 1983b; Hezel and Palme 2007; Alexander et al. 2008), or as open systems, with their compositions being modified during the chondrule forming event (e.g., Sears et al. 1996; Davis et al. 2005; Libourel et al. 2006). Below, we discuss whether the observed Fe/Mn systematics in type IIA chondrules could be related to inherited depletions of moderately volatile elements (including Mn) in the precursor material – for this section of the discussion, we assume closed system behavior. Then, we discuss another possibility, i.e. that there were different proportions of silicates, metals and sulfides in the precursor material, a model which appears to require open system behavior.

Are differences in Fe/Mn ratios the result of inherited depletions in moderately volatile elements?

Type IIA chondrules in CO chondrites have higher bulk Fe/Mn ratios than those in unequilibrated ordinary and CR chondrites (**Fig. 2.10**), which correspond to slightly lower Mn contents, but also higher Fe contents observed in CO type IIA bulk chondrule compositions compared to CR and UOC type IIA bulk compositions (**Fig. 2.9**). Because other moderately volatile elements (Cr, P, K) are also lower in CO type IIA bulk chondrule compositions (**Fig. 2.9**), we consider the possibility that the observed Fe/Mn trends in type IIA olivine (**Fig. 2.4**) could be related to a depletion of moderately volatile elements in the precursor material of CO type IIA chondrules.

A general depletion of moderately volatile elements (relative to CI chondrites) is commonly observed in bulk compositions of many carbonaceous chondrites, but it is not clear whether this depletion is mainly carried by chondrules, by matrix or both (e.g., Alexander 2005; Huss et al. 2005; Bland et al. 2005). Such depletions are not observed in bulk ordinary chondrites (e.g., Brearley and Jones 1998). The origin of moderately volatile element depletions in carbonaceous chondrites (and in the terrestrial planets) has been a subject of debate for decades and remains enigmatic (see review by Ciesla 2007). Recently, it has been suggested that the depletion could have been inherited from the molecular cloud (Yin 2005), although an incomplete condensation model, which calls upon diminishing nebular gas during the accretion of planets, has generally been favored (e.g., Cassen 2001).

If chondrules behaved as closed systems and if a moderately volatile element depletion was inherited from the precursor dust from which CO and CR type IIA chondrules formed, we would expect to see elemental depletions in the bulk chondrule compositions that correlate with volatility. Similar to bulk UOC compositions mentioned above, the bulk compositions of UOC type IIA chondrules are not significantly depleted in moderately volatile elements (**Fig. 2.9a,b**). However, CR type IIA bulk chondrule compositions are also not significantly depleted (**Fig. 2.9a,b**) while a depletion of moderately volatile elements is observed in bulk CR chondrites (e.g., Kong and Palme 1999). Compared to type IIA chondrules in UOC and CR chondrites, the mean bulk type IIA chondrule composition for Kainsaz (**Fig. 2.9b**) shows lower abundances of some moderately volatile elements (e.g., Cr, Mn, P, K) but not Na. The levels of depletion in Kainsaz type IIA chondrules do not correlate with the volatility of the elements and individual chondrule trends show even more complexity (**Fig. 2.9a**).

When compared to CI chondrite abundances, Mn shows little depletion in Kainsaz type IIA chondrules (**Fig. 2.9a,b**). We mentioned above that the low bulk Cr contents observed in our Kainsaz type IIA chondrules (**Fig. 2.9a,b**) could be an artifact of our MRA technique that is related to the onset of thermal metamorphism in Kainsaz, as it was impossible to obtain good EMP analyses on the exsolved chromites at the edges of olivine crystals. Also, as mentioned above, the lower K contents in Kainsaz type IIA chondrules could also be due to thermal metamorphism. On the other hand, higher

abundances of Na and K in UOC type IIA chondrules could be due to secondary processes as well, such as entry of these elements into chondrule mesostasis (e.g., Grossman and Brearley 2005). Taking further into account that bulk Fe contents of Kainsaz type IIA chondrules are much higher than those of UOC type IIA chondrules, while the difference in bulk Mn contents is actually quite small (**Table 2.4**), it seems that the observed Fe/Mn trends in type IIA chondrule olivines (**Fig. 2.4**) are difficult to reconcile with inherited moderately volatile element depletions from the precursor materials.

Are differences in Fe/Mn ratios the result of different proportions of silicates, metals and sulfides in the precursor materials of CO, CR and UOC type IIA chondrules?

The different Fe/Mn trends we observe in type IIA chondrule olivines in CO and UOC could be due to significant differences in the assemblage of precursor materials, such as varying amounts of silicates, metals and sulfides. Assuming that precursor silicates had the same Mg#, a higher proportion of metals and/or sulfides in the precursor material of CO chondrules would result in higher Fe/Mn ratios, whereas a higher proportion of silicates in the precursor material of UOC type IIA chondrules could explain lower Fe/Mn ratios. However, the observed modal abundances of Fe,Ni metal and sulfides are generally insignificantly small (typically <3 vol%) in type IIA chondrules from both CO and ordinary chondrites. Fe,Ni metal could have formed immiscible melts and then been lost when the chondrules were spinning in the nebula, but then we would expect to see at least a few chondrules which retained their high modal abundances of Fe,Ni metal. If a higher proportion of Fe,Ni metal was present in the CO type IIA precursor material, it must have been oxidized during the chondrule formation process. On the other hand, if a higher proportion of sulfides was present in the CO type IIA precursor material, S could have been volatilized during the chondrule-forming event and a higher amount of Fe could have been incorporated into CO type IIA chondrule olivine.

Another possibility is that precursor silicates of CO type IIA chondrules already had relatively high FeO contents and low proportions of metal/sulfides. Incidently, the Fe/Mn ratio of CO type IIA olivines (mean Fe/Mn = 99) is very similar to that of CI chondrites (Fe/Mn ratio = 92). The lower Fe/Mn ratios of CR and UOC type IIA olivines (**Fig.**

2.4c,d) might then relate to a CO-like precursor material that experienced reduction and metal loss, before the type IIA chondrules formed, that are now preserved in CR and UOC. It seems reasonable that reduction during chondrule formation combined with chondrule recycling could produce lower Fe/Mn ratios.

In summary, it appears that the different Fe/Mn trends observed in type IIA chondrule olivines in CO, CR and ordinary chondrites are more likely to be due to fundamental differences in the precursor materials than to inherited moderately volatile element depletions. However, in order to decide which of the possibilities stated above is most likely, we need to discuss open system behavior during chondrule formation, which is addressed in more detail below.

The role of chondrule formation in establishing Fe/Mn systematics

We can consider whether open system behavior is responsible for the different Fe/Mn trends in CO, CR and UOC type IIA chondrule olivines. A molar Fe/Mn vs. Fe/Mg diagram, such as introduced by Goodrich and Delaney (2000), can be used to make inferences about the behavior of Mn and Fe while olivine is crystallizing from a chondrule melt. **Figure 2.11a** shows a schematic illustration of the molar Fe/Mn vs. Fe/Mg diagram and possible processes that might be recorded in chondrule olivine. A trend parallel to the x-axis represents simple crystallization behavior of olivine without any Mn or Fe addition/loss. If Mn is being lost from the chondrule melt while olivine grains are crystallizing, one would expect to see a positive trend (**Fig. 2.11a**). However, a positive trend could also imply Fe addition to the silicate melt (e.g., via oxidation of metal), although in this case the trend should be shallower than for Mn loss (**Fig. 2.11a**). A negative trend indicates that the chondrule melt either gains Mn while olivine grains are crystallizing or that Fe is being lost from the silicate melt, for example by the reduction of FeO and physical loss of metal beads (**Fig. 2.11a**).

Figure 2.11b shows a schematic illustration of our observations for type IIA chondrule olivines from CO, CR and unequilibrated ordinary chondrites (see also **Fig. 2.4c,d** and **Fig. 2.5b**). CO type IIA chondrule olivines exhibit a trend parallel to the x-axis, indicating that no Mn or Fe loss/addition occurred while olivine grains were crystallizing. The Fe/Mn ratio stays constant (mean Fe/Mn ratio = 99) over a wide range

of Fe/Mg ratios during fractional crystallization to more Fe-rich compositions. Fe and Mn show similar behavior in CO type IIA chondrule olivine, which is illustrated in the schematic zoning profile shown in **Figure 2.11c.**

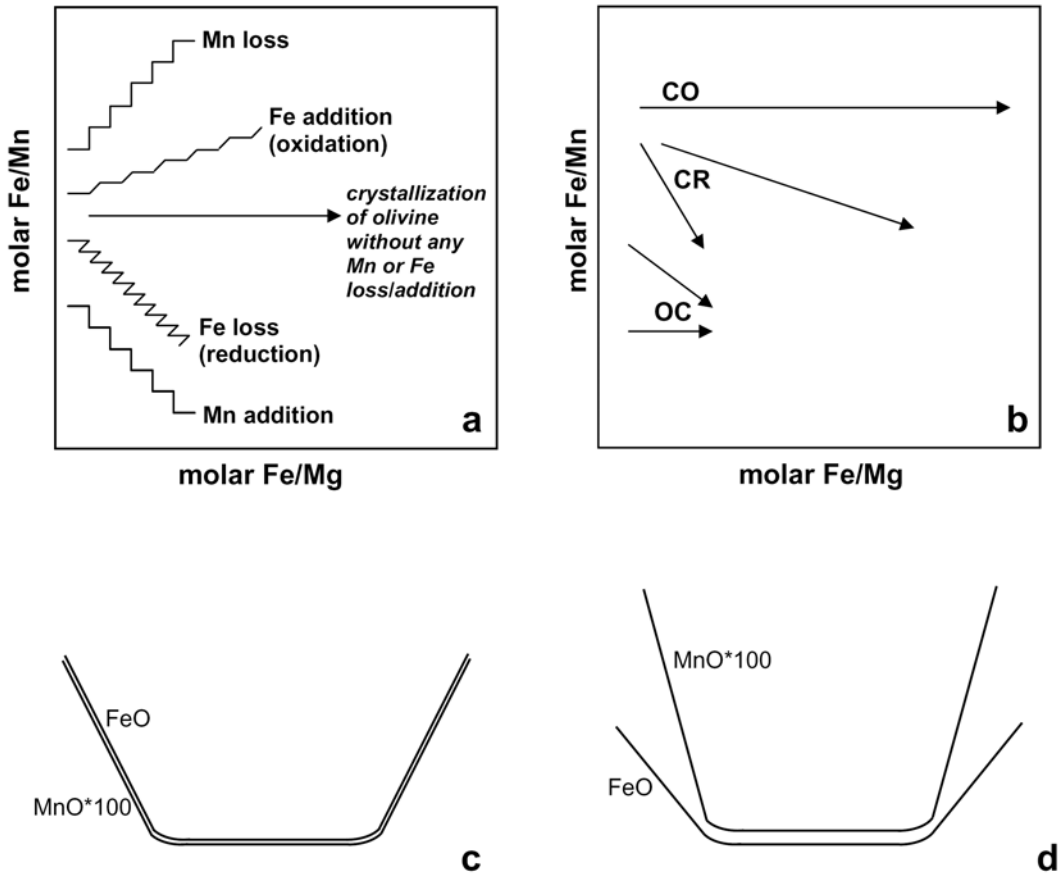

Fig. 2.11. a) Simplified illustration of Fe-Mn-Mg systematics in type IIA chondrule olivine in CO, CR and ordinary chondrites (OC). b) Illustration of crystallization trends. Negative trends are observed when Mn is added or Fe is lost (e.g., by reduction) during olivine crystallization. This is the case for CR and some OC chondrules. Positive trends imply Fe addition (e.g. oxidation of Fe,Ni metal) or Mn loss. Such trends were not observed in this study. The flat trend for CO is consistent with a simple crystallization trend without any Mn or Fe loss/addition. c) Schematic zoning profile for a CO type IIA chondrule olivine. The Fe/Mn ratio stays constant during olivine crystallization. d) Schematic zoning profile for a CR or OC type IIA chondrule olivine with a negative trend in the molar Fe/Mn vs. Fe/Mg diagram as shown in (b).

We suggested above that the precursor material of CO type IIA chondrules might have had a higher proportion of metals and/or sulfides than the precursor material of UOC type IIA chondrules. However, the observed modal abundances of Fe,Ni-metal and sulfides are very low (typically <3 vol%) in all type IIA chondrules. If Fe,Ni-metal was oxidized while olivine crystallized, we would expect to see a positive trend (Fe addition) in the molar Fe/Mn vs. Fe/Mg diagram (**Fig. 2.11a**), which we do not observe in our CO type IIA olivine data (**Fig. 2.4c** and **2.11b**). If oxidation of Fe,Ni metal took place prior to olivine crystallization, we would expect to at least see higher NiO contents in olivine, but most of our observed NiO contents in CO type IIA chondrule olivines are below the EMP detection limit (<0.04 wt%). It is therefore unlikely that oxidation of Fe,Ni metal occurred during the formation of CO type IIA chondrules.

However, as mentioned above, CO type IIA chondrules could also have had a higher proportion of sulfides in their precursor materials. If all S volatilized from the chondrule melt before olivine started crystallizing, a higher amount of Fe^{2+} could have been incorporated into CO type IIA chondrule olivine from the beginning, so that we would not necessarily expect to see a positive trend in the molar Fe/Mn vs. molar Fe/Mg diagram (**Fig. 2.11a**). Therefore, a higher proportion of sulfides in the CO type IIA precursor material seems to be a very reasonable argument to explain their higher Fe/Mn ratios.

In contrast to CO chondrules, CR and some UOC type IIA chondrule olivines show negative trends in the molar Fe/Mn vs. Fe/Mg diagram (**Fig. 2.11b**). This behavior implies that the chondrule melt either gained Mn while the olivines crystallized, which in turn resulted in increasing Mn contents in the olivine, or that Fe was lost from the silicate melt (e.g., via reduction of FeO) while the CR and UOC olivines crystallized (**Fig. 2.11a**). A schematic zoning profile for a CR (or UOC) type IIA chondrule olivine grain is shown in **Figure 2.11d**, demonstrating the behavior of Fe and Mn during olivine crystallization. It is difficult to constrain which of the two processes, Mn gain or reduction of FeO (or both), is responsible for the negative trends, because both processes have a similar slope in the molar Fe/Mn vs. Fe/Mg diagram (**Fig. 2.11a**).

Some CR and UOC type IIA chondrule olivines have significantly higher MnO contents (up to 1 wt%) than CO olivines (below 0.5 wt%). Bulk compositions of CR and

UOC type IIA chondrules also have higher Mn and K contents relative to CI chondrites (**Fig. 2.9**). Therefore, it seems possible that CR and some UOC type IIA chondrules gained volatile elements (including Mn) during chondrule formation while olivine grains were crystallizing. Libourel et al. (2006) and Nagahara et al. (2008) have argued that condensation of volatiles onto chondrule melt droplets during cooling is possible, based on the presence of concentration gradients for elements such as K, Na, Ca, Mn, Al and Si found in mesostasis glass in type I chondrules. We did not observe any zoning in the mesostasis of type IIA chondrules, but MnO contents of the mesostasis glass in CR and UOC are clearly higher than in CO type IIA chondrules (**Table 2.3**). It also seems likely that Mn addition would occur closer to the liquidus for type II than for type I chondrules, so that diffusion may have homogenized Mn in the remaining liquid that is now preserved as mesostasis. However, there is no apparent correlation between MnO contents and Na_2O or K_2O contents in our dataset of individual mesostasis analyses and K_2O contents of CR type IIA mesostases are higher than in UOC and CO type IIA mesostases (**Fig. 2.8b**). This latter observation is not consistent with the order of observed Fe/Mn trends in olivine (CR-UOC-CO vs. UOC-CR-CO).

Above, we also mentioned the possibility that the lower Fe/Mn ratios of CR and UOC type IIA olivines (**Fig. 2.4c,d**) might relate to an FeO-rich CO- or CI-like precursor material that experienced reduction and metal loss, before the type IIA chondrules formed, that are now preserved in CR and UOC. Reduction during chondrule formation could also be the reason for the negative trends we observe for CR and some UOC type IIA olivines in the molar Fe/Mn vs. Fe/Mg diagram (**Fig. 2.4d, 2.5b and 2.11b**). Remelting of such partially reduced chondrule material could explain the trends more parallel to the x-axis. However, if reduction of FeO occurred in the silicate melt or maybe even within the olivine grains while they were crystallizing, we would expect to observe abundant Ni-poor metal blebs in the CR and UOC type IIA chondrules that show negative trends in the molar Fe/Mn vs. Fe/Mg diagram (**Fig. 2.11a,b**). We did not observe such Ni-poor metal blebs, but it is possible that they are so small that a TEM investigation is needed in order to confirm their presence.

At this point in time, we can only speculate whether Mn gain or reduction of FeO caused the negative trends observed for CR and some UOC type IIA chondrule olivines

in the molar Fe/Mn vs. Fe/Mg diagram (**Fig. 2.4c,d**, **Fig. 2.5b** and **Fig. 2.11a,b**). They might also represent a combination of both. It is possible that reduction of FeO was more significant for UOC type IIA chondrules (see discussion below), while gain of volatile elements might be the dominant process recorded in CR type IIA chondrules as indicated by higher Na_2O and K_2O contents in CR type IIA mesostasis than in UOC type IIA mesostasis (**Fig. 2.8b**). The two populations observed in the CR data (**Fig. 2.4b,d**) could point to different amounts of volatile elements added while the precursor composition might have been similar to that of CO type IIA chondrules as indicated by high Fe/Mn ratios at the beginning of olivine crystallization. CR-Ch6 has higher MnO contents (**Table 2.3**) as well as higher K/Al and Na/Al ratios in the mesostasis glass (**Fig. 2.8b**) than CR-Ch13 and olivines show a steeper negative trend in the molar Fe/Mn vs. Fe/Mg diagram (**Fig. 2.4d**).

Most of the UOC type IIA chondrule olivine trends have fairly shallow negative slopes in the molar Fe/Mn vs. Fe/Mn diagram (**Fig. 2.5b**) compared to the steep slopes of the CR type IIA chondrule olivine trends (**Fig. 2.4d**). While the latter may have started crystallizing with an Fe/Mn ratio close to CO (and CI), Fe/Mn ratios of UOC type IIA chondrule olivines are significantly lower (**Fig. 2.4c,d** and **Fig. 2.5b**). This might indicate that either the UOC type IIA precursor material experienced significant reduction and metal loss before chondrule formation occurred or that UOC type IIA chondrules experienced reduction during chondrule formation and significant recycling that led to metal loss. Both possibilities would also explain the lack of Ni-poor metal as it might have been physically lost because of metal-silicate melt immiscibility. A potential reducing agent could have been the presence of carbon in the precursor material (e.g., Connolly et al. 1994) or a reducing nebular gas.

If reduction was a major process responsible for establishing the Fe/Mn trends, one would expect to see differences in the recorded oxygen fugacities between UOC, CR and CO type IIA chondrules. Sutton et al. (1996) found different Cr^{2+}/Cr^{3+} ratios in type II chondrule olivine from Semarkona ($Cr^{2+}/Cr^{3+} = 0.9$) and ALHA 77307 ($Cr^{2+}/Cr^{3+} = 0.3$), implying that CO type II chondrules might have crystallized under slightly more oxidizing conditions than UOC type II chondrules: this is consistent with the differences in Fe/Mn systematics.

In conclusion, CO type IIA chondrules record no evidence for Mn or Fe loss/addition while olivine grains were crystallizing (**Fig. 2.11a,b**). This is in contrast to CR and UOC type IIA chondrules, which show negative trends in the molar Fe/Mn vs. Fe/Mg diagram indicating that Mn gain and/or reduction of FeO occurred during the crystallization of olivine grains (**Fig. 2.11a,b**). CO type IIA chondrules could have had a higher proportion of sulfides in their precursor materials than CR and UOC type IIA chondrules. If all S volatilized from the chondrule melt before olivine started crystallizing, a higher amount of Fe^{2+} could have been incorporated into CO type IIA chondrule olivine. On the other hand, the precursor material of CO type IIA chondrules could have been FeO-rich prior to chondrule formation with a low modal proportion of sulfides and metal. The lower Fe/Mn ratios of CR and UOC type IIA olivines might then be related to an FeO-rich CO- or CI-like precursor material that experienced reduction, metal loss and recycling during chondrule formation.

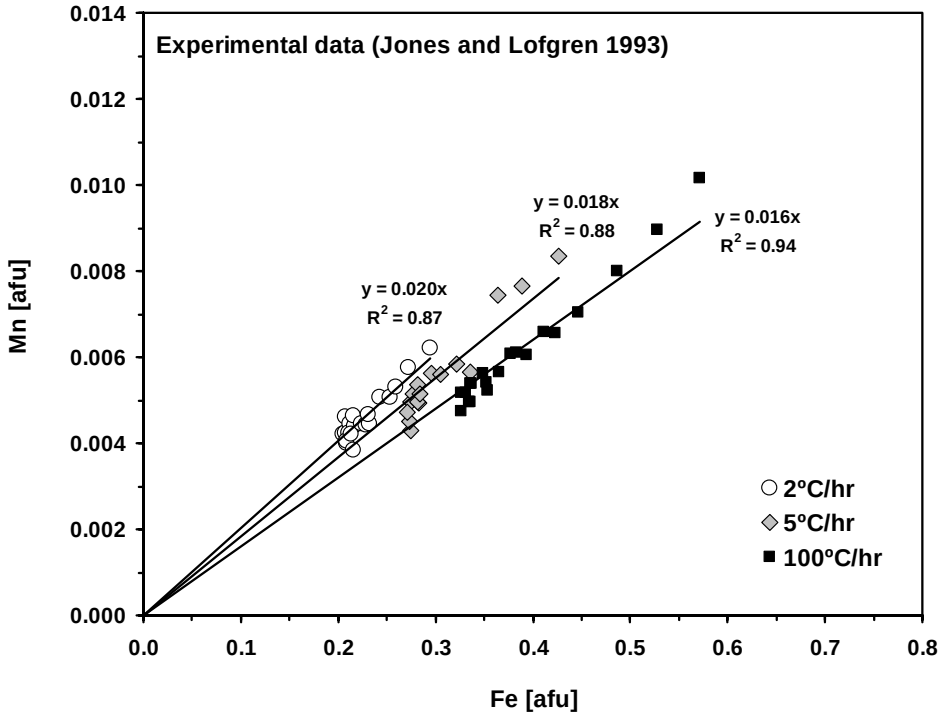

Fig. 2.12. Fe (afu) vs. Mn (afu) for olivine zoning profiles from experimental samples with different cooling rates (Jones and Lofgren 1993). Trendlines are best-fit linear regressions forced through the origin.

Do the Fe/Mn trends relate to differences in cooling rates?

Differences in cooling rates could be an explanation for the slightly different slopes we observe for each Semarkona chondrule in the Mn vs. Fe diagram (**Fig. 2.5a**). Jones and Lofgren (1993) performed experiments at different cooling rates (2, 5 and 100ºC/hr) with a starting composition that is very similar to the bulk composition of UOC type IIA chondrules. In **Fig. 2.12**, the experimental data for olivine from Jones and Lofgren (1993) are plotted as Mn vs. Fe. The slope of the trendlines becomes shallower with increasing cooling rate.

The experiments by Jones and Lofgren (1993) do not provide an explanation for the shallow slope (0.010) we observed for CO type IIA chondrule olivines in the Mn vs. Fe diagram. This slope would require a much higher cooling rate. However, at cooling rates in the range of 500 – 1000ºC/hr significantly different chondrule textures are observed (Lofgren 1989). The shallow slope for CO type IIA chondrules might be reproduced with a porphyritic texture if the starting composition of the experiment more closely resembles the bulk compositions of CO type IIA chondrules. Clearly, more experiments are needed to fully understand the effect of cooling rate on Fe/Mn systematics, but available evidence indicates that different cooling rates may only represent a second order effect.

Relict grains

Two types of relict grains (i.e., grains that did not crystallize *in situ* from the host chondrule melt) are frequently encountered in chondrules: relict forsterite or enstatite grains in FeO-rich chondrules and "dusty" olivine grains in FeO-poor chondrules (e.g., Jones 1996b and ref. therein; Jones and Danielson 1997; Weinbruch et al. 2000; Pack et al. 2004, 2005). In addition to these commonly described relicts, Jones and Carey (2006) showed evidence that Fo-rich relicts exist in type I chondrules. Wasson and Rubin (2003) also suggested that type II chondrules might contain ubiquitous high-FeO relict grains.

In this study, we tried to avoid relict forsterites in order to show true chondrule crystallization trends. Our MELTS modeling demonstrates that the first olivine to crystallize from a melt of type IIA bulk composition would be Fa_{4-6} for UOC and Fa_{7-10} for CO chondrules (**Table 2.4**). A few grains with Fa contents significantly below these values were excluded from **Figures 2.2** to **2.5**.

As a result of our detailed examination of Fe/Mn systematics, we have observed grains that we consider to be relicts that have not been described previously. These are FeO-rich grains that we can identify as relicts, because they have significantly different Fe/Mn ratios than melt-grown olivines in the host chondrules. (**Figs. 2.6** and **2.7).** The relict core of Grain 1 in Kainsaz chondrule K1-Ch8 (**Fig. 2.6a,b**) plots in a region of the Mn vs. Fe diagram that lies outside our data for type IIA chondrule olivine from all chondrites studied (**Fig. 2.6d**). The relict core of this grain is Fa_{20}. Its MnO content of 0.89 wt% (**Table 2.2**) is significantly higher than what we observe for olivines with a Fa content of 20 mol% in host chondrule olivines in type IIA chondrules in CO, CR and ordinary chondrites. A possible explanation for this relict is that it was initially significantly more FeO-rich, and that it underwent reduction before formation of the host chondrule. There is evidence for this in the form of small metal blebs (**Fig. 2.6b**). If the original grain had an Fe/Mn ratio similar to that in UOC type IIA chondrules, it would initially have had a composition of ~Fa_{42}. If its original Fe/Mn ratio was that of a CO type II chondrule, it would have had an initial composition of ~Fa_{95}. The latter is clearly unreasonable, and Fa_{42} is high for UOC, but not unreasonable (see **Fig. 2.2**). Nakamura et al. (2008) found olivines with compositions ($Fa_{20\text{-}21}$ and MnO = 0.8 wt%), very similar to the relict core of our Grain 1 (**Fig. 2.6**), in a chondrule-like object ("Torajiro") in samples collected by the Stardust mission from comet 81P/Wild 2.

The relict core of Grain 2 in Kainsaz chondrule K1-Ch8 (**Fig. 2.6a,c**) could also represent a grain that originally formed in a previous generation of UOC type IIA chondrules. Fe and Mn contents of this grain overlap with those observed in type I chondrules (indicated by the box in **Fig. 2.6d**), but it is rather unlikely that it was derived from a type I chondrule. The presence of small metal blebs (**Fig. 2.6c**) indicates that it underwent reduction, like Grain 1, either before or during the chondrule-forming event.

While the relict cores in Kainsaz chondrule K1-Ch8 are fairly easy to recognize because of their darker appearance in a BSE image (**Fig. 2.6a**), the relict grain in Semarkona chondrule 51 looks very similar to the host olivine grains in this chondrule (**Fig. 2.7a**). Its low Mn content suggests that it could potentially be a grain that originally formed in the CO chondrite formation region (**Fig. 2.7b**).

Relict grains provide a real physical record of chondrule precursor grains. Most relicts appear to be derived from previous generations of chondrules and hence represent evidence for recycling of material in the chondrule forming region(s). Jones (1996b) estimated that at least 15% of chondrules contain material that experienced at least two chondrule-forming events, with disruptive collisions probably occurring between the events. The prospect of finding more relict grains using Fe-Mn-Mg systematics (**Figs. 2.4**, **2.6**, and **2.7**) might result in a greater population of relicts in chondrules than previously estimated. We plan to determine the oxygen isotopic compositions of the relicts we have identified. Boesenberg et al. (2007) showed that O-isotope exchange between relict olivine and chondrule melt is much slower than Fe-Mg exchange. Therefore, even if Fe-Mg exchange occurred, chances are high that oxygen isotopes will help us to constrain the origin of newly identified relict grains in this study.

CONCLUSIONS

Type IIA chondrule olivines show positive correlations in a Mn (afu) vs. Fe (afu) diagram. Even though the slopes of the trends are slightly different for each chondrule, UOC type IIA chondrules show a significantly steeper correlation than CO type IIA chondrules (**Fig. 2.4a**). CR type IIA chondrule olivines show two populations. One population overlaps somewhat with UOC compositions, while the other has properties intermediate between unequilibrated ordinary and CO chondrites (**Fig. 2.4b**).

Differences observed in type IIA bulk chondrule compositions suggest that precursor materials for UOC, CR and CO type IIA chondrules were fundamentally different, while L and LL type IIA chondrules must have been derived from a common reservoir as has also been suggested based on oxygen isotopic compositions (e.g., Clayton et al. 1991). We also found evidence that the chondrule formation process might have played an important role in establishing the different Fe/Mn trends.

Differences in cooling rates could be an explanation for the slightly different slopes we observe in the Semarkona data (**Fig. 2.5a** and **Fig. 2.12**), but more experiments are clearly needed to fully understand the effect of cooling rate on the partitioning behavior of Mn.

The Fe/Mn trends for type IIA chondrule olivines in ordinary, CR and CO chondrites are very similar to those observed for olivine from martian (slope 0.0217), terrestrial (slope 0.0134) and lunar (slope 0.0095) basalts (Karner et al. 2003; Papike et al. 2003). While these planetary trends could be related to the volatility of Mn and the heliocentric distance from the Sun, our chondrule data indicate a considerable heterogeneity in the Fe/Mn ratio of reservoirs that are sampled by different chondrite bodies on scales less than 1 AU within the protoplanetary disk. This observation suggests that either very different processes are recorded in chondrites or that there is no simple relationship between volatile element depletions and distance from the Sun.

Fe-Mn-Mg systematics can be used to identify relict grains that have significantly different Fe/Mn ratios than the host olivines in type IIA chondrules. We have observed relict grains in a Kainsaz (**Fig. 2.6**) and in a Semarkona chondrule (**Fig. 2.7**) that could be derived from previous generations of chondrules, including chondrules from other chondrite groups.

CHAPTER 3 - CHONDRULES AND MATRIX IN KAKANGARI: EVIDENCE FOR WIDE-SPREAD REDUCTION AND SULFIDIZATION

ABSTRACT

In this study, the Kakangari chondrite was examined in detail by optical microscopy, scanning electron microscopy and electron microprobe analysis. The relative abundances of chondrule textural types were determined and twenty chondrules were chosen for a detailed study of mineralogy and petrography. Bulk compositions of these chondrules were obtained by modal recombination analysis (MRA) and matrix was analyzed using defocused beam analyses.

Kakangari has been thought of as a very primitive chondrite, but our study reveals that it records a complex series of events, including (1) formation of fine-grained FeO-rich precursor material, (2) formation of FeO-rich chondrules in early heating events in the solar nebula, (3) subsequent reduction of chondrules and fine-grained matrix materials in a later heating event(s) also in the nebula, (4) accretion, (5) thermal metamorphism and formation of apatite, (6) sulfidization of Ni-poor metal, and (7) low-temperature aqueous alteration leading to the formation of abundant ferrihydrite.

Kakangari chondrules, as they are preserved in the meteorite, are quite different from chondrules in ordinary and carbonaceous chondrites, but are similar to FeO-rich objects found in enstatite chondrites. Even though mesostasis compositions might point to a type I and type II chondrule population, other evidence (e.g., high MnO contents in olivine and presence of Ni-poor metal) suggests that silicates in all chondrules were initially FeO-rich and underwent reduction. The silicate portion of the fine-grained matrix in Kakangari is compositionally very similar to chondrule silicates, even after taking secondary overprints into account. Our results support a model in which Kakangari chondrules and matrix formed in close proximity in the solar nebula.

INTRODUCTION

Kakangari fell on June 4th, 1890 in Kangankarai, India (Silberrad 1932). It was recognized as a unique chondrite in the 1970s (e.g., Graham and Hutchison 1974; Davis et al. 1977). Weisberg et al. (1996) suggested that Kakangari, Lea County 002 (Zolensky et al. 1989; Prinz et al. 1991) and LEW 87232 (Weisberg et al. 1993b; Kallemeyn 1994) should form the Kakangari (K) chondrite grouplet. This classification has found acceptance; however, Krot et al. (2003) proposed that Lea County 002 should actually be classified as a CR chondrite, while Zolensky (pers. comm.) recommends that it should remain ungrouped.

Kakangari and LEW 87232 are type 3 chondrites that are characterized by high matrix abundances (>60 vol%) similar to carbonaceous chondrites, metal abundances (6-10 vol%) similar to H chondrites and average mafic silicate compositions that indicate an oxidation state intermediate between H and E chondrites (Weisberg et al. 1996). Bulk oxygen isotopic compositions plot close to CR chondrites, but chondrule and matrix oxygen isotopic compositions form a mixing line that distinguishes K from CR chondrites (Weisberg et al. 1996). A detailed TEM study by Brearley (1989) showed that Kakangari matrix differs from other chondrite groups in being dominated by enstatite, not olivine, and in exhibiting textures that indicate high temperature processing.

The motivation for this study was to examine the relationship between chondrules and matrix in Kakangari. Several studies have indicated that Kakangari is a very pristine chondrite (e.g., Brearley 1989; Scott and Krot 2005; Nuth et al. 2005). Furthermore, a unique feature of Kakangari is that chondrules and matrix are compositionally very similar, so similar in fact that Nehru et al. (1983) argued that Kakangari appears to consist of only one, rather than two components. In addition, although Kakangari matrix has been studied in detail (Brearley 1989), only a few cursory studies have been carried out on the chemical and petrographic properties of chondrules in K chondrites. Nehru et al. (1986) and Genge and Grady (1998) documented layered chondrules and different kinds of chondrule rims in Kakangari and also noticed that no type II chondrules (Fa > 10 mol%) are present in Kakangari. Genge and Grady (1998) suggested that the relative abundances of different textural types of chondrules in Kakangari are most similar to those in ordinary chondrites. McSween (1977a) determined bulk compositions of

chondrules in Kakangari by electron microprobe defocused beam analyses and also found that they overlap with those of ordinary chondrite chondrules. Oxygen isotopic compositions, on the other hand, suggest that there might be a genetic relationship between the chondrules in Kakangari and enstatite chondrites (Weisberg et al. 1996). To complicate matters further, the one matrix sample of Kakangari that was analyzed for oxygen isotopes has a considerably more ^{16}O-rich composition than the chondrules (Prinz et al. 1989; Weisberg et al. 1996).

Our detailed study of the mineralogy and bulk chemistry of chondrules and matrix in Kakangari reveals a very complex history that has not been recognized previously. Multiple events are recorded in the textural and mineralogical characteristics of Kakangari involving high-temperature processing, reduction, thermal metamorphism, sulfidization and low-temperature aqueous alteration. These processes have modified the primary nebular record of Kakangari to a significant extent. However, after taking secondary overprints into account, our observations allow an assessment of the relationship between chondrules and matrix as well as a more detailed comparison between chondrules in Kakangari and those in ordinary, carbonaceous, and enstatite chondrites. In addition, our data provide new constraints on both nebular and parent body processes that have affected chondritic meteorites.

SAMPLES AND ANALYTICAL TECHNIQUES

Two thin sections of Kakangari (UNM 559, UNM 585) were studied in detail by optical and scanning electron microscopy. A photomosaic of one of the thin sections (UNM 559) is shown in **Figure 3.1**. Electron imaging, semi-quantitative EDS, X-ray mapping and quantitative analyses were performed on a JEOL 8200 Superprobe in the Electron Microbeam Facility at the University of New Mexico. This electron microprobe is equipped with a Thermo Noran EDS system and five WDS spectrometers, including two high intensity spectrometers with smaller Rowland circles for precise minor element analysis.

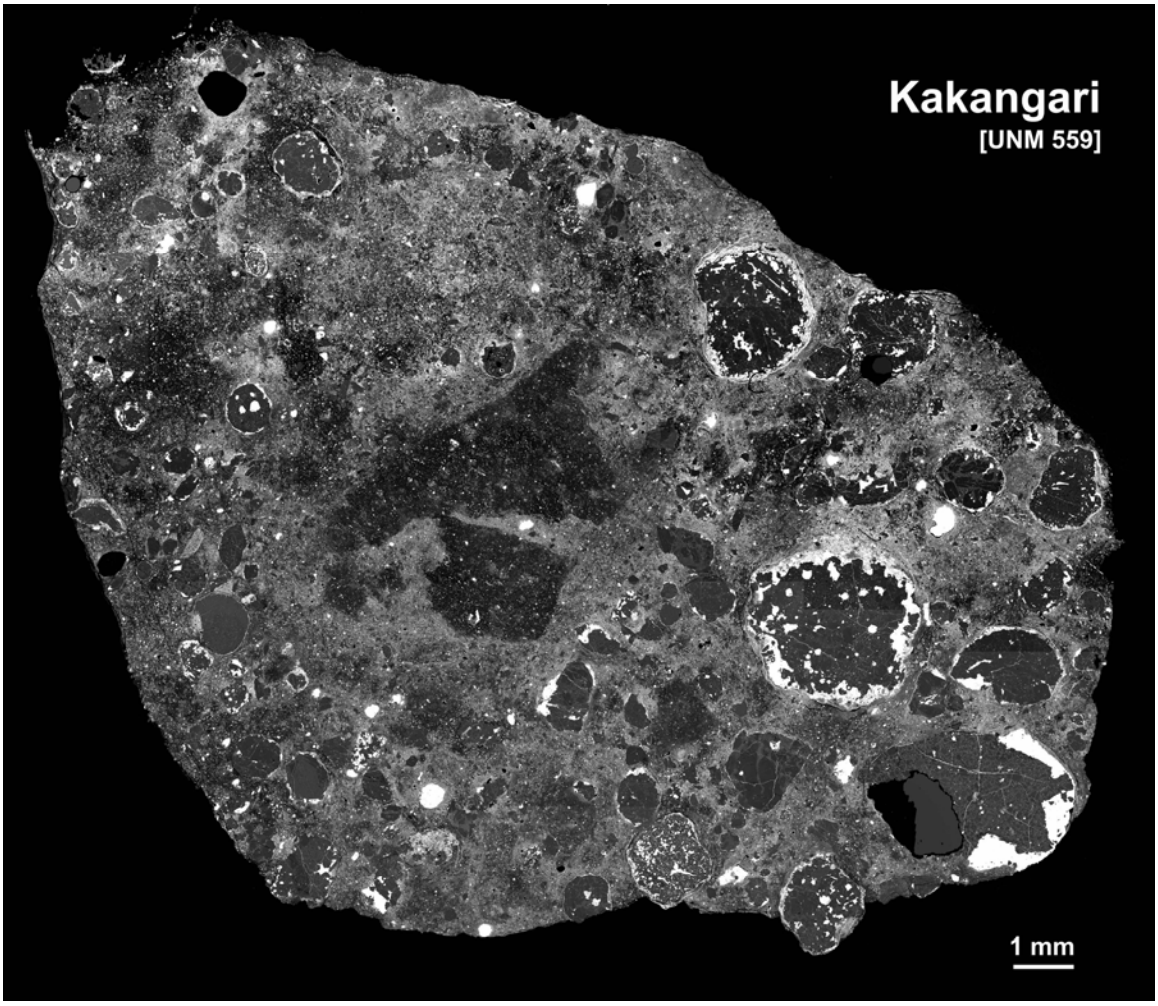

Fig. 3.1. Backscattered electron photomosaic of Kakangari thin section UNM 559. Two dark clasts of fine-grained material occur in the center of the thin section. Chondrules range in size from 0.25 to 3 mm. Metal/troilite rims around chondrules are very common. Matrix abundance is 76.8 vol% (Weisberg et al. 1996). The high compositional (atomic number) contrast of the matrix is caused by abundant fine-grained troilite and ferrihydrite.

Twenty chondrules were selected for detailed analysis. Chondrule labels #1 and #2 refer to their location in thin section UNM585 or UNM559, respectively. Quantitative analyses were obtained on all phases present in a chondrule and were then combined with their weighted modal proportions to obtain the bulk composition of the chondrule (refer to Appendix A). WDS element maps were used to identify the different phases present, but in order to avoid Na loss, mesostasis analyses were obtained first (15 keV, 5 μm beam diameter, 10 nA beam current) before element maps were collected. A rhyolitic glass standard (3.75 wt% Na_2O) and a basaltic glass standard (2.66 wt% Na_2O) were

analyzed along with the meteorite samples in order to maintain a reasonable accuracy for our Na values (±10%). Subsequently, the chondrules were mapped by WDS X-ray spectrometry using stage mapping with a beam current of 30 nA and a pixel-size between 0.5 and 1.5 μm (depending on chondrule size) for a suite of 5 elements (Al, Ca, Mg, Fe, S). In some cases, when we knew beforehand that silica was present in a chondrule, Si was mapped instead of Al. The collected element maps were then used to select spots for silicate, metal and sulfide point analyses. Silicate minerals were analyzed with an accelerating voltage of 15 keV and a beam current of 20 nA. Metals and sulfides were analyzed at 20 keV and a beam current of 40 nA. ZAF corrections were applied to the data and standards used include Taylor olivine (Si, Fe, Mg), diopside (Ca, Mg, Si), spessartine (Mn), albite (Na), orthoclase (K, Al), corundum (Al), rutile (Ti), chromite (Cr), apatite (P), pyrite (S), Ni-metal (Ni), and Co-metal (Co), as well as JEOL Fe-metal (Fe) and Si-metal (Si).

Figure 3.2 shows BSE images of two chondrules and their corresponding phase images that were assembled with the phase tool in Lispix Lx133P (public domain image analysis program for Windows, written and maintained by David Bright, National Institute of Standards and Technology) and/or Adobe Photoshop® based on collected X-ray maps. Modal abundances of the different phases present were determined with Lispix or with Scion Image. A comparison of both methods is provided in Appendix B.

Several matrix regions were analyzed with a defocused beam (30 μm diameter), a beam current of 20 nA and an accelerating voltage of 15 keV. The same setup was used to analyze the fine-grained clasts (**Fig. 3.1**). Analyses were placed randomly and small metal/sulfide grains (< 5 μm) within the matrix and fine-grained clasts were not avoided. Elements were measured as oxides and ZAF corrections were applied to the data. Totals lower than 80 wt% were assumed to be due to holes and/or cracks in the thin section and were therefore discarded. High totals, which are due to mixed metal/sulfide/silicate analyses and the fact that Fe, Ni and S were measured as FeO, NiO and SO_3, were not discarded. For the presentation of our matrix data, NiO and SO_3 were converted to element wt%. Individual grains of olivine and pyroxene in the matrix and fine-grained clasts were analyzed with the same setup that was used for chondrule silicates (15 keV, 20 nA and focused beam).

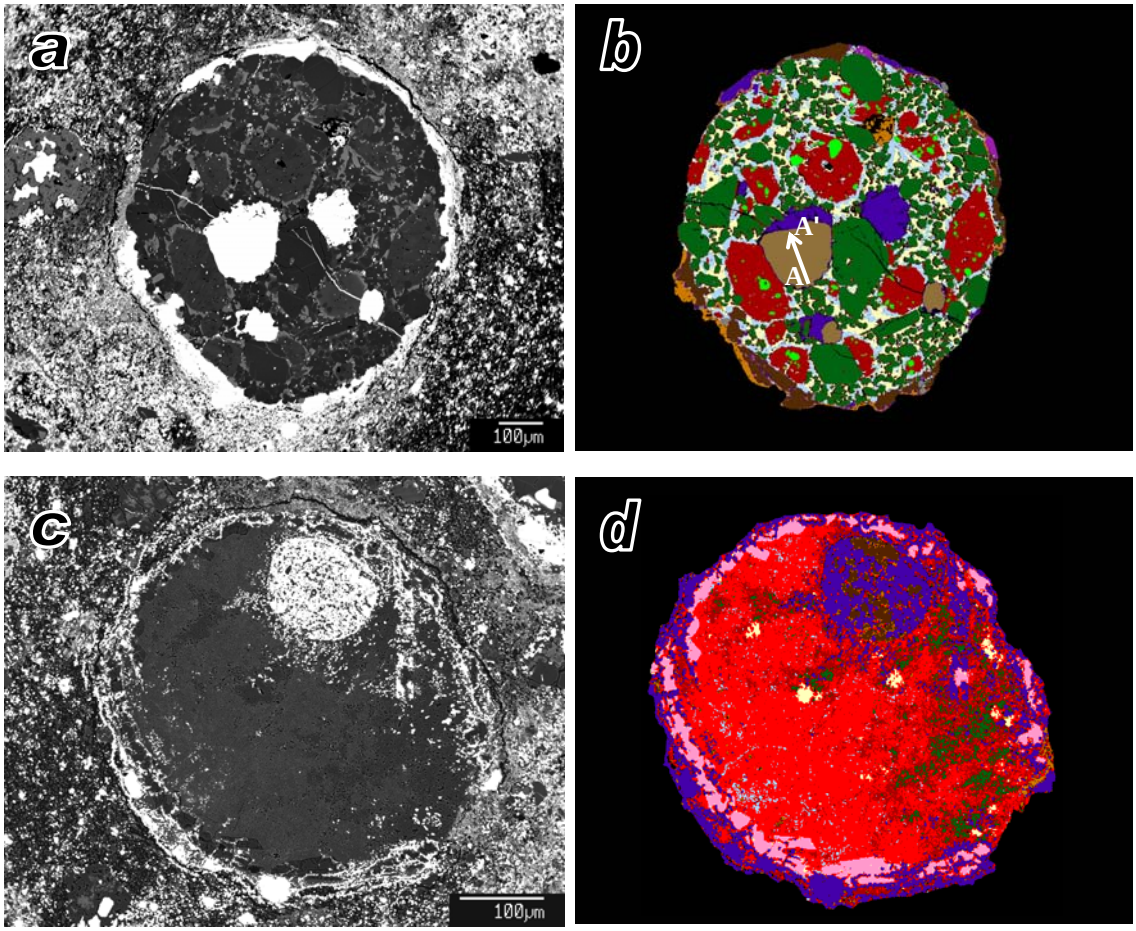

Color code for phase images:

= olivine 1	= olivine 2	= pyroxene 1	= pyroxene 2
= Ca-pyroxene	= mesostasis	= silica	= troilite
= kamacite	= taenite	= apatite	= Cr-spinel
= ferrihydrite			

Fig. 3.2. Examples of phase identification for modal recombination. a) Backscattered electron (BSE) image of a typical POP chondrule, #2-5. b) Phase image of the chondrule shown in Fig. 3.2a generated in Adobe Photoshop® using element maps to identify each phase. Such images were used to determine the modal abundances of the different phases with Scion Imaging software. The indicated taenite zoning profile is shown in Fig. 3.15. c) BSE image of a cryptocrystalline chondrule (#2-9) consisting of olivine, two pyroxenes (pyroxene 1 = $Fs_{3.2}Wo_{6.5}$; pyroxene 2 = $Fs_{4.6}Wo_{7.3}$) and silica. d) Phase image of the chondrule shown in Fig. 3.2c.

RESULTS

Chondrules

Chondrule textures

Chondrules constitute ~19 vol% of Kakangari (Weisberg et al. 1996). Their average diameter is 0.69 mm with many of them falling in the 0.25–0.5 mm range (Weisberg et al. 1996), but there are also a few larger chondrules present with sizes up to at least 3 mm (**Fig. 3.1**). Genge and Grady (1998) noticed a high abundance of chondrule fragments and described different types of chondrule rims. Virtually all chondrules have either a massive troilite/kamacite rim and/or a fine-grained porous troilite rim (**Fig. 3.1**), which Genge and Grady (1998) refer to as 'spongey'. Some fracture surfaces on chondrule or mineral fragments have a very thin troilite rim.

Table 3.1. Relative abundances (%) of different chondrule types.

		Kakan-gari	**Kakan-gari** (GG98)	**OC** (GK81)	**EH3** (RG87)	**EH3** (S02)	**EL3** (S02)	**CO** (R00)	**CV** (G88)
Porphyritic:	PO-II*	7.1	-	15-27	-	-	-	8	84.6
	PO	7.1	9.1						
	POP	40.0	36.3	47-52	4.6	11.8	17.6	69	7.5
	PP	21.9	8.4	9-11	76.2	56.6	58.8	18	1.9
Agglomeratic#:	AC	14.2	-	-	-	-	-	-	-
Granular:	GOP	-	22.1	2-5	1.4	18.4	10.6	<0.1	-
	GP	-	7.8	-					
Barred:	BO	-	-	3-4	-	-	-	2	6
Radial:	RP/(BP)	9.0	10.4	7-9	12.8	6.6	10.6	2	0.3
Crypto-crystalline:	CC	0.7	3.9	3-5	5.0	6.6	2.5	1	

*PO chondrules exhibiting a typical "type IIA"-texture (see text), but olivines are FeO-poor ($Fa_{2.5-3.5}$) in Kakangari.
#Chondrules consisting of very fine-grained silicates (grain size: <10 μm), abundant troilite/metal beads and larger troilite/metal grains with very ragged outlines. Low-Ca and Ca-pyroxene are more abundant than olivine. These chondrules are very similar to the material that constitutes fine-grained igneous rims around ~16% of chondrules in Kakangari, in fact, some of them contain larger relict grains and/or chondrule fragments.
GG98: Genge and Grady (1998)
GK81: Gooding and Keil (1981)
RG87: Rubin and Grossman (1987)
S02: Schneider et al. (2002)
R00: Rubin (2000)
G88: Grossman et al. (1988)

In this study, textures of 155 Kakangari chondrules and chondrule fragments were examined in detail by optical and electron microscopy. The relative abundances of different textural types are listed in **Table 3.1**, compared to data for Kakangari from Genge and Grady (1998) and ordinary, enstatite and carbonaceous chondrites from different authors. Similar to many other chondrite groups, porphyritic chondrules are the most abundant in Kakangari and show a textural continuum from porphyritic olivine (PO) to porphyritic olivine-pyroxene (POP) and porphyritic pyroxene (PP) chondrules.

Genge and Grady (1998) classified ~30% of Kakangari chondrules as granular, whereas we do not classify any chondrules as granular. Gooding and Keil (1981) defined a granular texture as one that exhibits a uniformly small grain size, with anhedral crystals and patches of mesostasis that are similar in size to the crystals. Genge and Grady (1998) acknowledge that in their study: *"Granular chondrules were identified as those which lack significant mesostasis or groundmass and might be classified as porphyritic in other studies.*" We prefer to use the Gooding and Keil (1981) definition and use the term porphyritic for such objects.

Several authors have noticed that Kakangari does not contain type II chondrules (e.g., Nehru et al. 1986; Weisberg et al. 1996; Genge and Grady 1998). However, we found that about half of the PO chondrule population exhibits a texture that is very similar to a typical "type IIA" chondrule texture (e.g., Scott and Taylor 1983; Jones 1990), but olivines are FeO-poor ($Fa_{2.5-3.5}$) and do not show normal igneous zoning (e.g., **Fig. 3.3a,c**). These chondrules are referred to as PO-II in **Tables 3.1**, **3.2**, and **3.5-3.7**. Their shapes can be rounded or irregular. Euhedral olivine phenocrysts in these chondrules range in grain sizes from 5–400 μm. In the most coarse-grained PO-II chondrule, the olivine grain size ranges from 100–800 μm. In these chondrules, olivine phenocrysts are typically embedded in a microcrystalline groundmass that contains abundant laths of Ca-pyroxene (**Fig. 3.3b**). Such Ca-pyroxene laths can be fairly large (up to 60 μm thick) and can have cores of low-Ca pyroxene and/or pigeonite (**Fig. 3.3c**). However, in chondrules with a "type IIA" texture, low-Ca pyroxene is never present as large phenocrysts at the periphery of the chondrule as would be typical for type I chondrules (e.g., Scott and Taylor 1983). Most of the Kakangari chondrules classified as having a "type IIA"-texture (PO-II in **Table 3.1**) contain only small amounts of opaque

phases in the form of μm-sized metal and/or troilite beads within the microcrystalline groundmass and frequently decorating the crystal faces of olivines (**Fig. 3.3b**). Larger troilite and/or metal grains can be present along the edge of a chondrule (**Fig. 3.3a**). A few chondrules, which were included in the PO-II category in **Table 3.1**, show all the characteristics of the "type IIA"-texture described above, but contain larger troilite/metal intergrowths (**Fig. 3.3d**) with very ragged outlines (**Fig. 3.3e**).

The chondrule shown in **Fig. 3.3d** is armored by an igneous rim (**Fig. 3.3f**) with an outermost layer of fine-grained troilite. In contrast to the center of the chondrule, the rim is dominated by small crystals (<10 μm) of low-Ca and Ca-rich pyroxenes; olivine and mesostasis are present but are not as abundant (**Fig. 3.3f**). Troilite and metal grains within the igneous rim show ragged outlines resembling the grains in the interior of the chondrule. Twenty-four out of the 155 chondrules studied exhibit igneous rims with similar texture. Another 22 chondrules (labeled "agglomeratic" in **Table 3.1**) seem to be almost entirely made up of material similar to igneous rims, but they could also simply represent slices through such rims. However, this is unlikely for the large agglomeratic chondrule shown in **Fig. 3.3g**. A more detailed view of a part of this chondrule (**Fig. 3.3h**) demonstrates the similarity to the igneous rim shown in **Fig. 3.3f**. In the optical microscope, these chondrules are easily identifiable by their high abundance of opaque minerals and their overall darker, brownish color, which is probably caused by the very fine-grained nature of the silicates. These chondrules are very similar to a class of objects that has been described by various authors with different terms: "dark-zoned chondrules" (Dodd and Van Schmus 1971), "aggregational chondrules" (Cohen et al. 1983), "coarse-grained lumps" (Rubin 1984), "aggregational inclusions" (Rubin et al. 1988) and "agglomeratic chondrules" (Weisberg and Prinz 1996). Whereas such chondrules consist mainly of fine-grained olivine and low-Ca pyroxene in ordinary and carbonaceous chondrites (e.g., Rubin 1984; Rubin et al. 1988; Weisberg and Prinz 1996), we found that those in Kakangari are dominated by low-Ca and high-Ca pyroxene with subordinate olivine (**Fig. 3.3g,h**).

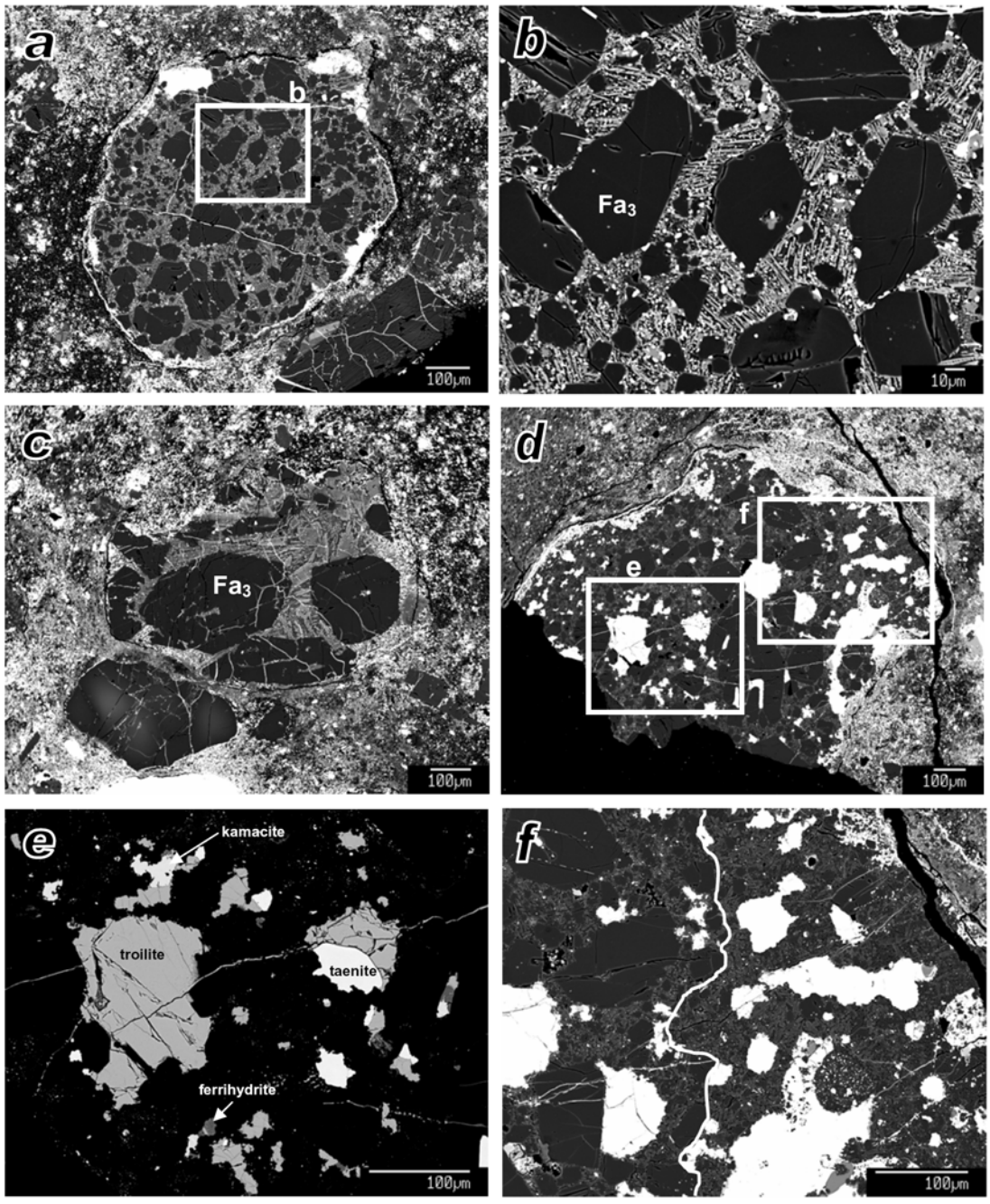

Fig. 3.3. BSE images of Kakangari chondrules showing different textural types. a) Kakangari chondrule #1-10 with a typical "type IIA"-texture, but FeO-poor olivines ($Fa_{2.5-3.5}$). b) Close-up image of the box outlined in Fig. 3.3a. The groundmass of chondrule #1-10 contains Ca-pyroxene laths and abundant metal/troilite blebs. c) Fragment of chondrule #2-4 with a typical "type IIA"-texture. Olivines are FeO-poor ($Fa_{2.5-3.5}$) and the Ca-pyroxene laths have low-Ca pyroxene cores. The large isolated olivine grain at the lower left is not included in the chondrule. It is zoned from Fa_{10} (core) – Fa_3 (edge). d) Porphyritic olivine chondrule #1-4 with large metal/troilite grains that have ragged outlines, typical of many Kakangari chondrules. This chondrule is armored by a fine-grained igneous rim (close-up image shown in Fig. 3.3f). e) Close-up image of box labeled "e" in Fig. 3.3d showing relationships between metals and trolite. f) Close-up image of box "f" in Fig. 3.3d. Fine-grained low-Ca and Ca-pyroxene dominate over olivine in the igneous rim (to the right of the white line), whereas large olivine grains are present in the center of this chondrule (left).

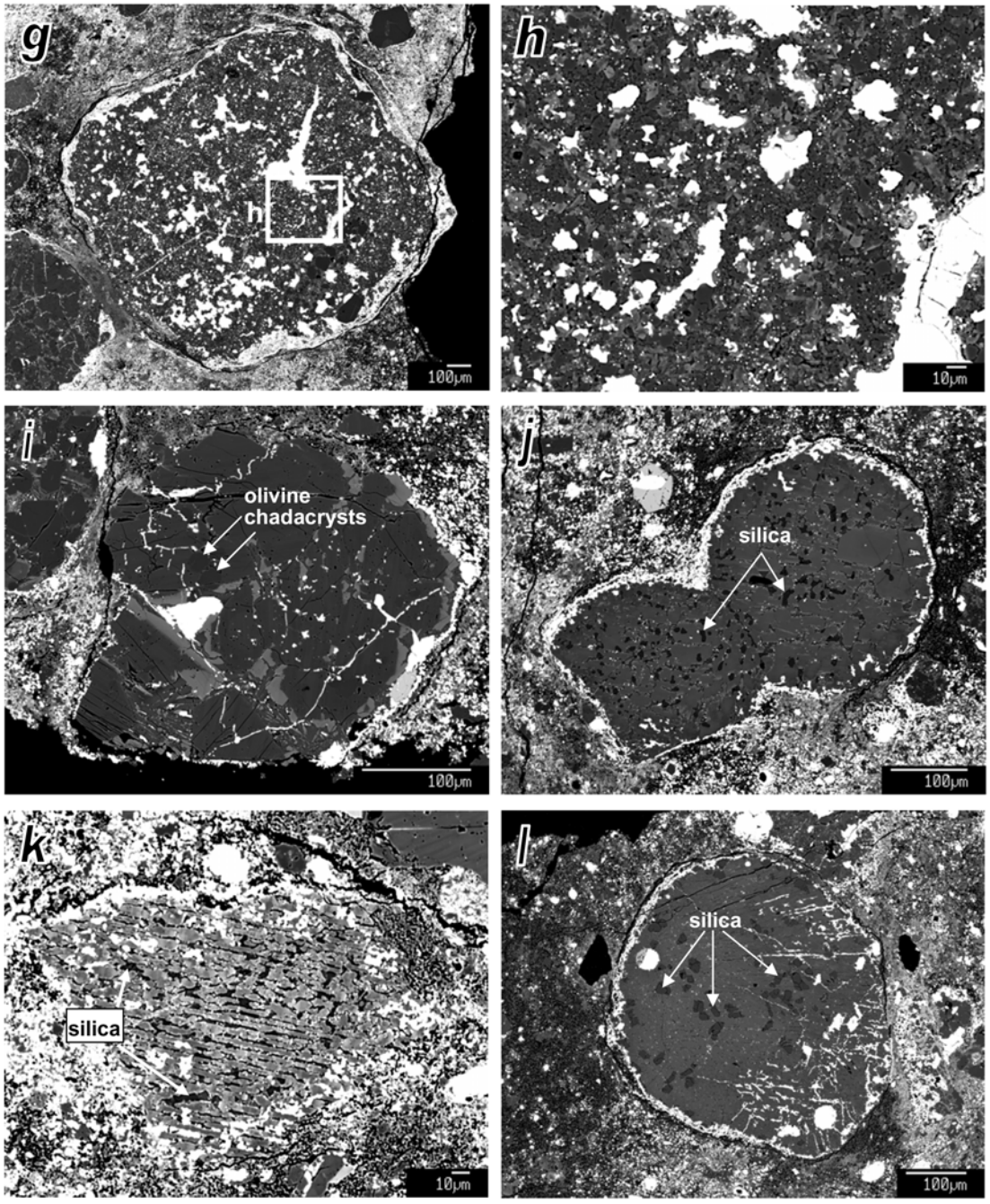

Fig. 3.3 continued. g) Agglomeratic chondrule with abundant metal/troilite grains showing ragged outlines. h) Close-up image of box outlined in Fig. 3.3g. The mineralogy and texture of agglomeratic chondrules is very similar to the fine-grained igneous rims found around ~16% of all Kakangari chondrules, such as the one shown in Fig. 3.3f. i) Porphyritic pyroxene chondrule (#1-7) with olivine chadacrysts. j) Compound chondrule (#2-3) consisting of two mineralogically identical barred/porphyritic pyroxene chondrules. Both contain abundant silica. k) BP chondrule (#1-11) consisting of low-Ca pyroxene (Fs_{5-14}) and abundant silica. l) RP chondrule (#2-7) with coarser-grained silica.

In general, PP chondrules (~22%) are more common in Kakangari than PO chondrules (~14%). Also, in many POP chondrules, pyroxene is more abundant than olivine. Olivine frequently occurs as chadacrysts within larger low-Ca pyroxene crystals (e.g., **Fig. 3.2a,b** and **Fig. 3.3i**). Troilite and metal grains with ragged outlines (**Fig. 3.3e**) are a very characteristic feature of Kakangari (**Fig. 3.1**) and occur mostly in chondrules with agglomeratic textures (**Fig. 3.3g,h**) and those chondrules that show a large range in grain sizes (**Fig. 3.3d,e**). Troilite and metal grains are more rounded in chondrules with a more uniform grain size of the silicates (e.g., **Fig. 3.3i**).

The abundance of radial pyroxene (RP) chondrules in Kakangari is more similar to ordinary and enstatite chondrites than to carbonaceous chondrites (**Table 3.1**). Some of the Kakangari chondrules that are included in the category of RP chondrules in **Table 3.1** have rather thick laths/bars of pyroxene (up to 50 μm) so that it is not exactly appropriate to describe them as RP chondrules (e.g. **Fig. 3.3j**). These are transitional between PP and RP chondrules, and we refer to them as barred pyroxene (BP) chondrules. Their textures are similar to coarse barred pyroxene chondrules described by Jones (1996a) in ordinary chondrites. However, many RP/BP chondrules in Kakangari contain abundant silica (e.g., **Fig. 3.3j,k,l**). Only one cryptocrystalline chondrule was found in this study (**Fig. 3.2c,d**).

Chondrule mineralogy

Twenty chondrules were selected for detailed analysis. The selection process was carried out in a somewhat subjective way, making sure that chondrules with different textures (all that were possibly available) were included. We feel confident that these chondrules are approximately representative for Kakangari. The supplementary CD contains Microsoft Office Excel® files with the collected and generated data for each chondrule (EMP data, BSE image, corresponding phase image and details of the modal recombination analysis). Here, we summarize important features of mineral compositions.

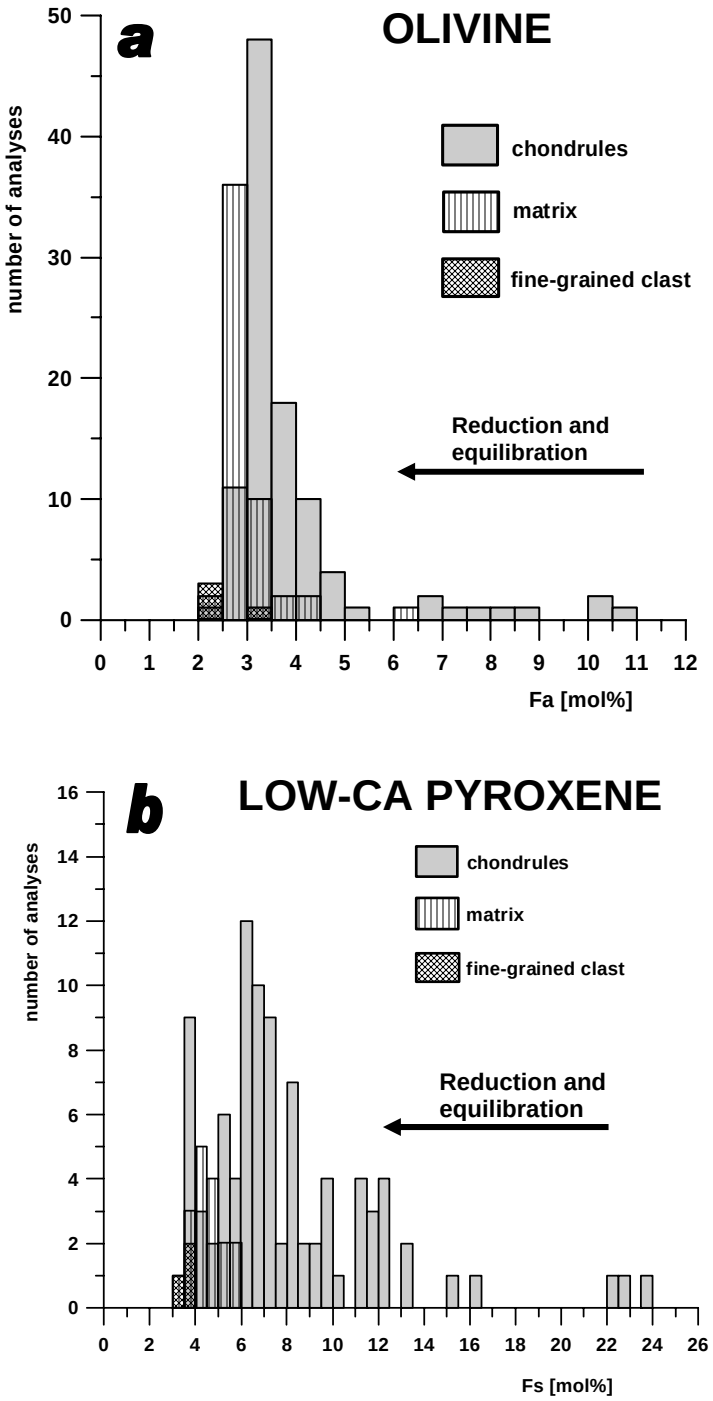

Fig. 3.4. Histograms showing a) Fa contents of olivines and b) Fs contents of low-Ca pyroxenes in Kakangari. Chondrule data are for the 20 chondrules chosen for bulk chondrule analysis in this study. Chondrule silicates (2–9 analyses per chondrule) show a wider range of compositions than those in the matrix and fine-grained clasts. The most FeO-rich compositions for both olivine and pyroxene are analyses of the cores of zoned grains. Note that low-Ca pyroxenes show a wider range of compositions than olivines.

Olivine, pyroxene and silica

Figure 3.4 shows histograms of Fa contents of olivines and Fs contents of low-Ca pyroxenes for the 20 Kakangari chondrules chosen for detailed study (2–9 analyses per chondrule). Compositions of most chondrule olivines fall within the narrow range 2.3<Fa<5.5, but there is a continuous distribution up to 11 mol% (highest Fa contents represent the cores of zoned olivine grains). Low-Ca pyroxenes show a much wider range of compositions (mostly 3.5<Fs<16.5) with a peak at 6–7 mol% and some outliers between 22 and 24 mol% (again, representing the cores of zoned grains). Arrows in **Figure 3.4** indicate the trends expected for reduction and equilibration, which are discussed in detail below. Our data are similar to those collected by Graham et al. (1977) and Brearley (1989), who surveyed olivine and low-Ca pyroxene compositions in Kakangari. Their observed ranges were $Fa_{3.2\text{-}9.3}/Fs_{3.3\text{-}14.3}$ and $Fa_{3.5\text{-}6}/Fs_{2.5\text{-}14}$, respectively. The results of previous studies (Graham and Hutchison 1974; Graham et al. 1977; Brearley 1989) and our study emphasize that Kakangari lacks chondrule silicates with Fa contents below 2 mol% and Fs contents below 3 mol%, in contrast to primitive chondrites from all other chondrite groups.

Tables 3.2 and **3.3** report representative electron microprobe analyses of chondrule olivines and pyroxenes, including analyses from the chondrules shown in **Fig. 3.2**, **Fig. 3.3a,i,l** and **Fig. 3.6**. The Cr_2O_3 contents of chondrule olivines in Kakangari are very low (<0.16 wt%, with more than 90% of all measured olivines having Cr_2O_3 contents below 0.04 wt%), whereas MnO contents of chondrule olivines are mostly higher than 0.38 wt% (average of all individual olivine analyses: 0.42 wt%). CaO contents of chondrule olivines are <0.3 wt% (average: 0.06 wt%).

Table 3.2. Representative electron microprobe analyses of olivines in Kakangari chondrules.

Chondrule	**#1-10**	**#2-2**	**#2-2**	**#2-5**	**#2-5**	**#2-9**
Texture	**PO-II**	**PO**	**PO**	**POP**	**POP**	**CC**
Fig.	**3a**	**6b**	**6b**	**2a,b**	**2a,b**	**2c,d**
Mineral	**olivine**	**dusty olivine (core)**	**dusty olivine (edge)**	**olivine chadacryst**	**olivine phenocryst**	**fine-grained olivine**
Oxide wt%						
SiO_2	42.1	41.1	41.8	41.6	42.0	42.9
TiO_2	<0.04	<0.04	<0.04	<0.04	<0.04	<0.04
Al_2O_3	<0.03	<0.03	<0.03	<0.03	<0.03	<0.03
Cr_2O_3	<0.02	<0.02	<0.02	<0.02	<0.02	<0.02
FeO	3.3	8.1	3.3	4.7	3.5	2.4
MnO	0.42	0.42	0.46	0.46	0.42	0.40
MgO	54.4	49.8	53.8	52.7	53.6	54.6
CaO	0.05	0.12	0.10	0.04	<0.02	0.05
NiO	<0.03	<0.03	<0.03	<0.03	<0.03	<0.03
Total	100.3	99.6	99.5	99.6	99.6	100.4
Cations (4 oxygens)						
Si	1.00	1.00	1.00	1.00	1.00	1.01
Ti	0.00	0.00	0.00	0.00	0.00	0.00
Al	0.00	0.00	0.00	0.00	0.00	0.00
Cr	0.00	0.00	0.00	0.00	0.00	0.00
Fe	0.06	0.17	0.07	0.09	0.07	0.05
Mn	0.01	0.01	0.01	0.01	0.01	0.01
Mg	1.93	1.81	1.92	1.89	1.91	1.92
Ca	0.00	0.00	0.00	0.00	0.00	0.00
Ni	0.00	0.00	0.00	0.00	0.00	0.00
Total	3.00	3.00	3.00	3.00	2.99	2.99
Fa (mol%)	3.3	8.4	3.3	4.8	3.5	2.4

Table 3.3. Representative electron microprobe analyses of pyroxenes and silica in Kakangari chondrules.

Chondrule	#2-5	#2-5	#1-7	#1-7	#1-9	#1-9	#2-2	#2-7	#2-9	#2-9
Texture	POP	POP	PP	PP	RP/BP	RP/BP	PO	RP	CC	CC
Fig.	2a,b	2a,b	3i	3i	6a	6a	6b	3l	2c,d	2c,d
Mineral	enstatite	augite	enstatite	augite	enstatite (core)	enstatite (edge)	enstatite	enstatite	pigeonite	silica
Oxide wt%										
SiO_2	58.2	54.0	59.0	52.4	57.3	58.6	55.9	57.3	57.7	99.6
TiO_2	<0.04	0.46	<0.04	0.65	<0.04	<0.04	0.07	<0.04	0.13	<0.04
Al_2O_3	0.25	2.0	0.18	3.7	0.10	0.25	0.46	0.39	1.9	0.13
Cr_2O_3	0.50	1.7	0.43	1.6	0.39	0.29	0.59	0.50	0.70	<0.02
FeO	4.4	4.0	2.8	2.4	8.0	3.8	11.7	6.7	3.2	0.11
MnO	0.33	0.51	0.32	1.1	1.0	0.70	0.36	0.44	0.56	0.03
MgO	35.6	19.2	37.5	19.5	32.7	36.2	29.8	33.6	33.5	0.04
CaO	0.25	17.6	0.18	18.5	0.54	0.73	1.2	0.69	2.7	<0.02
Na_2O	0.03	0.55	<0.02	0.28	0.07	0.04	0.05	0.11	0.47	0.04
K_2O	0.04	0.04	<0.02	<0.02	<0.02	<0.02	<0.02	<0.02	0.13	<0.02
Total	99.7	100.0	100.4	100.1	100.2	100.7	100.2	99.8	101.0	100.0
Cations (6 oxygens)										*(2 oxygens)*
Si	2.00	1.95	1.99	1.89	2.00	1.99	1.98	1.99	1.96	0.997
Ti	0.00	0.01	0.00	0.02	0.00	0.00	0.00	0.00	0.00	0.000
Al	0.01	0.08	0.01	0.16	0.00	0.01	0.02	0.02	0.08	0.002
Cr	0.01	0.05	0.01	0.05	0.01	0.01	0.02	0.01	0.02	0.000
Fe	0.13	0.12	0.08	0.07	0.23	0.11	0.35	0.19	0.09	0.001
Mn	0.01	0.02	0.01	0.03	0.03	0.02	0.01	0.01	0.02	0.000
Mg	1.82	1.03	1.89	1.05	1.70	1.83	1.57	1.74	1.70	0.001
Ca	0.01	0.68	0.01	0.71	0.02	0.03	0.05	0.03	0.10	0.000
Na	0.00	0.04	0.00	0.02	0.00	0.00	0.00	0.01	0.03	0.001
K	0.00	0.00	0.00	0.00	0.00	0.00	0.00	0.00	0.01	0.000
Total	3.99	3.99	4.00	4.00	4.00	4.00	4.00	4.00	4.00	1.001
Fs (mol%)	6.5	6.5	4.0	3.9	11.8	5.5	17.5	9.8	4.7	
Wo (mol%)	0.5	36.8	0.3	38.2	1.0	1.3	2.3	1.3	5.2	

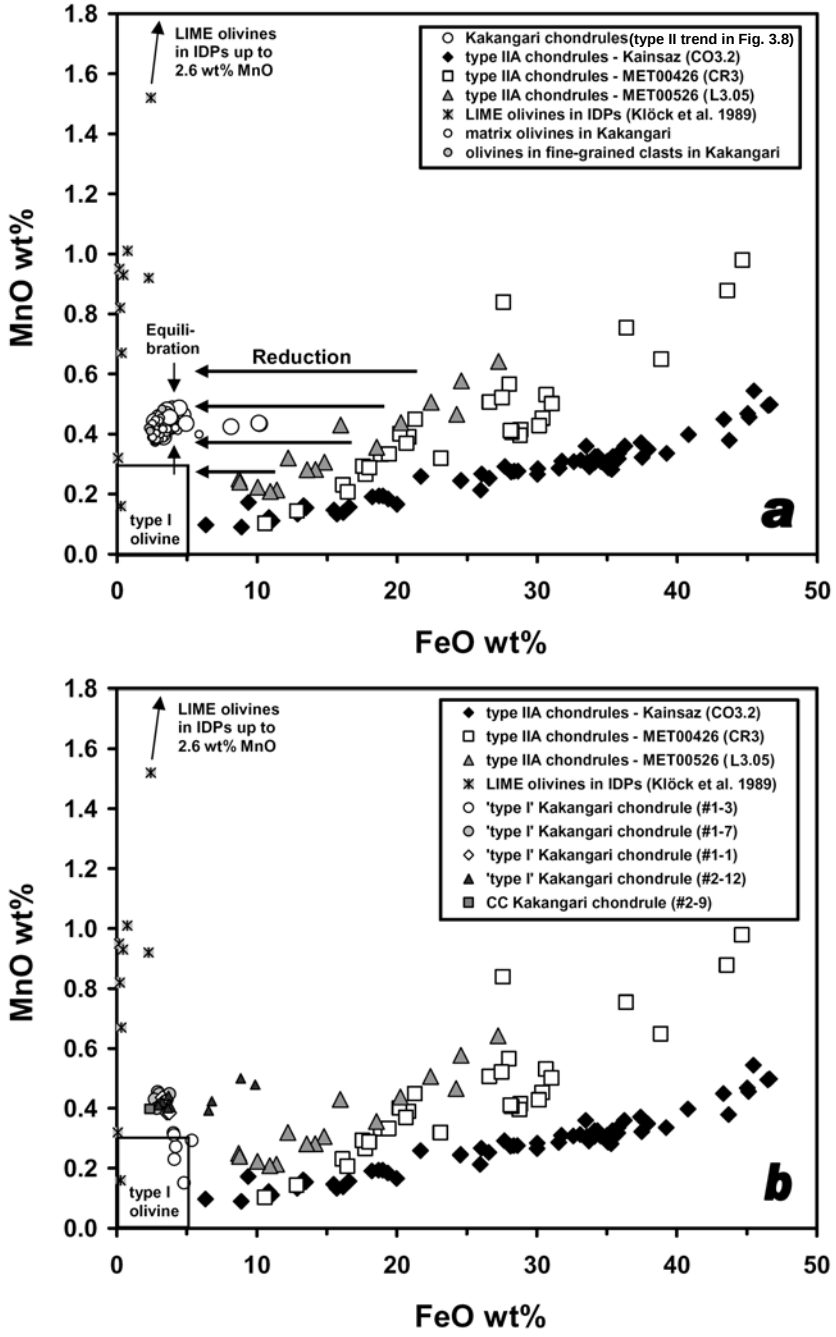

Fig. 3.5. MnO vs. FeO (wt%) in olivines in Kakangari compared to type IIA chondrule olivines from Kainsaz (CO3.2), MET 00426 (CR3.0) and MET 00526 (L3.05) (see Chapter 1) as well as LIME olivines in IDPs (Klöck et al. 1989). Outlined boxes at the origin indicate type I olivine compositions. Type IIA chondrule olivines in carbonaceous and ordinary chondrites show linear correlations between MnO and FeO contents. a) Olivines from Kakangari chondrules that follow the type II chondrule mesostasis trend in Fig. 3.8. The two analyses with FeO contents close to 10 wt% are from dusty olivines in chondrule #2-2 (Fig. 3.6b). Matrix olivines and olivines in fine-grained clasts have MnO contents similar to chondrule olivines. b) Olivines from Kakangari chondrules that follow the type I chondrule mesostasis trend in Fig. 3.8. Olivines from only one of these chondrules (#1-3, Fig. 3.6c) have MnO contents that overlap with those of typical type I chondrules in ordinary and carbonaceous chondrites. Olivine compositions in Kakangari can be explained by a combination of reduction and equilibration (see text).

Figure 3.5 shows MnO (wt%) versus FeO (wt%) for individual analyses of olivine in Kakangari chondrules. Mesostasis compositions in Kakangari chondrules follow two trends, which we describe as 'type I' and 'type II' trends (see below). We plotted olivine from these two groups of chondrules separately in **Figure 3.5** (**Fig. 3.5a** = type II trend, **Fig. 3.5b** = type I trend). For comparison, data for LIME (low-iron, manganese-enriched) olivines from IDPs (Klöck et al. 1989) are shown as well as data for chondrule olivines in L3.05 chondrite MET 00526, CR3.0 chondrite MET 00426, and Kainsaz (CO3.2). Type IIA chondrule olivines in these unequilibrated chondrites show positive correlations: MnO concentrations increase with increasing FeO contents (see Chapter 2), while MnO contents of olivines in type I chondrules are typically below 0.3 wt% (Chapter 1). Olivines in Kakangari chondrules that follow the 'type II' mesostasis trend plot in a unique field with low FeO contents and high MnO contents (**Fig. 3.5a**). However, their compositions are not equivalent to those of LIME olivines. Olivines in chondrules that follow the 'type I' mesostasis trend (**Fig. 3.5b**) have the same compositions as those that follow the the 'type II' trend, except for some analyses in Kakangari chondrule #1-3 (see **Figure 3.6c**) which fall within the typical type I range. Arrows in **Figure 3.5a** indicate the trends expected for reduction and equilibration, which are discussed in detail below.

Some chondrule silicates are zoned with FeO-rich cores and MgO-rich edges and contain abundant metal/troilite blebs. **Figure 3.6a** shows a RP/BP chondrule (#1-9) containing low-Ca pyroxene with Fs_{12} in the center and Fs_{7} at the edge, where it is associated with fine-grained troilite. **Figure 3.6b** shows an object (#2-2) consisting of FeO-rich low-Ca pyroxene in the center surrounded by several "dusty" olivines, which contain numerous micron-size troilite and some Ni-poor metal blebs. There is no mesostasis present in this object. Both the olivine and the pyroxene grains are zoned (Fa_{11-3}, Fs_{24-16}) with more MgO-rich compositions towards the edges. The "dusty" olivines are similar to those found in unequilibrated ordinary and carbonaceous chondrites (e.g., Jones and Danielson 1997; Leroux et al. 2003).

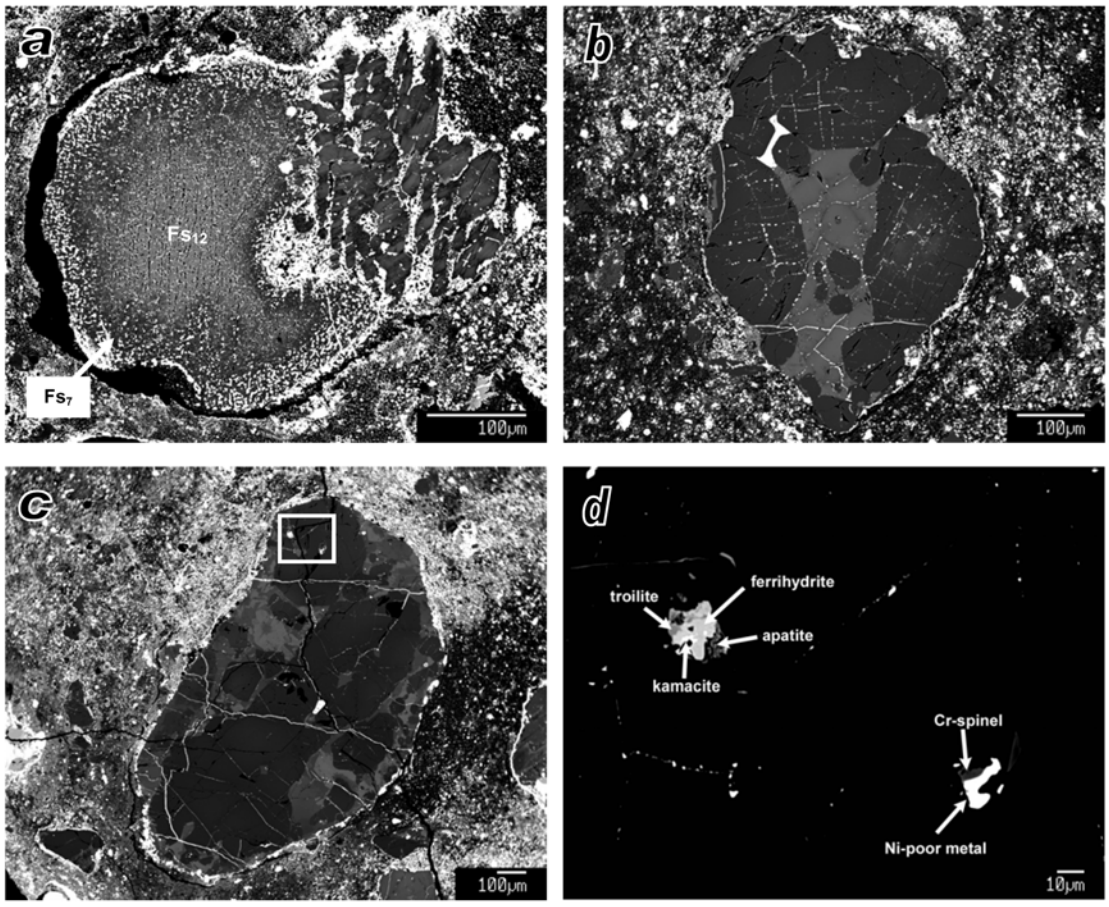

Fig. 3.6. BSE images of chondrules that show evidence for solid-state reduction. a) Fine-grained pyroxene chondrule (#1-9). Low-Ca pyroxene is FeO-rich in the center (Fs_{12}) and FeO-poor at the edge (Fs_7), where it is associated with fine-grained troilite. b) Object (#2-2) consisting of "dusty" olivines (core to rim, Fa_{11} to Fa_3) and very FeO-rich pyroxene (core to rim, Fs_{24} to Fs_{16}) in the center. Ni-poor metal blebs have high Cr contents (up to 1.8 wt%) and some of them have been sulfidized. White veins are troilite. c) POP chondrule (#1-3) in which olivines have somewhat lower MnO contents than other Kakangari chondrule olivines, overlapping with those of typical type I chondrules in ordinary and carbonaceous chondrites (Fig. 3.5b). d) Close-up image of box outlined in Fig. 3.6c. The presence of a large Ni-poor metal grain within one of the olivine crystals provides evidence that this chondrule also has undergone significant reduction.

Six of the twenty chondrules (e.g., **Fig. 3.2c,d** and **Fig. 3.3j,k,l**) contain abundant silica (the polymorphs were not determined). The cryptocrystalline chondrule shown in **Fig. 3.2c,d** is surrounded by a layer of silica (EMP analysis given in **Table 3.3**). This chondrule mainly consists of fine-grained pyroxene ($Fs_{4.6}Wo_{7.3}$) and olivine. The composition of the pyroxene next to the olivine is slightly more Mg-rich ($Fs_{3.2}Wo_{6.5}$) and Si-deficient (non-stoichiometric). A few patches of mesostasis and some fine-grained Ca-rich pyroxene were also identified.

Augite is common in Kakangari chondrules. In PO chondrules, augite occurs as laths in the groundmass (e.g., **Fig. 3.3a,b**), and it is frequently found overgrowing low-Ca pyroxene and/or pigeonite in POP and PP chondrules (e.g., **Fig. 3.2a,b** and **Fig. 3.3c,i**). Representative analyses of augite are given in **Table 3.3**. They show relatively high TiO_2, Al_2O_3, Cr_2O_3 and Na_2O contents.

Another typical feature of Kakangari chondrules is the presence of rounded olivine grains poikilitically enclosed in low-Ca pyroxene (e.g., **Fig. 3.2a,b** and **Fig. 3.3i**). Olivine chadacrysts have either higher or the same Fe/(Fe+Mg) as olivine phenocrysts in the same chondrule, but always lower Fe/(Fe+Mg) than the host pyroxene (e.g., **Table 3.2**). In some chondrules, low-Ca pyroxene shows patchy zoning in BSE images (e.g., **Fig. 3.6a** – chondrule fragment on the upper right hand side). The edges of these crystals are more MgO-rich than the cores.

Troilite, metal and Cr spinel

Representative analyses of troilite, kamacite and taenite are given in **Table 3.4**. Troilite is the only sulfide present in Kakangari and contains 0.15–0.25 wt% Cr. Kamacite has Ni contents between 3–7 wt%, with an average (of all individual kamacite analyses) of 6.3 wt% Ni. Taenite is common in the interior of Kakangari chondrules (it was observed in 8 of the 20 chondrules chosen for bulk chondrule analysis) and has grain sizes up to ~150 μm (e.g., **Fig. 3.2a,b**). It also makes up ~6 vol% of the igneous rim of chondrule #1-4 shown in **Fig. 3.3d** and **3.3f**, and is present in some of the agglomeratic chondrules. Weisberg et al. (1996) found two types of taenite in Kakangari and LEW87232, one with ~24 wt% Ni and the other 30–34 wt% Ni. We found that Ni contents in taenite vary continuously from 22 to 51 wt% Ni. The large taenite grain in chondrule #2-5 (**Fig. 3.2a,b**) has an M-shaped zoning profile with higher Ni contents toward the edges. This will be further addressed in the discussion section (see also **Fig. 3.15**). Core and edge compositions of the taenite grain are given in **Table 3.4**.

Table 3.4. Representative electron microprobe analyses of kamacite, taenite and troilite.

Chondrule	#2-5	#2-5	#2-5	#2-5
Texture	POP	POP	POP	POP
Figure	3.2a,b	3.2a,b	3.2a,b	3.2a,b
Mineral	kamacite	taenite (core)	taenite (edge)	troilite
Fe	93.1	78.3	69.8	63.1
Ni	6.5	22.1	29.6	<0.01
S	<0.01	<0.01	<0.01	36.6
Co	0.50	0.22	0.15	<0.01
Cr	0.13	<0.01	<0.01	0.23
Si	<0.02	<0.02	<0.02	<0.02
P	<0.02	<0.02	<0.02	<0.02
As	0.05	0.03	0.04	<0.02
Total	100.3	100.7	99.6	99.9

Numerous μm-sized troilite and metal blebs are found throughout all fine-grained chondrules (e.g., **Fig. 3.3g, h, and j-l**) and within the microcrystalline groundmass of chondrules with a "type IIA"-texture (e.g., **Figs. 3.3a-f**). In the latter, Ni-poor metal blebs (~1.1 wt% Ni) frequently decorate the crystal faces of olivines. A semi-quantitative EDS analysis of a Ni-poor metal bleb in chondrule #2-2 (shown in **Fig. 3.6b**) yielded 1.3 wt% Ni and 1.8 wt% Cr.

We also found a metal grain (~10 μm in size) with only 0.25 wt% Ni associated with a Cr-bearing spinel in chondrule #1-3 (**Fig. 3.6c,d**). This is the chondrule for which olivine analyses fall within the type I field of other chondrites (**Fig. 3.5b**) and mesostasis analyses follow the type I trend in **Figure 3.8**.

Cr spinel was observed in 5 of the 20 chondrules (grains up to 20 μm in size). The composition of the Cr spinels in chondrule #2-5 (**Fig. 3.2a,b**) is very similar to those found by Brearley (1989) in Kakangari matrix. They contain ~10 wt% MgO and ~5 wt% Al_2O_3. Others have higher MgO (up to 25 wt%) and Al_2O_3 contents (up to 35 wt%). All Cr spinels analyzed contain some ZnO (up to 1.2 wt%).

Virtually all chondrules in Kakangari have opaque rims (**Fig. 3.1**). Genge and Grady (1998) described two different types of opaque rims around Kakangari chondrules: massive rims consisting of irregular-shaped kamacite and/or troilite and porous ('spongey') rims consisting of small, interconnected grains of troilite that enclose silicate grains. Massive and porous rims are often found on the same chondrule with porous rims always forming the outermost layer. Some examples of metal/troilite rims are shown in

Figure 3.7. Our observations are similar to those by Genge and Grady (1998), but we also observed that many porous rims contain kamacite in addition to troilite (e.g., **Fig. 3.7a**). Some porous rims are clearly distinct from the surrounding matrix (e.g., **Fig. 3.7b**), whereas others are not (e.g., **Fig. 3.7a**). Apatite and ferrihydrite (see section 3.3.) are fairly common within both types of rims (e.g., **Fig. 3.2a,b**). In one massive kamacite rim around a large chondrule with a "type IIA" texture, we observed a rare assemblage: two oval-shaped objects consisting of troilite and Fe,Ni-phosphide (**Fig. 3.7c,d**). Most chondrules contain cross-cutting troilite veins that only rarely extend into the matrix (e.g., **Figs. 3.1**, **3.2a**, and **3.3**).

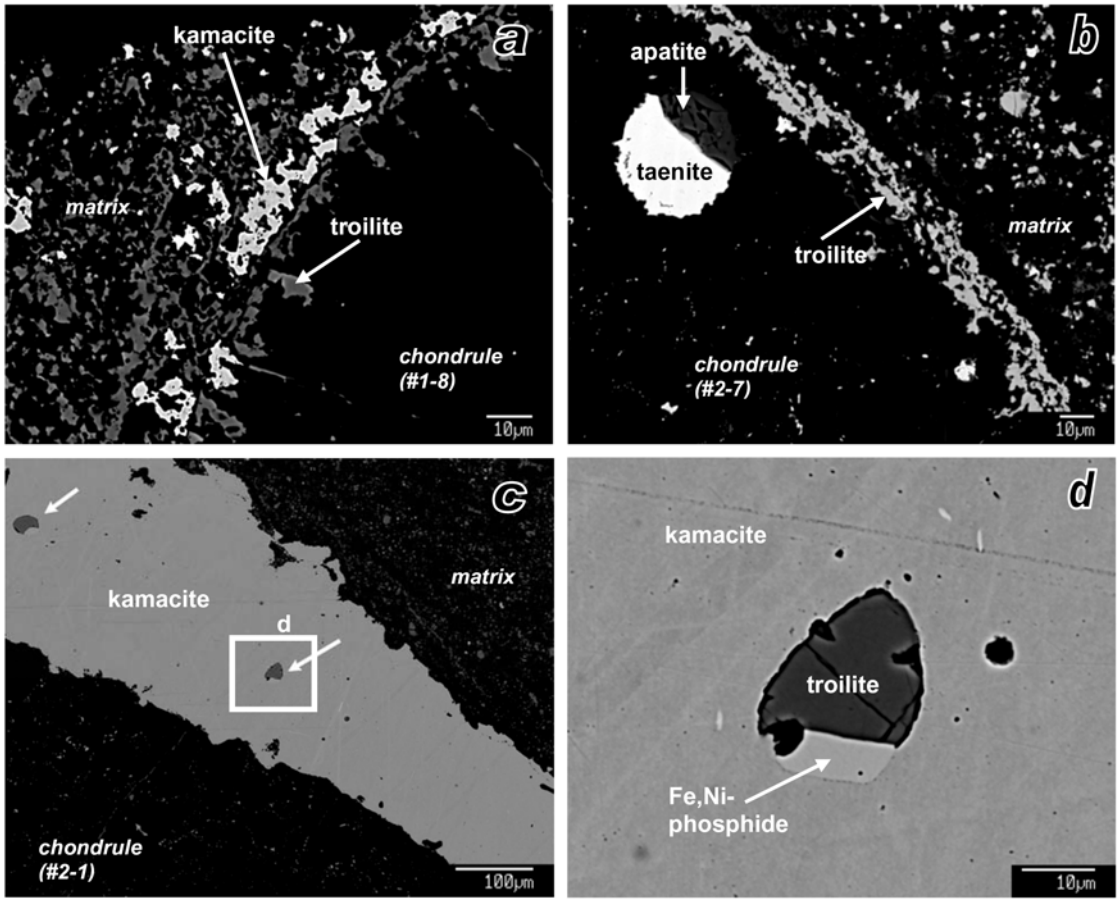

Fig. 3.7. Metal/troilite rims around chondrules. a) 'Spongey' rim consisting of troilite and kamacite. No clear distinction is visible between the rim and fine-grained troilite in the matrix. b) 'Spongey' rim consisting solely of fine-grained troilite. In contrast to the metal/troilite rim shown in Fig. 3.7a, there is a clear distinction between the troilite rim and surrounding matrix. The whole chondrule (#2-7) is shown in Fig. 3.3l. c) Massive kamacite rim containing troilite blebs associated with Fe,Ni-phosphide (arrowed). d) Close-up image of box outlined in Fig. 3.7c.

Mesostasis

Average compositions of mesostasis glass for all Kakangari chondrules are given in **Table 3.5**. The exception is the chondrule-like object #2-2, in which no mesostasis is present (**Fig. 3.6b)**. In all other chondrules, the modal abundance of mesostasis glass varies from 1–24 vol%. In most chondrules, the glass was analyzed with a beam diameter of 5 μm. However, when the patches of glass were very small, the beam diameter was decreased to 3 μm. Ca-rich pyroxene crystallites in the mesostasis were analyzed separately with a focused beam, because typically several crystals were present within a chondrule that were large enough to analyze (width >2 μm).

SiO_2 contents in chondrule mesostases range from 45–75 wt%. CaO and Al_2O_3 are negatively correlated with SiO_2, as has also been observed in ordinary and some carbonaceous chondrites (e.g., Brearley and Jones 1998). In a K/Al versus Na/Al plot (**Fig. 3.8**), our mesostasis analyses follow two significantly different trends that are similar to the general type I and type II chondrule trends observed in ordinary chondrites (Grossman and Brearley 2005). Most Kakangari chondrules have high Na/Al ratios and variable K/Al (type II chondrule trend), but six chondrules (indicated in **Table 3.5**) have low K/Al ratios and variable Na/Al ratios (type I chondrule trend). All of the PO-II and RP/BP chondrules fall in the type II group.

Three chondrules that fall in the type I group are CC chondrule #2-9 shown in **Figure 3.2c,d**, PP chondrule #1-7 shown in **Figure 3.3i** and POP chondrule #1-3 shown in **Figure 3.6c**. The range of Fa and Fs contents for silicates in chondrules that follow the type I trend ($2.3<Fa<10.1$ and $3.7<Fs<18.8$) is not significantly different from those that follow the type II trend ($2.7<Fa<10.6$ and $4.3<Fs<23.6$). These chondrules also do not show the typical textural characteristic of type I chondrules, such as abundant metal grains for example (e.g., Scott and Taylor 1983). In fact, there is no other characteristic that distinguishes them from the chondrules that follow the type II trend.

Table 3.5. Mesostasis compositions of Kakangari chondrules (means of 2 to 13 analyses per chondrule).

No.	Texture	vol% mesostasis	SiO_2	TiO_2	Al_2O_3	Cr_2O_3	FeO	MnO	MgO	CaO	Na_2O	K_2O	NiO	P_2O_5	S	Total
1-4	PO-II	6	71.3	0.59	17.4	0.39	0.76	0.05	0.80	1.1	6.0	2.0	<0.03	n.a.	n.a.	100.4
1-10	PO-II	15	67.9	0.46	12.4	0.21	2.5	0.06	4.0	3.9	6.8	1.3	0.11	0.15	0.11	100.1
2-4	PO-II	24	66.8	0.41	13.2	0.16	3.0	0.08	3.2	4.3	7.2	1.6	0.10	0.08	0.21	100.6
1-1*	POP	6	59.9	0.09	25.4	<0.03	0.39	<0.03	0.13	6.9	7.9	0.18	<0.03	<0.04	<0.03	101.1
1-3*	POP	5	53.3	0.46	23.5	0.21	1.8	0.13	6.0	11.2	3.9	0.12	0.05	<0.04	<0.03	100.6
1-13	POP	14	65.0	0.48	15.3	0.82	1.5	0.09	4.1	2.4	7.7	2.0	<0.03	0.26	0.18	100.0
1-14	POP	9	63.7	0.45	16.3	0.62	2.0	0.10	4.3	2.8	8.9	1.1	0.08	0.07	0.09	100.7
2-5	POP	11	68.4	0.44	17.3	0.20	0.55	0.04	0.88	1.2	8.9	1.8	<0.03	<0.04	0.06	100.0
2-11	POP	24	74.3	0.40	11.6	0.20	2.1	0.17	2.1	2.6	5.6	2.2	<0.03	<0.04	0.04	101.3
2-12*	POP	9	45.4	<0.06	35.2	0.05	0.57	<0.03	0.41	17.8	1.3	0.07	<0.03	<0.04	<0.03	100.8
1-7*	PP	11	58.4	0.15	24.8	<0.03	0.55	n.a.	0.81	7.6	7.2	0.19	0.08	<0.04	0.14	100.2
1-12	PP	17	70.7	0.45	13.4	0.19	1.7	n.a.	2.3	2.6	6.8	2.1	<0.03	<0.04	0.06	100.4
2-10*	PP	4	49.0	0.36	25.0	0.20	4.1	0.23	5.0	13.4	2.4	0.10	0.06	0.07	0.44	101.0
1-8	RP	8	66.7	0.43	15.8	0.25	0.99	n.a.	3.6	1.4	7.9	2.4	0.04	<0.04	0.04	99.5
1-9	RP/BP	2	64.6	0.19	6.0	0.52	6.8	0.43	13.8	3.6	3.2	0.38	0.12	<0.04	0.10	100.0
1-11	BP	9	69.6	0.29	8.8	0.43	3.4	0.68	9.7	2.4	4.1	1.0	0.04	<0.04	<0.03	100.0
2-3	BP	15	71.3	0.46	15.7	0.24	1.0	<0.03	0.51	0.35	7.5	3.0	<0.03	<0.04	0.08	100.3
2-7	RP	3	63.7	0.47	16.6	0.41	1.5	0.10	5.0	2.5	8.2	1.5	<0.03	<0.04	<0.03	100.1
2-9*	CC	1	55.2	<0.06	13.7	0.04	1.2	0.17	22.2	1.6	5.9	0.23	<0.03	<0.04	0.09	100.6

*Chondrules that follow the type I trend in Fig. 3.8.
n.a. = not analyzed

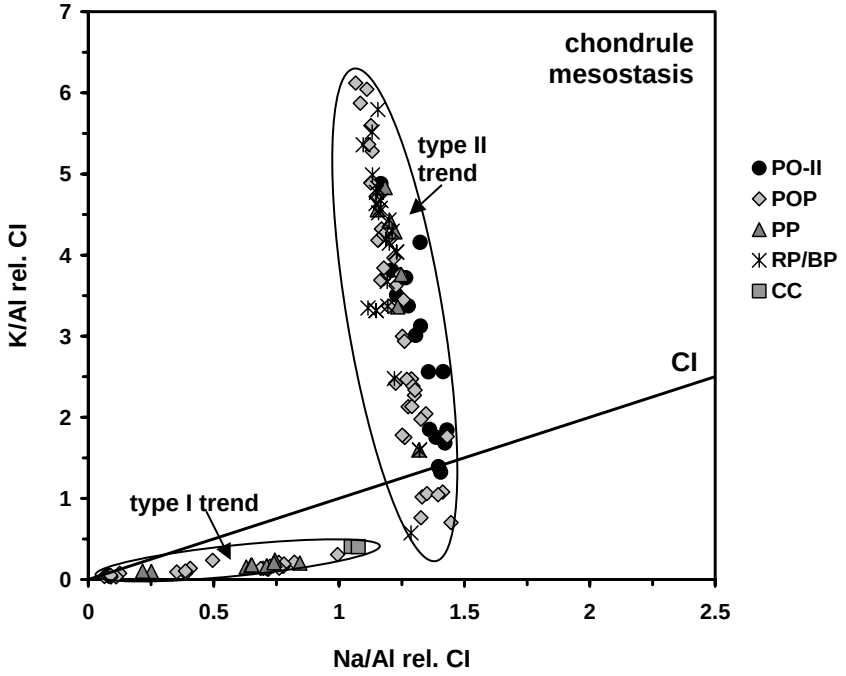

Fig. 3.8. K/Al vs. Na/Al (relative to CI) for individual mesostasis analyses in Kakangari chondrules (2-13 analyses per chondrule, refer to Table 3.5 for number of chondrules per textural type). Two trends are visible, resembling general type I and type II chondrule trends observed in ordinary chondrites (Grossman and Brearley 2005). Chondrules that follow the type I trend are: #1-1 (POP), #1-3 (POP), #2-12 (POP), #1-7 (PP), #2-10 (PP), and #2-9 (CC).

Chondrule bulk compositions

Bulk chondrule compositions were obtained using modal recombination analysis (MRA). The supplementary CD contains Microsoft Office Excel® files with the collected and generated data for each chondrule (EMP data, BSE image, corresponding phase image and details of the modal recombination analysis). Metal/troilite rims were included in bulk chondrule compositions. We agree with Genge and Grady (1998), who suggested that metal/troilite rims probably formed during chondrule melting events due to liquid immiscibility, so they belong to the chondrule and provide important information about the precursor material.

Bulk chondrule compositions are given in **Table 3.6** and data for the silicate portions only are given in **Table 3.7**. The variation in chemical composition between chondrules is shown in **Fig. 3.9**, an element abundance diagram for all elements that were

determined in this study, plotted as a function of increasing volatility. Element abundance patterns for Kakangari chondrules are relatively unfractionated compared to bulk compositions of chondrules in ordinary and enstatite chondrites that commonly show volatility-related trends (e.g., Grossman et al. 1988; Jones et al. 2005). There are no significant differences in bulk chondrule compositions between the chondrules that follow the type I and type II mesostasis trends in **Fig. 3.8**, except for somewhat higher K contents in chondrules that follow the type II trend.

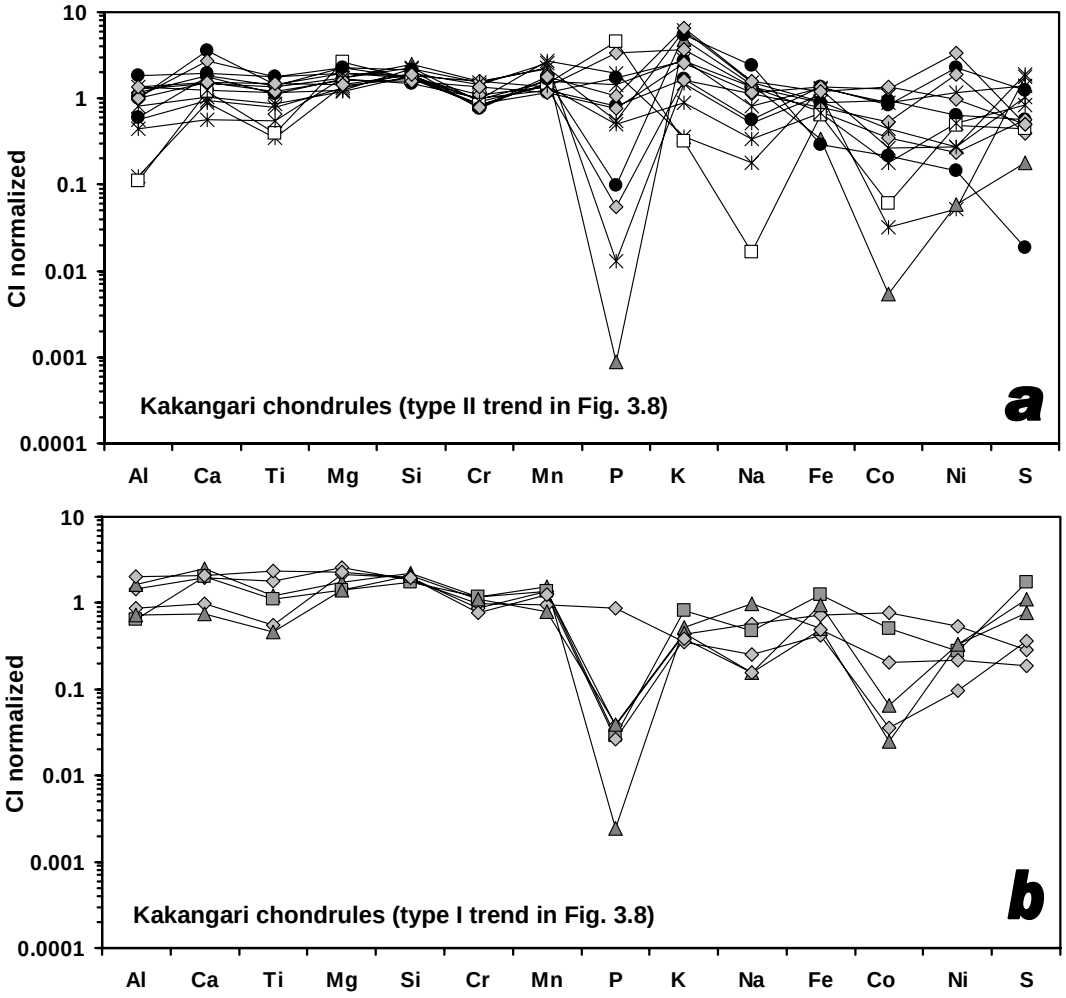

Fig. 3.9. Bulk chemical compositions of a) Kakangari chondrules that follow the type II trend in Figure 3.8 and b) chondrules that follow the type I trend in Figure 3.8. Elemental abundances are normalized to CI chondrite abundances (Lodders 2003). Elements on the ordinate are arranged in order of increasing volatility. Siderophile elements are plotted last.

Table 3.6. Bulk compositions of Kakangari chondrules (including metal-troilite rims) determined by EMP via modal recombination.

No.	Texture	SiO_2	TiO_2	Al_2O_3	Cr_2O_3	FeO[#]	MnO	MgO	CaO	Na_2O	K_2O	P_2O_5	Fe[*]	Co	Ni	S	Total	Fe^{tot}
1-4[a]	PO-II	34.1	0.08	0.96	0.38	4.4	0.30	26.7	2.3	0.38	0.11	0.17	21.4	0.04	2.4	6.7	100.5	24.8
1-10	PO-II	39.3	0.11	1.6	0.32	3.0	0.29	31.5	4.6	0.93	0.17	0.36	13.8	0.05	0.68	3.1	99.8	16.1
2-4	PO-II	48.9	0.13	2.9	0.29	4.4	0.42	36.1	2.5	1.6	0.35	<0.06	1.9	0.01	0.15	0.10	99.8	5.3
2-2	PO	38.5	<0.06	0.18	0.32	6.3	0.37	41.9	1.5	<0.02	0.02	0.95	6.8	<0.01	0.52	2.4	99.9	11.7
1-1	POP	45.3	<0.06	1.4	0.33	4.1	0.34	34.5	1.2	0.38	0.03	<0.06	10.0	0.04	0.56	1.5	99.8	13.2
1-3	POP	41.9	0.13	2.4	0.37	4.5	0.24	40.6	2.5	0.17	0.02	0.18	4.2	<0.01	0.10	1.9	99.2	7.7
1-13	POP	39.6	0.10	1.9	0.42	3.6	0.34	36.3	2.4	0.92	0.23	0.71	9.8	0.02	0.25	3.1	99.6	12.6
1-14	POP	41.4	0.13	1.7	0.60	3.8	0.33	31.1	3.4	0.77	0.10	<0.06	11.5	0.03	2.0	2.2	99.1	14.5
2-5	POP	35.9	0.09	1.6	0.52	3.5	0.28	26.0	2.0	0.78	0.16	0.16	21.9	0.07	3.6	2.7	99.2	24.6
2-11	POP	42.7	0.11	2.2	0.30	5.0	0.44	23.1	1.9	1.1	0.41	0.22	18.1	0.07	1.0	2.7	99.3	22.0
2-12	POP	44.5	0.17	3.3	0.29	6.0	0.31	36.7	2.7	0.11	0.02	<0.06	4.4	0.01	0.23	1.0	99.7	9.1
1-7	PP	49.9	0.09	2.7	0.44	2.5	0.38	27.9	3.1	0.67	0.03	<0.06	7.2	<0.01	0.36	4.1	99.4	9.1
1-12	PP	57.4	0.10	2.1	0.60	5.3	0.55	27.8	1.9	0.97	0.31	<0.06	2.1	<0.01	0.06	0.98	100.1	6.2
2-10	PP	48.1	<0.06	1.2	0.43	7.3	0.19	22.5	0.94	0.11	0.03	<0.06	11.9	<0.01	0.36	6.1	99.1	17.6
1-8	RP	41.6	0.06	1.3	0.37	4.4	0.40	19.3	1.3	0.55	0.18	0.30	21.0	0.05	1.2	7.6	99.6	24.4
1-9	RP/BP	39.9	<0.06	0.20	0.37	6.9	0.67	22.6	1.1	0.12	0.02	0.42	17.9	0.01	0.30	10.2	100.9	23.3
1-11	BP	44.3	0.06	0.92	0.55	6.8	0.63	21.2	1.2	0.35	0.09	<0.06	15.2	<0.01	0.06	9.7	101.0	20.5
2-3[b]	BP	49.9	0.09	2.2	0.59	4.9	0.57	20.0	1.6	1.0	0.39	0.12	12.8	0.02	0.29	5.7	100.1	16.6
2-7	RP	51.9	<0.06	0.71	0.35	4.0	0.34	27.2	0.72	0.23	0.06	0.10	9.3	0.01	0.55	4.5	100.0	12.4
2-9	C	40.2	0.08	1.0	0.45	2.6	0.34	22.2	2.6	0.32	0.05	<0.06	20.7	0.03	0.30	9.5	100.4	22.7

[#]FeO in silicates.
[*]Fe included in metals and sulfide.
[a]Bulk composition of chondrule No. 1-4 includes igneous rim (Figs. 3.3d,f).
[b]Compound chondrule (Fig. 3.3j). Bulk composition includes both chondrules; they have the same texture and mineral compositions.

Table 3.7. Bulk compositions of the silicate portion of Kakangari chondrules determined by EMP via modal recombination.

No.	Texture	SiO_2	TiO_2	Al_2O_3	Cr_2O_3	FeO	MnO	MgO	CaO	Na_2O	K_2O	Total
1-4[a]	PO-II	50.5	0.12	1.4	0.49	4.4	0.45	39.6	3.1	0.56	0.16	100.8
1-10	PO-II	48.8	0.13	2.0	0.36	3.0	0.36	39.1	5.2	1.1	0.21	100.3
2-4	PO-II	50.0	0.13	3.0	0.29	4.4	0.43	36.9	2.5	1.7	0.36	99.7
2-2	PO	44.3	<0.06	0.10	0.14	6.3	0.41	48.2	0.33	<0.02	0.02	99.9
1-1	POP	52.3	<0.06	1.6	0.36	4.1	0.39	39.8	1.4	0.44	0.03	100.5
1-3	POP	45.4	0.14	2.5	0.37	4.5	0.26	44.0	2.4	0.18	0.02	99.8
1-13	POP	47.0	0.12	2.3	0.36	3.6	0.40	42.8	1.7	1.1	0.28	99.6
1-14	POP	50.0	0.16	2.0	0.59	3.8	0.40	37.6	4.1	0.93	0.12	99.7
2-5	POP	51.7	0.12	2.3	0.39	3.5	0.39	37.4	2.6	1.1	0.23	99.7
2-11	POP	56.8	0.14	2.9	0.36	5.0	0.58	30.7	2.2	1.4	0.54	100.7
2-12	POP	47.7	0.19	3.5	0.30	6.0	0.33	39.4	2.9	0.11	0.02	100.4
1-7	PP	57.2	0.10	3.0	0.47	2.5	0.43	32.1	3.1	0.77	0.04	99.7
1-12	PP	59.8	0.10	2.1	0.61	5.3	0.57	29.0	1.9	1.0	0.32	100.6
2-10	PP	61.0	<0.06	1.5	0.47	7.3	0.24	28.5	1.2	0.12	0.03	100.4
1-8	RP	61.8	0.09	2.0	0.46	4.4	0.59	28.7	1.4	0.81	0.27	100.4
1-9	RP/BP	57.8	<0.06	0.29	0.42	6.9	0.98	32.9	0.88	0.17	0.03	100.5
1-11	BP	60.1	0.08	1.3	0.64	6.8	0.86	28.9	1.6	0.48	0.13	100.8
2-3[b]	BP	62.5	0.11	2.8	0.71	4.9	0.72	25.4	1.2	1.3	0.49	100.0
2-7	RP	61.3	<0.06	0.84	0.37	4.0	0.41	32.0	0.69	0.27	0.07	100.0
2-9	C	59.0	0.12	1.5	0.55	2.6	0.48	32.4	3.7	0.47	0.08	100.9

[a]Bulk composition of chondrule No. 1-4 includes igneous rim (Figs. 3.3d,f).
[b]Compound chondrule. Bulk composition includes both chondrules; they have the same texture and mineral compositions.

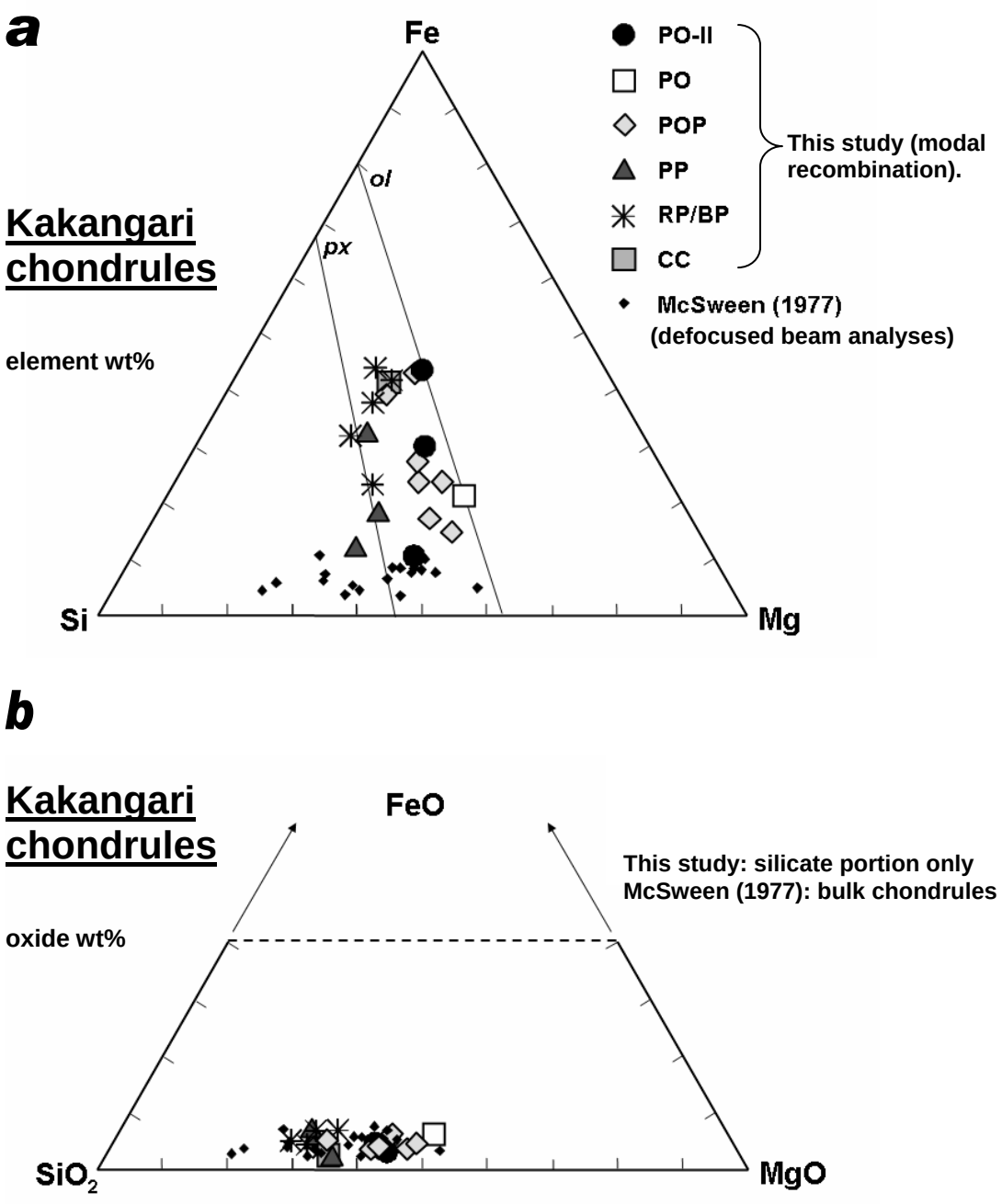

Fig. 3.10. a) Fe-Mg-Si ternary diagram showing bulk compositions of Kakangari chondrules. Data published by McSween (1977) are plotted for comparison. Fe contents are significantly lower in McSween's data, which is probably due to artifacts of his analytical method. b) Silicate portion of Kakangari chondrules plotted in a FeO-MgO-SiO_2 ternary diagram. McSween's bulk chondrule data are more similar in this diagram.

Fig. 3.10a shows that Kakangari chondrules are highly variable in bulk Fe content (5–25 wt%), which is essentially caused by different abundances of Fe,Ni metal and troilite. FeO contents of the silicate portion (**Fig. 3.10b**) show a more limited range (2.5–7.3 wt%: **Table 3.7**). Our data are significantly different from previously published data for Kakangari chondrules (McSween 1977a), having much higher bulk Fe contents (**Fig. 3.10a**). This is also true when metal/troilite rims are not included in the bulk chondrule compositions. Depending on the thickness of the metal/troilite rim, the bulk Fe contents drop between 1 and 13 wt%, but the overall range in bulk Fe contents (4-24 wt%) is still much higher than McSween's (1977a) data. McSween's (1977a) bulk chondrule compositions were obtained by defocused beam analyses. The low bulk Fe contents he observed are most likely due to the fact that analyses with totals higher than 103 wt% (mixed metal/silicate analyses) were excluded and that phase densities were not included in the normative correction method used (see Appendix A for more details). When we compare our data for the chondrule silicate portions to McSween's (1977a) bulk chondrule data, they are actually more similar (**Fig. 3.10b**).

Matrix and fine-grained clasts

Matrix in Kakangari is very different from matrix in ordinary and carbonaceous chondrites (Brearley 1989). The main constituent of the dominant non-clastic portion of the matrix is enstatite (~50 vol%), while olivine comprises only ~20 vol% (Brearley 1989). Olivines and pyroxenes in the matrix are very MgO-rich and show a narrower range in compositions ($Fa_{2\text{-}6.5}$, $Fs_{3\text{-}6}$) than those in chondrules (**Fig. 3.4a,b**). Matrix olivines have high MnO contents, like olivine in chondrules (**Fig. 3.5a**). Chromium contents of troilites in the matrix are also comparable to those in chondrules (0.15–0.25 wt% Cr, with a few outliers up to 0.6 wt% Cr).

The interchondrule matrix of Kakangari has a high compositional (atomic number) contrast in BSE images (e.g., **Figs. 3.1**, **3.11a** and **3.12**), which, in other chondrites, is normally related to the high FeO content of matrix silicates. This is not the case in Kakangari, as FeO contents of matrix silicates are very low. Instead, the reason is a high (but variable) abundance of fine-grained troilite (1-5 μm) and ferrihydrite (see below).

Abundances of troilite and ferrihydrite in matrix, determined from a false-color image (**Fig. 3.11b**) are ~28 vol% and ~31 vol%, respectively.

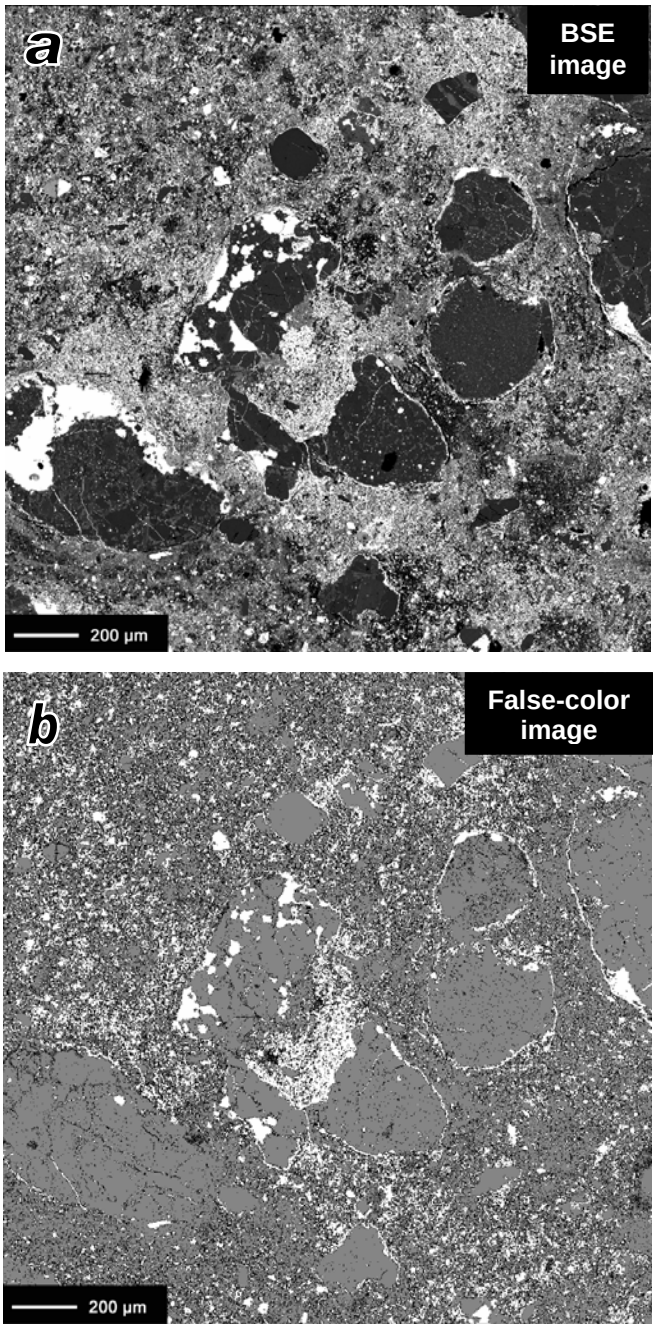

Fig. 3.11. Matrix textures in Kakangari. a) BSE image: abundant fine-grained troilite and ferrihydrite in matrix are the reason for the high compositional (atomic number) contrast. b) False-color image (based on a quantitative sulfur map) showing the abundance of troilite (white) and ferrihydrite (black). Ferrihydrite can contain up to 3 wt% S. Minerals that do not contain any sulfur (as well as cracks and holes) appear gray. Image analysis indicates that troilite makes up ~28 vol% and ferrihydrite ~31 vol% of matrix material in Kakangari.

The two fine-grained clasts visible in **Figure 3.1** have a much lower compositional contrast than the matrix because troilite is not as abundant as in the matrix and ferrihydrite only occurs at the edges of the clasts. The clasts are also very porous. A high magnification BSE image of a contact between matrix and one of the fine-grained clasts is shown in **Fig. 3.12**.

Mean bulk compositions of the matrix and the fine-grained clasts, determined by broad beam analyses, are given in **Table 3.8** compared to matrix data from McSween and Richardson (1977). Different analytical conditions are probably the reason for higher Al_2O_3 and Na_2O values in our data. The mean compositions of matrix and fine-grained clasts are very similar, except for the concentrations of Fe and S (see also **Fig. 3.13**), which are much lower in the fine-grained clasts. Interchondrule matrix in Kakangari has a very high mean S content of ~4 wt%. Bulk compositions of matrix and fine-grained clasts are similar to the range of compositions spanned by chondrules in the Fe-Mg-Si ternary (compare **Fig. 3.13** to **Fig. 3.10a**).

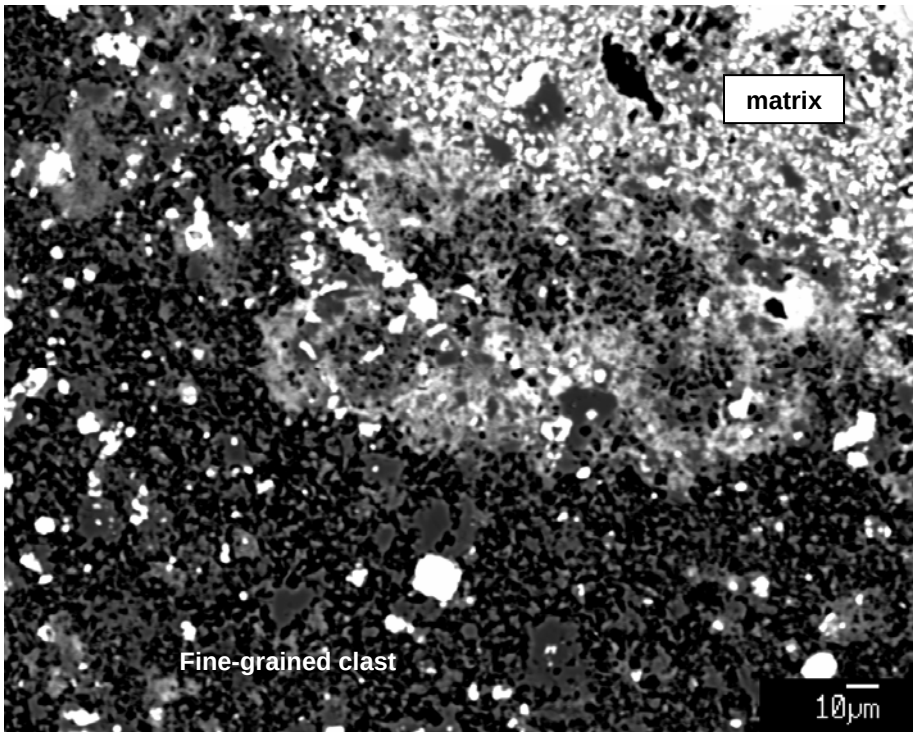

Fig. 3.12. BSE image of the contact between matrix and fine-grained clast. Troilite (white) and ferrihydrite (light gray) are more abundant in the matrix than in the fine-grained clast. The boundary of the fine-grained clast is not well defined and the center of the clast is mostly unaltered.

Table 3.8. Composition of Kakangari matrix (mean of 125 analyses) and fine-grained clasts (3 clasts, mean of 48 analyses) compared to data from McSween and Richardson (1977).

	Matrix[#]	Clasts[#]	Matrix (MR77[§])
SiO_2	36.4	40.5	35.3
TiO_2	0.10	0.14	0.10
Al_2O_3	3.0	3.3	1.9
Cr_2O_3	0.52	0.43	0.50
FeO[∞]	20.5	12.0	25.4
MnO	0.32	0.33	0.27
MgO	25.8	28.6	25.4
CaO	1.5	2.1	1.3
Na_2O	1.3	1.5	0.76
K_2O	0.18	0.17	0.13
P_2O_5	0.14	0.14	n.a.
Ni	1.0	1.1	1.3
S	4.0	0.55	2.7
Total	94.8	90.9	95.1

[#]Our analyses were obtained at 15 keV, with a beam current of 20 nA and a 30 μm beam diameter.
[§]McSween and Richardson (1977): Analytical conditions were 20 keV, 40 nA and 100 μm beam diameter.
[∞]all Fe as FeO

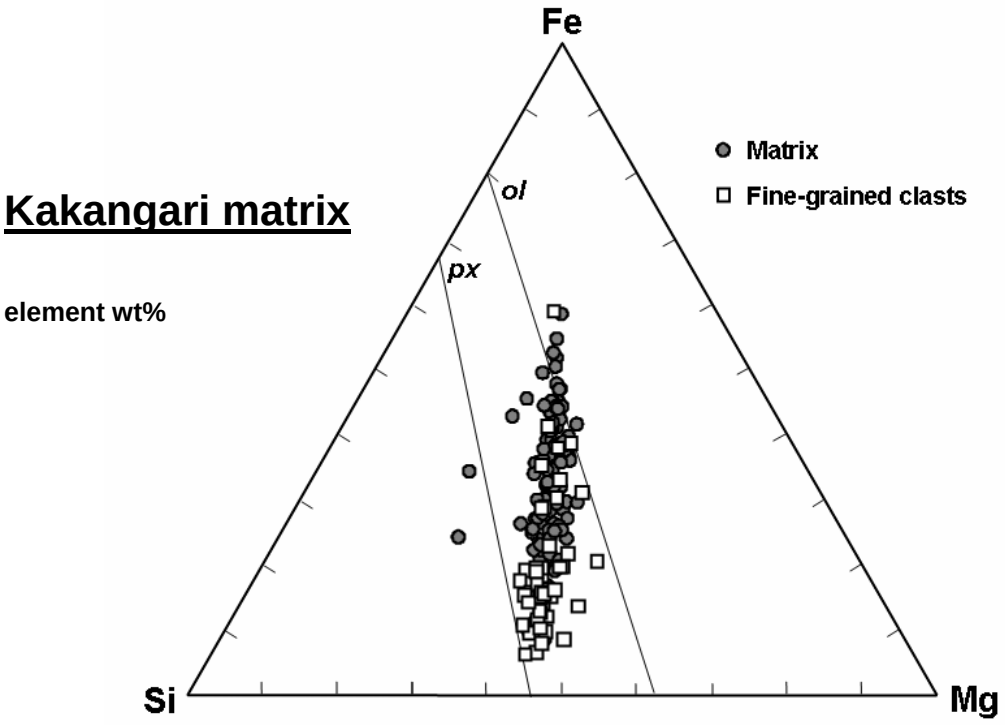

Fig. 3.13. Fe-Mg-Si ternary showing the composition of matrix and fine-grained clasts (broad-beam analyses, 30 μm beam diameter). The Fe content of the fine-grained clasts is generally lower than that of the matrix, because they contain much less troilite and ferrihydrite. Bulk compositions of matrix and fine-grained clasts are similar to the range of compositions spanned by chondrules in the Fe-Mg-Si ternary (Fig. 3.10a).

Secondary alteration products

Kakangari contains abundant apatite and ferrihydrite that we consider to be secondary (see discussion). **Figures 3.14a-c** show different occurrences of Cl-apatite in matrix. Grain sizes reach up to several tens of micrometers, which is unusually large for chondrites of petrologic type 3 (e.g., Huss et al. 2006). Apatite was also observed in the fine-grained clasts, within chondrules (e.g., **Fig. 3.7b**) and in metal/troilite rims around chondrules (e.g., **Fig. 3.2a,b**), almost always in close proximity to metal and/or troilite.

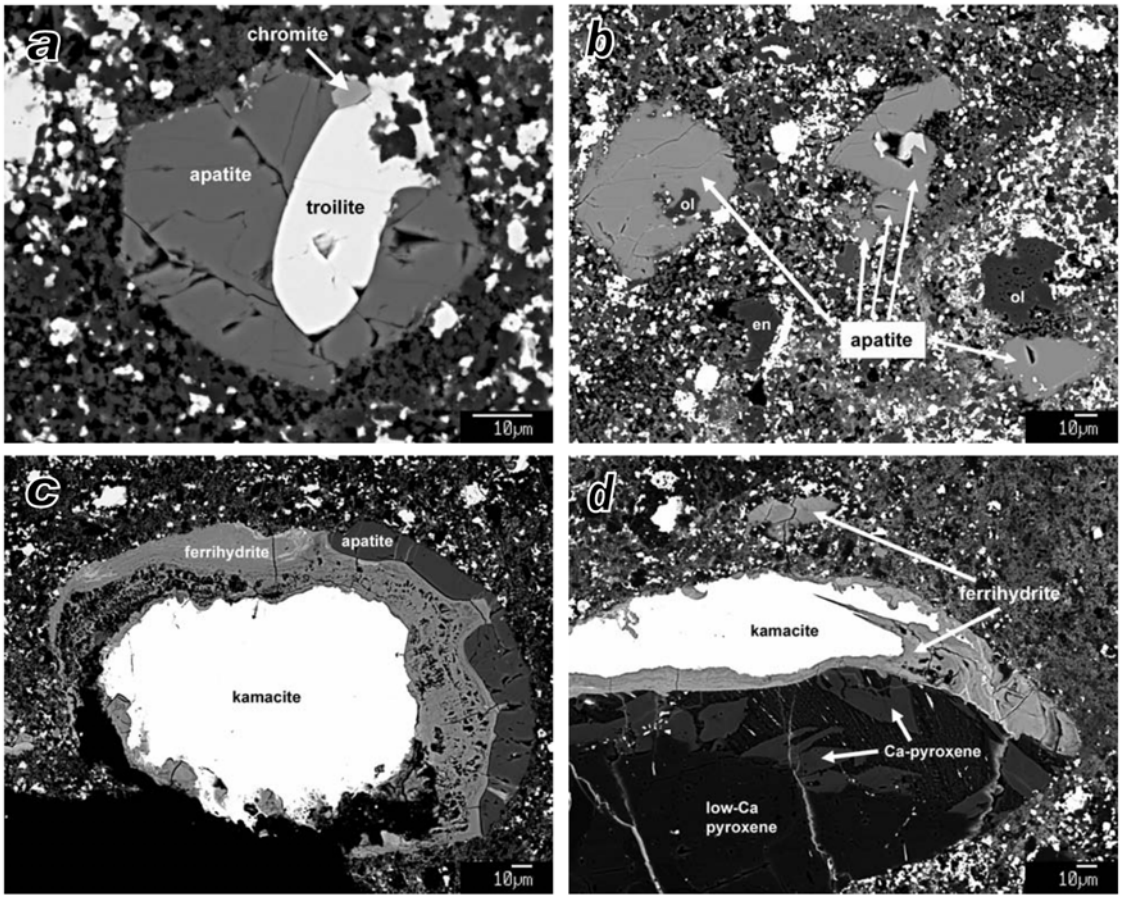

Fig. 3.14. Occurrences of apatite and ferrihydrite in Kakangari. a) Apatite crystal with troilite inclusion observed in the matrix. b) Several large apatite grains in the matrix. c) Kamacite grain in the matrix surrounded by ferrihydrite and apatite. d) Chondrule fragment with a massive kamacite rim. A large part of the rim has been replaced by ferrihydrite.

Brearley (1989) first identified ferrihydrite (ideally $5Fe_2O_3 \cdot 9H_2O$) in Kakangari matrix with electron diffraction patterns obtained by transmission electron microscopy. Like Genge et al. (1998), we base our identification of ferrihydrite on compositional data (here: EDS and quantitative analyses) and its characteristic acicular/sheet-like morphology. **Table 3.9** gives representative microprobe analyses of ferrihydrite. We observed significant concentrations of Ni, S, Si and Mg as did Brearley (1989). The low totals are a result of the high water content.

Genge et al. (1998) observed ferrihydrite as (1) rims (<10 μm thick) on corroded kamacite grains, both within the fine-grained matrix and at the margins of chondrules, (2) isolated irregular grains within the matrix and (3) veins adjacent to chondrules. In our study, we observed ferrihydrite as a dominant component of fine-grained matrix (see above). We also found much thicker rims of ferrihydrite (up to 50 μm) than Genge et al. (1998) around kamacite grains within the matrix (e.g., **Fig. 3.14c**) and along the margins of chondrules (**Fig. 3.14d**). In many cases, it also occurs in the interior of chondrules (**Fig. 3.2a,b** and **Fig. 3.3e**).

Table 3.9. Representative microprobe analyses of ferrihydrite from metal/troilite rims around chondrules.

	1	2	3	4	5	6
SiO_2	2.3	2.6	3.9	2.7	0.78	0.18
Al_2O_3	<0.04	<0.04	<0.04	0.14	<0.04	<0.04
Cr_2O_3	0.05	<0.03	<0.03	<0.03	<0.03	<0.03
Fe_2O_3	79.9	73.8	75.9	78.4	72.8	85.0
MnO	<0.04	0.04	<0.04	<0.04	<0.04	<0.04
MgO	1.8	2.3	2.0	1.8	1.4	1.1
CaO	0.32	0.69	0.64	0.37	0.25	0.18
Na_2O	0.10	0.24	0.31	0.35	0.24	0.26
K_2O	0.11	0.11	0.14	0.08	0.18	0.08
P_2O_5	0.17	0.36	0.26	0.08	0.15	0.15
NiO	5.2	8.3	6.3	7.0	8.5	2.8
SO_3	3.1	4.5	3.6	3.4	6.9	3.0
Total	93.1	92.9	93.1	94.3	91.3	92.8

DISCUSSION

Based on previous studies, Kakangari has been considered to be a very pristine chondrite (e.g., Brearley, 1989; Scott and Krot 2005; Nuth et al. 2005). Compared to other pristine chondrites, Kakangari exhibits the unique feature that chondrules and matrix are very similar in composition. This has been used to argue that chondrules formed from material that closely resembled the associated matrix and that matrix grains must have formed in close proximity to the chondrules (Scott and Krot 2005).

Our detailed study enables us to gain a better understanding of bulk chondrule compositions in Kakangari and the relationship between chondrules and matrix, we performed a detailed study of chondrules in Kakangari. Only a few brief studies of chondrules from Kakangari have been reported in the literature (McSween 1977a; Nehru et al. 1983, 1986; Weisberg et al. 1996; Genge and Grady 1998), whereas Kakangari matrix has been studied in detail (Brearley 1989). Our new data indicate that a more complex series of events is recorded by Kakangari than has been recognized previously, including high-temperature processing, reduction, thermal metamorphism, sulfidization and low-temperature aqueous alteration. Kakangari chondrules, as they are preserved, are quite different from chondrules in ordinary and carbonaceous chondrites. In particular, FeO-rich type II chondrules were previously thought to be absent (e.g., Nehru et al. 1986; Genge and Grady 1998). However, we have observed chondrules with textures (**Fig. 3.3a,c**) that resemble the typical type IIA chondrules found in ordinary and carbonaceous chondrites, but in which the Fa contents of olivine are much lower (~3 mol% Fa). Ni-poor metal grains decorating the crystal faces of olivines and high MnO contents of olivine (**Fig. 3.5a**) provide evidence that these chondrules experienced reduction. Furthermore, other porphyritic chondrules are clearly not typical type I chondrules (like those found in ordinary and carbonaceous chondrites) either as indicated by the lack of any chondrule silicates with Fa <2.5 mol% or Fs <3 mol%. Although mesostasis compositions (**Fig. 3.8**) might point to a type I chondrule population, there are no other significant features that distinguish these chondrules from those that follow the type II mesostasis trend.

In the following discussion we first focus on evidence for processes (thermal metamorphism and low-temperature aqueous alteration) that we argue have overprinted the primary, nebular characteristics of Kakangari. We then discuss evidence for nebular processes (high temperature processing and reduction) and the origin of troilite, before we compare Kakangari chondrules to those in ordinary, carbonaceous and enstatite chondrites. In conclusion, we provide a model for the formation of Kakangari and discuss whether secondary processing could have led to the similarity in chondrule and matrix compositions.

Evidence for processes that overprinted primary features in Kakangari

Thermal metamorphism

We observed many features in Kakangari which suggest that it experienced thermal metamorphism on the parent asteroid. These features include: (1) an M-shaped zoning profile for Ni in a large (~140 μm) taenite grain in chondrule #2-5 (**Fig. 3.15a** and **Fig. 3.2a,b**; **Table 3.4**), (2) the occurrence of large (>20 μm) apatite grains (**Fig. 3.14**), (3) high ZnO contents in Cr spinels, (4) equilibrated MnO contents of olivine (**Fig. 3.5**) and (5) the narrow range of Fa contents in olivine (**Fig. 3.4a**).

M-shaped zoning profiles for Ni in taenite require temperatures of at least 500-600ºC for an extended period of time (e.g., Wood 1964; Willis and Goldstein 1981). The zoning profile for a large taenite grain in chondrule #2-5 is shown in **Figure 3.15a** (refer to **Figure 3.2b** for the location of the zoning profile). **Figure 3.15b** shows the central Ni content (wt%) of all taenite grains analyzed in this study versus the radius of each grain (in μm). Using the "central Ni content" method (e.g., Wood 1964; Rasmussen 1981; Willis and Goldstein 1981; Saikumar and Goldstein 1988), the derived curve suggests a cooling rate between 1 and 10 K/Myr. This can be seen as strong evidence that thermal metamorphism must have occurred on the Kakangari parent body.

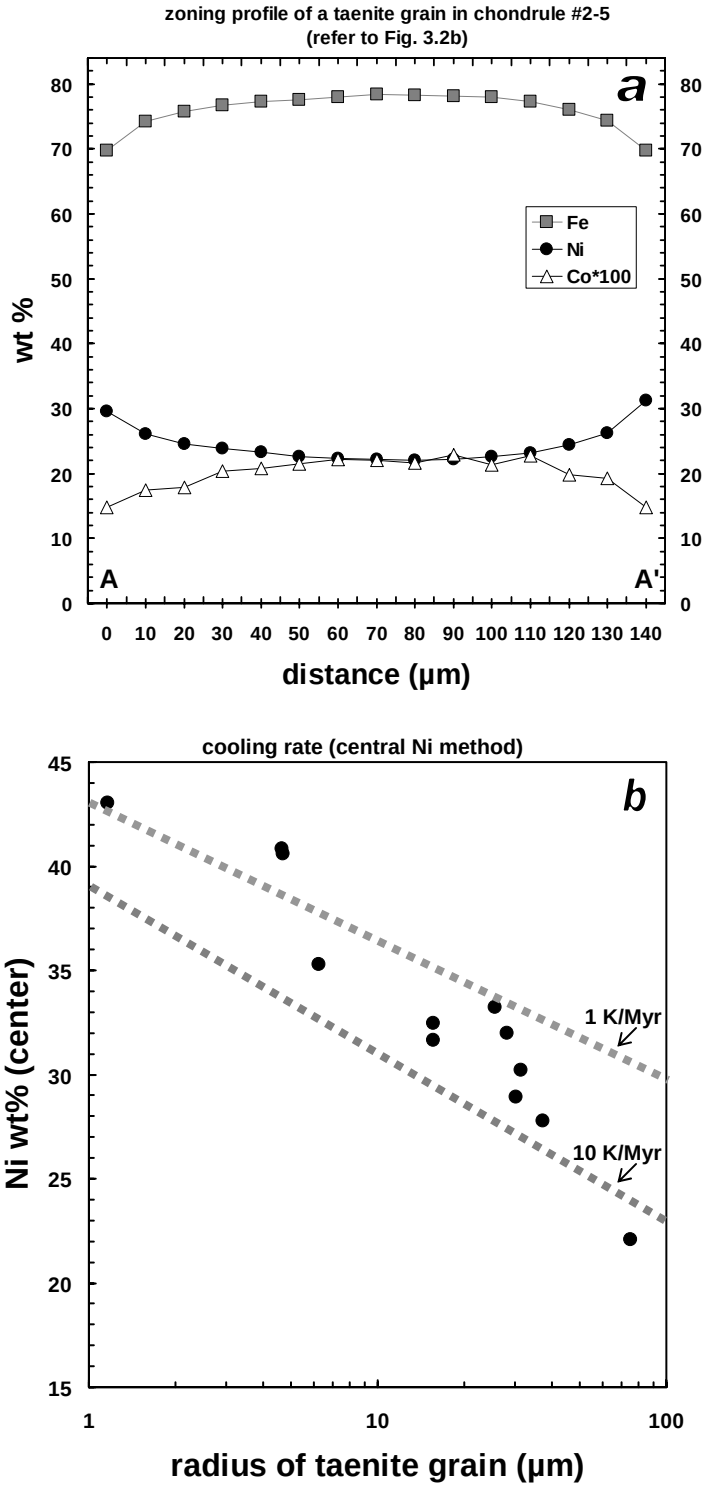

Fig. 3.15. a) Zoning profile of a taenite grain in chondrule #2-5 (refer to Fig. 3.2b for location). b) Ni content (wt%) in the center versus radius (μm) of all taenite grains analyzed in Kakangari in this study. The "central Ni content" method (e.g., Wood 1964; Rasmussen 1981; Willis and Goldstein 1981; Saikumar and Goldstein 1988) suggests a cooling rate between 1 and 10 K/Myr. Approximate cooling rate curves (gray dashed lines) for 1 and 10 K/Myr are from Willis and Goldstein (1981).

Large grains of chlorapatite (>20 μm) are common in Kakangari and occur in the matrix, in the fine-grained clasts, in metal/troilite rims around chondrules and even within chondrules (e.g., **Fig. 3.2a,b**, **3.7b** and **3.14a-c**). Such large apatite grains are usually only found in chondritic meteorites with petrologic types higher than 3.5 (e.g., Huss et al. 2006). The close spatial relationship of apatite and metal support an initially siderophile character of P and formation of apatite by oxidation (e.g., Ahrens 1970; Rambaldi and Rajan 1982; Hutchison and Bevan 1983; Rubin and Grossman 1985; Zanda et al. 1994). Solar-composition metal contains 93.8 wt% Fe, 5.4 wt% Ni, 0.3 wt% Co and 0.6 wt% P when the siderophile elements are fully condensed (Anders and Grevesse 1989). The P content of kamacite in Kakangari is very low (≤0.08 wt% P), consistent with the suggestion that P has left the metal to form apatite. It is likely that the two nodules containing Fe,Ni-phosphide shown in **Figure 3.7c,d** were protected from oxidation and reaction with Ca and Cl by the surrounding kamacite.

We observed relatively high ZnO contents (up to 1.2 wt%) in Cr spinels in Kakangari. Johnson and Prinz (1991) showed that chromites in type 3.0 chondrites have ZnO below detection limits, whereas chromites in chondrites of higher petrologic type contain >0.1 wt% ZnO, supporting the suggestion by Grossman et al. (1979) that mild reheating may redistribute Zn. Johnson and Prinz (1991) proposed that chromite re-equilibrates with troilite, in which sphalerite has a small but sufficient solubility (Barton and Toulmin 1966).

MnO contents of chondrule olivines are high (average 0.42 wt%), but also very equilibrated as olivine grains in the matrix have similar compositions (**Fig. 3.5**). In ordinary chondrites, MnO contents of olivine equilibrate between petrologic type 3.4 and 3.8 (DeHart et al. 1992). The fairly narrow range of Fa contents of olivine in chondrules (**Fig. 3.4a**) is probably due to Fe-Mg exchange between the originally more FeO-rich chondrule olivines and relatively MgO-rich matrix olivines. Low-Ca pyroxenes preserve a much wider range of compositions (**Fig. 3.4b**), which can be related to the fact that diffusion rates in pyroxene are slow compared with those in olivine (e.g., Freer 1981). For our limited dataset, the coefficient of variation of Fa contents in olivine is 41, which corresponds to a petrologic subtype of 3.5 according to Sears and Dodd (1988).

More than 90% of all analyzed olivines in Kakangari chondrules have Cr_2O_3 contents below 0.04 wt%. Grossman and Brearley (2005) showed that at the onset of metamorphism a Cr-rich phase (probably chromite) exsolves from chondrule olivine with FeO > 2 wt%, which leads to very low Cr contents in the olivines at petrologic types higher than 3.2. However, a mobilization of Cr could also have occurred during reduction along with Fe (e.g., Weisberg et al. 2005; Bendersky et al. 2007), which is discussed below.

Low-temperature aqueous alteration

Ferrihydrite is the only hydrous phase that was observed in Kakangari and it is likely the source for the 2.3 wt% H_2O reported by Mason and Wiik (1966) in their bulk chemical analysis of Kakangari. We found ferrihydrite in larger aggregates than previously described by Genge et al. (1998), partially replacing kamacite grains in the matrix (**Fig. 3.14c**) and in metal/troilite rims along chondrule margins (**Fig. 3.14d**). Brearley (1989) estimated that ferrihydrite constitutes approximately 10 vol% of the matrix, whereas our image analysis of X-ray element maps indicates ~31 vol% (**Fig. 3.11**). We also found ferrihydrite within chondrules (**Fig. 3.2a,b** and **Fig. 3.3e**). These occurrences indicate wide-spread low-temperature aqueous alteration.

Ferrihydrite is a poorly crystalline, hydrated Fe^{3+} oxide and typically forms nanometer-sized crystals resulting in aggregates with an extremely high surface area. The most commonly cited ideal chemical formula of ferrihydrite is $5Fe_2O_3 \cdot 9H_2O$ (e.g., Jambor and Dutrizac 1998), but its detailed structure is still being debated (e.g., Michel et al. 2007). Ferrihydrite is generally classified according to its number of X-ray diffraction lines (e.g., Eggleton and Fitzpatrick 1988; Jambor and Dutrizac 1998) into 2-line ferrihydrite (less crystalline variety) and 6-line ferrihydrite (more crystalline variety). Electron diffraction data of ferrihydrite in Kakangari obtained by Brearley (1989) are most consistent with 6-line ferrihydrite as described by Janney et al. (2001).

In terrestrial settings, ferrihydrite commonly occurs in young soils and sediments when groundwater is present and forms at pH > 3 by rapid oxidation of Fe^{2+} from silicates or sulfides and hydrolysis (e.g., Cornell and Schwertmann 1996). Therefore, ferrihydrite in Kakangari must have formed at low temperatures in the presence of an

aqueous fluid. The close association of ferrihydrite with metal/troilite in Kakangari indicates that the main sources of Fe were metal and troilite. Additional evidence includes high concentrations of Ni and S in electron microprobe analyses of ferrihydrite in Kakangari (**Table 3.9**). Minor amounts of Fe might also have been released from silicates as some Si and Mg is present in the ferrihydrite analyses as well, but metal and troilite are clearly more susceptible to oxidation by water than the Mg-rich silicates. Iron might have been transported as Fe^{2+} through a network of interconnected pores in the matrix, but the mobility of Fe^{3+} in aqueous solution is restricted due to its rapid hydrolysis and precipitation.

The conditions Kakangari experienced after ferrihydrite formed are significantly constrained by the fact that ferrihydrite is metastable. It easily transforms into crystalline Fe-oxides and/or Fe-hydroxides. However, the rate of transformation and the maximum temperature under which ferrihydrite is preserved depend on several factors like water activity (aqueous transformation versus dry thermal transformation), pH (during aqueous transformation), presence of adsorbed ions and whether ferrihydrite is present as 2-line or 6-line ferrihydrite (e.g., Jambor and Dutrizac 1998). Schwertmann et al. (2004) performed experiments to observe transformation rates under aqueous conditions at temperatures between 4 and 25ºC. They showed that at neutral pH's (7–8) ferrihydrite quickly (within 10-12 years) transforms into hematite by dehydration and structural rearrangement, whereas the formation of goethite is favored at lower and higher pH's (maxima at 2–5 and 10–14) via dissolution of ferrihydrite followed by nucleation and precipitation of goethite from solution. In contrast, when heated under dry conditions, 6-line ferrihydrite dehydrates without significant changes in cell parameters or structure up to a temperature of 127 ºC where maximum OH loss occurs without conversion to hematite (Stanjek and Weidler 1992). Our ferrihydrite analyses (**Table 3.9**) indicate lower water contents than what is typically observed (e.g., Jambor and Dutrizac 1998), implying that some dehydration occurred. It is further likely that the system dried out fairly quickly, otherwise we would observe hematite or goethite instead of ferrihydrite. The maximum temperature under which ferrihydrite is preserved also depends significantly on adsorbed ions (e.g., Jambor and Dutrizac 1998). One element that strongly retards transformation rates is Si, which is present in varying amounts in our

microprobe analyses of ferrihydrite in Kakangari (**Table 3.9**). Experiments performed by Vempati et al. (1990) suggest a direct relationship between the Si/Fe molar ratio of the ferrihydrite and the temperature at which hematite is first observed. Their results applied to Si/Fe ratios of ferrihydrite in Kakangari indicate that it might have been stable up to temperatures between 300–550ºC.

Brearley (1989) cautioned that ferrihydrite might be of terrestrial origin (i.e., due to storage of samples in a moist environment). Genge et al. (1998) found no ferrihydrite within ~200 μm of the fusion crust of Kakangari, suggesting that ferrihydrite was removed by heating during atmospheric entry and, therefore, must have formed by aqueous alteration on the Kakangari parent body. [Regrettably, the two thin sections studied here did not contain any parts of the fusion crust.] A major piece of evidence that ferrihydrite probably formed on the Kakangari parent body is the large size of the aggregates (up to 50 μm).

Genge et al. (1998) suggested that H_2O ice was accreted along with the chondritic components of Kakangari and subsequent shock heating could then have been responsible for melting the H_2O-ice and triggering ferrihydrite formation. We suggested above that thermal metamorphism occurred on the Kakangari parent body. H_2O ice would not have survived this heating episode. Therefore, we propose that ferrihydrite formation post-dated metamorphism because its formation and preservation requires lower temperatures. Possibly, H_2O ice could still have been a source for the liquid water needed for ferrihydrite formation, if it accreted as a late veneer. The mostly unaltered nature of the fine-grained clasts can be explained either by the fact that the clasts contain much less fine-grained troilite and were therefore less affected, or brecciation occurred when the water/rock ratio was low enough so that precipitation of ferrihydrite was limited to the matrix-clast boundary (**Fig. 3.12**).

Evidence for nebular processes

High-temperature processing

Despite the secondary alteration present in Kakangari, it is still possible to unravel the early high-temperature history of Kakangari chondrules and matrix. At least two

episodes of high-temperature events are recorded in Kakangari, which must have been brief events that occurred in the solar nebula. Our interpretation of the sequence of processes experienced by Kakangari is summarized in the schematic diagram shown in **Figure 3.16**. The first heating event was responsible for the formation of chondrules (T>1600ºC). The original chondrule population probably consisted mostly of FeO-rich chondrules which experienced reduction (see discussion below) during a second heating event at somewhat lower temperatures (~1000–1500ºC).

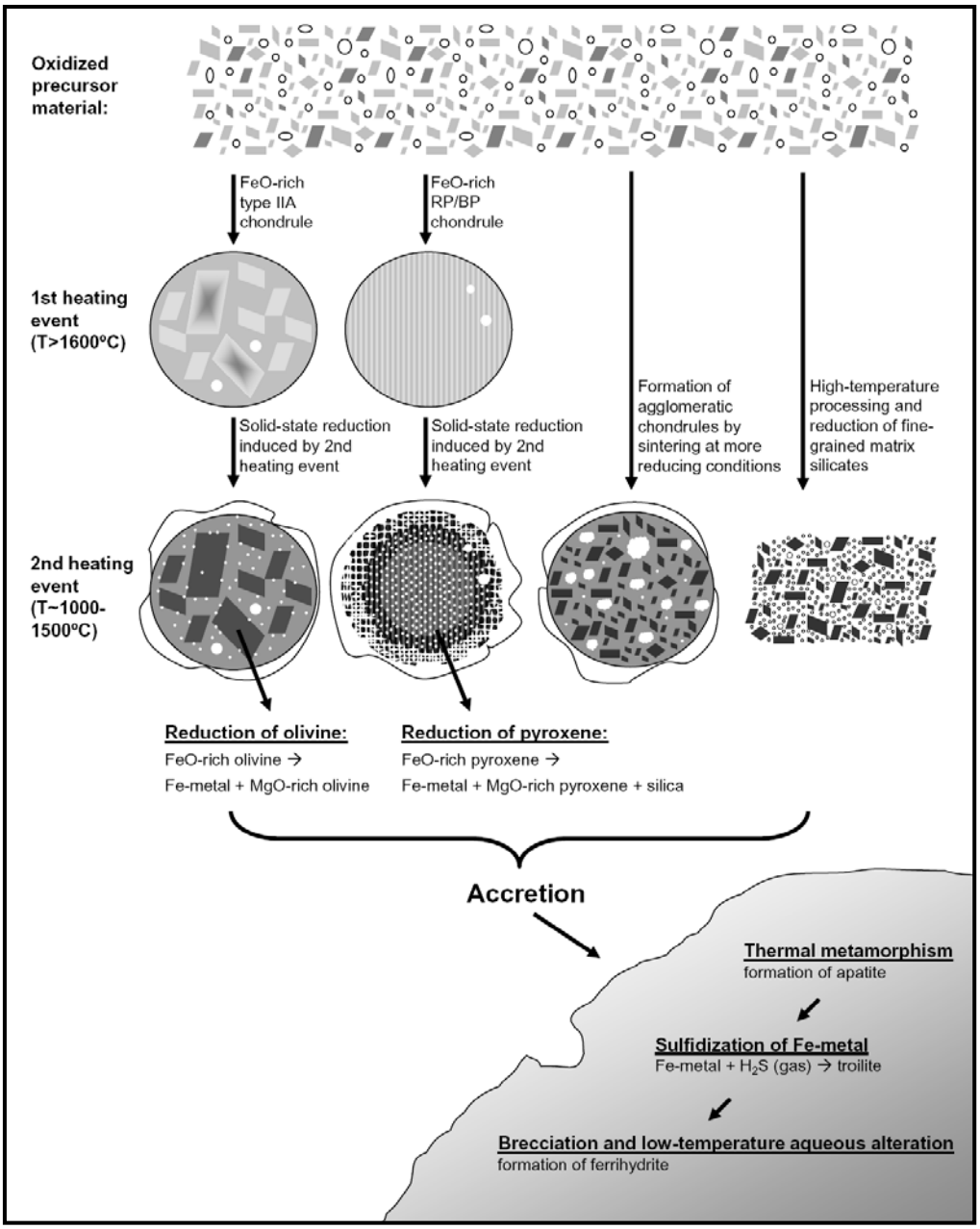

Fig. 3.16. Simplified illustration of the complex series of events recorded in Kakangari.

Agglomeratic chondrules, which are very abundant in Kakangari (**Table 3.1**), represent temperatures of ~1200ºC that caused sintering and partial melting of fine-grained precursor material (Weisberg and Prinz 1996). It appears that the silicate portion of the matrix was also affected by a brief heating event(s) with temperatures >1000ºC as is evident in the microstructures of low-Ca pyroxene (Brearley 1989). Our results indicate that Kakangari matrix probably experienced reduction as well (see discussion below). If Kakangari chondrules and matrix were located in close proximity in the solar nebula, the same heating event could have been responsible for the reduction of FeO-rich chondrules, the formation of agglomeratic chondrules and the reduction and high-temperature processing of matrix silicates (**Fig. 3.16**). The progressively lower temperatures experienced by chondrules, agglomeratic chondrules and matrix might relate to a decreasing distance from the center of the heating event. It is likely that igneous rims, which are mineralogically and texturally very similar to agglomeratic chondrules, also formed during this (second) heating period.

Reduction

Several lines of evidence are present in Kakangari that lead us to suggest that the silicate portion of most chondrules and of the fine-grained matrix material was originally FeO-rich and subsequently became more MgO-rich as the result of a reheating event under reducing conditions, most likely in the solar nebula. Our observations can be summarized as follows: (1) Dusty olivines and pyroxenes present in some chondrules provide direct evidence for solid-state reduction. (2) Several chondrule silicates and larger isolated grains in the matrix show zoning with FeO-rich cores and MgO-rich edges. (3) Some chondrules have a typical “type IIA”-texture, indicating that they originally might have had higher FeO contents. (4) Many chondrules contain silica. (5) Matrix and chondrule olivines have high MnO contents (average ~0.42 wt%). (6) Fine-grained matrix silicates, which might have been more susceptible to reduction, have the most MgO-rich compositions. (7) Troilite in chondrules and matrix contains 0.15–0.25 wt% Cr, which is indicative of reducing conditions. We discuss the implications of each of these observations below.

Dusty olivine and pyroxene, zoning and chondrules with "type IIA"- textures

Only a few chondrules in Kakangari contain typical dusty olivines or dusty pyroxene (e.g., **Fig. 3.6a,b**), but they provide direct evidence that solid-state reduction occurred. Dusty olivines in Kakangari are similar to those found in primitive ordinary and carbonaceous chondrites (e.g., Nagahara 1981; Rambaldi 1981; Jones and Danielson 1997). Their textures have been reproduced experimentally by heating Fe^{2+}-bearing olivine at temperatures between 1100ºC and 1740ºC and oxygen fugacities between the IW and C/CO buffer (e.g., Boland and Duba 1981; Nagahara 1985, 1986; Connolly et al. 1994; Danielson and Jones 1995; Lemelle et al. 2000, 2001; Leroux et al. 2003). The specific range of conditions under which solid-state reduction of olivine occurs, and under which different reaction products form, has not been explored experimentally in detail, although it has been treated thermodynamically (e.g., Nitsan 1974; Matas et al. 2000). Possible reaction mechanisms include:

$$Fe_2SiO_4 \rightarrow 2\ Fe^0_{(metal)} + SiO_2 + O_2 \quad (1)$$

(referred to as "OSI" = olivine – silica/iron)

$$FeMgSiO_4 \rightarrow Fe^0_{(metal)} + MgSiO_3 + \tfrac{1}{2}\ O_2 \quad (2)$$

(referred to as "OPI" = olivine – pyroxene/iron)

Boland and Duba (1981) and Nagahara (1985, 1986), who cooled their experiments slowly, found pyroxene as a reaction product in their experiments, whereas others, who quenched their experiments, did not (e.g., Danielson and Jones 1995; Libourel and Chaussidon 1995; Leroux et al. 2003). Crystalline SiO_2 polymorphs were not observed in any of the studies mentioned above. Libourel and Chaussidon (1995) suggested that SiO_2 might get absorbed into the chondrule melt, which was further confirmed in experiments by Leroux et al. (2003), who also found that some SiO goes into the gas phase:

$$Fe_2SiO_4 \rightarrow 2\ Fe^0_{(metal)} + x\ SiO_{2\ (in\ melt)} + (1\text{-}x)\ SiO_{(gas)} + (3\text{-}x)/2\ O_2 \quad (3)$$

Experiments by Leroux et al. (2003) produced dusty olivines that show an outer zone free of metal blebs, which is similar to our observations of dusty olivines in Kakangari shown in **Figure 3.6b**. Others (e.g., Nagahara 1986) observed metal blebs throughout the reduced zone at the edges of the olivine grains. The grain boundaries of dusty olivines in Kakangari chondrule #2-2 (**Fig. 3.6b**) are decorated with metal blebs, indicating that Fe atoms diffused along defects in the olivine and coalesced at the surface. We observed such decorated grain boundaries also on olivines in chondrules with "type IIA"-texture (e.g., **Fig. 3.3a-c**) and on isolated olivines in the matrix that are zoned with more MgO-rich compositions towards the edges (e.g., **Fig. 3.3c**). The metal blebs in chondrules with a "type IIA"-texture contain ~1.1 wt% Ni, which would correspond to a NiO content of ~0.2 wt% in the original olivine (~Fa_{20}) before reduction occurred. Many metal blebs in chondrules #1-9 and #2-2 (**Fig. 3.6a,b**) are now troilite, but the fact that we observe several Ni-poor metal blebs that were not sulfidized, makes us confident that we can exclude the following reaction mechanism (e.g., DuFresne and Anders 1962; Lewis 1967):

$$Fe_2SiO_4 + 2\ H_2S \rightarrow 2\ FeS + SiO_2 + 2\ H_2O \qquad (4)$$

Instead, we interpret the presence of troilite as the product of sulfidization, which occurred on the parent body (see discussion below).

Reduction reactions and kinetics for pyroxene are less well understood than those for olivine. Dusty pyroxenes (which have also been called "black" pyroxenes, because they lack cathodoluminescence) are common in primitive enstatite chondrites (e.g., Lusby et al. 1987; Weisberg et al. 1994). As a possible reaction mechanism, Weisberg et al. (1994) suggested:

$$2\ (Fe,Mg)SiO_3 \rightarrow Fe^0\ (metal) + MgSiO_3 + SiO_2 + \tfrac{1}{2}O_2 \qquad (5)$$

Experiments reported by Nagahara (1986), Allen et al. (1993a,b) and Britt (1993) support this mechanism and show that reaction kinetics for the reduction of pyroxene are much slower than for olivine. This is evident in the chondrule shown in **Fig. 3.6b**, where

olivine grains show a higher degree of reduction (dusty and zoned) than the pyroxene in the center (thin Mg-rich edges and metal blebs along grain boundaries only).

Silica

According to reactions (1) and (3), silica should be a typical product of reduction reactions; however, as we mentioned above, it is rarely observed in experiments. Six of the 20 Kakangari chondrules studied contain silica (polymorphs were not determined). Four of these chondrules have a RP/BP texture, where silica occurs interstitially and in close proximity to the mesostasis (e.g., **Fig. 3.3j-l**). This indicates that silica was not absorbed into the melt and/or lost via a gas phase as indicated in reaction (3). However, the silica rim around a cryptocrystalline chondrule (#2-9, **Fig. 3.2c,d**) can be seen as evidence that some SiO went into the gas phase and later recondensed onto the chondrule.

MnO contents of olivine

Even though MnO contents of chondrule olivine are equilibrated, they are mostly too high to represent equilibration of a typical type I chondrule population as found in ordinary and carbonaceous chondrites (**Fig. 3.5**). A simple explanation is that the original chondrule olivines were FeO-rich (such as type II chondrules in OC or CC), and then reduction occurred, shifting FeO contents of olivines to lower values, but maintaining the original MnO contents. As a last step, equilibration of MnO contents followed during thermal metamorphism (refer to arrows in **Fig. 3.5a**). If the high MnO contents of Kakangari chondrule olivines provide an indication for the original Fa content before reduction occurred, the precursor material was probably more comparable to ordinary chondrite type IIA chondrules than to carbonaceous type IIA chondrules (**Fig. 3.5a**).

Matrix olivines also have high MnO contents, very similar to those observed in chondrule olivines (**Fig. 3.5a**). Even though MnO contents equilibrated during thermal metamorphism, it seems likely that matrix silicates also experienced reduction in the solar nebula. The chondrule abundance in Kakangari is only 19 vol% and the fine-grained matrix is very MgO-rich. If only the chondrules experienced reduction and had high MnO contents in their olivines, and if they equilibrated with FeO-poor matrix olivines with

much lower MnO contents, the equilibrated MnO content of olivines in chondrules and matrix would probably not be as high as is observed.

Matrix

Although the silicate portion of the fine-grained matrix is unusually MgO-rich in Kakangari compared to ordinary and carbonaceous chondrites (Brearley 1989), the bulk composition of Kakangari matrix is still fairly Fe-rich because it contains abundant troilite. The reduction of previously FeO-rich matrix olivines could have produced the MgO-rich compositions and simultaneously resulted in the formation of abundant Ni-poor metal grains, which could have later been sulfidized (see discussion below). Matrix silicates do not show dusty textures, but their fine-grained nature makes it likely that precipitated metal blebs diffused to the grain boundaries (e.g., Allen et al. 1993; Lemelle et al. 2001).

Temperatures reached by matrix silicates were constrained by Brearley (1989), who found abundant clino-orthopyroxene intergrowths indicating temperatures in excess of 1000ºC and cooling rates of approximately 1000ºC/hr. The high modal abundance of low-Ca pyroxene in Kakangari matrix (~50 vol%; Brearley 1989) is consistent with reduction in several ways. According to reaction (2), MgO-rich pyroxene can be the direct reaction product of the reduction of FeO-rich olivine. Another possible reaction product is silica (reactions 1 and 3), which would likely react with any remaining olivine to form pyroxene:

$$Mg_2SiO_4 + SiO_2 \rightarrow 2\ MgSiO_3 \qquad (6)$$

Brearley (1989) found corroded inclusions of olivine that frequently occur within enstatite, which could suggest that some enstatite formed by the reaction of olivine with a silica polymorph. There is no evidence in Kakangari's matrix that silica survived (Brearley 1989), but olivine is still fairly abundant (~20 vol%), so it was not all reacted away. Some SiO (gas) might also have left the system (reaction 3) or reacted with other components to form feldspar for example.

Cr contents of troilite

Troilite in Kakangari contains between 0.15 to 0.25 wt % Cr, which is indicative of reducing conditions, but not as reducing as in primitive enstatite chondrites where troilite contains up to 2.4 wt% Cr (e.g., Ikeda 1989). Analyses of Ni-poor metal blebs in dusty olivines and chondrules with "type IIA"-textures yield variable Cr contents, between 0.05 and 1.8 wt% Cr. It is therefore possible that Cr was reduced along with Fe from olivine and incorporated into Ni-poor metal (Weisberg et al. 2005; Bendersky et al. 2007), which was later sulfidized to troilite (see discussion below). As mentioned above, an alternative or additional possibility is that Cr was mobilized at the onset of thermal metamorphism (e.g., Jones and Lofgren 1993; Grossman and Brearley 2005) leading to the observed low Cr_2O_3 contents in chondrule olivines in Kakangari. The latter might be supported by the fact that dusty olivines in primitive ordinary and carbonaceous chondrites have high Cr_2O_3 contents, between 0.2–0.7 wt% (e.g., Jones and Danielson 1997; Leroux et al. 2003) and that Leroux et al. (2003) did not detect Cr in metal blebs in dusty olivines in Bishunpur in their ATEM study. On the other hand, conditions that were responsible for producing dusty olivines in ordinary and carbonaceous chondrites might not have been as reducing as in Kakangari.

When and where did reduction take place?

Reduction most likely occurred in the solar nebula and was probably induced by a second heating event (or events) related to chondrule formation (**Fig. 3.16**). Three main arguments supporting this hypothesis are: (1) reaction kinetics are too slow for reduction to have occurred at the maximum temperatures reached during thermal metamorphism on the parent asteroid, (2) all grains within a chondrule show similar features, indicating that reduction of silicates happened in the solid state after the chondrules formed, but different degrees of reduction are observed from chondrule to chondrule, and (3) nucleation of many small metal grains throughout silicates (**Fig. 3.6a,b**) is consistent with high temperatures for a short period of time.

When compared to other type 3 chondrites, textural and mineralogical evidence indicates that Kakangari cannot have experienced temperatures higher than ~600ºC on the parent asteroid (e.g., Huss et al. 2006). Experimental studies that have investigated the reduction of olivine and pyroxene were carried out at high temperatures (1100–

1740ºC) in order to get reactions to proceed on reasonable timescales in the laboratory (e.g., Boland and Duba 1981; Nagahara 1985, 1986; Connolly et al. 1994; Danielson and Jones 1995; Lemelle et al. 2000, 2001; Leroux et al. 2003). When experimental results are extrapolated to low temperatures, it becomes apparent that reduction cannot have occurred on the parent body. For example (using data by Nagahara 1986), after 10 million years at 500ºC the reduced width from the surface of an olivine with original Fa content of 17 mol% would only be 0.03 μm wide and after 100 million years only 0.08 μm wide. Because we observe much wider reduced zones in olivines (e.g., **Fig. 3.3c** and **3.6b**) and pyroxenes (**Fig. 3.6a**), the latter having much slower reduction reaction kinetics than olivine, we are confident that reduction must have occurred in the solar nebula before material was accreted into an asteroidal parent body.

In individual Kakangari chondrules, all silicates show similar features (e.g., **Fig. 3.3a,c** and **3.6a,b**) indicating that reduction must have happened in the solid state, after the chondrules formed. This is in contrast to dusty olivines in chondrules of ordinary and carbonaceous chondrites, which are often relict grains with higher FeO contents than the host chondrule olivines suggesting that reduction took place prior to or during chondrule formation (e.g., Jones and Danielson (1997). A comparison of the Fa contents and zoning characteristics of olivines in different chondrules and fragments further shows that different chondrules experienced various degrees of reduction, which is not what one would expect if reduction had occurred on the parent asteroid. The zoned olivine in **Figure 3.6b** has a zoning profile that is very similar to the large isolated olivine in **Figure 3.3c** (core: 10-11 mol%; edge: ~ 3 mol%), but one of them is dusty (**Fig. 3.6b**) whereas the other one is not (**Fig. 3.3c**). In contrast, olivines in chondrules with "type IIA"-texture (**Fig. 3.3a,c**) are not zoned and have Fa contents between 2.5 and 3.5 mol%. The fine-grained nature of metal blebs in dusty olivines and pyroxenes (**Fig. 3.6a,b**) further supports a brief heating event (or events) at high temperatures in the nebula, whereas a smaller number of metal grains with larger sizes would be expected under prolonged heating at low temperatures in a parent body environment.

Reducing agent

Experiments by Danielson and Jones (1995) in H_2 and Ar atmospheres showed that it is the absence of oxygen rather than the presence of H_2 that drives a reduction reaction. Therefore, it is possible that simply lower dust/gas ratios were responsible for the more reducing conditions during the second heating event (**Fig. 3.16**). Another possibility is that the system was buffered by the presence of reduced carbon (e.g., Connolly et al. 1994) so that oxygen would have been consumed to form CO:

$$FeMgSiO_4 + C \rightarrow Fe_{(metal)} + MgSiO_3 + CO \quad (7).$$

Origin of troilite

There are several lines of evidence that a major sulfidization event is recorded in Kakangari. Troilite is the only major sulfide phase present in Kakangari and the sulfide mineralogy is therefore much simpler than in other chondrites. However, the modal abundance of troilite in chondrules (up to 26 vol%) and in the matrix (~28 vol%, **Fig. 3.11**) of Kakangari is, in general, much higher than in other chondrites. Bulk chemical sulfur abundances in Kakangari (5.5 wt%) are similar to CI (5.41 wt%) and EH chondrites (5.6 wt%), whereas all other chondrite groups have much lower bulk sulfur abundances (e.g., Lodders and Fegley 1998).

Is any troilite primary?

It is likely that sulfides were present in the precursor material of chondrules. Above, we suggested that most of the precursor chondrule and matrix material (silicate portion) of Kakangari was originally more FeO-rich than what is currently observed. The formation of FeO-rich silicates in the solar nebula requires high dust/gas ratios in equilibrium condensation models, which makes Fe-sulfides stable at temperatures higher than 700 K (e.g., Wood and Hashimoto 1993; Ebel and Grossman 2000). For example, according to Wood and Hashimoto (1993), Fe-sulfides are stable at temperatures below 1264 K at 10^{-5} bar and 1000x dust-enrichment. Ebel and Grossman's (2000) calculations predict direct condensation of iron-sulfide liquids at high total pressures and dust enrichments (i.e., 1330 K at 10^{-3} bar and 500x). In the past decades, it has been

recognized that presolar dust survival, conditions far from equilibrium and kinetics need to be considered when discussing solar nebula condensation models (e.g., Nuth et al. 2005; Grossman et al. 2008), which again makes the presence of FeO-rich silicates and Fe-sulfides more likely in the precursor material of chondrules in Kakangari.

Primary troilite is typically defined as troilite that crystallized from molten sulfide melt in chondrules (e.g., Rubin et al. 1999; Tachibana and Huss 2005), which implies that chondrule precursor materials contained sulfur-bearing phases and heating times were short enough to avoid complete evaporative loss of sulfur (e.g., Yu et al. 1996). In order to assess whether any troilite present in Kakangari chondrules is primary (= igneous), isotopic studies such as the one performed by Tachibana and Huss (2005) and/or REE data are needed (e.g., Kong et al. 2000; Donnelly and Brearley 2007). It is further possible, that some sulfur recondensed as sulfide veneers around chondrules during or shortly after the chondrule-forming event (e.g., Zanda et al. 1995).

Was Ni-poor metal sulfidized preferentially?

Classic equilibrium condensation calculations (e.g., Grossman 1972) predict sulfidization of iron metal in a cooling gas of solar composition (10^{-3}atm) via a gas-solid reaction below 700 K:

$$Fe^0 + H_2S \rightarrow FeS + H_2 \quad (8).$$

Taking Ni into account, Kerridge et al. (1979) predicted formation of a troilite rim around a kamacite–taenite metal core (under equilibrium conditions):

$$\text{kamacite } (\alpha) + H_2S \rightarrow \text{kamacite } (\alpha) + \text{taenite } (\gamma) + FeS + H_2 \quad (9).$$

However, experimental studies by Lauretta et al. (1997b, 1998) did not produce the predicted assemblage (reaction 9), but Ni-bearing sulfides (monosulfide solid solution) and even pentlandite. We did not observe any Ni-bearing sulfides or pentlandite in Kakangari, which might imply that Ni-poor metal (reaction 8) was preferentially sulfidized over kamacite. Lauretta et al. (1998) compared experimental sulfidization of kamacite and pure Fe and found that kamacite sulfidization is generally faster than that of

Fe metal. However, we frequently found that μm-sized opaque grains, that must have been Ni-poor metal blebs produced by the reduction process described above, are now preserved as troilite, while larger rounded kamacite and taenite grains within the same chondrules do not show any evidence for sulfidization (e.g., **Fig. 3.3l** and **3.6a**).

Evidence for a major sulfidization event on the parent asteroid

Our observations place constraints on when and where sulfidization occurred. We can present several arguments for a major secondary sulfidization event that must have occurred on the parent asteroid of Kakangari. Our major argument is that the fine-grained, interstitial nature of troilite (1-5 μm) in the matrix of Kakangari (e.g., **Fig. 3.12**) requires that a secondary sulfidization event occurred after thermal metamorphism on the parent body, otherwise the fine-grained troilite would have been mobilized and coarsened (e.g., Lauretta et al. 1997a; Grossman and Brearley 2005).

The sulfidization event affected both matrix and chondrules (especially the fine-grained metal blebs within dusty olivines and pyroxenes), although some of the troilite in chondrules might be of igneous origin. We suggested above that the precursor material for most chondrules and matrix was very similar and that both experienced solid-state reduction in the solar nebula. This could imply that chondrules and matrix formed within very close proximity in the nebula, which in turn requires a fairly rapid accretion of the parent asteroid. The sulfidization of metal via reaction (8) might have begun in the nebula (e.g., Lauretta et al. 1996a,b), but most likely did not go to completion within this short time frame (e.g., Pasek et al. 2005). As mentioned above, nebular sulfidization can certainly not be responsible for the abundant fine-grained troilite in the matrix of Kakangari.

On the other hand, troilite within the fine-grained clasts could potentially be of nebular origin or the clasts originated from a part of the parent body that was not as severely affected by the secondary sulfidization event. The modal abundance of troilite is much lower in the clasts compared to the matrix (**Fig. 3.12**), but the bulk chemical composition of clasts and matrix is very similar, except for Fe and S contents (**Table 3.8**). The fine-grained clasts also contain abundant Cl-apatite and therefore must have experienced thermal metamorphism on the parent body as well.

Conditions probably changed significantly on the Kakangari parent body over time (**Fig. 3.16**). Thermal metamorphism occurred under conditions that were oxidizing enough so that P was oxidized from the metal leading to the formation of apatite. Minor amounts of Cr present in the troilite indicate that sulfidization, probably via H_2S gas, took place under more reducing conditions. Subsequently, the formation of ferrihydrite required highly oxidizing conditions and the presence of water. This is very different from what has been observed in oxidized CV chondrites, where oxidation, sulfidization and carburization occurred simultaneously in the presence of C-O-S fluids (e.g., Blum et al. 1989; Krot et al. 1995, 1998). In Kakangari, there was no oxidant in the fluid that caused sulfidization. However, oxidizing fluids could have been present before sulfidization, causing the formation of apatite during thermal metamorphism, and definitely were present after sulfidization during the formation of ferrihydrite. This suggests that fluid convection might have occurred on the parent asteroid (e.g., Cohen and Coker 2000). The last stage of aqueous alteration occurred at very low temperatures so that troilite was preserved and not transformed into pyrrhotite and pentlandite like in CI and oxidized CV3 chondrites (Bullock et al. 2005; Krot et al. 1995, 1998).

Comparison of Kakangari chondrules to chondrules in ordinary, carbonaceous and enstatite chondrites

Chondrule textures

Genge and Grady (1998) suggested that the relative abundances of different textural types of chondrules in Kakangari are most similar to chondrules in ordinary chondrites, but our interpretation is that they are intermediate between ordinary and enstatite chondrites (**Table 3.1**). The abundance of PO chondrules is certainly higher in Kakangari (14.2%) than in enstatite chondrites, which do not contain any PO chondrules (Rubin and Grossman 1987; Schneider et al. 2002), but slightly lower than in ordinary chondrites (15-27% Gooding and Keil 1981). We found that PP chondrules are approximately twice as abundant in Kakangari (~22%) as in ordinary chondrites (9-11%; Gooding and Keil 1981), while they make up more than 50% of chondrules in enstatite chondrites (Rubin and Grossman 1987; Schneider et al. 2002). BO chondrules are absent in Kakangari and enstatite chondrites, but constitute 3–4% of ordinary chondrite chondrules (Gooding and

Keil 1981). A comparison to chondrule textures in carbonaceous chondrites is difficult at this point in time, because of the scarcity of detailed data in the literature (e.g., Grossman et al. 1988; Rubin 2000; Scott and Krot 2003). It seems that the abundance of radial pyroxene chondrules is much lower in carbonaceous chondrites (≤2%) than in Kakangari (9–10.4%), ordinary (7–9%) and enstatite chondrites (6.6–12.8%).

We further found a high relative abundance of agglomeratic chondrules in Kakangari (14.2%), which are mineralogically very similar to the igneous rims that are present around 16% of all chondrules. Agglomeratic chondrules could simply represent cross sections through such rims, but this is fairly unlikely for at least some of them, as they are quite large (e.g., **Fig. 3.3g**). The data for ordinary, enstatite and carbonaceous chondrites listed in **Table 3.1** do not include estimates for the abundance of agglomeratic chondrules. According to Weisberg and Prinz (1996), agglomeratic chondrules make up ~2 vol% of ordinary chondrites, but have much higher abundances in carbonaceous chondrites (e.g., Rubin 2000), for example 13.7 vol% in Ningqiang (Rubin et al. 1988). The absolute modal abundance of agglomeratic chondrules in Kakangari corresponds to approximately 2.7 vol%, similar to ordinary chondrites.

Chondrule mineralogy

Mesostasis compositions in Kakangari chondrules follow two distinct trends in a K/Al vs. Na/Al diagram (**Fig. 3.8**) that are similar to those observed in type I (FeO-poor) and type II (FeO-rich) chondrules in type 3 ordinary chondrites (Grossman and Brearley 2005). However, FeO contents of chondrule silicates in Kakangari do not show two distinct populations (**Fig. 3.4**), but are intermediate between typical type I and type II chondrules in primitive ordinary and carbonaceous chondrites. Below, we first discuss whether these observations can be attributed to thermal metamorphism or if it represents a primitive feature of Kakangari chondrules. Then we compare Kakangari chondrules with those in ordinary, carbonaceous and especially enstatite chondrites in more detail.

Six of the twenty Kakangari chondrules studied follow the type I trend in the K/Al vs. Na/Al diagram in **Figure 3.8**, whereas all other chondrules follow the type II trend. The terms type I and type II have been specifically used for porphyritic chondrules (e.g., Grossman et al. 1988), but in **Figure 3.8** all Kakangari chondrules are plotted. The type I trend includes a CC chondrule, three POP and two PP chondrules. All of the chondrules

that show a “type IIA”-texture (PO-II) and all of the RP/BP chondrules fall on the type II trend. Many Kakangari chondrules that follow the type II trend have mesostasis compositions with K/Al ratios (relative to CI) > 3, which could be indicative of the onset of albite crystallization, hence a residual glass that becomes more K-rich during mild thermal metamorphism (e.g., Grossman and Brearley 2005). This accentuates the two distinct trends.

Despite the differences in mesostasis compositions, the chondrules that follow the type I trend share many characteristics with those that follow the type II trend. Silicates in chondrules that follow the type I trend in **Figure 3.8** have a range of Fa and Fs contents (2.3<Fa<10.1 and 3.7<Fs<18.8) that is similar to those that follow the type II trend (2.7<Fa<10.6 and 4.3<Fs<23.6). For most chondrules, CaO contents of olivine in the type I and type II trends are similarly low (<0.03 wt%) and MnO contents of olivine are similarly high (**Fig. 3.5a,b**). Chondrule #1-3 (**Fig. 3.6c**) is an exception: some MnO values fall into the range of typical type I chondrules in ordinary and carbonaceous chondrites (**Fig. 3.5b**). However, this chondrule also contains a large Ni-poor metal bleb (**Fig. 3.6d**) indicating that it also must have undergone reduction as we suggested for other chondrules above. The range of MnO contents observed in olivine in chondrule #1-3 (**Fig. 3.5b**) can be explained by reduction of olivine that was originally not as FeO-rich as others plus limited equilibration. Overall, it is clear that chondrules that follow the type I trend in **Figure 3.8** are not typical type I chondrules as found in ordinary and carbonaceous chondrites.

A typical cut off value between type I and type II chondrules that has been used for ordinary and carbonaceous chondrites is Fe/(Fe+Mg) = 10% (e.g., Jones et al. 2005). In the most primitive ordinary and carbonaceous chondrites, there is a significant population of chondrules with Fa<1 (e.g., Jones et al. 2005), while Fe-Mg exchange between chondrules and matrix leads to higher FeO contents in type I chondrule silicates in chondrites that have experienced mild thermal metamorphism (Scott and Jones 1990; Jones and Rubie 1991). Fe-Mg exchange between chondrules and matrix in Kakangari cannot have produced the high FeO contents preserved in olivines and pyroxenes in chondrules that follow the type I trend in **Figure 3.8,** because matrix silicates in Kakangari are MgO-rich (**Fig. 3.4**). Chondrule silicates with Fa < 2 mol% and Fs < 3

mol% were not observed in our and other studies of Kakangari (Graham and Hutchison 1974; Graham et al. 1977; Brearley 1989) and neither did we observe any normal zoning that would suggest that Fe-Mg exchange between a typical type I chondrule population (with Fa<1) and the matrix ($Fa_{2\text{-}6.5}$) led to the lowest observed Fe/(Fe+Mg) ratios in chondrule silicates. Because we have evidence that thermal metamorphism occurred on the Kakangari parent body (see above), it is likely that Fe-Mg exchange between chondrule and matrix silicates took place. However, it is not possible to differentiate between how much reduction and how much Fe-Mg exchange contributed to the shift to lower MgO contents in chondrule silicates, but the reduced nature of Kakangari chondrules was clearly produced in the solar nebula.

Reduced chondrules are common in enstatite chondrites. Most chondrules in enstatite chondrites are very FeO-poor (Fa < 1 mol% and Fs < 4 mol%; Lusby et al. 1987), but ubiquitous FeO-rich objects consisting mainly of FeO-rich pyroxene have been observed (e.g., Lusby et al. 1987; Weisberg et al. 1994). Oxygen isotopic compositions of these objects are identical to FeO-poor chondrule silicates in enstatite chondrites (Perron and Bourot-Denise 2001; Kimura et al. 2003; Clayton and Mayeda 1985), and these are also identical to Kakangari chondrules (Weisberg et al. 1996). The range of silicate compositions of FeO-rich objects in primitive enstatite chondrites, $Fs_{5\text{-}34}$ and minor olivine with $Fa_{3\text{-}14}$ (Lusby et al. 1987; Weisberg et al. 1994), is very similar to that of Kakangari chondrules. Many of these objects also record evidence for reduction in the form of dusty pyroxenes (and olivines) with Ni-poor metal/sulfide blebs, zoning with more MgO-rich compositions towards grain edges and abundant silica (e.g., Weisberg et al. 1994). The presence of silica makes Kakangari chondrules more similar to chondrules in enstatite chondrites than to those in carbonaceous and ordinary chondrites, where silica is only a minor constituent (e.g., Olsen 1983; Brigham et al. 1986; Hezel et al. 2006). On the other hand, some FeO-rich objects in enstatite chondrites contain FeO-poor (Fs<3) enstatite relict grains and/or rims (Lusby et al. 1987; Weisberg et al. 1994), a feature that is not observed in Kakangari chondrules. Furthermore, troilites found in FeO-rich objects in enstatite chondrites have higher Cr contents (1.5–3 wt%) than troilite in Kakangari (0.15–0.25 wt%) and contains some Ti as well (Kimura et al. 2003), whereas Ti is below EMP detection limits in Kakangari troilite. FeO-rich objects in enstatite chondrites bear

many similarities to Kakangari chondrules, but they experienced an even more complex history.

In Chapter 1, we described two reduced chondrules in a primitive L chondrite (MET 00526) which are very similar to Kakangari chondrules because they show clear evidence for solid-state reduction. Kakangari chondrules can be seen as intermediate between these reduced chondrules in ordinary chondrites and FeO-rich objects in enstatite chondrites.

CONCLUSIONS

Up until now, Kakangari has been thought of as a very pristine chondrite (e.g., Brearley 1989; Scott and Krot 2005; Nuth et al. 2005). Based on observations initially made by Nehru et al. (1986) and Brearley (1989), Scott and Krot (2005) suggested that Kakangari chondrules formed from material that closely resembled the associated matrix and that chondrules and matrix must have formed in close proximity in the solar nebula. However, our study shows that caution needs to be exercised when making such statements, because Kakangari has experienced a complex history of secondary processing and alteration, which could also have been responsible for the compositional similarity between chondrules and matrix.

The simplified illustration in **Figure 3.16** summarizes the series of events we propose for Kakangari. These include: (1) formation of fine-grained FeO-rich precursor material, (2) formation of chondrules in a first heating event in the solar nebula, (3) reduction of chondrules and fine-grained matrix materials in a second heating event, (4) accretion, (5) thermal metamorphism, (6) sulfidization, and (7) low-temperature aqueous alteration.

APPENDIX A - DETERMINING BULK CHEMICAL COMPOSITIONS OF CHONDRULES BY ELECTRON MICROPROBE: MODAL RECOMBINATION ANALYSIS (MRA) VERSUS DEFOCUSED BEAM ANALYSES (DBA).

INTRODUCTION

Many scientists have employed the 'quick and dirty' method of using defocused beam analyses (DBA) to determine bulk chondrule compositions and still continue to do so (e.g., McSween 1977a; Dodd 1978b; Kimura and Yagi 1980; Lux et al. 1980; Ikeda 1980; Jones and Scott 1989; Jones 1990, 1994; 1996a; Kimura et al. 2005), even though Albee et al. emphasized in 1977 that *"most probe analysts recognize that large errors are involved and … many probe analysts strongly discourage or actively oppose the publication of DBAs."* In order to account for the heterogeneous target in DBA, various correction methods have been proposed, including a normative correction (e.g., Albee et al. 1977; Bower et al. 1977) and empirical correction factors (e.g., Ikeda 1980). But it was not until a couple of years later, that it was realized that the densities of the different phases excited by the electron beam need to be taken into account as well (e.g., Jones and Scott 1989; Warren et al. 1997).

In contrast to DBA, modal recombination analysis (MRA) is very time-consuming as it requires obtaining the compositions of all phases present in a chondrule as well as determining the modal abundances of the different phases. The latter can be done much faster these days using image analysis software instead of tedious point-counting. However, Grossman and Wasson (1983a) pointed out that minor elements tend to be less precise in MRA, especially when accessory phases are not taken into account.

In the beginning of this study, we considered using DBA, but as we became increasingly aware of the many problems with this analytical technique, we decided to obtain a dataset of MRA and DBA for the same chondrule (from the CV3 chondrite Vigarano). The results of this "experiment" are presented and discussed below, in order to demonstrate why we chose to use MRA for this study.

MODAL RECOMBINATION ANALYSIS (MRA)

For modal recombination analysis, mesostasis glass was analyzed first (15 keV, 10 nA, 5 µm beam diameter) in order to minimize Na loss (e.g., Jbara et al. 1995; Nielsen and Sigurdsson 1981; Morgan and London 2005; Grossman and Brearley 2005). Subsequently, WDS element maps were collected (15 keV, 30 nA, 1 µm beam diameter) and used to identify each phase. Olivine and pyroxene were analyzed at 15 kV with a focused beam and a beam current of 20 nA, whereas a beam current of 40 nA was used for metal and sulfide analyses.

Figure A.1a shows the phase image of the chondrule, which was constructed in Adobe Photoshop® based on the WDS element maps. It was used to determine the modal abundance of each phase with Scion Image software. The bulk composition of the chondrule was calculated for each element according to the following equation:

$$Element\ A = conc_{phase\ 1}^{Element\ A} \cdot \left[\frac{vol\%_{phase\ 1} \cdot \rho_{phase\ 1}}{\sum_{1}^{n} (vol\%_{phase} \cdot \rho_{phase})} \right] + conc_{phase\ 2}^{Element\ A} \cdot \left[\frac{vol\%_{phase\ 2} \cdot \rho_{phase\ 2}}{\sum_{1}^{n} (vol\%_{phase} \cdot \rho_{phase})} \right] + \ldots + conc_{phase\ n}^{Element\ A} \cdot \left[\frac{vol\%_{phase\ n} \cdot \rho_{phase\ n}}{\sum_{1}^{n} (vol\%_{phase} \cdot \rho_{phase})} \right]$$

where ρ is the density of the phase analyzed and the concentration *conc* is given in element wt%. Mineral densities from Deer et al. (1992) and at http://www.webmineral.com were used. The density of the mesostasis glass was determined using a model calculation by Fluegel (2007). The bulk chondrule composition determined via MRA is shown in **Table A.1**. in column A. In **Table A.1.**, column B we also show the bulk composition determined via MRA without including the phase densities, because this is such a commonly made mistake.

DEFOCUSED BEAM ANALYSES (DBA)

Defocused beam analyses were acquired with an accelerating voltage of 15 keV and a beam current of 20 nA. 75 analyses with a beam diameter of 50 µm were obtained on a grid (100 µm apart), so that they covered the entire chondrule (**Fig. A.1b**). A regular ZAF correction (for a homogeneous target) was applied to the data.

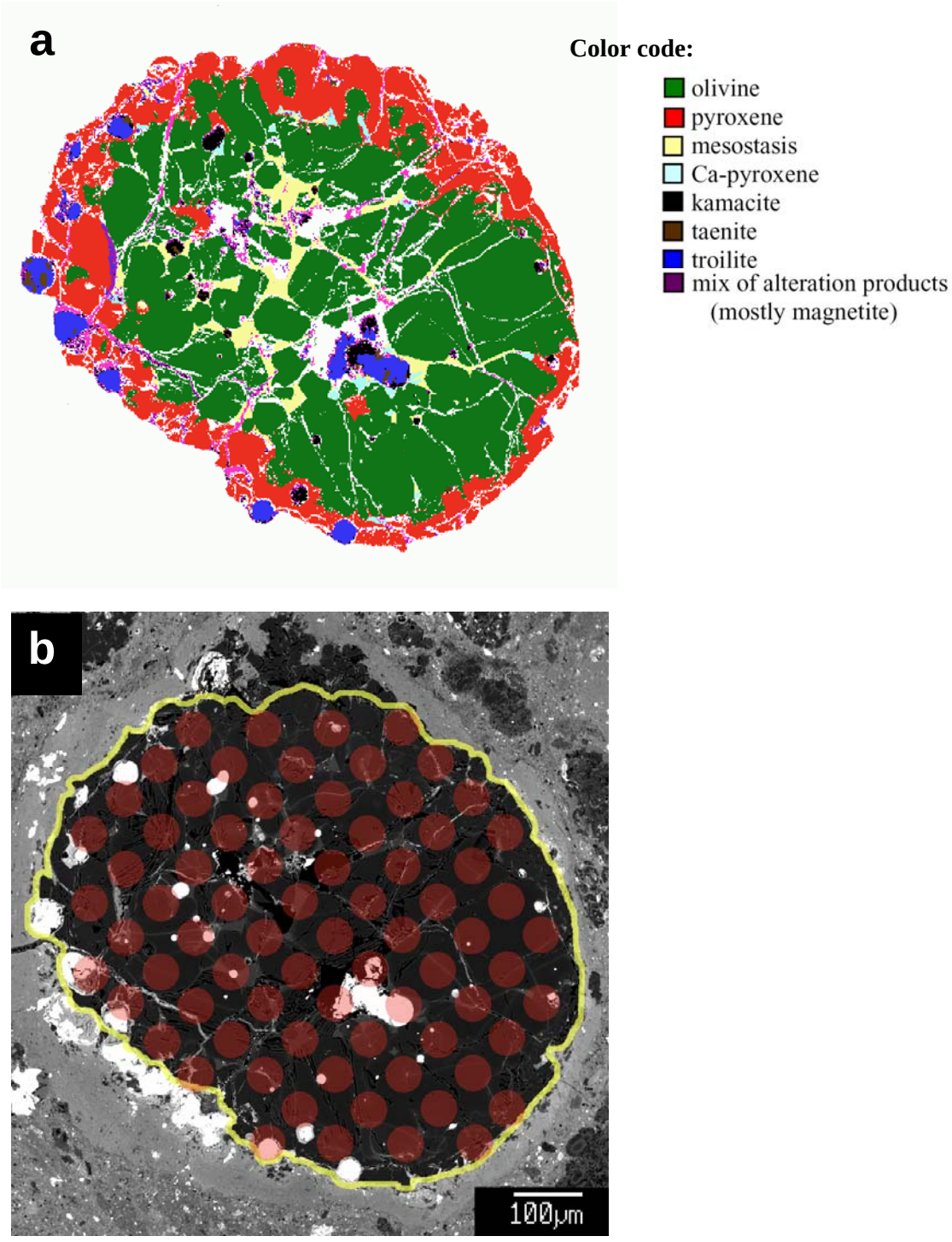

Fig. A.1. a) Phase image of the Vigarano chondrule used in MRA. b) BSE image of the Vigarano chondrule with DBA spots.

The first big problem that becomes apparent when doing DBA is how to deal with analyses that do not have acceptable totals. High totals often correspond to mixed analyses (silicate + metal/sulfides) and the fact that Fe is present in two oxidation states (as Fe^{2+} in silicates and as Fe^{0} in metal). Instead of simply normalizing these analyses to 100 wt%, we corrected them by converting some of the FeO into Fe until the total converged to ~100 wt%. Low totals resulted from spots where cracks or holes are present. Analyses with totals between 90 and 97 wt% were normalized to 100 wt%. The bulk chondrule composition (**Table A.1**, column C) was calculated by simple averaging (10 analyses were discarded). Oxide wt% were converted to element wt%, so that the data can be easily compared to the results obtained by MRA. Because the modal abundances of the phases and their average element concentrations were exactly known from our MRA, we were able to calculate "unequal host-phase density correction factors" (β_ρ) as suggested by Warren (1997) and apply them to our DBA (**Table A.1**, column D). The correction factors are given in column E in **Table A.1**.

Table A.1. Bulk compositions obtained via modal recombination analysis (MRA) and defocused beam analyses (DBA) for the chondrule shown in Figure A.1.

	A MRA (incl. phase densities)	**B** MRA (w/o phase densities)	**C** DBA (ZAF, but no ρ corr. applied)	**D** DBA (ρ-corrected, β_ρ given in **E**)	**E** correction factor β_ρ (Warren 1997)
Si	19.1	20.0	20.2	19.2	*0.95*
Ti	0.06	0.06	0.05	0.05	*0.93*
Al	**0.66**	**0.75**	**1.39**	**1.24**	***0.89***
Cr	0.41	0.4	0.45	0.46	*1.01*
Fe	**8.8**	**5.3**	**4.6**	**7.6**	***1.64***
Mn	0.04	0.04	0.04	0.04	*0.96*
Mg	24.9	26.0	27.0	26.0	*0.96*
Ca	1.45	1.7	1.08	0.92	*0.86*
Na	**0.14**	**0.18**	**0.24**	**0.19**	***0.81***
K	0.01	0.01	0.02	0.02	*0.94*
P	0.03	0.02	0.02	0.02	*1.35*
Ni	**0.57**	**0.25**	**0.16**	**0.36**	***2.31***
S	**1.74**	**1.27**	**0.64**	**0.88**	***1.37***

DISCUSSION

The main argument for using the DBA method has been that the error related to 2D vs. 3D composition is probably greater than the analytical error related to the heterogeneous target in DBA (e.g., Albee et al. 1977; Hezel 2007). However, this has never been quantified. Evidently, 2D and 3D bulk compositions should be very similar when the phases that are present in a 2D section have approximately the same modal proportions as in the 3D object. New techniques, such as 3D synchrotron X-ray micro-tomography, will soon provide us with a better understanding of the 3D structure of chondrules (e.g., Ebel et al. 2008). Hezel (2007) tried to assess the errors related to 2D EMP analysis using a numerical model, but he did not take phase densities into account.

Above, we show that a very large error is introduced in both EMP methods, DBA and MRA, when phase densities are not taken into account. **Table A.1** and **Figure A.2** show how large the differences can be, when bulk compositions are obtained by MRA and DBA, with and without taking phase densities into account. In **Figure A.2**, the results of each technique are compared to MRA with phase densities included. A 1:1 line for this technique is displayed as a reference. **Figure A.2b** shows an enlargement for the points near the origin (minor elements) in **Figure A.2a**. Elements (e.g., Fe, Ni and S) that are concentrated in the more dense phases such as Fe,Ni metal and sulfides are significantly underestimated in DBA and MRA, when densities are not included. As a major element, Fe is underestimated by a factor of ~2 (**Fig. A.2a**, see also Fig. 18 in Chapter 1). On the other hand, elements (e.g., Al, Na) concentrated in the less dense mesostasis glass are overestimated (**Fig. A.2b**). Elements that are affected most are basically those, for which the correction factors (**Table A.1**, column E) deviate most from 1.

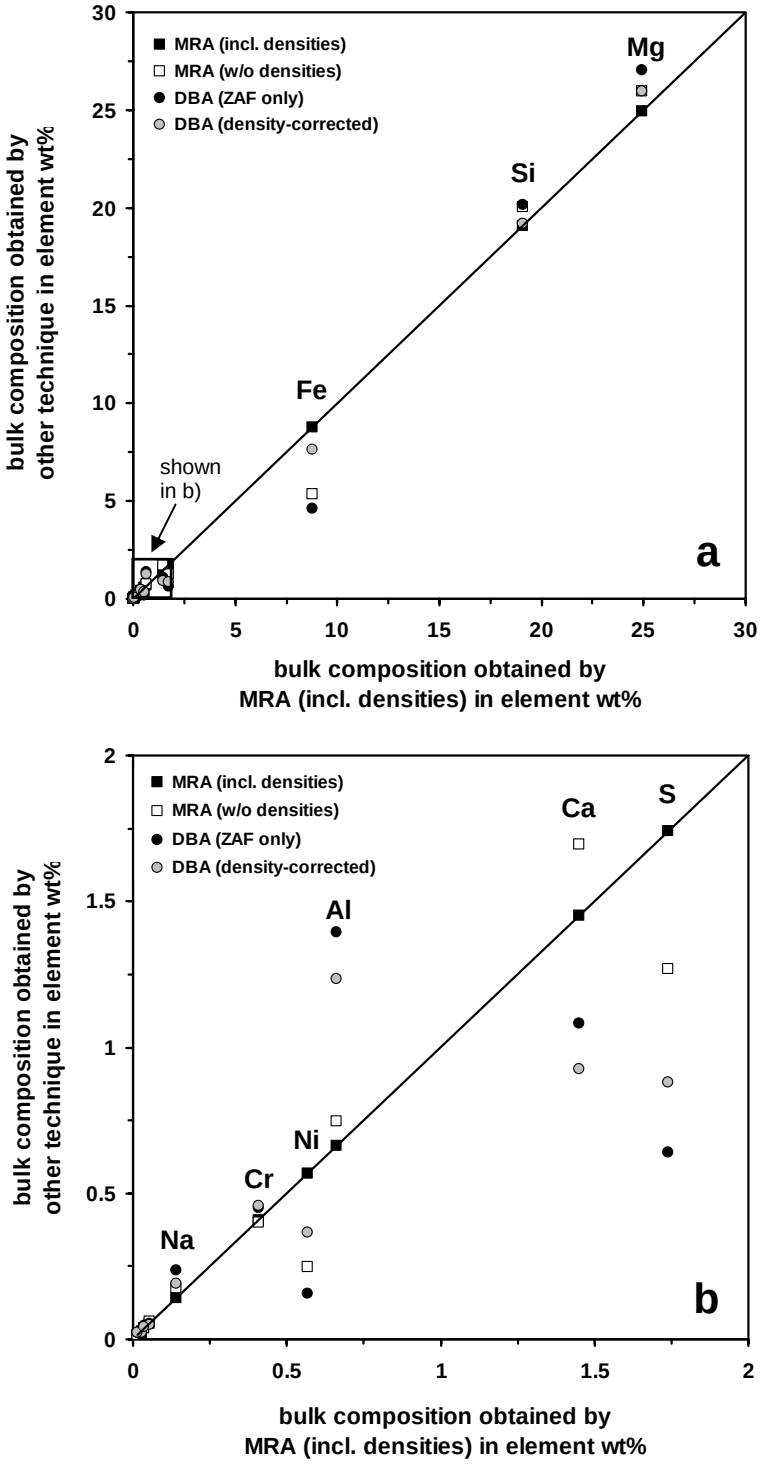

Fig. A.2. Bulk compositions obtained by MRA (squares) and DBA (circles), with and without taking phase densities into account (see legend) versus MRA including densities. A 1:1 line for MRA including densities is displayed as a reference. b) Enlargement for the points near the origin (minor elements) in a).

Our results show how important it is to take phase densities into account when calculating a bulk chondrule composition from EMP data. **Figure A.3** shows a summary of the variety of techniques that have been used to collect EMP datasets of bulk chondrule compositions. Only a few of these datasets were collected taking phase densities into account. Jones and Scott (1989) and Jones (1990, 1994, 1996a) performed a normative correction procedure (see also Bower et al. 1977), but they also accounted for the densities of Fe,Ni metal and sulfides. At this point in time, we cannot comment on how reliable this kind of correction procedure is, however, at least an effort was made to include metal and sulfide phase densities and therefore, these DBA analyses should be more accurate than others, where phase densities were not taken into account.

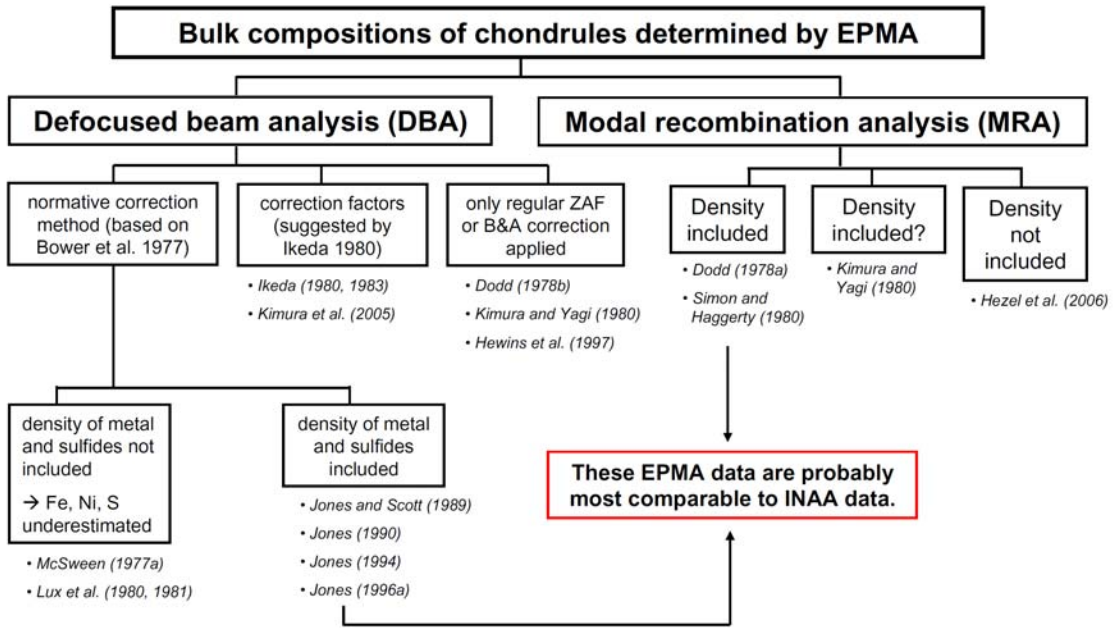

Fig. A.3. Flowchart representing a summary of the techniques used for the bulk chondrule EMP data that are currently available in the literature. In only a few datasets, the phase densities were taken into account.

Calculating the "unequal host-phase density correction factors" (Warren 1997), given in **Table A.1**, column E, was only possible because the modal abundances of the phases and their average element concentrations were exactly known from our MRA. But even when these correction factors are applied to our DBA (**Table A.1**, column D), only the values for some elements (Fe, Mg, and Ni) become more similar to those obtained by MRA (**Table A.1**, column A). The reason for that could be that the correction factors as listed in **Table A.1**, column E were simply applied to the final bulk composition given in **Table A.1**, column C, which was obtained by averaging the collected DBA. If the correction factors would have been calculated for, and applied to, each single DBA spot (**Fig. A.1b**), the density-corrected DBA values might have been more similar those obtained by MRA including phase densities. But, of course, if MRA needs to be done in order to correct DBA properly, the bulk compositions could be calculated by MRA in the first place. Carpenter et al. (2009) are currently working on new type of correction procedure for DBA, that simulates X-ray production and emission from multiphase samples. We conclude that, until a reliable correction method for DBA is established, MRA should be the preferred method.

APPENDIX B – COMPARISON OF THE TWO METHODS USED FOR MODAL RECOMBINATION ANALYSIS (MRA)

Until August 2008, bulk chondrule compositions were obtained using Adobe Photoshop® and Scion Image (**Method 1**). This includes all Kainsaz and Kakangari chondrules, as well as several chondrules in MET 00426 (CR-Ch1, CR-Ch6, CR-Ch13, CR-Ch17, CR-Ch18) and in MET 00526 (L-Ch1, L-Ch4, L-Ch7 and L-Ch9).

After August 2008, bulk chondrule compositions were obtained using the 'Phase Tool' (**Method 2**) in Lispix Lx133P (http://www.nist.gov/lispix/doc/contents.htm, public domain image analysis program for Windows, written and maintained by David Bright, National Institute of Standards and Technology). This includes all other chondrules in MET 00426 (CR) and MET 00526 (L) not mentioned above. Below we provide detailed instructions for using these two techniques and discuss how their results compare.

METHOD 1 (ADOBE PHOTOSHOP® & SCION IMAGE)

Chondrule phase images were produced in Adobe Photoshop® based on multi-color WDS element maps that were transferred from the JEOL 8200 electron microprobe via tif screen-captures. In order to have optimum contrast between the different phases, it was sometimes necessary to modify the levels of a certain map. Combination maps (e.g., Ca+Al+Mg, Fe+S, etc.) were obtained as well.

All WDS element maps of a certain chondrule were assembled as layers within a single Adobe Photoshop® file (1300 x 1300 pixel). The layers were labeled so that it was easy to navigate between the element maps. A transparent layer was added on top of the other layers and a rough mask was drawn with the 'Pencil Tool' to only expose the chondrule and the color scale. The maps that were most useful to distinguish between certain phases (e.g., Mg to distinguish between olivine and pyroxene) were saved as separate tif-files with the mask.

Within each tif-file, the pixels that belong to a certain phase were selected with the 'Magic Wand Tool' (it is easiest when this is done directly on the color scale). By holding down the Shift key, pixels of other colors were added until all pixels that

correspond to a certain phase were selected. Then, the phase was tinted with a single color using the 'Pencil Tool'. Using the key combinations Ctrl+c and Ctrl+v, the phase was copied and pasted into a separate psd-file for the phase image. The step was repeated for all phases present in the chondrule using the most suitable element map or combination map (e.g., CaMgSi combination map for Ca-rich pyroxene, FeS for metal and sulfides, etc.). While the phase image was assembled this way, the obtained quantitative analyses were organized in order to make sure that every phase was properly recognized and included. In the final phase image psd-file, each layer was labeled with the name of the respective phase it represents.

As a last step, a new transparent layer was added for the final mask to only expose the chondrule. We found that it was easier to recognize the outline of the chondrule in the phase image rather than in the BSE image. The psd-file was then saved and transferred into grayscale, so that the image could be used in Scion Image to determine the modal abundances of the phases. In Scion Image, the 'Density Slice' function was used to select each phase and measure the number of pixels covered by that phase.

METHOD 2 (LISPIX)

An advantage of Lispix is that phase images can be obtained within minutes (not hours as with Method 1) and that the modal proportions of the phases are being calculated directly in Lispix from the produced phase image. In order to only count the pixels that belong to the chondrule (i.e., exclude similar phases present in the surrounding matrix), a mask was placed on each WDS element map using the same technique in Adobe Photoshop® as described above in Method 1. This was done before element maps were loaded into Lispix.

Detailed instructions for using the 'Phase Tool' in Lispix can be found at: http://www.nist.gov/lispix/doc/tutorials/Tutorial%204%20Phase%20Tool.htm. One significant difference to Method 1 described above, is that grayscale WDS element maps are used instead of multi-color maps, which makes it a little bit more difficult for the human eye to distinguish between phases that exhibit similar shades of gray in a map. However, because we were aware of that, we always referred to multi-color single element and combination maps when producing phase images of chondrules in Lispix.

COMPARISON OF THE TWO METHODS

In **Table B.1**, the modal proportions and bulk compositions obtained using both methods are shown for two chondrules. While the modal abundance of a certain phase might differ by a few %, the bulk chondrule compositions obtained with both methods are fairly similar.

While modal recombination is more accurate than defocused beam analyses (DBA), it is still a very subjective method (e.g., choosing the outline of a chondrule). However, according to Maloy and Treiman (2007), having an educated individual prepare the phase images seems to generate more accurate results than if multispectral image classification software is used.

Table B.1. Modal proportions and bulk compositions obtained with both MRA methods for one chondrule in MET 00526 (L-Ch1) and one chondrule in Kainsaz (K2-Ch8).

	L-Ch1 Method 1	**L-Ch1 Method 2**	**K2-Ch8 Method 1**	**K2-Ch8 Method 2**
Modal proportions (area %)				
olivine	46.63	44.32	42.42	46.35
low-Ca pyroxene	5.17	5.43	39.01	37.38
Ca-rich pyroxene	5.84	4.87	5.57	4.69
mesostasis 1	20.38	17.86	11.04	10.51
mesostasis 2	19.71	25.42	-	-
kamacite	0.01	0.02	1.13	0.48
taenite	-	-	0.30	0.46
MSS	2.25	2.08	0.52	0.15
Bulk composition (element wt%)				
Si	22.10	22.50	22.35	22.53
Ti	0.23	0.23	0.10	0.09
Al	3.69	3.98	2.08	1.99
Cr	0.33	0.33	0.24	0.23
Fe	2.70	2.53	3.79	2.17
Mn	0.09	0.10	0.06	0.06
Mg	20.50	19.62	23.88	24.90
Ca	4.30	4.32	2.10	1.96
Na	0.60	0.83	0.19	0.18
K	0.05	0.07	0.02	0.02
Ni	0.01	0.01	0.46	0.60
Co	0.00	0.00	0.02	0.01
P	0.01	0.01	0.00	0.00
S	1.24	1.14	0.27	0.08

Method 1: Adobe Photoshop® + Scion Image
Method 2: Lispix

REFERENCES

Abreu N. M. 2007. Fine-scale mineralogical study of the matrices of CR carbonaceous chondrites: Insights on early solar system processes. Ph.D. thesis, University of New Mexico, Albuquerque, NM, USA.

Abreu N. M. and Brearley A. J. Forthcoming. Early solar system processes recorded in the matrices of two highly pristine CR3 carbonaceous chondrites, MET 00426 and QUE 99177. *Geochimica et Cosmochimica Acta*.

Ahrens L. H. 1970. The composition of stony meteorites (VIII). Observations on fractionation between the L and H chondrites. *Earth and Planetary Science Letters* 9:345-347.

Ahrens L. H., Willis J. P. and Erlank A. J. 1973. The chemical composition of Kainsaz and Efremovka. *Meteoritics* 8:133-139.

Albee A. L., Quick J. E., and Chodos A. A. 1977. Source and magnitude of errors in "broad-beam analysis" (DBA) with the electron probe. 8th Lunar and Planetary Science Conference. pp. 7-9.

Allen C. C., Morris R. V., Lauer H. V. Jr., and McKay D. S. 1993a. Microscopic iron metal on glass and minerals – A tool for studying regolith maturity. *Icarus* 104:291-300.

Allen C. C., Morris R. V., Lauer H. V. Jr., and McKay D. S. 1993b. Effects of microscopic iron metal on the reflectance spectra of glass and minerals. 24th Lunar and Planetary Science Conference. pp. 17-18.

Alexander C. M. O'D. 1995. Trace element contents of chondrule rims and interchondrule matrix in ordinary chondrites. *Geochimica et Cosmochimica Acta* 59:3247-3266.

Alexander C. M. O'D. 2005. Re-examining the role of chondrules in producing the elemental fractionations in chondrites. *Meteoritics and Planetary Science* 40:943-965.

Alexander C. M. O'D. and Grossman J. N. 2005. Alkali elemental and potassium isotopic compositions of Semarkona chondrules. *Meteoritics and Planetary Science* 40:541-556.

Alexander C. M. O'D, Barber D. J., and Hutchison R. 1989a. The microstructure of Semarkona and Bishunpur. *Geochimica et Cosmochimica Acta* 53:3045-3057.

Alexander C. M. O'D, Hutchison R., and Barber D. J. 1989b. Origin of chondrule rims and interchondrule matrices in unequilibrated ordinary chondrites. *Earth and Planetary Science Letters* 95:187-207.

Alexander C. M. O'D, Grossman J. N., Ebel D. S., and Ciesla F. J. 2008. The formation conditions of chondrules and chondrites. *Science* 320:1617-1619.

Anders E. and Grevesse N. 1989. Abundances of the elements: Meteoritic and solar. *Geochimica et Cosmochimica Acta* 53:197-214.

Barton P. B. Jr. and Toulmin P. III 1966. Phase relations involving sphalerite in the Fe-Zn-S system. *Economic Geology* 61:815-849.

Bendersky C., Weisberg M. K., Connolly H. C., and Ebel D. S. 2007. Olivine and the onset of thermal metamorphism in EH3 chondrites (abstract #2077). 38th Lunar and Planetary Science Conference. CD-ROM.

Benoit P. H., Akridge G. A., Ninagawa K., and Sears D. W. G. 2002. Thermoluminescence sensitivity and thermal history of type 3 ordinary chondrites: Eleven new type 3.0-3.1 chondrites and possible explanations for differences among H, L, and LL chondrites. *Meteoritics and Planetary Science* 37:793-805.

Berlin J., Jones R. H., and Brearley A. J. 2006a. Disentangling the diversity of bulk chondrule compositions: Did CO chondrites sample two very distinct chondrule populations? *Meteoritics and Planetary Science* 41:A21.

Berlin J., Jones R. H., and Brearley A. J. 2006b. Determining the bulk chemical composition of chondrules by electron microprobe; a comparison of different approaches (abstract #2370). 37th Lunar and Planetary Science Conference. CD-ROM.

Berlin J., Jones R. H., and Brearley A. J. 2007a. A closer look at chondrules and matrix in Kakangari; evidence for widespread reduction and sulfurization (abstract #2395). 38th Lunar and Planetary Science Conference. CD-ROM.

Berlin J., Jones R. H., and Brearley A. J. 2007b. A common origin for FeO-rich silicates in Kakangari and enstatite chondrite chondrules? *Meteoritics and Planetary Science* 42:A18.

Berlin J., Jones R. H., and Brearley A. J. 2007c. Reduction of FeO-rich chondrules in Kakangari and enstatite chondrites. *Geochimica et Cosmochimica Acta* 71:A84.

Berlin J., Jones R. H., and Brearley A. J. 2008a. Fe/Mn systematics of chondrule olivine: Significant differences between type II chondrules in CO, CR, and ordinary chondrites (abstract #2490). 39th Lunar and Planetary Science Conference. CD-ROM.

Berlin J., Jones R. H., Brearley A. J., and Spilde M. N. 2008b. Determining bulk chemical compositions of chondrules by electron microprobe: Modal recombination versus defocused beam analyses. *Proceedings Microscopy and Microanalysis* 14 (Suppl. 2):110-111.

Berlin J., Jones R. H., and Brearley A. J. 2009. Identification of FeO-rich relict olivines in type IIA chondrules using Fe-Mn systematics (abstract #2399). 39th Lunar and Planetary Science Conference. CD-ROM.

Bland P. A., Alard O., Bendix G. K., Kearsley A. T., Menzies O. N., Watt L. E., and Rogers N. W. 2005. Volatile fractionation in the early solar system and chondrule/matrix complementarity. *Proceedings of the National Academy of Sciences of the United States* 102:13755-13760.

Blum J. D., Wasserburg G. J., Hutcheon I. D., Beckett J. R., and Stopler E. M. 1989. Origin of opaque assemblages in C3V meteorites - Implications for nebular and planetary processes. *Geochimica et Cosmochimica Acta* 53:543-556.

Boesenberg J. S., Cosarinsky M., McKeegan K. D., Chaussidon M. and Hewins R. H. 2007. An experimental study of Fe-Mg and oxygen isotope exchange between relict olivine and chondrule melt (abstract #1621). 38th Lunar and Planetary Science Conference. CD-ROM.

Boland J. N. and Duba A. 1981. Solid-state reduction of iron in olivine – planetary and meteoritic evolution. *Nature* 294:142-144.

Bonal L., Bourot-Denise M., Quirico E., Montagnac G., and Lewin E. 2007. Organic matter and metamorphic history of CO chondrites. *Geochimica et Cosmochimica Acta* 71:1605-1623.

Boss A. P. 1996. A concise guide to chondrule formation models. In *Chondrules and the protoplanetary disk,* edited by Hewins R. H., Jones R. H., and Scott E. R. D. Cambridge: Cambridge University Press. pp. 257-263.

Bower J. F., Wood J. A., Richardson S. M., McSween H. Y. and Ryder G. 1977. Rock compositions by defocused beam analysis. 8th International Conference on X-ray optics and microanalysis and 12th Annual Conference of the Microbeam Analysis Society, 182A-182C.

Brearley A. J. 1989. Nature and origin of matrix in the unique type 3 chondrite, Kakangari. *Geochimica et Cosmochimica Acta* 53:2395-2411.

Brearley A. J. 1993. Matrix and fine-grained rims in the unequilibrated CO3 chondrite, ALHA 77307; origins and evidence for diverse, primitive nebular dust components. *Geochimica et Cosmochimica Acta* 57:1521-1550.

Brearley A. J. 1994. Metamorphic effects in the matrices of CO3 chondrites; compositional and mineralogical variations. 25th Lunar and Planetary Science Conference. pp. 165-166.

Brearley A. J. 1996. Nature of matrix in unequilibrated chondrites and its possible relationship to chondrules. In *Chondrules and the protoplanetary disk,* edited by Hewins R. H., Jones R. H., and Scott E. R. D. Cambridge: Cambridge University Press. pp. 137-151.

Brearley A. J. 2006. The action of water. In *Meteorites and the early solar system II,* edited by Lauretta D. S. and McSween Jr. H. Y. Tucson: The University of Arizona Press. pp. 587-624.

Brearley A. J. and Jones R. H. 1998. Chondritic meteorites. In *Planetary Materials,* edited by Papike J. J. Reviews in Mineralogy, vol. 36. Washington, D.C.: The Mineralogical Society of America. pp. 3-1–3-398.

Brearley A. J., Scott E. R. D., Keil K., Clayton R. N., Mayeda T. K., Boynton W. V., and Hill D. H. 1989. Chemical, isotopic and mineralogical evidence for the origin of matrix in ordinary chondrites. *Geochimica et Cosmochimica Acta* 53:2081-2093.

Brearley A. J., Bajt S. A., and Sutton S. R. 1995. Distribution of moderately volatile trace elements in fine-grained chondrule rims in the unequilibrated CO3 chondrite, ALH A77307. *Geochimica et Cosmochimica Acta* 59:4307-4316.

Brigham C. A., Yabuki H., Ouyang Z., Murrell M. T., El Goresy A., and Burnett D. S. 1986. Silica-bearing chondrules and clasts in ordinary chondrites. *Geochimica et Cosmochimica Acta* 50:1655-1666.

Britt D. T. 1993. The spectral effects of subsolidus reduction of olivine and pyroxene (abstract). 24th Lunar and Planetary Science Conference. pp. 195-196.

Bullock E. S., Gounelle M., Lauretta D. S., Grady M. M., and Russell S. S. 2005. Mineralogy and texture of Fe-Ni sulfides in CI1 chondrites: Clues to the extent of aqueous alteration on the CI1 parent body. *Geochimica et Cosmochimica Acta* 69:2687-2700.

Burger P. V. 2005. Incipient aqueous alteration of meteorite parent bodies: Hydration, mobilization, precipitation and equilibration. M.S. thesis, University of New Mexico, Albuquerque, NM, USA.

Carpenter P. K., Zeigler R. A., Jolliff B. L., Vicenzi E. P., Davis J. M., and Donovan J. J. 2009. Advances in Electron-Probe Microanalysis and Compositional Mapping: Applications to Lunar Samples (abstract #2531). 40th Lunar and Planetary Science Conference. CD-ROM.

Cassen P. 2001. Nebular thermal evolution and the properties of primitive planetary materials. *Meteoritics and Planetary Science* 36:671-700.

Chizmadia L. J., Rubin A. E. and Wasson J. T. 2002. Mineralogy and petrology of amoeboid olivine inclusions in CO3 chondrites: Relationship to parent-body aqueous alteration. *Meteoritics and Planetary Science* 37:1781-1796.

Choi B.-G., McKeegan K. D., Leshin L. A., and Wasson J. T. 1998. Extreme oxygen-isotope compositions in magnetite from unequilibrated ordinary chondrites. *Nature* 392:577-579.

Ciesla F. J. 2005. Chondrule-forming processes - An overview. In *Chondrites and the protoplanetary disk,* edited by Krot A. N., Scott E. R. D., and Reipurth B. San Francisco: Astronomical Society of the Pacific pp. 811-820.

Ciesla F. J. 2007. Radial transport in the solar nebula: Implications for moderately volatile element depletions in chondritic meteorites. *Astrophysics* eprint:0702032.

Clayton R. N. and Mayeda T. K. 1985. Oxygen isotopes in chondrules from enstatite chondrites: Possible identification of a major nebular reservoir. 16th Lunar and Planetary Science Conference. pp. 142-143.

Clayton R. N., Mayeda T. K., Goswami J. N. and Olsen E. J. 1991. Oxygen isotope studies of ordinary chondrites. *Geochimica et Cosmochimica Acta* 55:2317-2337.

Clayton R., N, 2003. Oxygen isotopes in meteorites. In *Meteorites, comets and planets,* edited by Davis A. M. Treatise on Geochemistry, vol. 1. Oxford, U.K.: Elsevier-Pergamon. pp. 129-142.

Cohen B. A. and Coker R. F. 2000. Modeling of liquid water on CM meteorite parent bodies and implications for amino acid racemization. *Icarus* 145:369-381.

Cohen B. A., Hewins R. H., and Yu Y. 2000. Evaporation in the young solar nebula as the origin of 'just-right' melting of chondrules. *Nature* 406:600-602.

Cohen R. E., Kornacki A. S., and Wood J. A. 1983. Mineralogy and petrology of chondrules and inclusions in the Mokoia CV3 chondrite. *Geochimica et Cosmochimica Acta* 47:1739-1757.

Connolly H. C., Hewins R. H., Ash R. D., Zanda B., Lofgren G. E., and Bourot-Denise M. 1994. Carbon and the formation of reduced chondrules. *Nature* 371:136-139.

Connolly H. C., Huss G. R., and Wasserburg G. J. 2001. On the formation of Fe-Ni metal in Renazzo-like carbonaceous chondrites. *Geochimica et Cosmochimica Acta* 65:4567-4588.

Connolly H. C., Weisberg M. K., Huss G. R., Nagashima K., Ebel D. S., Schrader D. L., and Lauretta D. S. 2007a. On the nature and origins of type II chondrules in CR2 chondrites (abstract #1571). 38th Lunar and Planetary Science Conference. CD-ROM.

Connolly H. C., Zipfel J., Folco L., Smith C., Jones R. H., Benedix G., Righter K., Yamaguchi A., Chennaoui Aoudjehane H., and Grossman J. N. 2007b. The Meteoritical Bulletin, No. 91, 2007 March. *Meteoritics and Planetary Science* 42:413-466.

Connolly H. C., Huss G. R., Nagashima K., Weisberg M. K., Ash R. D., Ebel D. S., Schrader D. L., and Lauretta D. S. 2008. Oxygen isotopes and the nature and origins of type-II chondrules in CR2 chondrites (abstract #1675). 39th Lunar and Planetary Science Conference. CD-ROM.

Cornell R. M. and Schwertmann U. 1996. In *The iron oxides.* Weinheim: VCH Verlagsgesellschaft. 573 p.

Cyr K. E., Sears W. D., and Lunine J. I. 1998. Distribution and evolution of water ice in the solar nebula: Implications for solar system body formation. *Icarus* 135:537-548.

Danielson L. R. and Jones R. H. 1995. Experimental reduction of olivine: Constraints on formation of dusty relict olivine in chondrules. 26th Lunar and Planetary Science Conference. pp. 309-310.

Davis A. M., Alexander C. M. O'D., Nagahara H., and Richter F. M. 2005. Evaporation and condensation during CAI and chondrule formation. In *Chondrites and the protoplanetary disk,* edited by Krot A. N., Scott E. R. D., and Reipurth B. San Francisco: Astronomical Society of the Pacific. pp. 432-455.

Davis A. M., Grossman L., and Ganapathy R. 1977. Yes, Kakangari is a unique chondrite. *Nature* 265:230-232.

Deer W. A., Howie R. A., and Zussman J. 1992. *An introduction to the rock-forming minerals*. Pearson Prentice Hall. 696 p.

DeHart J. M., Lofgren G. E., Lu J., Benoit P. H. and Sears D. W. 1992. Chemical and physical studies of chondrites: X. Cathodoluminescence and phase composition studies of metamorphism and nebular processes in chondrules of type 3 ordinary chondrites. *Geochimica et Cosmochimica Acta* 56:3791-3807.

Desch S. J., Ciesla F. J., Hood L. L., and Nakamoto T. 2005. Heating of chondritic materials in solar nebula shocks. In *Chondrites and the protoplanetary disk,* edited by Krot A. N., Scott E. R. D., and Reipurth B. San Francisco: Astronomical Society of the Pacific. pp. 849-872.

Dodd R. T. 1978a. The composition and origin of large microporphyritic chondrules in the Manych (L-3) chondrite. *Earth and Planetary Science Letters* 39: 52-66.

Dodd R. T. 1978b. Compositions of droplet chondrules in the Manych (L-3) chondrite and the origin of chondrules. *Earth and Planetary Science Letters* 40:71-82.

Dodd R. T. and Van Schmus W. R. 1971. Dark-zoned chondrules. *Chemie der Erde* 30:59-69.

Donnelly C. and Brearley A. J. 2007. Minor and trace elements in sulfides in reduced and oxidized CV3 carbonaceous chondrites; potential recorders of nebular and parent body processes (abstract #1959). 38th Lunar and Planetary Science Conference. CD-ROM

DuFresne E. R. and Anders E. 1962. On the chemical evolution of the carbonaceous chondrites. *Geochimica et Cosmochimica Acta* 26:1085-1114.

Dymek R. F., Albee A. L., Chodos A. A., and Wasserburg G. J. 1976. Petrography of isotopically-dated clasts in the Kapoeta howardite and petrologic constraints on the evolution of its parent body. *Geochimica et Cosmochimica Acta* 40:1115-1130.

Ebel D. S. and Grossman L. 2000. Condensation in dust-enriched systems. *Geochimica et Cosmochimica Acta* 64:339-366.

Ebel D. S., Weisberg M. K., Hertz J., and Campbell A. J. 2008. Shape, metal abundance, chemistry, and origin of chondrules in the Renazzo (CR) chondrite. *Meteoritics and Planetary Science* 43:1725-1740.

Eggleton R. A. and Fitzpatrick R. W. 1988. New data and a revised structural model for ferrihydrite. *Clays and Clay minerals* 36:111-124.

Engler A., Varela M. E., Kurat G., Ebel D., and Sylvester P. 2007. The origin of non-porphyritic pyroxene chondrules in UOCs: Liquid solar nebula condensates? *Icarus* 192:248-286.

Floss C. and Stadermann F. 2009. Auger Nanoprobe analysis of presolar ferromagnesian silicate grains from primitive CR chondrites QUE 99177 and MET 00426. *Geochimica et Cosmochimica Acta* 73:2415-2440.

Fluegel A. 2007. Global model for calculating room-temperature glass density from the composition. *Journal of the American Ceramic Society* 90:2622-2625.

Freer R. 1981. Diffusion in silicate minerals and glasses; a data digest and guide to the literature. *Contributions to Mineralogy and Petrology* 76:440-454.

Genge M. J. and Grady M. M. 1998. The textures and abundances of chondrules in the Kakangari chondrite (abstract #1670). 29th Lunar and Planetary Science Conference. CD-ROM.

Genge M. J., Clark R. J. H., Firth S., Batchelder M., and Grady M. M. 1998. Parent body aqueous alteration of kamacite in the Kakangari chondrite (abstract #1665). 29th Lunar and Planetary Science Conference. CD-ROM.

Gooding J. L. and Keil K. 1981. Relative abundances of chondrule primary textural types in ordinary chondrites and their bearing on conditions of chondrule formation. *Meteoritics* 16:17-43.

Goodrich C. A. and Delaney J. S. 2000. Fe/Mg-Fe/Mn relations of meteorites and primary heterogeneity of primitive achondrite parent bodies. *Geochimica et Cosmochimica Acta* 64:149-160.

Grady M. M. 2000. *Catalogue of meteorites.* Cambridge University Press, 689p.

Graham A. L. and Hutchison R. 1974. Is Kakangari a unique chondrite? *Nature* 251:128-129.

Graham A. L., Easton A. J., and Hutchison R. 1977. Forsterite chondrites; the meteorites Kakangari, Mount Morris (Wisconsin), Pontlyfni and Winona. *Mineralogical Magazine* 41:201-210.

Greshake A. 1997. The primitive matrix components of the unique carbonaceous chondrite Acfer 094: A TEM study. *Geochimica et Cosmochimica Acta* 61:437-452.

Grossman L. 1972. Condensation in the primitive solar nebula. *Geochimica et Cosmochimica Acta* 36:597-619.

Grossman J. N. 1999. The Meteoritical Bulletin, No. 83, 1999 July. *Meteoritics and Planetary Science* 34:169-186.

Grossman J. N. and Brearley A. J. 2005. The onset of metamorphism in ordinary and carbonaceous chondrites. *Meteoritics and Planetary Science* 40:87-122.

Grossman J. N. and Wasson J. T. 1983a. The composition of chondrules in unequilibrated chondrites: An evaluation of models for the formation of chondrules and their precursor materials. In *Chondrules and their origins,* edited by King E. A. Houston: Lunar and Planetary Institute. pp. 88-121.

Grossman J. N. and Wasson J. T. 1983b. Refractory precursor components of Semarkona chondrules and the fractionation of refractory elements among chondrites. *Geochimica et Cosmochimica Acta* 47:759-771.

Grossman J. N., Kracher A., and Wasson J. T. 1979. Volatiles in Chainpur chondrules. *Geophysical Research Letters* 6:597-600.

Grossman J. N., Rubin A. E., Nagahara H., and King E. A. 1988. Properties of chondrules. In *Meteorites and the Early Solar System,* edited by Kerridge J. F. and Matthews M. S. Tucson: The University of Arizona Press. pp. 619-659.

Grossman J. N., Alexander C. M. O'D., Wang J., and Brearley A. J. 2000. Bleached chondrules; evidence for widespread aqueous processes on the parent asteroids of ordinary chondrites. *Meteoritics and Planetary Science* 35:467-486.

Grossman J. N., Alexander C. M. O'D., Wang J., and Brearley A. J. 2002. Zoned chondrules in Semarkona: evidence for high- and low-temperature processing. *Meteoritics and Planetary Science* 37:49-73.

Grossman L., Beckett J. R., Fedkin A. V., Simon S. B., and Ciesla F. J. 2008. Redox Conditions in the Solar Nebula: Observational, Experimental, and Theoretical Constraints. In *Oxygen in the solar system,* edited by MacPherson G. J. Reviews in Mineralogy and Geochemistry, vol. 68. Chantilly: Mineralogical Society of America. pp. 93-140.

Guan Y., McKeegan K. D., and MacPherson G. J. 2000. Oxygen isotopes in calcium-aluminum-rich inclusions from enstatite chondrites: new evidence for a single CAI source in the solar neubla. *Earth and Planetary Science Letters* 181:271-277.

Hewins R. H. 1991. Retention of sodium during chondrule formation. *Geochimica et Cosmochimica Acta* 55:935–942.

Hewins R. H. and Radomsky P. M. 1990. Temperature conditions for chondrule formation. *Meteoritics* 25:309-318.

Hewins R. H., Klein L. C., and Fasano B. V. 1981. Conditions of formation of pyroxene excentroradial chondrules. *Proceedings*, 12th Lunar and Planetary Science Conference. pp. 1123-1133.

Hewins R. H., Yu Y., Zanda B., and Bourot-Denise M. 1997. Do nebular fractionations, evaporative losses, or both, influence chondrule compositions? *Antarctic Meteorite Research* 10:275-298.

Hewins R. H., Connolly H. C., Lofgren G. E., and Libourel G. 2005. Experimental Constraints on Chondrule Formation. In *Chondrites and the Protoplanetary Disk ,* edited by Krot A. N., Scott E. R. D., and Reipurth B. San Francisco: Astronomical Society of the Pacific. pp. 286-316.

Hezel D. C. 2007. A model for calculating the errors of 2D bulk analysis relative to the true 3D bulk composition of an object, with application to chondrules. *Computers and Geosciences* 33:1162-1175.

Hezel D. C. and Palme H. 2007. The conditions of chondrule formation; Part I, Closed system. *Geochimica et Cosmochimica Acta* 71:4092-4107.

Hezel D. C. and Palme H. 2008. Constraints for chondrule formation from Ca-Al distribution in carbonaceous chondrites. *Earth and Planetary Science Letters* 265:716-725.

Hezel D. C., Palme H., Nasdala L., and Brenker F. E. 2006. Origin of SiO_2-rich components in ordinary chondrites. *Geochimica et Cosmochimica Acta* 70:1548-1564.

Horányi M., Morfill G., Goertz C. K., and Levy E. H. 1995. Chondrule formation in lightning discharges. *Icarus* 114:174-185.

Huss G. R., Keil K., and Taylor G. J. 1981. The matrices of unequilibrated ordinary chondrites - Implications for the origin and history of chondrites. *Geochimica et Cosmochimica Acta* 45:33-51.

Huss G. R., Alexander C. M. O., Palme H., Bland P. A., and Wasson J. T. 2005. Genetic relationship between chondrules, fine-grained rims, and interchondrule matrix. In *Chondrites and the protoplanetary disk,* edited by Krot A. N., Scott E. R. D., and Reipurth B. San Francisco: Astronomical Society of the Pacific. pp. 701-731.

Huss G. R., Rubin A. E., and Grossman J. N. 2006. Thermal metamorphism in chondrites. In *Meteorites and the early solar system II,* edited by Lauretta D. S. and McSween H. Y. Jr. Tucson: The University of Arizona Press. pp. 567-586.

Hutchison R. and Bevan A. W. R. 1983. Conditions and time of chondrule accretion. In *Chondrules and their origins,* edited by King E. A. Houston: Lunar and Planetary Institute. pp. 162-179.

Hutchison R., Alexander C. M. O., and Barber D. J. 1987. The Semarkona meteorite; first recorded occurrence of smectite in an ordinary chondrite, and its implications. *Geochimica et Cosmochimica Acta* 51:1875-1882.

Ikeda Y. 1980. Petrology of Allan HILLS-764 Chondrite (LL3). *Proceedings of the National Institute of Polar Research*, 5th Symposium on Antarctic Meteorites. pp. 50-82.

Ikeda Y. 1983. Major element chemical compositions and chemical types of chondrules in unequilibrated E, O, and C chondrites from Antarctica. *Proceedings of the National Institute of Polar Research*, 8th Symposium on Antarctic Meteorites. pp. 122-145.

Ikeda Y. 1989. Petrochemical study of the Yamato-691 enstatite chondrite (E3) IV: Descriptions and mineral chemistry of opaque-mineral nodules. *Proceedings of the National Institute of Polar Research*, 13th Symposium on Antarctic Meteorites. pp. 109-146.

Ikeda Y. and Kojima H. 1991. Terrestrial alteration of Fe-Ni metals in Antarctic ordinary chondrites and the relationship to their terrestrial ages. *Proceedings of the National Institute of Polar Research*, 15th Symposium on Antarctic Meteorites. pp. 307-318.

Jambor J. L. and Dutrizac J. E. 1998. Occurrence and constitution of natural and synthetic ferrihydrite, a widespread iron oxyhydroxide. *Chemical Reviews* 98:2549-2585.

Janney D. E., Cowley J. M., and Buseck P. R. 2001. Structure of synthetic 6-line ferrihydrite by electron nanodiffraction. *American Mineralogist* 86:327-335.

Jbara O., Cazaux J. and Trebbia P. 1995. Sodium diffusion in glasses during electron irradiation. *Journal of Applied Physics* 78:868-875.

Johnson C. A. and Prinz M. 1991. Chromite and olivine in type II chondrules in carbonaceous and ordinary chondrites: Implications for thermal histories and group differences. *Geochimica et Cosmochimica Acta* 55:893-904.

Jones R. H. 1990. Petrology and mineralogy of type II, FeO-rich chondrules in Semarkona (LL3.0): Origin by closed-system fractional crystallization, with evidence for supercooling. *Geochimica et Cosmochimica Acta* 54:1785-1802.

Jones R. H. 1992. On the relationship between isolated and chondrule olivine grains in carbonaceous chondrite ALHA 77307. *Geochimica et Cosmochimica Acta* 56:467-482.

Jones R. H. 1994. Petrology of FeO-poor, porphyritic pyroxene chondrules in the Semarkona chondrite. *Geochimica et Cosmochimica Acta* 58:5325-5340.

Jones R. H. 1996a. FeO-rich, porphyritic pyroxene chondrules in unequilibrated ordinary chondrites. *Geochimica et Cosmochimica Acta* 60:3115-3138.

Jones R. H. 1996b. Relict grains in chondrules: Evidence for chondrule recycling. In *Chondrules and the protoplanetary disk*, edited by Hewins R. H., Jones R. H. and Scott E. R. D. Cambrigde: Cambridge University Press. pp. 163-172.

Jones R. H. and Carey E. R. 2006. Identification of relict forsterite grains in forsterite-rich chondrules using cathodoluminescence (abstract #1783). 37th Lunar and Planetary Science Conference, CD-ROM.

Jones R. H. and Danielson L. R. 1997. A chondrule origin for dusty relict olivine in unequilibrated chondrites. *Meteoritics and Planetary Science* 32:753-760.

Jones R. H. and Lofgren G. E. 1993. A comparison of FeO-rich, porphyritic olivine chondrules in unequilibrated chondrites and experimental analogues. *Meteoritics* 28:213-221.

Jones R. H. and Rubie D. C. 1991. Thermal histories of CO3 chondrites; application of olivine diffusion modelling to parent body metamorphism. *Earth and Planetary Science Letters* 106:73-86.

Jones R. H. and Scott E. R. D. 1989. Petrology and thermal history of type IA chondrules in the Semarkona (LL3.0) chondrite. *Proceedings*, 19th Lunar and Planetary Science Conference. pp. 523-536.

Jones R. H., Grossman J. N., and Rubin A. E. 2005. Chemical, Mineralogical and Isotopic Properties of Chondrules: Clues to Their Origin. In *Chondrites and the Protoplanetary Disk,* edited by Krot A. N., Scott E. R. D., and Reipurth B. San Francisco: Astronomical Society of the Pacific. pp. 251-285.

Jurewicz A. J. G. and Watson E. B. 1988. Cations in olivine; Part 1, Calcium partitioning and calcium-magnesium distribution between olivines and coexisting melts, with petrologic applications. *Contributions to Mineralogy and Petrology* 99:176-185.

Kallemeyn G. W. 1994. Compositional study of Kakangari and LEW 87232 (abstract). *Meteoritics* 29:479.

Karner J., Papike J. J. and Shearer C. K. 2003. Olivine from planetary basalts: Chemical signatures that indicate planetary parentage and those that record igneous setting and process. *American Mineralogist* 88:806-816.

Kerridge J. F., MacDougall J. D., and Marti K. 1979. Clues to the origin of sulfide minerals in CI chondrites. *Earth and Planetary Science Letters* 43:359-367.

Kimura M. and Yagi K. 1980. Crystallization of chondrules in ordinary chondrites. *Geochimica et Cosmochimica Acta* 44:589-602.

Kimura M., Hiyagon H., Lin Y., and Weisberg M. K. 2003. FeO-rich silicates in the Sahara 97159 (EH3) enstatite chondrite: Mineralogy, oxygen isotopic compositions, and origin. *Meteoritics and Planetary Science* 38:389-398.

Kimura M., Weisberg M. K., Lin Y., Suzuki A., Ohtani E., and Okazaki R. 2005. Thermal history of the enstatite chondrites from silica polymorphs. *Meteoritics and Planetary Science* 40:855-868.

Kita N. T., Nagahara H., Tomomura S., Tachibana S., and Valley J. W. 2006. Systematic oxygen isotopic variations among chondrules from the least equilibrated ordinary chondrites; improved ion microprobe precision (abstract #1496). 37th Lunar and Planetary Science Conference. CD-ROM

Kita N. T., Nagahara H., Tachibana S., Founelle J. H., and Valley J. W. 2007. Oxygen isotopic compositions of chondrule glasses in Semarkona (LL3.0); search for ^{16}O-depleted components in chondrules (abstract #1791). 38th Lunar and Planetary Science Conference. CD-ROM

Klerner S. 2001. Materie im frühen Sonnensystem: Die Enstehung von Chondren, Matrix und refraktären Forsteriten. Ph.D. thesis. University of Cologne, Köln, Germany.

Klerner S. and Palme H. 1999a. Origin of chondrules and matrix in carbonaceous chondrites (abstract #1272). 30th Lunar and Planetary Science Conference. CD-ROM

Klerner S. and Palme H. 1999b. Origin of chondrules and matrix in the Renazzo Meteorite. *Meteoritics and Planetary Science* 34:64-65.

Klerner S. and Palme H. 2000. Large titanium/aluminum fractionation between chondrules and matrix in Renazzo and other carbonaceous chondrites. *Meteoritics and Planetary Science* 35:89.

Klöck W., Thomas K. L., McKay D. S., and Palme H. 1989. Unusual olivine and pyroxene composition in interplanetary dust and unequilibrated ordinary chondrites. *Nature* 339:126-128.

Kong P. and Palme H. 1999. Compositional and genetic relationship between chondrules, chondrule rims, metal, and matrix in the Renazzo Chondrite. *Geochimica et Cosmochimica Acta* 63:3673-3682.

Kong P., Deloule E., and Palme H. 2000. REE-bearing sulfide in Bishunpur (LL3.1), a highly unequilibrated ordinary chondrite. *Earth and Planetary Science Letters* 177:1-7.

Kring D. A. 1991. High temperature rims around chondrules in primitive chondrites: Evidence for fluctuating conditions in the solar nebula. *Earth and Planetary Science Letters* 105:65–80.

Krot A. N., Scott E. R. D., and Zolensky M. E. 1995. Mineralogical and chemical modification of components in CV3 chondrites: Nebular or asteroidal processing? *Meteoritics* 30:748-775.

Krot A. N., Zolensky M. E., Wasson J. T., Scott E. R. D., Keil K., and Ohsumi K. 1997. Carbide-magnetite assemblages in Type-3 ordinary chondrites. *Geochimica et Cosmochimica Acta* 61:219-237.

Krot A. N., Petaev M. I., Scott E. R. D., Choi B., Zolensky M. E., and Keil K. 1998. Progressive alteration in CV3 chondrites: More evidence for asteroidal alteration. *Meteoritics and Planetary Science* 33:1065-1085.

Krot A. N., Meibom A., Weisberg M. K., and Keil K. 2002. The CR chondrite clan; implications for early solar system processes. *Meteoritics and Planetary Science* 37:1451-1490.

Krot A. N., Keil K., Goodrich C. A., and Scott E. R. D. 2003. Classification of meteorites. In *Meteorites, comets, and planets*, edited by Davis A. M. Treatise on Geochemistry, vol. 1. Oxford: Elsevier. pp. 83-128.

Krot A. N., Yurimoto H., McKeegan K. D., Leshin L. A., Chaussidon M., Libourel G., Yoshitake M., Huss G. R., Yunbin G., and Zanda B. 2006. Oxygen isotopic compositions of chondrules: implications for evolution of oxygen isotopic reservoirs in the inner solar nebula. *Chemie der Erde* 66:249-276.

Kunihiro T., Rubin A. E., McKeegan K. D., and Wasson J. T. 2004. Oxygen-isotopic compositions of relict and host grains in chondrules in the Yamato 81020 CO3.0 chondrite. *Geochimica et Cosmochimica Acta* 68:3599-3606.

Kurahashi E., Kita N. T., Nagahara H., and Morishita Y. 2008. ^{26}Al- ^{26}Mg systematics of chondrules in a primitive CO chondrite. *Geochimica et Cosmochimica Acta* 72:3865-3882.

Lauretta D. S. and Buseck P. R. 2003. Opaque minerals in chondrules and fine-grained chondrule rims in the Bishunpur (LL3.1) Chondrite. *Meteoritics and Planetary Science* 38:59-79.

Lauretta D. S., Kremser D. T., and Fegley B. Jr. 1996a. The rate of iron sulfide formation in the solar nebula. *Icarus* 122:288-315.

Lauretta D. S., Fegley B. Jr., Lodders K., and Kremser D. T. 1996b. The kinetics and mechanism of iron sulfide formation in the solar nebula. *Proceedings of the National Institute of Polar Research*, 20th Symposium on Antarctic Meteorites pp. 111-126.

Lauretta D. S., Lodders K., Fegley B., and Kremser D. T. 1997a. The origin of sulfide-rimmed metal grains in ordinary chondrites. *Earth and Planetary Science Letters* 151:289-301.

Lauretta D. S., Lodders K., and Fegley B. 1997b. Experimental simulations of sulfide formation in the solar nebula. *Science* 277:358-360.

Lauretta D. S., Lodders K., and Fegley B. 1998. Kamacite sulfurization in the solar nebula. *Meteoritics and Planetary Science* 33:821-833.

Lauretta D. S., Buseck P. R., and Zega T. J. 2001. Opaque minerals in the matrix of the Bishunpur (LL3.1) chondrite; constraints on the chondrule formation environment. *Geochimica et Cosmochimica Acta* 65:1337-1353.

Lee M. R. and Bland P. A. 2004. Mechanisms of weathering of meteorites recovered from hot and cold deserts and the formation of phyllosilicates. *Geochimica et Cosmochimica Acta* 68:893-916.

Lemelle L., Guyot F., Fialin M., and Pargamin J. 2000. Experimental study of chemical coupling between reduction and volatilization in olivine single crystals. *Geochimica et Cosmochimica Acta* 64**:**3237-3249.

Lemelle L., Guyot F., Leroux H., and Libourel G. 2001. An experimental study of external reduction of olivine single crystals. *American Mineralogist* 86:47-54.

Leroux H., Libourel G., Lemelle L., and Guyot F. 2003. Experimental study and TEM characterization of dusty olivines in chondrites: Evidence for formation by in situ reduction. *Meteoritics and Planetary Science* 38:81-94.

Lewis J. S. 1967. A possible origin for sulfates and sulfur in meteorites. *Earth and Planetary Science Letters* 2:29-32.

Libourel G. 1999. Systematics of calcium partitioning between olivine and silicate melt: implications for melt structure and calcium content of magmatic olivines. *Contributions to Mineralogy and Petrology* 136:63-80.

Libourel G. and Chaussidon M. 1995. Experimental constraints on chondrule reduction (abstract). *Meteoritics* 30:536-537.

Libourel G., Krot A. N., and Tissandier L. 2006. Role of gas-melt interaction during chondrule formation. *Earth and Planetary Science Letters* 251:232-240.

Lodders K. 2003. Solar system abundances and condensation temperatures of the elements. *The Astrophysical Journal* 591:1220-1247.

Lodders K. and Fegley B. Jr. 1998. *The Planetary Scientist's companion*. New York: Oxford University Press. 371p.

Lofgren G. 1989. Dynamic crystallization of chondrule melts of porphyritic olivine composition: Textures experimental and natural. *Geochimica et Cosmochimica Acta* 53:461-470.

Lofgren G. and Lanier A. B. 1990. Dynamic crystallization study of barred olivine chondrules. *Geochimica et Cosmochimica Acta* 54:3537-3551.

Lofgren G. and Russell W. J. 1986. Dynamic Crystallization of Chondrule Melts of Porphyritic and Radial Pyroxene Composition. *Geochimica et Cosmochimica Acta* 50:1715-1726.

Lusby D., Scott E. R. D., and Keil K. 1987. Ubiquitous high-FeO silicates in enstatite chondrites. *Journal of Geophysical Research* 92:E679-E695.

Lux G., Keil, K. and Taylor G. J. 1980. Metamorphism of the H-group chondrites - Implications from compositional and textural trends in chondrules. *Geochimica et Cosmochimica Acta* 44:841-855.

Lux G., Keil K., and Taylor G. J. 1981. Chondrules in H3 chondrites; textures, compositions and origins. *Geochimica et Cosmochimica Acta* 45:675-685.

Maloy A. K. and Treiman A. H. 2007. Evaluation of image classification routines for determining modal mineralogy of rocks from X-ray maps. *American Mineralogist* 92:1781-1788.

Mason B. and Wiik H. B. 1966. The composition of the Bath, Frankfort, Kakangari, Rose City, and Tadjera meteorites. *American Museum Novitates* 2272:1-24.

Matas J., Ricard Y., Lemelle L. and Guyot F. 2000. An improved thermodynamic model of metal-olivine-pyroxene stability domains. *Contributions to Mineralogy and Petrology* 140:73-83.

Matsuda H., Nakamura N., and Noda S. 1990. Alkali (Rb/K) abundances in Allende barred-olivine chondrules; implications for the melting conditions of chondrules. *Meteoritics* 25:137-143.

Matsunami S., Ninagawa K., Nishimura S., Kubono N., Yamamoto I., Kohata M., Wada T., Yamashita Y., Lu J., Sears D. W. G., and Nishimura H. 1993. Thermoluminescence and compositional zoning in the mesostasis of a Semarkona group A1 chondrule and new insights into the chondrule-forming process. *Geochimica et Cosmochimica Acta* 57:2101-2110.

McSween H. Y. 1977a. Chemical and petrographic constraints on the origin of chondrules and inclusions in carbonaceous chondrites. *Geochimica et Cosmochimica Acta* 41:1843-1845.

McSween H. Y. 1977b. Carbonaceous chondrites of the Ornans type; a metamorphic sequence. *Geochimica et Cosmochimica Acta* 41:477-491.

McSween H. Y. 1977c. On the nature and origin of isolated olivine grains in carbonaceous chondrites. *Geochimica et Cosmochimica Acta* 41:411-418.

McSween H. Y. and Richardson S. M. 1977. The composition of carbonaceous chondrite matrix. *Geochimica et Cosmochimica Acta* 41:1145-1161.

Metzler K., Bischoff A., and Stöffler D. 1992. Accretionary dust mantles in CM chondrites - Evidence for solar nebula processes. *Geochimica et Cosmochimica Acta* 56:2873-2897.

Michel F. M., Ehm L., Antao S. M., Lee P. L., Chupas P. J., Liu G., Strongin D. R., Schoonen M. A. A., Phillips B. L., and Parise J. B. 2007. The structure of ferrihydrite, a nanocrystalline material. *Science* 316:1726-1728.

Mittlefehldt D. W. 2008. Appendix: Meteorites – A brief tutorial. In *Oxygen in the solar system,* edited by MacPherson G. J. Reviews in Mineralogy and Geochemistry, vol. 68. Chantilly: Mineralogical Society of America. pp. 571-590.

Miyamoto M., Furuta T., Fujii N., McKay D. S., Lofgren G. E., and Duke M. B. 1993. The Mn-Fe negative correlation in olivines in ALHA 77257 ureilite. *Journal of Geophysical Research* 98(E3):5301-5307.

Morgan G. B. and London D. 2005. Effect of current density on the electron microprobe analysis of alkali aluminosilicate glasses. *American Mineralogist* 90:1131-1138.

Nagahara H. 1981. Evidence for secondary origin of chondrules. *Nature* 292:135-136.

Nagahara H. 1985. Experimental reduction of olivine and its application to the reduction in enstatite chondrites (abstract). *Meteoritics* 20:715-716.

Nagahara H. 1986. Reduction kinetics of olivine and oxygen fugacity environment during chondrule formation. 17th Lunar and Planetary Science Conference. pp. 595-596.

Nagahara H., Kita N. T., Ozawa K., and Morishita Y. 2008. Condensation of major elements during chondrule formation and its implication to the origin of chondrules. *Geochimica et Cosmochimica Acta* 72:1442-1465.

Nakamura T., Noguchi T., Tsuchiyama A., Ushikubo T., Kita N. T., Valley J. W., Zolensky M. E., Kakazu Y., Sakamoto K., Mashio E., Uesugi K., and Nakano T. 2008. Chondrulelike objects in short-period comet 81P/Wild2. *Science* 321:1664-1667

Nehru C. E., Prinz M., Weisberg M. K., and Delaney J. S. 1983. The Kakangari chondrite and its relationship to carbonaceous chondrite (abstract). *Meteoritics* 18:361-362.

Nehru C. E., Weisberg M. K., and Prinz M. 1986. Chondrules in the Kakangari chondrite (abstract). *Meteoritics* 21:468.

Nehru C. E., Prinz M., Okulewicz S. C., and Weisberg M. K. 1988. Glassy, cryptocrystalline and radial pyroxene chondrules in type 3 ordinary chondrites. *LPI Contribution* 665:C-3.

Nielson C. H. and Sigurdsson H. 1981. Quantitative methods for electron microprobe analysis of sodium in natural and synthetic glasses. *American Mineralogist* 66:547-552.

Nitsan U. 1974. Stability field of olivine with respect to oxidation and reduction. *Journal of Geophysical Research* 79:706-711.

Nuth J. A. III., Brearley A. J., and Scott E. R. D. 2005. Microcrystals and amorphous material in comets and primitive meteorites: Keys to understanding processes in the early solar system. In *Chondrites and the protoplanetary disk*, edited by Krot A. N., Scott E. R. D., and Reipurth B. San Francisco: Astronomical Society of the Pacific. pp. 675-700.

Olsen E. J. 1983. SiO_2-bearing chondrules in the Murchison (C2) meteorite. In *Chondrules and their Origin*, edited by King E. A. Houston: Lunar and Planetary Institute. pp. 223-234.

Pack A. and Palme H. 2003. Partitioning of Ca and Al between forsterite and silicate melt in dynamic systems with implications for the origin of Ca, Al-rich forsterites in primitive meteorites. *Meteoritics and Planetary Science* 38:1263-1281.

Pack A., Yurimoto H., and Palme H. 2004. Petrographic and oxygen-isotope study of refractory forsterites from R-chondrite Dar al Gani 013 (R3.5-6), unequilibrated ordinary and carbonaceous chondrites. *Geochimica et Cosmochimica Acta* 68:1135-1157.

Pack A., Palme H. and Shelley J. M. G. 2005. Origin of chondritic forsterite grains. *Geochimica et Cosmochimica Acta* **69**, 3159-3182.

Palme H. and Klerner S. 2000. Formation of chondrules and matrix in carbonaceous chondrites. *Meteoritics and Planetary Science* 35:124.

Papike J. J., Karner J. M., and Shearer C. K. 2003. Determination of planetary basalt parentage: A simple technique using the electron microprobe. *American Mineralogist* 88:469-472.

Pasek M. A., Milsom J. A., Ciesla F. J., Lauretta D. S., Sharp C. M., and Lunine J. I. 2005. Sulfur chemistry with time-varying oxygen abundance during solar system formation. *Icarus* 175:1-14.

Perron C. and Bourot-Denise M. 2001. Oxygen isotopes in the Sahara 97096 EH3 chondrite (abstract #2187). 32nd Lunar and Planetary Science Conference. CD-ROM.

Prinz M., Weisberg M. K., Nehru C. E., MacPherson G. J., Clayton R. N., and Mayeda, T. K. 1989. Petrologic and stable isotope study of the Kakangari (K-Group) chondrite: Chondrules, matrix, CAI's. 20th Lunar and Planetary Science Conference. pp. 870-871.

Prinz M., Chatterjee N., Weisberg M. K., Clayton R. N., and Mayeda T. K. 1991. Lea Co. 002: A second Kakangari-type chondrite. 22nd Lunar and Planetary Science Conference. pp. 1097-1098.

Rambaldi E. R. 1981. Relict grains in chondrules. *Nature* 293:558-561.

Rambaldi E. R. and Rajan R. S. 1982. Evidence for primitive phosphates in highly unequilibrated ordinary chondrites (abstract). *Meteoritics* 17:271-272.

Rambaldi E. R. and Wasson J. T. 1984. Metal and associated phases in Krymka and Chainpur; nebular formational processes. *Geochimica et Cosmochimica Acta* 48:1885-1897.

Rasmussen K. L. 1981. The cooling rates of iron meteorites - A new approach. *Icarus* 45:564-576.

Righter K. 2007. Curator's comments. *Antarctic Meteorite Newsletter* 30:1-4.

Rubin A. E. 1984. Coarse-grained chondrule rims in type 3 chondrites. *Geochimica et Cosmochimica Acta* 48:1779-1789.

Rubin A. E. 1989. Size-frequency distributions of chondrules in CO3 chondrites. *Meteoritics* 24:179-189.

Rubin A. E. 2000. Petrologic, geochemical and experimental constraints on models of chondrule formation. *Earth Science Reviews* 50:3-27.

Rubin A. E. and Grossman J. N. 1985. Phosphate-sulfide assemblages and Al/Ca ratios in type-3 chondrites. *Meteoritics* 20:479-489.

Rubin A. E. and Grossman J. N. 1987. Size-frequency-distributions of EH3 chondrules. *Meteoritics* 22:237-251.

Rubin A. E. and Wasson J. T. 1988. Chondrules and matrix in the Ornans CO3 Meteorite; possible precursor components. *Geochimica et Cosmochimica Acta* 52:425-432.

Rubin A. E. and Wasson J. T. 2005. Non-spherical lobate chondrules in CO3.0 Y-81020; general implications for the formation of low-FeO porphyritic chondrules in CO chondrites. *Geochimica et Cosmochimica Acta* 69:211-220.

Rubin A. E., Wang D., Kallemeyn G. W., and Wasson J. T. 1988. The Ningqiang meteorite: Classification and petrology of an anomalous CV chondrite. *Meteoritics* 23:13-23.

Rubin A. E., Sailer A. L., and Wasson J. T. 1999. Troilite in the chondrules of type-3 ordinary chondrites; implications for chondrule formation. *Geochimica et Cosmochimica Acta* 63:2281-2298.

Russell S. S., Zipfel J., Grossman J. N., and Grady M. M. 2002. The Meteoritical Bulletin, No. 86, 2002 July. *Meteoritics and Planetary Science* 37:157-184.

Saikumar V. and Goldstein J. I. 1988. An evaluation of the methods to determine the cooling rates of iron meteorites. *Geochimica et Cosmochimica Acta* 52:715-726.

Schmitt R.A. and Laul J.C. 1973. A survey of the selenochemistry of major, minor and trace elements. *The Moon* 8:182-209.

Schneider D. M., Symes S. J. K., Benoit P. H., and Sears D. W. G. 2002. Properties of chondrules in EL3 chondrites, comparison with EH3 chondrites, and the implications for the formation of enstatite chondrites. *Meteoritics and Planetary Science* 37:1401-1416.

Schrader D. L., Connolly Jr H. C., and Lauretta D. S. 2008. Opaque phases in type-II chondrules from CR2 chondrites: Implications for CR parent body formation. *Geochimica et Cosmochimica Acta* 72:6124-6140.

Schwertmann U., Stanjek H., and Becher H.-H. 2004. Long-term in vitro transformation of 2-line ferrihydrite to goethite/hematite at 4, 10, 15 and 25ºC. *Clay Minerals* 39:433-438.

Scott E. R. D. and Jones R. H. 1990. Disentangling nebular and asteroidal features of CO3 carbonaceous chondrite meteorites. *Geochimica et Cosmochimica Acta* 54:2485-2502.

Scott E. R. D. and Krot A. N. 2003. Chondrites and their Components. In *Meteorites, comets, and planets*, edited by Davis A. M. Treatise on Geochemistry, vol. 1. Oxford: Elsevier. pp. 143-200.

Scott E. R. D. and Krot A. N. 2005. Thermal processing of silicate dust in the solar nebula: Clues from primitive chondrite matrices. *Astrophysical Journal* 623:571-578.

Scott E. R. D. and Taylor G. J. 1983. Chondrules and other components in C, O, and E chondrites: Similarities in their properties and origins. *Proceedings,* 14th Lunar and Planetary Science Conference, *Journal of Geophysical Research* 88:B275-B286.

Scott E. R. D., Taylor G. J., and Keil K. 1982. Origin of ordinary and carbonaceous type 3 chondrites and their components. *Lunar and Planetary Science* XIII:704-705.

Scott E. R. D., Rubin A. E., Taylor G. J., and Keil K. 1984. Matrix material in type 3 chondrites; occurrence, heterogeneity and relationship with chondrules. *Geochimica et Cosmochimica Acta* 48:1741-1757.

Scott E. R. D., Barber D. J., Alexander C. M. O., Hutchison R., and Peck J. A. 1988. Primitive material surviving in chondrites: Matrix. In *Meteorites and the early solar system,* edited by Kerridge J. F. and Matthews M. S. Tucson: The University of Arizona Press. pp. 718-745.

Scott E. R. D., Jones R. H., and Rubin A. E. 1994. Classification, metamorphic history, and pre-metamorphic composition of chondrules. *Geochimica et Cosmochimica Acta* 58:1203-1209.

Sears D. W. G. and Dodd R. T. 1988. Overview and classification of meteorites. In *Meteorites and the Early Solar System*, edited by Kerridge J. F. and Matthews M. S. Tucson: The University of Arizona Press. pp. 3-31.

Sears D. W. G., Huang S., and Benoit P. H. 1996. Open-system behavior during chondrule formation. In *Chondrules and the protoplanetary disk,* edited by Hewins R. H., Jones R. H., and Scott E. R. D. Cambridge: Cambridge University Press. pp. 221-231.

Sears D. W. G., Morse A. D., Hutchison R., Guimon R. K., Lu J., Alexander C. M. O., Benoit P. H., Wright I., Pillinger C., Xie T., and Lipschutz M. E. 1995. Metamorphism and aqueous alteration in low petrographic type ordinary chondrites. *Meteoritics* 30:169-181.

Shu F. H., Shang H., Glassgold A. E., and Lee T. 1997. X-rays and fluctuating x-winds from protostars. *Science* 277:1475-1479.

Shu F. H., Shang H., Gounelle M., Glassgold A. E., and Lee T. 2001. The origin of chondrules and refractory inclusions in chondritic meteorites. *The Astrophysical Journal* 548:1029-1050.

Silberrad C. A. 1932. In *Mineralogical Magazine* 23:296.

Simon S. B. and Haggerty S. E. 1980. Bulk compositions of chondrules in the Allende meteorite. *Proceedings*, 11th Lunar and Planetary Science Conference. pp. 901-927.

Stanjek H. and Weidler P. G. 1992. The effect of dry heating on the chemistry, surface area, and oxalate solubility of synthetic 2-line and 6-line ferrihydrites. *Clay Minerals* 27:397-411.

Stöffler D., Keil K., and Scott E. R. D. 1991. Shock metamorphism of ordinary chondrites. *Geochimica et Cosmochimica Acta* 55:3845-3867.

Sutton S. R., Bajt S., and Jones R. 1996. In situ determination of chromium oxidation state in olivine from chondrules. 27th Lunar and Planetary Science Conference. pp. 1291-1292.

Tachibana S. and Huss G. R. 2005. Sulfur isotope composition of putative primary troilite in chondrules from Bishunpur and Semarkona. *Geochimica et Cosmochimica Acta* 69:3075-3097.

Takagi M., Huber H., Rubin A. E., and Wasson J. T. 2004. Distribution of FeO/(FeO+MgO) in Semarkona chondrules: Implications for chondrule formation and nebular evolution (abstract #5217). *Meteoritics and Planetary Science* 39 (Supplement).

Taylor S. R. 2001. *Solar system evolution - A new perspective*. Cambridge: Cambridge University Press. 460 p.

Tsuchiyama A., Nagahara H., and Kushiro I. 1980. Experimental reproduction of textures of chondrules. *Earth and Planetary Science Letters* 48:155-165.

Tsuchiyama A., Osada Y., Nakano T., and Uesugi K. 2004. Experimental reproduction of classic barred olivine chondrules: open system behavior of chondrule formation. *Geochimica et Cosmochimica Acta* 68:653-672.

Varela M. E., Kurat G., and Zinner E. 2006. The primary liquid condensation model and the origin of barred olivine chondrules. *Icarus* 184:344-364.

Vempati R. K., Loeppert R. H., Sittertz-Bhatkar H., and Burghardt R. C. 1990. Infrared vibrations of hematite formed from aqueous- and dry-thermal incubation of Si-containing ferrihydrite. *Clays and Clay Minerals* 38:294-298.

Warren P. H. 1997. The unequal host-phase density effect in electron probe defocused beam analysis: An easily correctable problem (abstract #1406). 28th Lunar and Planetary Science Conference. CD-ROM.

Wasson J. T. and Rubin A. E. 2003. Ubiquitous low-FeO relict grains in type II chondrules and limited overgrowths on phenocrysts following the final melting event. *Geochimica et Cosmochimica Acta* 67:2239-2250.

Wasson J. T., Kallemeyn G. W., and Rubin A. E. 2000. Chondrules in the LEW85332 ungrouped carbonaceous chondrite; fractionation processes in the solar nebula. *Geochimica et Cosmochimica Acta* 64:1279-1290.

Weinbruch S., Palme H. and Spettel B. 2000. Refractory forsterite in primitive meteorites: Condensates from the solar nebula? *Meteoritics and Planetary Science* 35:161-171.

Weisberg M. K. 1986. Barred olivine chrondules in carbonaceous chondrites (abstract). *LPI Contribution* 600:81.

Weisberg M. K. 1987. Barred olivine chondrules in ordinary chondrites. *Journal of Geophysical Research* 92:E663-E678.

Weisberg M. K. 2001. Sahara 00182, the first CR3 chondrite and formation of multi-layered chondrules. *Meteoritics and Planetary Science* 36:222-223.

Weisberg M. K. and Huber H. 2007. The GRO 95577 CR1 chondrite and hydration of the CR parent body. *Meteoritics and Planetary Science* 42:1495-1503.

Weisberg M. K. and Prinz M. 1996. Agglomeratic chondrules, chondrule precursors, and incomplete melting. In *Chondrules and the protoplanetary disk*, edited by Hewins R. H., Jones R. H., and Scott E. R. D. Cambridge: Cambridge University Press. pp. 119-127.

Weisberg M. K., Prinz M., Clayton R. N., and Mayeda T. K. 1993. The CR (Renazzo-type) carbonaceous chondrite group and its implications. *Geochimica et Cosmochimica Acta* 57:1567-1586.

Weisberg M. K., Prinz M., Clayton R. N., Mayeda T. K., Grady M. M., and Franchi, I. A. 1993. Petrology and stable isotopes of LEW 87232, a new Kakangari-type chondrite. *Meteoritics* 28:458-459.

Weisberg M. K., Prinz M., and Fogel R. A. 1994. The evolution of enstatite and chondrules in unequilibrated enstatite chondrites: Evidence from iron-rich pyroxene. *Meteoritics* 29:362-373.

Weisberg M. K., Prinz M., Clayton R. N., Mayeda T. K., Grady M. M., and Pillinger C. T. 1995. The CR chondrite clan. *Proceedings of the National Institute of Polar Research*, 19th Symposium on Antarctic Meteorites pp. 11-32.

Weisberg M. K., Prinz M., Clayton R. N., Mayeda T. K., Grady M. M., Franchi I., Pillinger C. T., and Kallemeyn G. W. 1996. The K (Kakangari) chondrite grouplet. *Geochimica et Cosmochimica Acta* 60:4253-4263.

Weisberg M. K., Kimura M., McCoy T. J., and Lin Y. 2005. Olivine and the thermal history of the E chondrite parent body (abstract #1420). 36th Lunar and Planetary Science Conference. CD-ROM.

Willis J. and Goldstein J. I. 1981. Solidification zoning and metallographic cooling rates of chondrites. *Nature* 293:126-127

Wood J. A. 1964. The cooling rates and parent planets of several iron meteorites. *Icarus* 3:429-459.

Wood J. A. 1985. Meteoritic constraints on processes in the solar nebula. In *Protostars and Planets II,* edited by Black D. C. and Matthews M. S. Tucson: The University of Arizona Press. pp. 687-702.

Wood J. A. 2005. The chondrite types and their origins. In *Chondrites and the protoplanetary disk*, edited by Hewins R. H., Jones R. H. and Scott E. R. D. Cambrigde: Cambridge University Press. pp. 953-971.

Wood J. A. and Hashimoto A. 1993. Mineral equilibrium in fractionated nebular systems. *Geochimica et Cosmochimica Acta* 57:2377-2388.

Yin Q.-Z. 2005. From dust to planets: The tale told by moderately volatile elements. In *Chondrites and the protoplanetary Disk*, edited by Krot A. N., Scott E. R. D., and Reipurth B. San Francisco: Astronomical Society of the Pacific. pp. 632-644.

Yu Y., Hewins R. H., and Zanda B. 1996. Sodium and sulfur in chondrules: Heating time and cooling curves. In *Chondrules and the protoplanetary disk,* edited by Hewins R. H., Jones R. H., and Scott E. R. D. Cambridge: Cambridge University Press. pp. 213-219.

Yurimoto H., Krot A. N., Choi B.-G., Aleon J., and Kunihiro T. 2008. Oxygen Isotopes of Chondritic Components. In *Oxygen in the solar system,* edited by MacPherson G. J. Reviews in Mineralogy and Geochemistry, vol. 68. Chantilly: Mineralogical Society of America. pp. 141-186.

Zanda B. 2004. Chondrules. *Earth and Planetary Science Letters* 224:1-17.

Zanda B., Bourot-Denise M., Perron C., and Hewins R. H. 1994. Origin and metamorphic redistribution of silicon, chromium, and phosphorus in the metal of chondrites. *Science* 265:1846-1849.

Zanda B., Bourot-Denise M., and Hewins R. H. 1995. Condensate sulfide and its metamorphic transformations in primitive chondrites. *Meteoritics* 30:605.

Zolensky M. E., Score R., Clayton R. N., Mayeda T. K., and Schutt J. W. 1989. Lea County 001, an H5 chondrite, and Lea County 002, an ungrouped type 3 chondrite. *Meteoritics* 24:227-232.

Zolensky M. E., Barrett R., and Browning L. 1993. Mineralogy and composition of matrix and chondrule rims in carbonaceous chondrites. *Geochimica et Cosmochimica Acta* 57:3123-3148.